EXPERIMENTAL METHODS FOR UNDERSTANDING THE BEHAVIOR AND RESIDUAL CAPACITY OF BOLTS AND STEEL BOLTED CONNECTIONS UNDER IMPULSIVE LOADS

A Thesis
Presented to
The Academic Faculty

By

Marc J. Sanborn

In Partial Fulfillment
Of the Requirements for the Degree
Doctor of Philosophy in Civil Engineering

Georgia Institute of Technology

May 2018

EXPERIMENTAL METHODS FOR UNDERSTANDING THE BEHAVIOR AND RESIDUAL CAPACITY OF BOLTS AND STEEL BOLTED CONNECTIONS UNDER IMPULSIVE LOADS

Approved by:

Dr. Lauren K. Stewart, Advisor
School of Civil & Environmental Engineering
Georgia Institute of Technology

Dr. Laurence J. Jacobs
College of Engineering
Georgia Institute of Technology

Dr. Lawrence F. Kahn
School of Civil & Environmental Engineering
Georgia Institute of Technology

Dr. T. Russell Gentry
College of Design
Georgia Institute of Technology

Dr. Paul F. Mlakar
U.S. Army Engineer Research & Development Center
U.S. Army Corps of Engineers

Date Approved: March 1, 2018

To my parents for the inspiration and to
Kathryn for the strength of will

ACKNOWLEDGEMENTS

As career U.S. Army officers, the opportunity for Kathryn and I to pursue doctorates would never have been possible without the first class faculty in the Department of Civil & Mechanical Engineering at the United States Military Academy who put their trust and confidence in us to earn our degrees and return to our alma mater as senior faculty members. I am grateful to COL Fred Meyer, COL Joseph Hanus, and COL Brad Wambeke for their mentorship, guidance, words of encouragement and, most of all, their unconditional support of the difficult career decisions we have had to make over the past three years. Dr. Chris Conley has provided mentorship, coaching, and guidance to me since I was a student in his mechanics course 20 years ago and continues to do so to this day, pushing and inspiring me through his ceaseless intellectual curiosity. A heartfelt thanks to all of you and, of course, Beat Navy!

I could not imagine navigating this process with an advisor other than Dr. Lauren Stewart. Her understanding, appreciation, and support of my constrained timeline was absolutely critical to ensuring I remained on track and on task. When I began investigating graduate programs, I was repeatedly advised to avoid experimental research. I am forever grateful that I ignored conventional wisdom and was afforded the tremendous opportunity to work with Dr. Stewart. Thank you for providing me a multitude of opportunities, timely and sound guidance, and the support necessary to learn, grow, and be successful in this program.

This work would not have been possible without the commitment of the other members of my committee, Dr. Laurence Jacobs, Dr. Lawrence Kahn, Dr. Russell Gentry,

and Dr. Paul Mlakar. Thank you for your time, feedback, and guidance throughout this process. I have enjoyed working with all of you and sincerely appreciate your willingness to be a part of this work.

Full scale experimental research simply cannot be done alone. Much of this research would not have been possible without the help and support of the Stewart Research Group. A very special thanks to Dr. Giovanni Loreto, who provided hours of technical assistance, physical labor, and much needed support and guidance throughout the process. Fellow students Genevieve Pezzola, Dr. Nan Gao, Rebecca Nylen, CPT Brian Riser as well as undergraduate researchers Chris Foster, Chris Miller, and Alex Herdt all spent countless, mind numbing hours waiting for the blast simulator to warm up followed by an hour of hard labor - only to repeat the process again and again. Thank you all for your time, efforts, and positive attitudes when I am certain there is something more productive you could have been doing.

In addition to other students, this project also received the support of the staff at the Structural Engineering and Materials Research Laboratory and the School of Civil and Environmental Engineering support staff. I am particularly grateful to Mr. Jeremy Mitchell for ensuring that my limbs remained intact and for all of his support throughout this project. Thank you for being flexible when I needed to close half the lab down for several weeks and keeping all of the infrastructure running that made this work possible. Mr. Andy Udell and Mr. Blake Baklini were tremendously helpful in modifying and fine tuning the experimental setup when my brilliant ideas turned out to be not so brilliant. Their common sense approach and exceptional fabrication skills were greatly needed and appreciated.

I would be remiss if I did not acknowledge all of the paratroopers and Soldiers that I have had the pleasure of serving with over the past 17 years. While not directly involved in this work, the superiors, peers, and subordinates that I served with have greatly influenced who I am as a person, my core values, and who I aspire to be. Senior leadership has been supportive of my academic pursuits, peers have proved exceptional teammates in the best and worst of times, and noncommissioned officers and Soldiers have given me a reason to be better each and every day. It is because of them that I was able to pursue this work. My only hope is that in some small way I will probably never know, this work will be of some benefit to them and those that will serve in the future.

The unending love and support of my family has been and will continue to be a constant source of inspiration and strength. Observing both of my parents pursue higher education later in life has instilled in me a love of learning and a strong belief in the joys and benefits of lifetime learning. My big sister is and always will be my best friend and I believe, was put on this earth to keep me humble. Thank you for your support and unconditional love.

Finally, absolutely none of this would be possible without the love and support of my wife, Kathryn. She is my confidant, my sounding board, and my reason for getting up in the morning (besides the dogs barking, that is). When conducting experimental tests, she was right by my side assisting when she had her own research demands. She has heard me repeatedly rehearse presentations, edited my often abysmal writing, and been a sanity check when I have come dangerously close to the edge of the cliff. Thank you for being you and all that you do. As always, I look forward to where our next adventures will take us and writing the next chapter together.

TABLE OF CONTENTS

LIST OF TABLES

LIST OF FIGURES

LIST OF ABBREVIATIONS

ANOVA	Analysis of variance
ASCE	American Society of Civil Engineers
AISC	American Institute of Steel Construction
ASTM	American Society for Testing and Materials
BG	Blast generator; blast simulator
DAQ	Data acquisition system
DIF	Dynamic increase factor
ELFORM	Element formulation
EXP	Explosive
FAIL	Maximum effective plastic strain at failure
FE	Finite element
Gr	Grade
HSV	High speed video
LOP	Level of protection
LVDT	Linear variable displacement transducer
MAT	Material
MDOF	Multi-degree of freedom
MSE	Mean squared error
MXEPS	Maximum effective plastic strain at failure
NI	National Instruments
PCC	Phantom Camera Control application

RCRBSJ	Research Council on Riveted and Bolted Structural Joints
RCSC	Research Council on Structural Connections
SDOF	Single degree of freedom
SHPB	Split Hopkinson Pressure Bar
SIF	Static increase factor
START	National Consortium for the Study of Terrorism and Responses to Terrorism
TNT	Trinitrotoluene
UNC	Unified National Course thread series

LIST OF SYMBOLS

A_b	Nominal bolt cross-sectional area
$a_{part}(t)$	Acceleration time history of LS-DYNA model part
A_s	Reduced area of threaded portion of a structural bolt
A_w	Area of web, W-section
b	Waveform parameter
C	Width across points
d	Distance between center line of shear plates
D	Cowper-Symonds model parameter
d_b	Nominal bolt diameter
d_H	Diameter of bolt hole
D_m	Mesh density
d_p	Mean pitch diameter
d_r	Root (minor) thread diameter
$d_{rebound}$	Rebound displacement
d_{slip}	Slip displacement
E	Modulus of Elasticity
E_k	Kinetic energy
F	Width across flats
$F(t)$	Force-time history
$F_I(t)$	Force-time history, impact load cells
F_p	Bolt pretension or preload

$F_R(t)$	Force-time history, reaction load cells
f_t	Tensile stress
f_{ut}	Ultimate tensile stress
f_v	Shear stress
f_y	Tensile yield stress
$f_{y,dyn}$	Dynamic yield stress
G	Modulus of rigidity
H_H	Bolt head height
H_N	Nut length
I	Area moment of inertia
i_r	Positive reflected impulse
i_s	Specific impulse
K	Torque friction coefficient
k	Stiffness
K_L	Equivalent load factor
K_{LM}	Equivalent mass-load factor
K_M	Equivalent mass factor
k_s	Slip coefficient of faying surfaces
K_S	Equivalent stiffness factor
L	Length
l	Fixed height in determination of shear strain
L_b	Nominal bolt length, excluding head
L_c	Bolt Shank length

L_g	Grip length
L_t	Thread length
m	Mass
m_s	Number of slip planes in a joint
n	Number of threads per inch
n_b	Number of bolts in a joint
n_{LC}	Number of load cells
Ø	Diameter
p	Thread pitch, distance between threads, $1/n$
P	Applied load
P_{exp}	Experimental slip load
P_o	Ambient air pressure
P_{peak}	Peak impulsive load
P_r	Peak reflected pressure
$P_s(t)$	Pressure time history of blast load
P_{sim}	Simulated slip load
P_{slip}	Force required to connection to slip; slip load
P_{so}	Peak positive overpressure
q	Cowper-Symonds parameter
Q_{EXP}	Mass specific energy of an explosive substance
Q_{TNT}	Mass specific energy of TNT
R	Perpendicular distance to point of interest
$R(x)$	Non-linear resistance function

R^2	Coefficient of determination
r_n	Effective radius of contact between the nut and joint surface
r_t	Effective contact radius of threads
R_u	Maximum moment resistance
S	Impulse
$S_{f,I}$	Impulsive friction loss, impact side of system
$S_{f,R}$	Impulsive friction loss, reaction side of system
T	Bolt tightening torque
t	Time
t_A	Arrival time of blast pressure
T_{bolt}	Tensile force in bolt
T_{break}	Break torque
t_D	Duration of load
t_{plate}	Thickness of shear plate
t_{so}	Positive phase duration
v	Velocity
V	Shear force
$V(t)$	Shear resistance function
V_{bolt}	Shear force in bolt
VC	Viscous coefficient, $\sigma_y/\sqrt{3}$
V_n	Shear resistance
v_{rel}	Relative velocity
V_u	Maximum shear resistance; ultimate shear force

W_{EXP}	Explosive weight
W_f	Work due to friction
W_{TNT}	Equivalent explosive weight in TNT
x	Displacement or distance
Z	Scaled distance
γ	Shear strain
$\dot{\gamma}$	Shear strain rate
γ_p	Residual plastic shear strain
δ	Shear deformation
Δx	Change in displacement
ε	Normal strain
$\dot{\varepsilon}$	Normal strain rate
ε_f	Engineering normal fracture strain
ε_p	Engineering residual plastic normal strain
ε_T	True normal strain
ε_u	Engineering normal strain at ultimate
θ	Shear plate rotation angle
λ	Decay coefficient
μ_c	Coefficient of friction at a given relative velocity, v_{rel}
μ_d	Coefficient of dynamic friction
μ_n	Coefficient of friction between face of nut and upper surface of joint
μ_s	Coefficient of static friction
μ_t	Coefficient of friction between nut and bolt threads

ν	Poisson’s ratio, 0.30 for steel
σ_T	True normal stress
$\sigma_{T,u}$	Ultimate normal true stress
τ	Shear stress

SUMMARY

Explosive threats continue to be a primary tactic of terrorist organizations in today's international security environment, often impacting civil structures and infrastructure. When structures are subjected to blast events, the potential for progressive collapse of the structure due to the loss of load bearing members is a significant concern. A more thorough understanding of the behavior of bolted steel connections during and after extreme loading events is necessary to be able to predict and prevent progressive collapse of the structures. Connections ensure ductility and transfer loads to surviving structural elements after an extreme loading event. Relatively little experimental research has been done on the behavior of structural bolts under impulsive shear and no research has evaluated the residual shear capacity of bolts or bolted connections after an extreme loading event. The research presented in this thesis aims to fill that gap with the development of an experimental method and a proof of concept experimental test program.

An experimental residual capacity test system was developed to subject bolts and bolted connections to an impulsive shear event and then test the residual static capacity of the bolt in-situ after the event. In the test system, impulsive loads were generated through the use of a high speed hydraulic actuator to accelerate a flyer mass to a desired impact velocity. A modular system was designed to be installed within the impulsive setup to apply a quasi-static load after the impulsive event. While a single structural bolt served as the primary specimen for this research, the system can be adapted to accommodate any number of bolted connection configurations. The system can also be easily adapted to

investigate different types of bolts, pins, rods, dowels or connected plate materials and surface treatments.

The residual capacity experimental test system was used to investigate three fundamental aspects of bolted steel connections under impulsive loads: 1) the response and behavior of structural bolts during an impulsive event; 2) the residual capacity of structural bolts after an impulsive event; and 3) the response and behavior of clamping force and friction during and after an impulsive event in slip-critical connections.

The response and behavior of structural bolts during an impulsive event was investigated by subjecting ASTM A307 and ASTM A325 structural bolts to varying impulsive loads. Impulsive loads were generated in the intermediate strain rate range, typical of the structural response strain rate from a blast load. Key findings of this investigation included an observed increase in the rigidity of structural bolts within the tested strain rate range, recommended static and dynamic increase factors for structural bolts for design and simplified analysis, a linear relationship between impact energy and residual permanent shear strain in the bolt, and decreased ductility as compared to static ductility at higher rates.

Investigation of the residual capacity of structural bolts after an impulsive load was conducted by quasi-statically testing impulsively damaged ASTM A307 and ASTM A325 structural bolts. Key findings of this investigation included the observation that below a certain impact energy threshold, the residual capacity of a structural bolt is equivalent to the virgin capacity of the bolt. The residual ductility of the damaged bolt was found to decrease with increased impact energy. However, the total ductility, considering both the residual permanent shear deformation from the impulsive event and the residual

deformation, was generally equivalent to the ductility of a virgin bolt. Finally, a model to predict the residual strain and resulting residual capacity for a bolt subjected to an impulsive shear load was developed. The model accounts for the four apparent behavior zones based on the impact energy applied to the bolt.

The response, behavior, and residual capacity of slip-critical connections subjected to an impulsive load was investigated by using the residual capacity experimental test system to test single bolt, slip-critical connections fabricated using current design standards. Key findings of this investigation included a lower peak friction resistance under impulsive loads than static loads and work due to fiction increases linearly with increased impact energy. As a result, only 20 to 30% of the initial impact energy is transferred to the structural bolt in bearing. Because the friction resistance increases with the number of structural bolts in the connection, friction resistance has the potential to significantly protect structural bolts from damage in a structural bolt and should not be neglected.

Finally, a numerical study was conducted to investigate how well high fidelity physics based models capture the behavior observed in the impulsive, residual capacity, and slip-critical experimental tests. The investigation employed common modeling methodologies inherent to the finite element solver, LS-DYNA. Representative simulations of the experimental test series were conducted and results compared to the experimental data. In general, the models predict the overall impulsive and residual capacity behavior observed in experimental tests. However, due to lack of data and methods to evaluate important material parameters, the models significantly over predict the ductility in the connections. Similarly, in slip-critical simulations the models fail to

accurately predict relaxation of preload in the bolt and subsequently over predict the friction resistance observed in slip-critical connections.

CHAPTER 1

INTRODUCTION

1.1 Problem Statement

Domestic and international terror attacks continue to be a primary means for both state and non-state actors to achieve their desired political and economic ends [2-4]. According to the National Consortium for the Study of Terrorism and Responses to Terrorism (START), of the 170,000 terrorist attacks in the world since 1970, 52% of these attacks used an explosive device and the number of attacks involving explosives has grown exponentially over that same period [7]. Though the majority of these attacks are concentrated in just ten countries, the potential for attacks outside these areas presents both a real and present threat to the United States [7].

Aside from the senseless and catastrophic loss of life, the use of explosive devices in terrorist attacks pose a significant risk to critical infrastructure and the built environment. Even a modestly planned, coordinated and executed explosive terror attack has the potential to inflict significant structural damage. For example, the bombing of the Manchester Arena in Manchester, U.K. in May 2017 and subsequent closing of the adjacent Victoria Rail Station due to structural damage highlights the ever present nature of the threat and the cost in terms of human life and the built environment [5].

Events like the Manchester Arena bombing require that engineers consider the potential effects of extreme loadings on structures, especially given the higher frequency of attacks in recent years. In truth, engineers and researchers have been investigating the effects of explosives on structures since the Second World War due to the widespread destruction caused by extensive bombing campaigns [11]. In the 1950s and 1960s the U.S. Department of Defense conducted several tests involving explosives to develop a tri-service regulatory design manual, "Structures to Resist the Effects of Accidental Explosions" [13], presumably to assist in the construction of ammunition storage depots. However, the design manual – now Unified Facilities Criteria (UFC) 3-340-02 – remains the standard design guide for blast loadings today, though it has been updated extensively since the initial release.

The first bombing of the World Trade Center in New York in 1992 and the bombing of the Alfred P. Murrah Federal Building in Oklahoma City in 1995 sparked a renewed interest for structural engineers to investigate the effects of blast loads on structures. Researchers investigated methods to enhance the protection and resistance of structures to blast loadings, be they accidental or intentional [1]. The events of September 11, 2001 further underscored the issue of progressive collapse after an extreme loading event. Progressive collapse occurs with the loss of one or more load carrying elements due to an extreme event. As the loads are redistributed to non- or less-damaged elements, the capacity of those elements is exceeded and the structure subsequently collapses in a nonlinear dynamic process [8]. The progressive collapse of the World Trade Center towers in New York demonstrated the lack of redundancy and energy absorption capability of the steel frame.

Because of the complex, non-linear dynamic nature of progressive collapse, more research is needed to better predict behavior after an extreme loading such as a blast event. Efforts to prevent progressive collapse after a blast loading or an extreme event should focus on achieving three objectives: 1) achieve structural stability for a period of time sufficient to evacuate all occupants and surrounding areas; 2) protect first responders and emergency personnel who need to enter the structure; and 3) minimize damage to adjacent structures and property [6]. To achieve these objectives, the behavior of the entire structural system must be well understood.

In their critical review of the literature, design codes, and procedures regarding progressive collapse, Ellingwood and Dusenberry point to connection behavior as a critical link for a more thorough understanding of progressive collapse phenomena:

> "Connection behavior during and after extreme events must be thoroughly understood, as this understanding is essential to providing for alternate load path development and for achieving continuity and ductility" [6].

Bolted structural steel connections are one of the most common connection types in structural steel buildings due to their low cost and efficient installation [10]. However, as will be seen in the following chapters, the behavior of bolts and bolted connections under impulsive loads is not well understood. Current simplified prediction tools idealize connections in analysis [12]. Current high fidelity physics based (HFPB) models fail to accurately capture localized behavior in connections due to lack of validation data [9]. Even less understood than the behavior of bolts and bolted steel connections under dynamic loads is their residual capacity after an extreme loading event.

Therefore, the proposed research seeks to investigate the behavior of structural bolts and bolted connections subjected to impulsive loads in a simple connection as a

critical first step in understanding connection behavior both during and after extreme loading events. While this research focuses on full-scale structural connections, bolts and bolted connections are ubiquitous; therefore, the research has applications beyond civil structures. Bolted connections are used in a wide range of structures and components because they are generally cost efficient and not permanent, facilitating disassembly and reassembly for repairs and other requirements. As a result, bolted connections are used in many applications where they are subjected to shock loadings, especially in military materiel. Ground combat vehicles, ships, and airframes all rely on bolted connections either as a fundamental part of the structural system or to secure sensitive equipment. The results of this research can be used to improve these and other systems. Non-military applications of this research include biomedical structures, machine parts and tools, and the automotive industry.

1.2 Thesis Outline

Chapter 2 discusses the relevant background information on structural steel bolts and steel bolted connections. This chapter focuses on the fundamentals of steel bolted connections and the properties of individual structural bolts under static and dynamic loading conditions. An overview of blast loadings and experimental methods to simulate blast loadings in the laboratory is also discussed.

Chapter 3 provides the objectives and scope of the proposed research. The project's research questions and hypotheses are presented.

Chapter 4 presents the concept and design for a new experimental method developed to investigate dynamic shear in bolts and connections. The results from preliminary tests and subsequent improvements made to the experimental method for further testing are also presented.

Chapter 5 presents the methodology and findings of an experimental program conducted to investigate the behavior of ASTM A307 and A325 structural bolts during an impulsive event. The results from baseline quasi-static tests, average strain rate, modulus of rigidity under impulsive loadings, as well as proposed static and dynamic increase factors for structural bolts are presented.

Chapter 6 presents the methodology and findings of an experimental program conducted to investigate the residual capacity of ASTM A307 and A325 structural bolts following an impulsive loading event. The residual strength and residual ductility of structural bolts are presented. Additionally, overall response of the combined impulsive and quasi-static events are compared to the virgin response of the bolt under quasi-static loads.

Chapter 7 presents the methodology and findings of an experimental program conducted to investigate the slip resistance of a bolted slip-critical connection as well as the residual slip resistance after an impulsive event. The energy dissipation through friction during an impulsive event and the net impact on the bolt is presented.

Chapter 8 presents the findings of a numerical investigation into the accuracy and validity of common modeling methods to predict both the behavior of a structural bolt during an impulsive event and the residual capacity of the bolt. A description of the model

developed, the material models of the structural bolt, and the results of the simulation compared to experimental data are presented.

Finally, Chapter 9 discusses the key conclusions of the research as well as the contributions and significance of the research. Recommendations for future work based on the results of the project are also presented.

1.3 References

[1] D. O. Dusenberry, Ed. *Handbook for Blast Resistant Design of Buildings*. Hoboken, NJ: John Wiley & Sons, 2010.

[2] U.S. Department of Defense. (2014). *Quadrennial Defense Review*. Available: http://archive.defense.gov/pubs/2014_Quadrennial_Defense_Review.pdf

[3] U.S. Department of Homeland Security. (2014). *Quadrennial Homeland Security Review*. Available: https://www.dhs.gov/sites/default/files/publications/2014-qhsr-final-508.pdf

[4] Joint Chiefs of Staff. (2015). *National Military Strategy of the United States of America*. Available: http://www.jcs.mil/Portals/36/Documents/Publications/National_Military_Strategy_2015.pdf

[5] Bardsley, A., "Victoria Station to remain closed after it was structurally damaged in Manchester Arena terror attack," *Manchester Evening News*, May 26, 2017. Accessed on: July 17, 2017, Available: http://www.manchestereveningnews.co.uk/news/greater-manchester-news/victoria-station-closed-manchester-arena-13099152

[6] Ellingwood, B. R. and D. O. Dusenberry, "Building design for abnormal loads and progressive collapse," *Computer-Aided Civil and Infrastructure Engineering*, vol. 20, no. 3, pp. 194-205, 2005.

[7] Miller, E. and M. Distler. (2017). *Background Report: Mass Casualty Explosives Attacks in Iraq and Afghanistan*. Available: https://www.start.umd.edu/pubs/START_MassCasualtyExplosivesAttacksIraqAfghanistan_BackgroundReport_June2017.pdf

[8] Mohamed, O. A., "Progressive collapse of structures: annotated bibliography and comparison of codes and standards," *Journal of Performance of Constructed Facilities*, vol. 20, no. 4, pp. 418-425, 2006.

[9] Morrill, K. B., J. E. Crawford, J. M. Magallanes, and H. J. Choi, "Development of simplified tools to predict blast response of steel beam-column connections," in *Structural Engineering Research Frontiers*, 2007, pp. 1-10.

[10] Salmon, C. G., J. E. Johnson, and F. A. Malhas, *Steel Structures: Design and Behavior*, 5th ed. Upper Saddle River, NJ: Pearson Prentice Hall, 2009.

[11] Smith, P., M. Byfield, and D. Goode, "Building robustness research during World War II," *Journal of Performance of Constructed Facilities*, vol. 24, no. 6, pp. 529-535, 2010.

[12] Stewart, L. K., "Course Notes, CEE 8813: Multi-hazard Analysis and Design," 2015.

[13] Zehrt, J., William H and P. F. Acosta, "Revision of Army Technical Manual 5-1300/NAVFAC P-397/AFR 88-22,"Structures to Resist the Effects of Accidental Explosions"," in *Structures Congress 2005: Metropolis and Beyond*, 2005, pp. 1-12.

CHAPTER 2

BACKGROUND

Threaded fasteners – screws, bolts, and nuts – have been in use for over 500 years [12] and continue to be a versatile and inexpensive method for connecting two or more components, especially when disassembly and reassembly is required. The use of bolts in civil structures began in the 1950s as a more economical alternative to riveted joints [44]. Despite their widespread use, there are still significant gaps in knowledge regarding the behavior and performance of bolted structural connections in service, particularly under dynamic and impact loadings.

The following sections discuss the fundamentals of bolted steel structural connections under static load, discuss the fundamentals of blast loads on steel structures and methods for experimentally investigating blast loadings, review the relevant studies on the dynamic properties of structural bolts and structural steel connections, and review relevant studies on the residual capacity of structures after extreme loading events.

2.1 Fundamentals of Bolted Connections

2.1.1 Types of Bolted Connections

Bolted connections (used interchangeably with bolted joints) are used to join two or more structural members together, allowing the external loads to smoothly transfer from one joint member to the other joint member(s). Bolted connections are classified by the orientation of the bolt's longitudinal axis to the direction of the external load. Tension

connections carry external load parallel to the longitudinal axis of the bolt whereas shear connections carry load transverse to the longitudinal axis of the bolt [12]. Bolted connections may also consist of combined tension and shear. Figure 2.1(a) illustrates the two types of bolted joints and Figure 2.1(b) illustrates an example of a bolted joint with combined tension and shear. In Figure 2.1(a), the bolts that connect the structural plate to the structural angles create a shear joint. The bolts that connect the structural angles to the steel wide flange section (W-section) create a tension joint. In Figure 2.1(b), the eccentricity of the load causes the bolts to resist tensile forces (parallel to the bolt longitudinal axis) as well as shear forces (transverse to the bolt longitudinal axis).

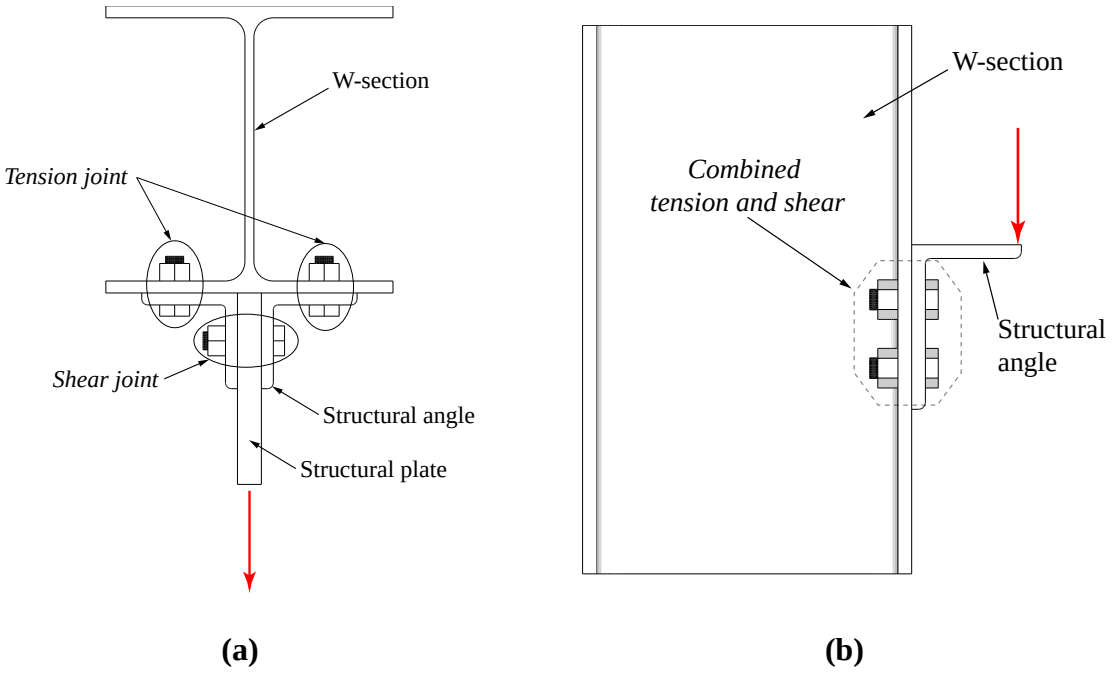

Figure 2.1: Types of bolted connections: **(a)** bolted connection illustrating a tension joint and a shear joint; **(b)** bolted connection illustrating a combined tension and shear joint.

Additionally, there are two types of shear connections as illustrated in Figure 2.2. A lap joint (Figure 2.2a) consists of one joint member overlaid on top of another joint

member. In this configuration, there is only one shear plane (denoted by a red line through the bolt shaft) and so the bolts are in single shear. Use of lap joints are generally discouraged due to the unbalanced nature of the load, which can develop tensile stresses in the bolt as well as shear stresses [9]. In a butt joint (Figure 2.2b), however, the joint members are connected by means of two additional plates. The lines of action of the external loads are the same, creating pure axial loading. In this configuration, there are two shear planes per bolt and so the bolts are in double shear. In double shear, only half of the shear capacity of the bolts is required if the same external load, *P*, is applied to both joints, which has been validated experimentally [9].

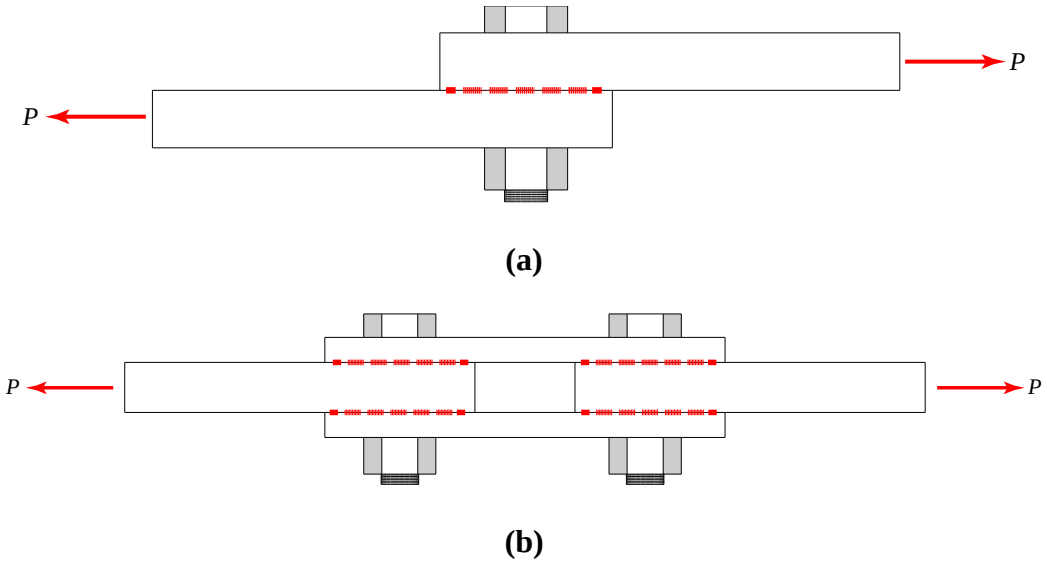

Figure 2.2: Types of shear connections: **(a)** lap joint with a single shear plane; **(b)** butt joint with two shear planes per bolt.

Bolted connections can transfer force between two connected members through either the dowel action of a bolt or pin or through friction in the connection. The American Institute of Steel Construction (AISC) specifies two performance categories for high-

strength bolted connections: 1) bearing-type connections; and 2) slip-critical connections, historically referred to as friction-type connections [44, 65]. These performance categories will be discussed in detail in the following sections.

2.1.1.1 Bearing-type Connections

Bearing-type connections are among the simplest means of transferring external force from one joint member to another. Bearing-type connections rely only on the bolt, pin or dowel shank to transfer an applied force from one joint member to the other. Bolts in a bearing-type connection are typically tightened only enough to keep the joint members in full contact [44]. Therefore, in a bearing-type connection, the effects of friction between the plates are negligible.

Figure 2.3 shows a bearing-type connection of a lap joint and the associated free body diagrams of each component. The free body diagram of the bolt shank demonstrates that the applied load, *P*, is transferred from Plate A to Plate B through shear in the bolt. Because applied load, *P*, creates an unbalanced moment and the bolt holes are slightly larger than the nominal diameter of the bolt, some minor rotation of the bolt will occur, creating both tension and shear in the bolt shank. However, the induced tension in the bolt is generally negligible compared to the shear [11].

2.1.1.2 Slip-critical Connections

Slip-critical connections do not rely on bearing between the plate and the bolt to transfer the load between joint members. Instead, pretensioning of the bolt creates a clamping force between the connected members and the joint relies on friction to transfer the load between joint members. Slip-critical connections are often used to prevent fatigue failure of the bolt in cases where the direction of the load frequently changes. It is

important to note that slip-critical connections are a serviceability requirement and the capacity of the joint is ultimately determined by the bearing capacity of the bolt and joint members [3, 65].

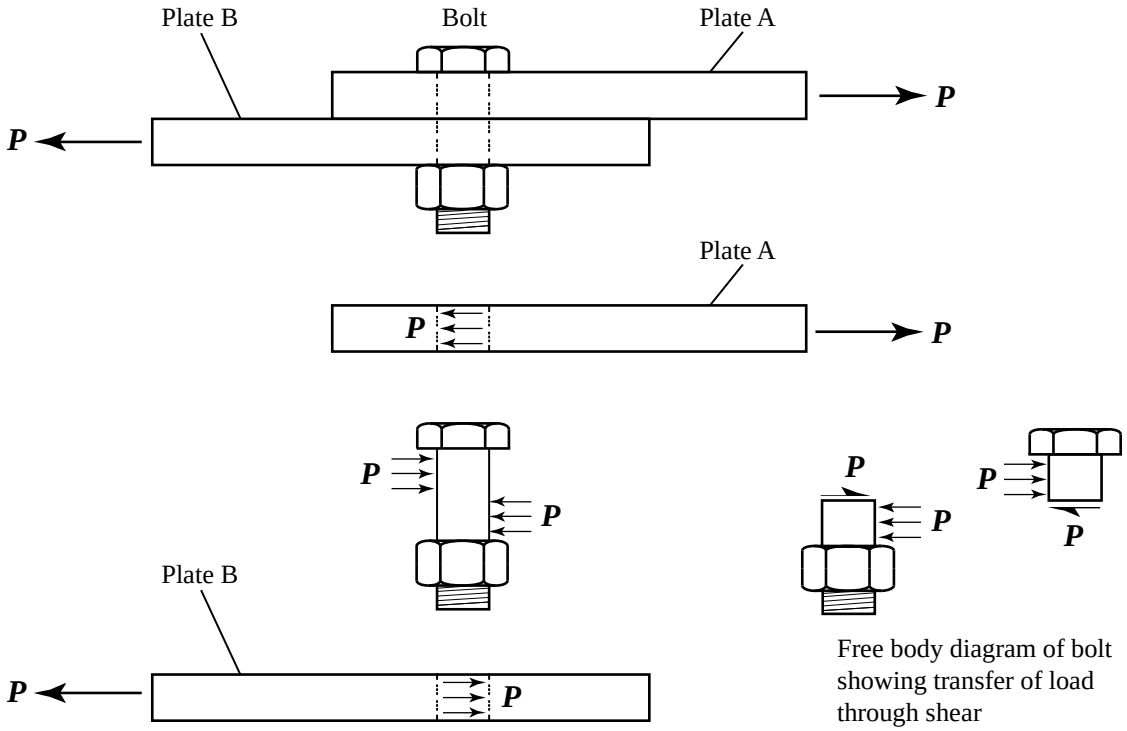

Figure 2.3: Analysis of a bearing-type lap joint demonstrating load transfer through shear in the bolt shank (adapted from [65]).

Figure 2.4 illustrates the general load-deformation behavior of a slip-critical joint. As an increasing external load is applied, the load is transferred between the joint members by friction. When the applied load is larger than the frictional resistance, major slip occurs in the joint and the joint members and bolt become in contact. After slipping, the connection essentially behaves as a bearing connection until the failure of the joint.

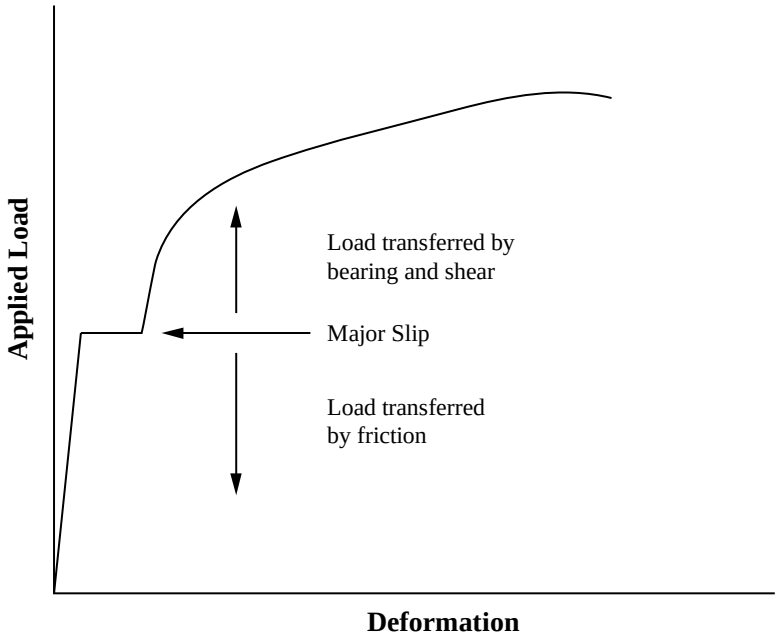

Figure 2.4: Behavior of a slip-critical connection.

Figure 2.5 shows a slip-critical connection and the associated free body diagrams of the components. The pretension in the bolt compresses the joint members together. The resulting frictional forces (μT) provide the resistance necessary to prevent Plates A and B from sliding past one another and the plates from bearing on the bolt. The force required for the connection to slip, P_{slip}, is directly proportional to the sum of the pretension, F_p, in each of n_{bolt} bolts in the connection, the slip coefficient of the faying surfaces, k_s, and the number of slip planes in the joint, m:

$$P_{slip} = k_s m_s \sum_{i=1}^{n_b} F_{p_i} \tag{2.1}$$

The slip coefficient can only be determined experimentally and researchers have conducted extensive tests to determine the slip coefficient for different steels, surface treatments, and conditions [10, 23, 25, 26, 44], concluding that the slip coefficient for

structural steel (A36) with clean mill scale surfaces is 0.33 on average. Values can be as low as 0.06 for painted surfaces and as high as 0.54 for grit blasted surfaces [44, 52].

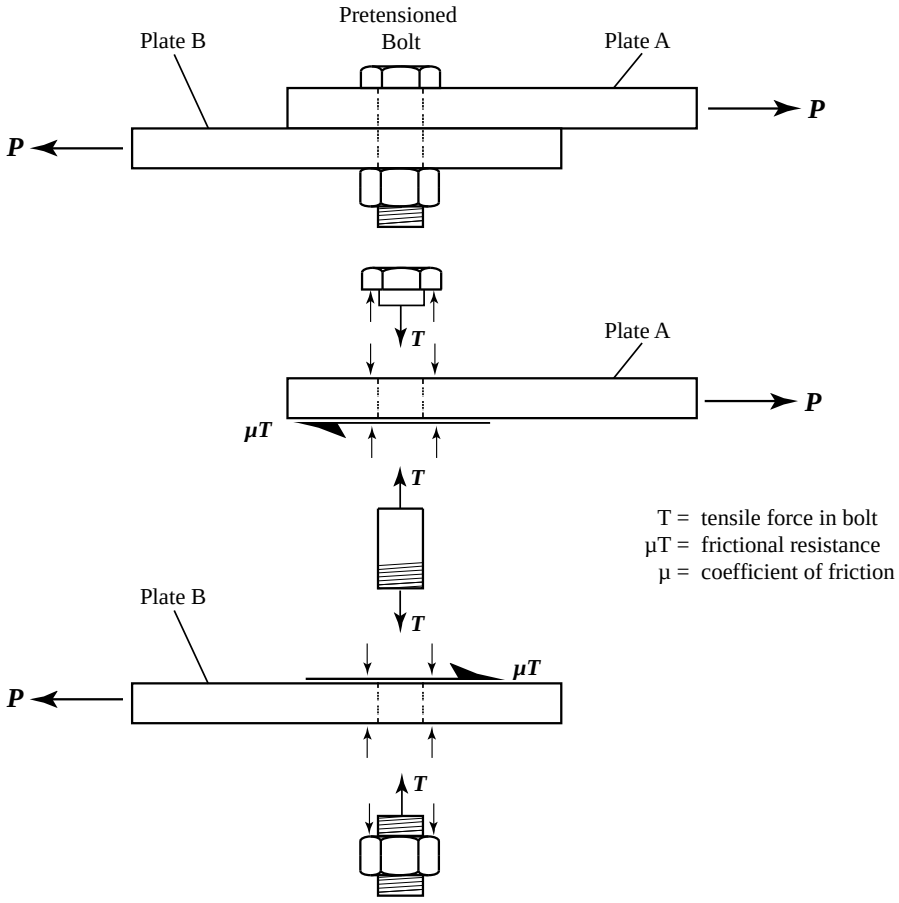

Figure 2.5: Analysis of a slip-critical lap joint demonstrating load transfer through friction induced by a pre-tensioned bolt (adapted from [65]).

Pretension in the bolt is the other critical factor in determining the slip load, P_{slip}. Lower pretension in the bolt corresponds to a lower clamping force and therefore a reduced slip load. Ideally, bolts are pretensioned to the maximum possible load without causing permanent deformation in the bolt to generate the maximum clamping force in the connection [65]. In practice, pretensioning high-strength bolts to a specified load level is

highly variable [44]. Methods for installing pretensioned bolts will be discussed further in Section 2.2.2.2, Installation of Structural Bolts.

2.1.2 Bolted Steel Connection Failure Modes

There are seven primary failure modes for bolted connections. Failure may occur either in the bolt or in the connected members depending on the relative material properties of the bolt and connected members. Figures 2.6(a) – (g) illustrate the various failure modes of bolted connections. For each of these failure modes, the connection is a bearing-type connection as any frictional resistance in the connection has been overcome by the external loads [44].

In the bolt, failure may occur by shear, bearing, tension, or bending failure of the bolt. In all cases, the applied load exceeds the material capacity of the bolt. Shear failure (a) occurs along the shear plane of the connection when the bearing capacity of the connected members exceeds the shear capacity of the bolt. Bearing failure (b) is characterized by localized yielding of the bolt shank and occurs when the bearing capacity of the connected members is greater than the bearing capacity of the bolt. Tensile failure (c) occurs when the applied load in tension exceeds the direct tension capacity of the bolt. Finally, bending failure (d) may occur in longer bolts when the applied load and bearing capacity of the connected members exceed the tensile capacity of the bolt.

Similarly, in the connected members, failure may occur by shear, bearing, or tensile failure. Shear failure (e) of the connected members is characterized by tear-out behind the bolt hole and occurs when the bearing and shear capacity of the bolt exceeds the shear capacity of the plate. Bearing failure (f) of the plate is characterized by excessive elongation of the

bolt hole and occurs when the bearing capacity of the bolt is greater than the bearing and shear capacity of the bolt. Finally, tensile failure (g) in the plate is characterized by splitting of the connected member along the bolt hole and occurs when the tensile capacity of the connected member is lower than the bearing and shear capacity of the bolt.

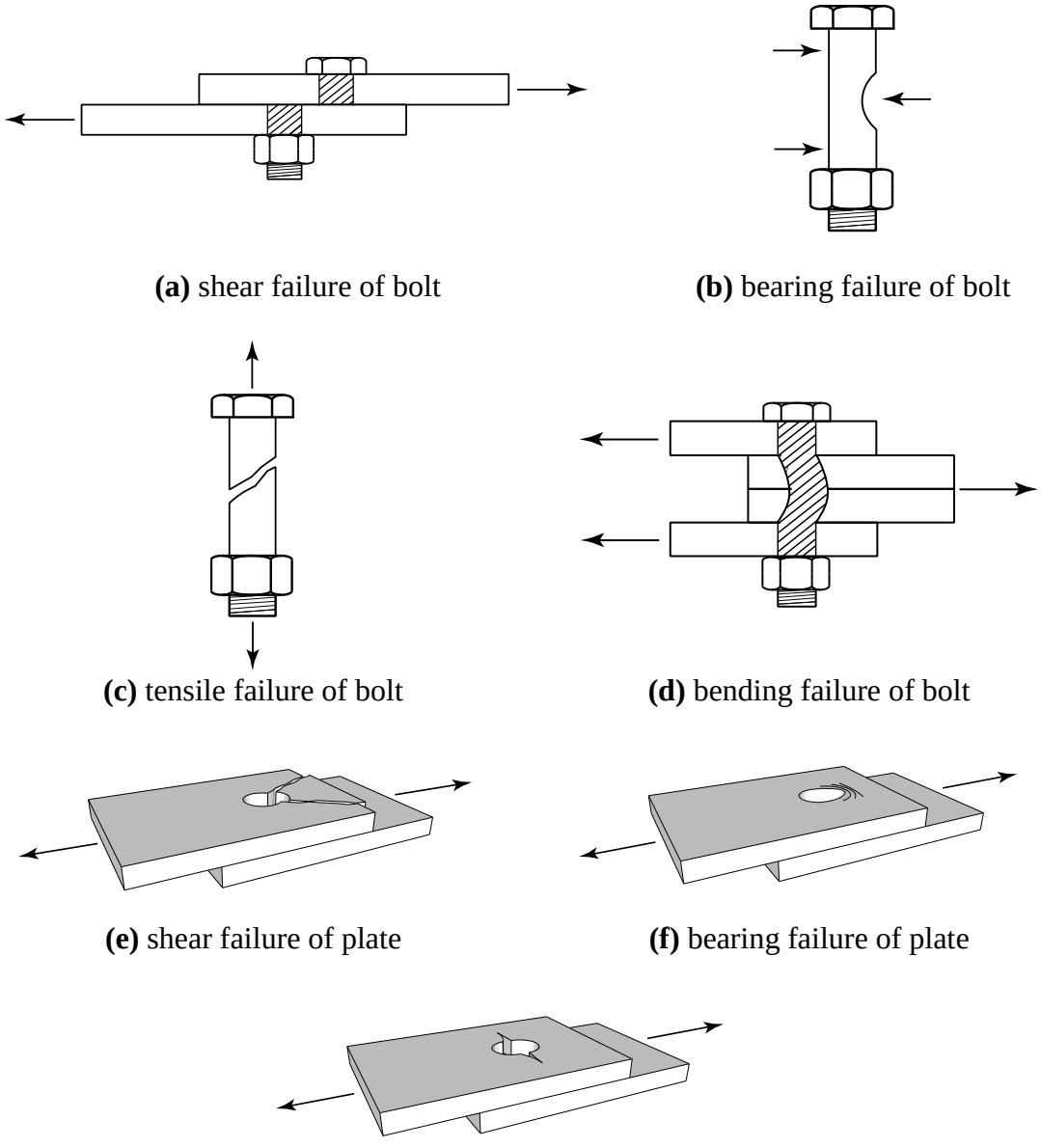

(a) shear failure of bolt

(b) bearing failure of bolt

(c) tensile failure of bolt

(d) bending failure of bolt

(e) shear failure of plate

(f) bearing failure of plate

(g) tensile failure of plate

Figure 2.6: Failure modes of bolted connections (adapted from [65]).

2.2 Structural Bolts

Researchers have been investigating the properties of bolts and threaded fasteners since the late 19th century [42]. Much of the work centered on the use of bolts in machines as rivets were the primary method of joining members in early iron- and steel-framed buildings [41, 80]. In 1934, experiments by Batho and Bateman [8] suggested that bolts could be used in place of rivets for structural steel connections. Further testing [81] demonstrated the efficacy of using bolts in connections and led to the formation of the Research Council on Riveted and Bolted Structural Joints (RCRBSJ) in 1947. During the 1950s and 1960s, the RCRBSJ directed several studies on structural bolts to better understand their properties and behavior. The overarching outcome from this research thrust was that structural bolts could safely and more efficiently replace rivets in steel structures on a one-to-one basis [65].

This section reviews the types of structural bolts currently recognized by AISC and the Research Council on Structural Connections (RCSC; successor to the RCRBSJ), the geometry of structural bolts, the installation procedures for bolts, and finally discusses the tensile strength, shear strength and combined tension and shear strengths under static loadings of individual structural bolts.

2.2.1 Types of Structural Bolts

AISC and RCSC recognize three common types of structural bolts, shown in Table 2.1 [4, 5, 44]. ASTM A307-14 grade A carbon steel bolts (A307) are general purpose bolts used in light-duty, static, or temporary applications [44, 65]. A307 bolts are generally only

used in bearing-type connections due to their limited ability to generate clamping force [44, 61].

Introduced in 2015, ASTM F3125-15a combined ASTM A325-14 (A325) and ASTM A490-14a (A490) under a single standard for high-strength bolts with A325 and A490 re-designated as grades under the new standard [5]. A325 and A490 bolts are the most common structural bolts and are used in bolted connections designed for both bearing-type and slip-critical connections [65]. A490 bolts were specifically designed for connections of high-strength structural steel joint members [44].

Table 2.1: Common Types of Structural Bolts [4, 5].

ASTM Designation	Grade	Material Type	Bolt Diameter (in)	Minimum Tensile Strength (psi)
ASTM A307-14	A	Carbon steel	1/4 – 4	60,000
ASTM F3125-15a	A325	Quenched and tempered medium carbon steel	1/2 – 1 1/2	120,000
ASTM F3125-15a	A490	Quenched and tempered alloy steel	1/2 – 1 1/2	150,000

2.2.2 Properties of Individual Structural Bolts

2.2.2.1 Geometry of Structural Bolts

The geometry of a structural bolt is shown in Figure 2.7. A325 and A490 bolts are often referred to as heavy hex head due to their oversized head and nut. A307 bolts can be either regular hex head or heavy hex head.

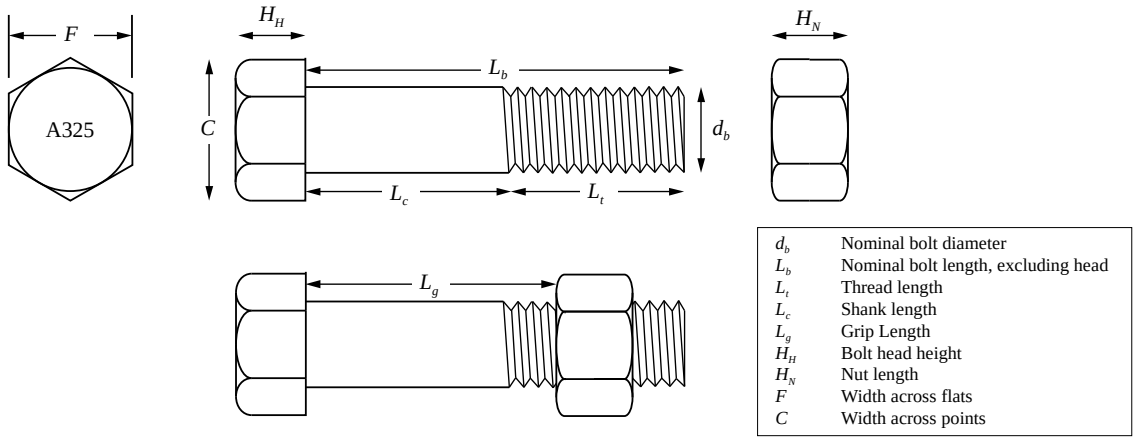

Figure 2.7: Structural bolt geometry.

High-strength bolts are marked with the specific type and grade on the bolt head while A307 bolts are simply marked with the manufacturer's symbol. High-strength A325 and A490 bolts have a shorter thread length, L_t, than A307 bolts to reduce the probability that the threaded portion is located in the shear plane of the connection [44].

The presence of threads in structural steel bolts has a significant influence on the tensile and shear strength of the bolts. Threads reduce the area available to resist load and so in strength tests, structural bolts always fail in the threaded portion of the bolt [44]. A307, A325, and A490 structural bolts all abide by the Unified National Course (UNC) thread series. Figure 2.8 shows the basic thread geometry for the UNC thread series.

In order to account for the reduction in capacity, the reduced area of the threaded portion, A_s, must be considered. The nominal (major) diameter of the bolt, d_b, is reduced by the mean pitch diameter, d_p, or the average of the major and minor diameter, d_r. Equation 2.2 shows the resulting tensile stress area of structural bolt:

$$A_s = \frac{\pi}{4}\left(d_b - \frac{d_b + d_r}{2}\right)^2 \tag{2.2}$$

Based on the geometry of the UNC thread standards discussed above, Equation 2.1 reduces to Equation 2.3, where n is the number of threads per inch ($1/p$).

$$A_s = 0.785\left(d_b - \frac{0.9743}{n}\right)^2 \tag{2.3}$$

Other methods to determine the stress area may also be used, including reducing the nominal diameter by the minor diameter, d_r, instead of the mean pitch diameter, d_p, but experimental studies on structural bolts have shown the mean pitch diameter and Equation 2.3 to be a sufficient approximation [12].

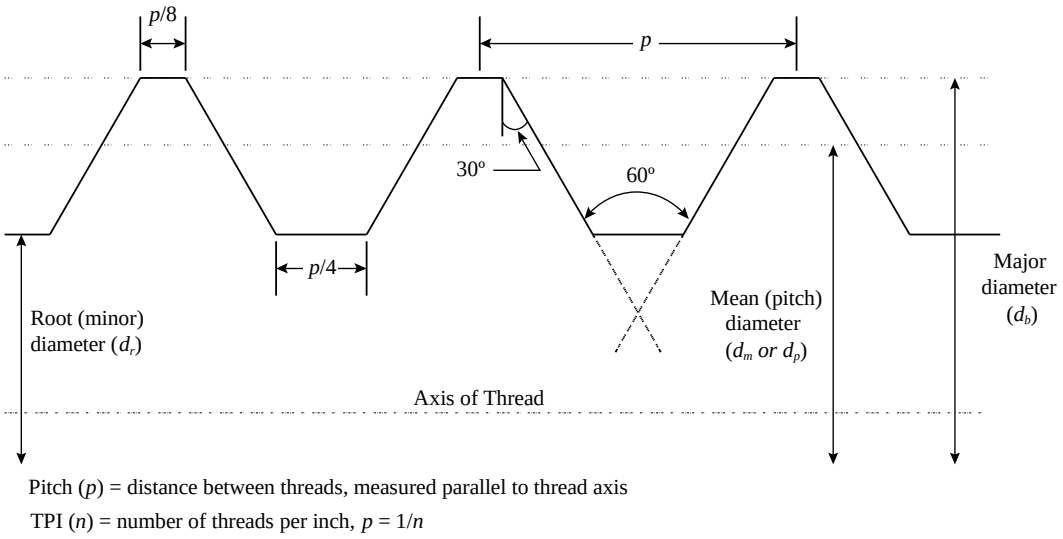

Figure 2.8: Unified National Course (UNC) thread series [55].

2.2.2.2 Installation of Structural Bolts

The installation of structural bolts in a bolted joint influences the behavior and strength of the connection. Whether threads are included or excluded from the shear plane, the diameter of the bolt hole in the connected members, and the pretension induced in the

bolt for slip-critical connections are all important factors in a bolted connection. If threads are included in the shear plane, the stress area must be reduced to account for the threads.

Table 2.2 shows the specification for standard, oversize, and maximum sizes of bolt holes for various structural bolt sizes. To ensure proper alignment of connected parts, bolt holes are often enlarged or slotted to ensure proper fit. Researchers have found that while oversize holes have no influence on the bearing strength of a bolted connection, oversized holes result in a loss of preload in bolts of approximately 15% compared to standard sized holes [6].

For slip-critical joints, the amount of pretension in the bolt is critical to developing the appropriate clamping force in the joint. Bolts are required to be tightened to 70% of their minimum tensile strength (AISC). AISC and RCSC approve of three methods to pretension high-strength structural bolts: 1) the Turn-of-the-Nut Method; 2) the Calibrated Wrench Method; and 3) Direct Tension Indicators.

Turn-of-the-nut and direct tension indicators are displacement control methods while the calibrated wrench is a torque control method. All methods start from the snug tight condition, which is defined as the result of "a few impacts of an impact wrench or the full effort of an ironworker using an ordinary spud wrench" [65]. While there is much variability in the snug tight condition, the appropriate level of preload can be induced so long as the bolt remains elastic [44].

Table 2.2: Bolt hole sizes for various structural bolts [44].

	Hole Diameter (in)			
Bolt Ø (in)	**Standard**	**Oversize**	**Short Slot (Width x Length)**	**Long Slot (Width x Length)**
1/2	9/16	5/8	9/16 x 11/16	9/16 x 1 1/4
5/8	11/16	13/16	11/16 x 7/8	11/16 x 1 9/16
3/4	13/16	15/16	13/16 x 1	13/16 x 1 7/8
7/8	15/16	1 1/16	15/16 x 1 1/8	15/16 x 2 3/16
1	1 1/16	1 1/4	1 1/16 x 1 5/16	1 1/16 x 2 1/2
≥ 1 1/8	d + 1/16	d + 5/16	(d + 1/16) x (d + 3/8)	(d + 1/16) x (2.5 x d)

In the turn-of-the-nut method, the nut or bolt head is turned a specified number of turns based on the diameter and length of the bolt – typically 1/3 turn to 1 full turn – to achieve the desired pretension. Several researchers have investigated the turn-of-the-nut relationship to bolt tension to develop current code requirements [44]. The calibrated wrench method uses a manual torque wrench that slips at the desired torque. The calibrated wrench method requires the use of a hardened washer under the turned element to reduce friction variability. Additionally, the wrench must be calibrated for each bolt lot using a calibrating device that measures the direct tension in the bolt. Theoretically, the torque, T, required for a given preload, F_P, may be estimated by the following equation,

$$T = F_P(Kd_b) \tag{2.4}$$

where K is the torque coefficient and d_b is the bolt nominal shank diameter [12]. The product of the torque coefficient and the bolt diameter is given by [12],

$$T = F_P \left(\frac{p}{2\pi} + \frac{\mu_t r_t}{\cos \beta} + \mu_n \, r_n \right) \tag{2.5}$$

where p = thread pitch
μ_t = coefficient of friction between nut and bolt threads
r_t = effective contact radius of threads
β = the half-angle of the threads
μ_n = coefficient of friction between the face of the nut and the upper surface of the joint
r_n = effective radius of contact between the nut and joint surface

As can be seen from Equation 2.5, the complexity in determining the numerous parameters to calculate the torque required to generate a specified pretension yields significant variability. The calibrated wrench method, even with daily calibration, is the least accurate of the three methods, with variability reported as much as 30% [65].

Direct tension indicators typically consist of hardened washers with protrusions that flatten as the appropriate preload level is met. Direct tension indicators must also be calibrated to ensure that the appropriate level of preload is achieved in the structural bolt. For ease of use and consistency of results in practice, the turn-of-the-nut method is the preferred method by the RCSC [44].

2.2.2.3 Tensile Strength

During the 1950s and 1960s, the tensile strength of structural bolts was studied extensively [17, 62, 67]. Tests were typically conducted on 3/4-in, 7/8-in, 1-in, and 1 1/4-in A325 and A490 bolts from various lots and manufacturers. Figure 2.9 shows a comparison of the load-deformation curves for different types of structural bolts in direct tension. In general, as the tensile strength of the bolt increases, the deformation capacity of the bolt decreases.

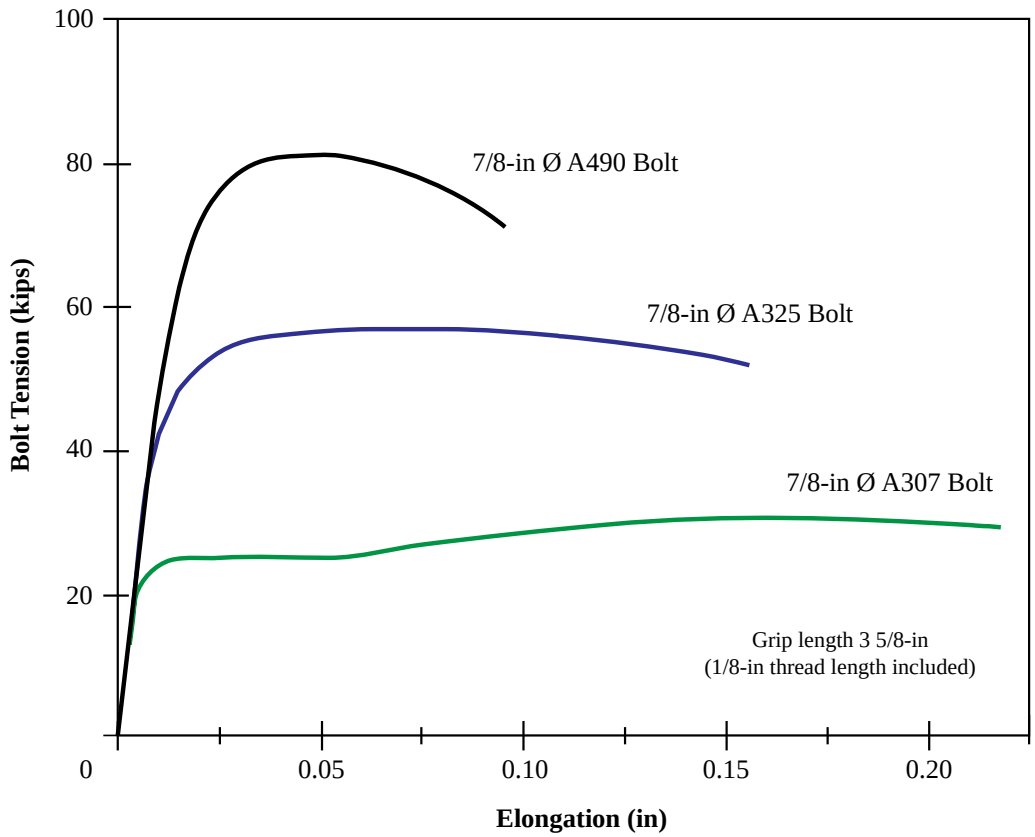

Figure 2.9: Comparison of bolt types in direct tension from [44].

High-strength bolts were tested in both direct tension as specified by ASTM and in torqued tension. In torqued tension tests, tension in the bolt was induced by means of turning the nut until failure. Researchers observed an increased deformation capacity in direct tension tests and noted an average decrease of 15% in the ultimate tensile strength of bolts in the torqued tension [17, 62, 67]. However, researchers found that loading structural bolts in direct tension after pretensioning the bolts to the proof load does not significantly reduce the ultimate tensile strength of the bolt [17, 62]. These studies also concluded that the tensile strength of structural bolts were 18% higher than the minimum required tensile strength [17, 62, 67] and that grip length had little effect on the tensile strength of the bolt [62].

In the early 1990s, researchers reexamined the earlier research on the tensile strength of high-strength bolts using improved experimental techniques, including a servo-controlled universal testing machine and a computerized data acquisition system [64]. They found that the ultimate tensile strength of the bolts was 16% higher than earlier findings, but found similar elongation in the bolts [64]. Contrary to earlier findings, they found an increase in ultimate strength and decrease in ductility as the number of threads in the grip length increased [64].

2.2.2.4 Shear Strength

During the same period that tensile tests were being conducted, extensive tests were conducted on the shear strength of high-strength bolts. Tests were conducted on the same bolt diameters and materials as the tensile tests. In general, bolts with a higher tensile strength exhibited higher shear strengths and decreased shear deformation capacity [79]. On average, researchers found the shear strength of a bolt to be 62% of the ultimate tensile strength [79]. Figure 2.10 shows the relationship between tensile strength and shear strength for A325 and A490 bolts. The data points are average values from various bolt lots. As a result of this data, the shear strength of a bolt is generally taken to be 62% of the tensile strength [3, 65].

Researchers found that the shear strength of a bolt was influenced by the type of test conducted. Bolts shear tested in a compression jig had a 6 to 13% higher shear strength than those tested in tension jigs [79]. Figure 2.11 shows typical tension and compression jigs used to determine the shear strength as well as their influence on the load-deformation curve, likely caused by the prying action of the plates in the tension jig, which induces a

small amount of axial tension as well as shear [68, 79]. All of the tests were conducted with the bolts in double shear.

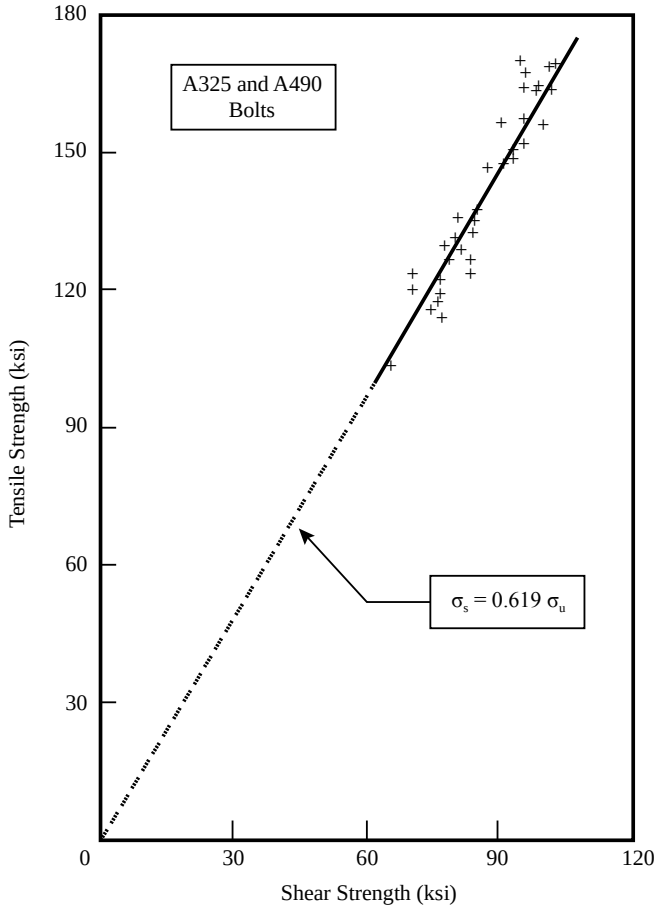

Figure 2.10: Shear strength versus tensile strength [44].

As expected, the location of the shear planes with respect to the bolt shank and the threads also significantly influences the shear strength of the bolt. Bolts where both shear planes were through threaded regions resulted in a significant decrease compared to bolts tested with the shear planes only through the bolt shank [79]. The reduced strength corresponds to the 30% reduction in stress area due to the threaded portion [44].

However, researches did not observe any appreciable change in shear capacity due to preloading of bolts [10, 23, 25]. Researchers found that any preload in the bolt is released due to shear deformations as the bolt approaches the ultimate load [10, 23].

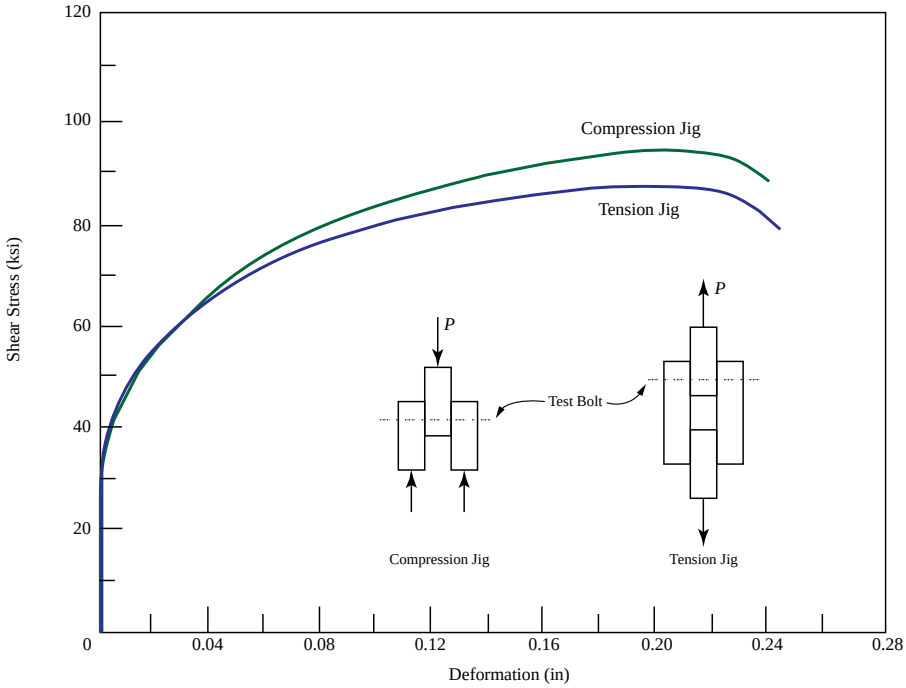

Figure 2.11: Influence of compression jig versus tension jig for shear stress [44].

2.2.2.5 Combined Tension and Shear Strength

In addition to direct tension and shear tests, researchers have investigated strength and behavior characteristics of bolts loaded under combined tension and shear [16]. In testing, researchers varied several factors including the bolt grip length, bolt diameter, type of bolt (A325 and A354 BD), and the type of material gripped by the bolt. From these tests, researchers concluded that the bolt diameter, type of bolt, and type of material gripped by the bolt had little influence on the ultimate strength of the bolt [16]. The only factor that

influenced the strength of the bolt was the grip length. Increased grip length allows for more bending in the bolt thereby slightly increasing the strength of the bolt when compared to shorter grip lengths [44]. Additionally, researchers found that in combined tension and shear, tensile stresses up to 30% of the ultimate tensile load have little influence in the ultimate shear strength of the bolt [16].

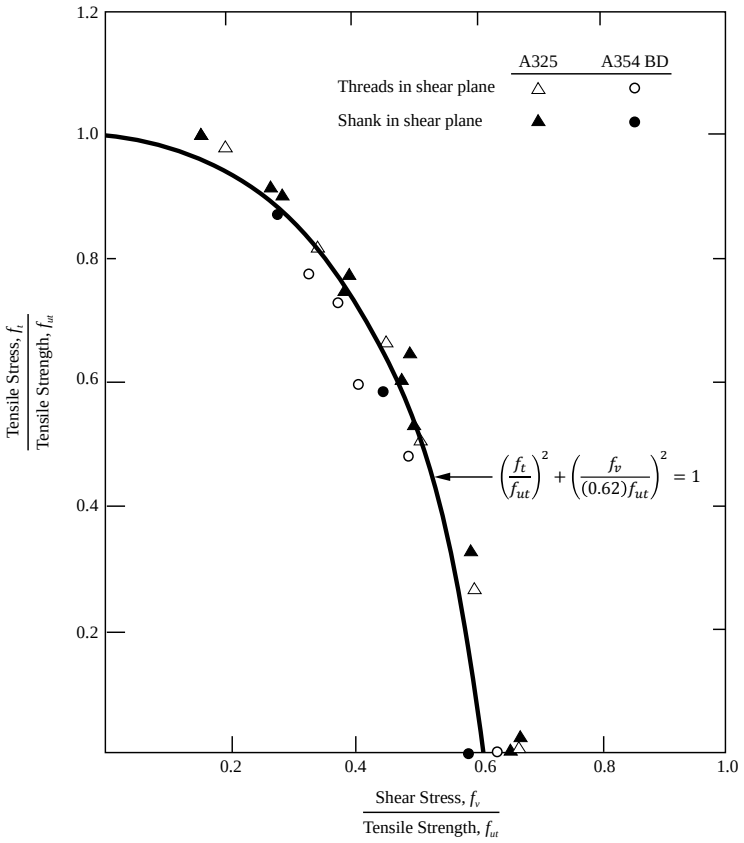

Figure 2.12: Interaction curve for bolts, combined tension and shear [44].

Figure 2.12 summarizes the researchers' findings and shows the interaction for combined tension and shear of high strength bolts. Tensile stress was calculated using the stress area and shear stress was determined using either the stress area if the threads were in the shear plane or the nominal area if the shank was in the shear plane. More recent

studies evaluating European design codes have confirmed the interaction of tension and shear in high-strength bolts [60].

2.3 Fundamentals of Blast Loadings

Transient excitations concern the application of force over a period of time and result in dynamic loadings on structures. Dynamic loads are characterized by the duration of the loading compared to the natural period of the structure. Typical dynamic loads on structures include wind, traffic, and seismic loadings. In these types loadings, the period of the structure and the duration of the loading are similar, with the load occurring on the order of seconds. However, structures may also be subjected to extreme loadings such as impulsive loadings, which are characterized by a large application of force over a very short period of time. In an impulsive loading environment, the duration of the impulse is much, much less than the period of the structure – on the order of milliseconds – and the loading results in an environment where a shock wave propagates through the structure and connected components. The shock environment is characterized by an abrupt change in force, position, velocity, or acceleration [77]. There are several means of generating the shock environment. These include impact, the dropping or falling of a mass, or blast loads caused by explosive events. In light of global security concerns and the use of explosives as a preferred terrorist tactic, blast loads are of particular concern in the built environment.

The following sections provide an overview of explosive events that generate a shock environment, discuss methods for determining blast parameters, discuss the current

methodology for the design and analysis of steel structures for blast resistance, and review methods to experimentally investigate blast loadings.

2.3.1 Explosive Events

Blast loads are generated by accidental or intentional explosive threats that are caused by violent thermochemical events resulting in a sudden release of energy through high temperature and pressure gases. During a blast event in free air, the rapid release of energy at the source creates a pressure disturbance away from the source in all directions. The pressure disturbance is created by the expanding gases and subsequent compression of surrounding air particles. The resulting shock wave travels at a velocity faster than the speed of sound and is characterized by an instantaneous peak pressure followed by a rapid exponential decay [46, 70]. As the shock wave expands, the gases cool and pressures drop below atmospheric pressure, resulting in a negative phase or suction back towards the source. Figure 2.13 shows the behavior of an incident shock wave from detonation. The exponential decay of the shock wave can be calculated using the Friedlander equation,

$$P_s(t) = P_{so}\left[1 - \frac{t}{t_{so}}\right] e^{\left(-\frac{bt}{t_{so}}\right)} \tag{2.6}$$

where b is the waveform parameter. The specific impulse, i_s, is the area under the positive phase of the pressure-time history and is given by,

$$i_s = \int_{t_A}^{t_A + t_{so}} P_s(t)\, dt \tag{2.7}$$

Triangular approximations for the decay and resulting specific impulse are often sufficient for design and analysis [70].

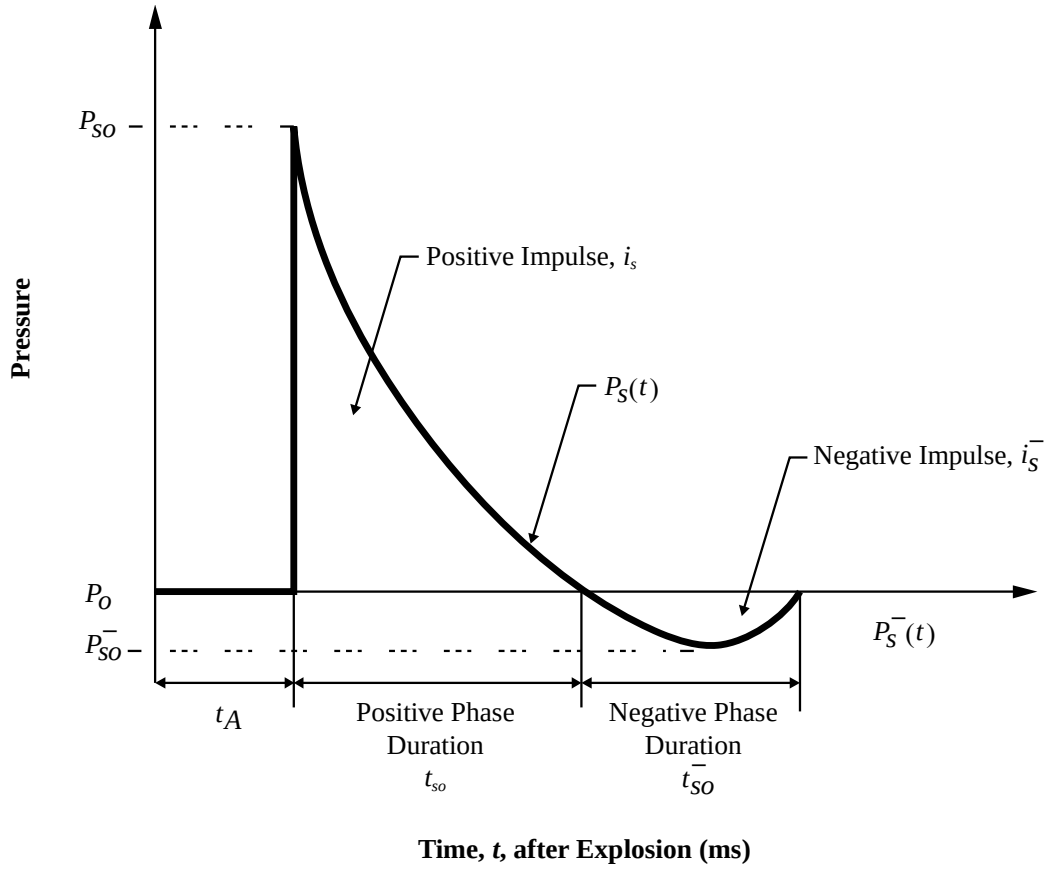

Figure 2.13: Pressure-time history of shock wave from detonation [46, 70].

In reality, the expansion of the shock wave is typically impeded by a physical object such as the ground or a structure which reflects the incident shock wave. In environments such as airbursts (not free air) or surface bursts, the incident wave and the reflected waves merge. The resulting pressure-time history for a reflected shock wave is shown in Figure 2.14. The peak reflected pressure, p_r, and impulse, i_r, are significantly higher than the peak incident peak pressure and impulse.

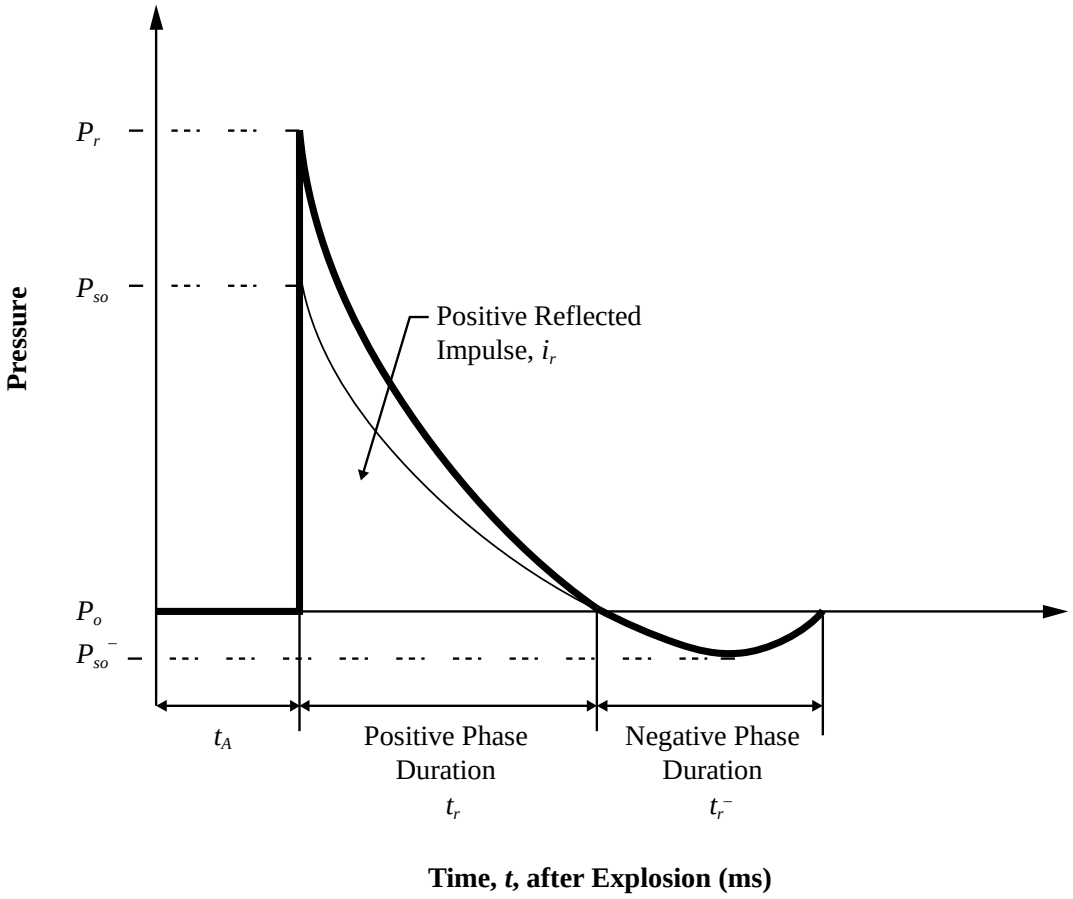

Figure 2.14: Pressure-time history of reflected shock wave from detonation [46, 70].

2.3.2 Blast Parameters

Graphical methods are most often used to empirically determine the blast parameters for explosive events based on a series of experiments conducted by the U.S. Department of Defense in the 1950s and 1960s [47]. The Unified Facilities Criteria (UFC) [1] provides a graphical method to predict blast parameters. Figure 2.15 shows the relevant curves for a free air burst. Peak incident and reflected pressures and impulses as well as time of arrival and duration of the positive phase can be determined from the figure. In order to use graphical methods to determine blast parameters, information regarding the type of explosive and distance of the source from the point of interest must be considered.

A wide variety of explosives exist with varying chemical compositions, sensitivity to detonation, and explosive energies [70]. Because of the wide variation in explosives, in any analysis of blast loadings the explosive is normalized to its equivalent weight of trinitrotoluene (TNT) using the ratio of the mass specific energy of the individual explosive, Q_{EXP}, to the mass specific energy of TNT, Q_{TNT}:

$$W_{TNT} = \frac{Q_{EXP}}{Q_{TNT}} W_{EXP} \tag{2.8}$$

where W_{TNT} is the equivalent weight of TNT and W_{EXP} is the weight of the explosive. The mass specific energies of common explosives are well known and tabulated [46, 47].

The distance between the charge and the point of interest has a significant influence on the resulting blast parameters. In addition to longer arrival time for events that occur farther away, the peak incident or reflected pressure will be lower due to the dissipation of energy throughout the event [54]. Therefore the pressures at different points of interest must be scaled based on their proximity to the charge. For spherical charges using the Hopkinson and Cranz cube root scaling law, the scaled distance, Z, is given by,

$$Z = \frac{R}{\sqrt[3]{W_{TNT}}} \tag{2.9}$$

where R is the perpendicular distance to the point of interest [70].

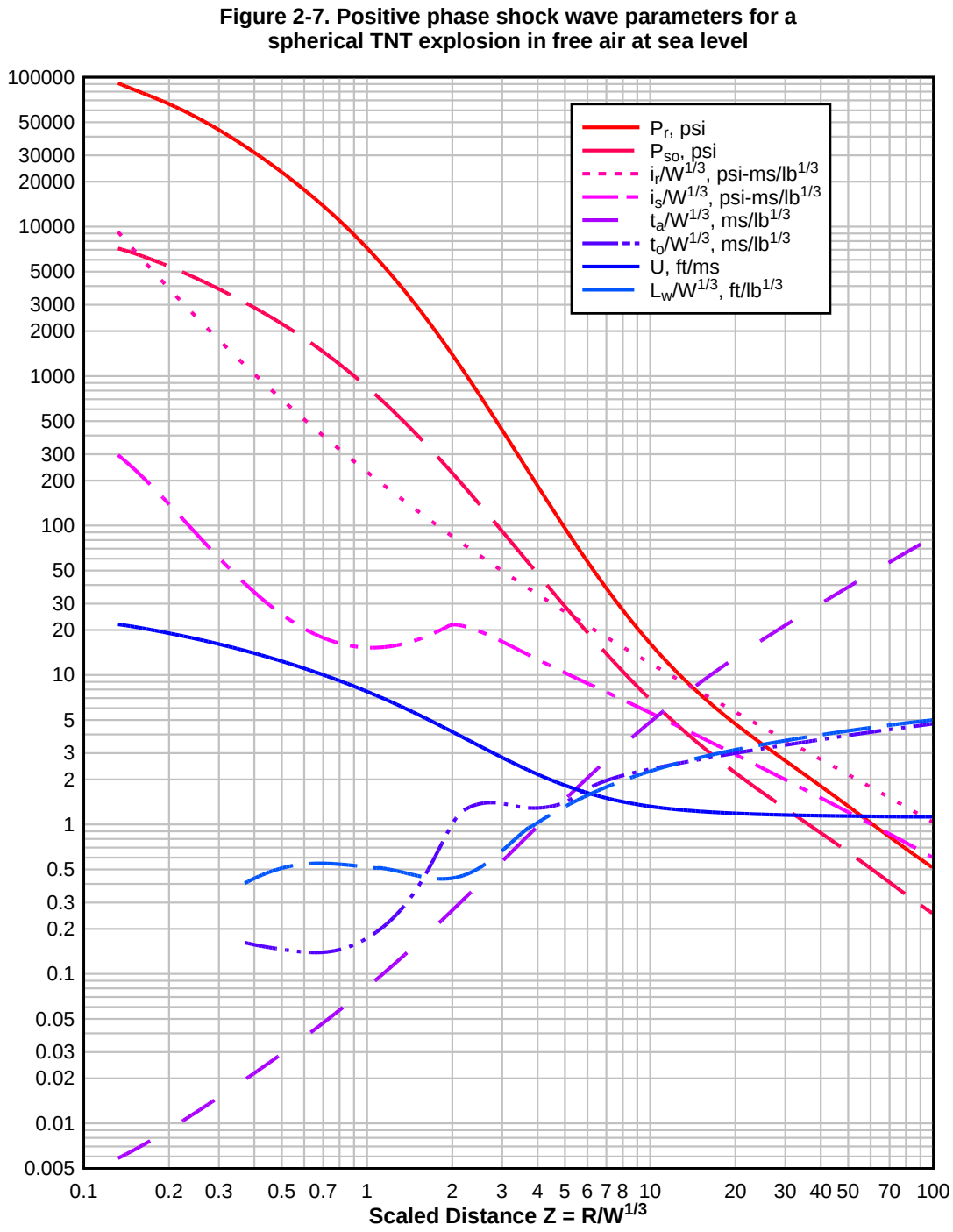

Figure 2.15: Blast parameters for TNT free air bursts from UFC 3-340-02 [1].

2.3.3 Strain Rate Response of Blast Loadings

The resulting shock wave from an explosive event produces a dynamic loading on the structure. Material properties vary considerably with the rate at which the load is applied. Higher loading rates result in higher strain rates. Under high strain rates, researchers have observed an increase in the strength of metals, alloys, and many non-metallic and composite materials [66]. Table 2.3 shows commonly used strain rate classifications, the influence of inertia forces with those classifications, and the dynamic considerations associated with each regime. While strain rate classifications are useful in determining general effects of the loading rate, actual strain rates should be noted due to the considerable influence differing strain rates can have within a regime and because no standard definitions of the regimes exist [83]. In low strain rate environments, such as creep and quasi-static loadings, the inertia forces are neglected because these forces are extremely small compared to the applied loading. In the higher strain rate regimes, however, inertial effects are much more significant to the response and cannot be neglected.

Table 2.3: Strain rate classifications (adapted from [83]).

Classification	Strain Rate (s^{-1})	Inertia Forces	Dynamic Considerations
Creep	$< 10^{-7}$	Neglected	Strain vs. time
Quasi-static	10^{-7} to 10^{-1}	Neglected	Constant strain rate
Intermediate	10^{-1} to 10^{2}	Important	Mechanical resonance
High	10^{2} to 10^{4}	Important	Elastic-plastic wave propagation
Very High	$> 10^{4}$	Important	Shock wave propagation

Inertia effects significantly influence the loading rate, strain rate, and structural response from the shock wave of an explosive event. As a result, it is necessary to distinguish between the material response to a shock wave and the structural response to the event [35]. The material response is insensitive to how the load is applied and the geometry of the structural element while the structural response is sensitive to both of these considerations [66].

As the shock wave propagates through the structure, the resulting strain rate in terms of material response is in the very high regime. However, the shock wave passes through the structure in such a short period of time that the larger structure and its components, due to their mass and bulk volume, have not yet responded. Once the structure begins to respond and deform, the structure and its components experience a much lower average strain rate than the material response. The structural response is typically in the intermediate regime with strain rates up to 10^2 s^{-1} [35]. Experimental testing using live explosives on concrete structures have shown strain rates of structural components ranging from 0.75 s^{-1} to 10 s^{-1} [13, 56].

2.3.4 SDOF Methods to Predict Response of Steel Components

Once the blast loading environment is known, the resulting pressure-time history can be applied to the structure. Typically, the analysis of structures subjected to blast loadings is conducted at the component level rather than as a structural system. Each individual structural component's response to the blast loading must be analyzed and then its dynamic reactions transferred to connected components for further analysis. Currently, no simplified design or analysis procedures exist to analyze structural response at the

system level to blast loadings. Alternatively, high fidelity physics based models can be generated to predict localized behavior, but requires specialized expertise and comes at a significant computational cost.

In lieu of high fidelity physics based models, engineers use an equivalent single degree of freedom system (SDOF) to predict the behavior of structural components under blast loadings. Figure 2.16(a) shows a model of a real system where $P(t)$ is the reflected pressure-time history discussed in Section 2.3.1. The simply supported steel beam shown has mass, m, stiffness, k, and length, L. The maximum displacement of the beam at midspan at any given time is denoted as $x_{max}(t)$. Applying Newton's Law, the equation of motion for a SDOF model of the real system is given by,

$$m\ddot{x}(t) + c\dot{x} + kx(t) = F(t) = P(t)A \tag{2.10}$$

where c is the damping coefficient and A is the area over which the blast load is applied.

Figure 2.16(b) shows the equivalent SDOF system for the beam under a blast loading. An equivalent force, $F_e(t)$ is applied to an equivalent mass, m_e, and an equivalent stiffness, $k_e(x)$, that is a function of the maximum displacement, $x_{max}(t)$, of the equivalent mass at any given time. The damping coefficient in the equivalent SDOF system is generally ignored because the structural component will reach its maximum response due to the impulse before any significant damping in the system can occur.

For the equivalent system, the equation of motion is similar to Equation 2.10, but described in terms of equivalent variables. With the damping force ignored, the equation of motion for the equivalent system is,

$$m_e\ddot{x}(t) + k_e x(t) = F_e(t) \tag{2.11}$$

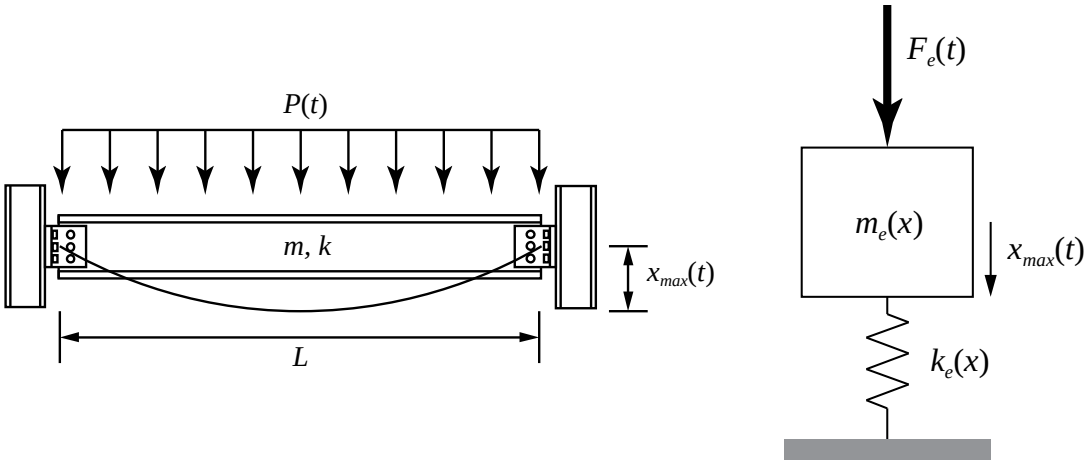

Figure 2.16: Structural steel component under blast loading: **(a)** real system and **(b)** equivalent SDOF system.

The equivalent mass, stiffness, and load can be expressed as a factor, K_X, describing the ratio of the equivalent mass, stiffness, or force to the actual mass, stiffness, or force of the real system:

$$K_M = \frac{m_e(t)}{m}, \qquad K_S = \frac{k_e(t)}{k}, \qquad K_L = \frac{F_e(t)}{F(t)} \tag{2.12}$$

Substituting these factors into the equation of motion for the equivalent system and deducing that $K_S = K_L$ from the static case ($\ddot{x} = 0$), the equation of motion becomes

$$K_M m\ddot{x}(t) + kx(t) = K_L F(t) \tag{2.13}$$

$$\frac{K_M}{K_L} m\ddot{x}(t) + kx(t) = F(t) \tag{2.14}$$

$$K_{LM} m\ddot{x}(t) + kx(t) = F(t), \qquad K_{LM} = \frac{K_M}{K_L} \tag{2.15}$$

Under an impulsive loading event, the stiffness of the component will vary non-linearly with time as the component transitions from elastic response to plastic response and back

to elastic response during rebound. Therefore, the equation of motion is typically written as

$$K_{LM}\ddot{x}(t) + R(x) = F(t) \tag{2.16}$$

where $R(x)$ is a non-linear resistance function of the displacement, x. The load-mass factor, K_{LM}, is determined based on boundary conditions, deformed shape, and equivalent strain energy [70]. In the analysis of components under blast loadings, the boundary conditions (connections) are typically idealized either as frictionless pins or completely rigid, though the energy dissipation of the connections is not well understood.

An elastic-perfectly plastic resistance function for the steel component shown in Figure 2.16(a) can be derived from mechanics. The steel component has modulus of elasticity, E, and an area moment of inertia, I. Figure 2.17 shows the resistance for the component, R_u, as a function of the displacement of the component, x, at midspan. Assuming frictionless pins at the supports, the component will be loaded elastically until yielding occurs at mid-span, the location of the maximum moment in the component. Once yielding occurs, a plastic hinge forms at mid-span and the component continues to displace without any additional resistance. From mechanics, the maximum elastic moment (Equation 2.17) and displacement (Equation 2.18) in the component are given by,

$$M_{max,e} = \frac{P(t)L^2}{8} \tag{2.17}$$

$$x_e = \frac{5P(t)L^4}{384EI} \tag{2.18}$$

Equation 2.17 can be solved for the force required to resist the maximum moment, R_u, by solving for $P(t)$ and dividing by the length of the component, L. The elastic resistance of the component is therefore,

$$R_u = \frac{8M_{u,dyn}}{L} \quad [Force] \tag{2.19}$$

Similarly, that resisting force can be substituted into Equation 2.18 and so the maximum elastic displacement of the beam is

$$x_e = \frac{5R_u L^3}{384EI} \quad [R_u \rightarrow Force] \tag{2.20}$$

The resulting elastic stiffness of the component is therefore,

$$k = \frac{R_u}{x_e} \tag{2.21}$$

In Equation 2.19, $M_{u,dyn}$ is the ultimate dynamic moment capacity of the component and is determined by multiplying the yield or ultimate strengths of the steel by dynamic and static increase factors (DIF and SIF, respectively). The SIF takes into account the fact that the actual yield and ultimate strengths are higher than minimum standards. For steels with a yield strength of less than 50,000 psi (345 MPa), the actual strength is approximately 10% higher than the minimum [70]. At rapid strain rates, the strength of the material increases beyond its static strength. The DIF for the ultimate stress of steel has been experimentally determined to be [54]

$$DIF = \left(\frac{\dot{\varepsilon}}{10^{-4}}\right)^{\alpha_{fy}}, \quad \alpha_{fy} = 0.074 - 0.04\left(\frac{f_y}{414}\right) \tag{2.21}$$

where f_y is in MPa. More conservatively, a simple DIF of 10 – 12% is used for yield stress depending on the failure mode and a DIF of 5% is used for the ultimate strength [70].

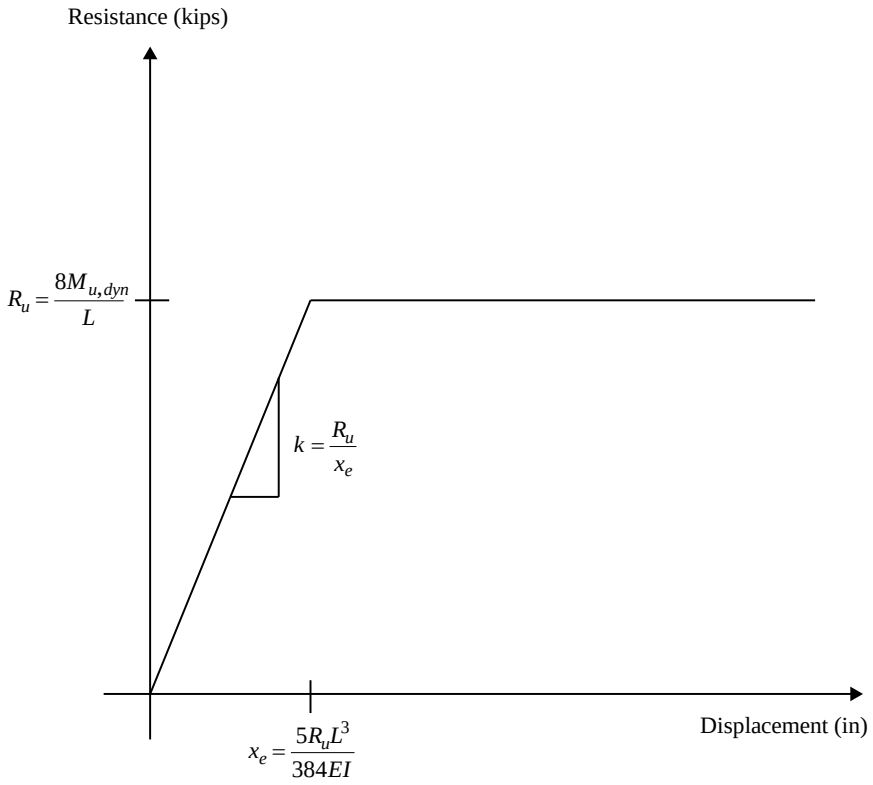

Figure 2.17: Resistance function for a simply supported steel component with uniform blast loading from [70].

A resistance function for the dynamic shear capacity of the component can likewise be derived. The shear capacity of the beam is assumed to be 55% of the tensile yield stress,

$$V_n = 0.55 f_{y,dyn} A_w \tag{2.22}$$

and the component's ultimate resistance to shear is given by,

$$V_u = \frac{R_u}{2} \tag{2.23}$$

The shear resistance must be compared to the flexural resistance of the component. If the shear resistance governs the behavior, then the shear resistance function must be used to solve the equation of motion.

The dynamic reactions for the component shown in Figure 2.16(a) are important for determining the loads on the connections and transferring the force-time history to connected components. It is therefore important to note that just because the external loading on a structure is impulsive in nature, the load on the connection may not be and will result in differing strain rates. The dynamic reactions are a function of the applied load, the boundary conditions, the deflected shape of the component, and the inertial forces of the component. In the elastic range, the dynamic reaction for the simply supported beam with a uniform blast load is given by,

$$V(t) = 0.39R(t) + 0.11F(t) \tag{2.24}$$

This force-time history can then be applied to connected members for further analysis. The dynamic reactions for different loading and boundary conditions have been calculated and tabulated [70].

Given the resistance function, $R(x)$, the load-mass factor, K_{LM}, and the pressure-time history, the equation of motion in Equation 2.16 can be solved to predict the response of the structural steel component. Typically the equation of motion is solved using Newmark's numerical integration procedure. In the procedure, a linear acceleration between time-steps is generally assumed and the displacement at each time-step is calculated using the results of the previous time-step and the current time-step. The displacement is used to determine whether the response is in the elastic region, plastic region, rebounding in the elastic region, or rebounding in the plastic region.

The results of the component-level, SDOF analysis can be used to characterize the damage from an explosive event to determine a level of acceptable risk. The American Society of Civil Engineers (ASCE) established performance goals depending on the level

of acceptable damage [2]. These Levels of Protection (LOP) range from *superficial* where there is no permanent deformation to *hazardous* where the component is likely to fail. Expected element damage can be determined based on the LOP and whether the component is a primary, secondary, or nonstructural element. For steel components, the maximum displacement and rotation of the components are used to determine response limits to determine the LOP provided by the component. The maximum response limits are governed by the type of load carried (flexure or compression) and the type of cross-section of the component.

2.3.5 Blast Loading Experimental Methods

Several experimental methods have been developed to simulate the shock environment from the material level to full-scale structural components for blast loadings. While field tests with live explosives generate the most realistic shock environment to investigate blast effects, their implementation is problematic. Field tests are expensive [72], difficult to achieve repeatability [77], and often unable to generate useful data due to survivability issues with instrumentation [32, 72]. Due to the inherent limitations of field testing, mechanically generated impulses have been used to simulate blast loadings. The Split Hopkinson Pressure Bar (SHPB) and gas guns have been used to investigate strain-rate effects on material behavior [73]. To investigate full-scale components and systems, drop towers, impact pendulums, shock tables, and shock tubes are commonly used [72]. More recently, the use of high-speed actuators at the University of California, San Diego and the Georgia Institute of Technology have been used to simulate blast loadings in a variety of applications [30, 71-73].

The Georgia Tech Blast, Shock, and Impact Laboratory has one MTS Single Channel Shock Impactor, commonly referred to as a blast generator (BG), that can be used to simulate blast loads on structural components. Figure 2.18 shows a schematic of the key components of the BG. In the system, nitrogen and pressurized hydraulic oil from an external hydraulic pump are charged in the pressure accumulator. Upon initiating the test, a servo valve controls the flow of oil into the BG, accelerating the piston rod and attached impactor mass towards the specimen at the desired acceleration. As the piston rod moves forward, the nitrogen gas in the deceleration chamber compresses and slows the piston rod to the desired impact velocity. After impact, a servo valve on the return side controls the flow of oil out of the BG, allowing the piston rod to retract. The BG can be used to directly impact the specimen with the programmer/impactor mass combination or it can be outfitted with a lightweight pusher plate to accelerate a flyer mass to impact the specimen [72]. The combination of the flow of oil into the BG, the preset pressure in the deceleration chamber, the opening of the return valves, and the programmer material create an impulse characteristic of a blast shockwave on the specimen [30].

The programmer material significantly influences the shape of the impulse on the specimen but can be difficult to quantify and predict its behavior. The BG primarily uses a non-linear, polyurethane-based rubber elastomer programmer that has been investigated, modeled, and reported on by Freidenberg [29] and Freidenberg et al. [31]. However, other types of programmers have been used and investigated, including leather, confined sand, and a combination of confined sand and leather [20]. Softer materials, such as foam and neoprene rubber have also been used to generate different impulses. The use of different materials to influence the shape of the pulse is often used in SHPB tests. Researchers have

experimented with soft metals, paper, felt, and a wide variety of materials to generate a pulse with a specific shape [15].

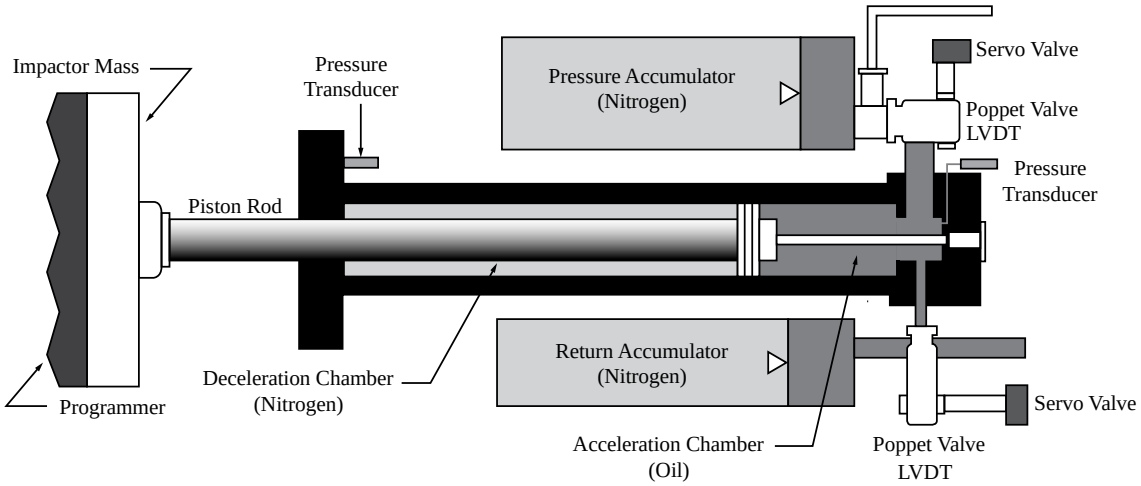

Figure 2.18: Single channel shock impactor schematic (adapted from [32]).

2.4 Dynamic Properties and Behavior of Bolts and Bolted Connections

The dynamic properties and behavior of bolts and bolted connections are significantly different than their static properties due to the nature of the loading. The following sections discuss the relevant literature on individual bolts subjected to shock, impact, and blast loadings as well as the relevant literature on bolted connections subjected to the same types of loadings.

2.4.1 Behavior of Bolts under Impulsive Loads

Researchers have been investigating the dynamic properties of bolts and threaded fasteners since the early 20th century. Early studies observed an increase in the tensile

capacity of bolts under impact loading compared to the static capacity of bolts, most often characterized by the work required to rupture the bolt. In their exhaustive study of different bolt materials, thread types, and bolt diameters, Whittemore et al. found that steel bolts subject to impact tensile loads experienced a 20-30% increase in capacity compared to their static capacity [80]. Early experimental methods for applying impulsive loads to bolts included modified Charpy impact hammers and steam powered impact hammers [80]. Deformation in the bolts was measured after impact [80].

In the 1950s and 1960s, the U.S. Navy investigated both tension and shear for hold down bolts subjected to shock loadings. Clements [19] investigated bolts manufactured from mild carbon steels and high-strength steels in different lengths and shank diameters subjected to shock loads. Tensile shock loadings were applied to a consistently torqued bolt by means of a shock anvil table (Navy High-Impact Shock Machine) which generated inertial forces in weights secured by the specimen bolt. The same impact was applied for each test and individual bolts were repeatedly tested until fracture with the total bolt elongation recorded. Strain gauges were used to determine the peak dynamic strain in the bolts for each impact and velocity meters were used to measure the inertia of the system. Clements concluded that high-strength alloys provided the best resistance to shock and mild carbon steels should be avoided for hold down situations due to large deformations.

Using the same Navy High-Impact Shock Machine as Clements, Vigness, et al. [78] investigated the shear behavior of 3/4-in and 1 1/14-in Grade 2 steel bolts in single shear arranged in a simple lap joint to investigate the influence that chamfering the bolt holes has on shear behavior of the bolt. For comparative purposes of the influence of the bolt head and nut, additional tests were also conducted on dowels. Load was applied by means of

dropping a weight from a specified height and velocity meters were used to determine the force-time history. The bolts were again subjected to successive blows until fracture with the shear displacement measured after each blow. Vigness et al. concluded that chamfered bolt holes provide greater energy absorption for bolts loaded in shear.

More recent studies on the behavior of bolts under impulsive loads have incorporated improved experimental methods and measurement techniques. Mouritz [49] and Munoz-Garcia et al. [50] investigated the tensile strength and failure mechanisms of mild steel bolts at different strain rates using different methods of inducing the shock load, including quasi-static direct tension, a drop tower, and underwater explosives. Tests used a single bolt size and constant torque level to achieve pretension in the bolt. Mouritz noted a linear increase in plastic strain in the bolts with increased input energy. Munoz-Garcia et al. concluded that bolts have reduced tensile capacity and ductility when dynamically loaded despite the common assumption that high strain rates increased the tensile strength of bolts [50, 74].

Fransplass, et al. [27, 28] examined threaded fasteners in both tension and combined tension and shear using modified tensile Split Hopkinson Pressure Bar equipment. They observed increase strength and ductility at higher rates [27] and similar failure modes in combined tension in shear tests as those found in static tests [28]. Fransplass, et al. also developed numerical models for various loading rates of the threaded portion of fasteners.

Horsfall, et al. [36] examined medium carbon steel bolts in shear subjected to blast loadings using live explosives, impact loadings using a drop tower, and quasi-static loadings in the same experimental setup. The researchers tested single or double bolts in

single shear with a simple lap joint in a compression jig and varied impulse energy for the dynamic tests. Bolts were tightened to a consistent torque-level prior to each test. Load-displacement curves were generated for the quasi-static tests and high speed video (HSV) was used to capture the explosive events. In all cases the researchers noted ductile failure of the bolts and concluded the impact loadings were consistent with blast loadings using live explosives.

In conjunction with the Engineer Research and Development Center (ERDC), U.S. Army Corps of Engineers (USACE), Rabalais [59] conducted dynamic and static direct shear tests of A307 bolts in various bolt patterns, in both single and double shear, and using pretensioned and non-pretensioned bolts to compare their performance to similarly constructed riveted joints. A tension jig using a 200-kip Dynamic Loader was used to shear the bolts, which were loaded at a high rate until fracture. Rabalais noted a 75% increase in the dynamic capacity in A307 bolts compared to their static capacity and their dynamic capacity was not affected by shear type (single or double) or bolt configuration in the joint.

Hadjioannou, et al. [34] conducted static and dynamic testing of mild carbon steel bolts in order to develop a simplified numerical modeling approach for bolted connections. Single bolts were tested in a tension jig with a simple lap joint using a 2,250-lb pendulum. Strain data was collected using digital image correlation. The data collected from tests were used to generate a numerical model that simulated the behavior of the bolt through fracture.

2.4.2 Bolted Connections under Impulsive Loads

Much of the experimental and numerical research on bolted steel connections under dynamic loads have centered on low rate, cyclic loadings in response to seismic events. These studies examined the ductile behavior of steel connections [14], cyclic-loading performance of various bolted steel connection configurations [22, 76], slip characteristics [22, 24, 57], and developed numerical methods for predicting energy dissipation through slip [18]. Ibrahim and Pettit [37] reviewed the relevant research to provide an overview of the uncertainties in predicting behavior of a bolted connection subjected to low rate, cyclic loadings. These uncertainties stem from the variability in initial bolt preload, interfaces of the materials, tolerances used in construction, and relaxation of preload during the dynamic event.

Few experimental studies have investigated these uncertainties in bolted joints subjected to shock loads [63]. Sabuwala, et al. [63] attempted to extrapolate experimental results from seismic testing into a numerical model that predicted behavior with blast loads applied to the same structure. However, the structural response to an impulsive load is markedly different than a slower, cyclic loading [43]. Direct correlations are problematic and so it is difficult to truly validate the model at the higher loading rates of an explosive event [21].

Several different types of connections under impulsive loads have been researched. Neubert and Poeth [53] investigated the behavior of pre-loaded connections subjected to a shock load parallel to the axis of the bolts. Karpanan [39] investigated a small-scale, simple lap joint cantilever beam that tested two bolts in tension as well as a small-scale bolted hat-

plate structure that tested four bolts in combined tension and shear to calibrate a numerical model.

In addition to small-scale components, full-scale structural connections have also been investigated. Stoddart [75] and Stoddart, et al. [74] conducted full-scale tests of a flexible end-plate connection and a shear tab connection. Both connections included multiple bolts tested primarily in shear with the connection primarily in tension. Based on the behavior of the connection in the experiment, a simplified numerical model was developed to match the behavior. Grimsmo, et al. [33] conducted similar experiments on full-scale fixed end-plate joints, concluding that shear failure in joints subjected to impulsive loads should be avoided due to the brittle nature of their failure. In both of these full-scale tests, the joints were tested to failure under quasi-static conditions and under impulsive loadings for comparative purposes.

Finally, field tests using live explosives have been used to investigate the response of bolted steel connections [45, 48, 58] and compared to high fidelity physics based (HFPB) models developed prior to the test. Two connections were used in the test. The first connection was a moment resisting beam-column connection and the second connection was a moment resisting column-reinforced concrete baseplate connection. While the models captured the global response of the event well, the models did not capture the behavior of the connection well due to the difficulty in identifying the fracture mechanisms of the materials.

2.5 Residual Capacity after a Blast Event

After an impulsive loading event on a structure, components that were damaged and exhibit plastic deformation but did not fracture continue to have some level of capacity under normal static loads. The remaining capacity in the component is referred to as its residual capacity. Understanding the residual capacity of structural components after an extreme event is critical to assessing the soundness of the structure for enabling occupants to safely exit the structure and allowing first responders to enter and assist occupants with reduced risk for progressive collapse.

Several studies have investigated the residual capacity of reinforced concrete components. Bao and Li [7], Wu et al. [82], Jayasooriya et al. [38], and Keliher and Sutton-Swaby [40] conducted numerical simulations to investigate the residual capacity of damaged components. Bao and Li examined reinforced concrete columns and through a parametric study, developed a formula for predicting the residual axial capacity of reinforced concrete columns. Wu et al. examined localized damage of reinforced concrete columns. Jayasooriya et al. and Keliher and Sutton-Swaby examined a multi-story reinforced concrete building and concluded that both global and detailed investigations are needed to adequately predict residual capacity following a blast event.

Only one study has examined the residual capacity of steel structures or components after an impulsive loading. Stewart and Morrill [69] developed a physics-based fast running model using an artificial neural network (ANN) to predict the residual capacity of a steel column subjected to a blast load.

The residual capacity of structural bolts and steel bolted connections after impulsive loadings has also not been meaningfully investigated. Clements [19] conducted static tensile tests on a small sample of mild carbon steel bolts that had been subjected to repeated impact loads and aged from two hours to 96 days to determine the influence of strain-aging after impact. In all other investigations, the bolts were either tested to failure [34, 49, 59, 78, 80] or the bolt damage was noted, but not tested [33, 36, 74, 75].

2.6 Conclusions

Based on a review of the available literature, the following conclusions can be made regarding the current body of knowledge of structural bolts and connections, particularly with respect to impulsive loadings:

1. The static behavior and properties of structural bolts and structural steel bolted connections have been studied extensively and are well known. Numerous bolt configurations, conditions, and factors have been investigated with statistically significant design guidelines and rules developed for implementation of bearing-type and slip-critical bolted connections [44, 51].

2. Comparatively few studies have examined the behavior of structural bolts or connections under dynamic or impulsive loadings, which introduce significantly different stress conditions on both the bolts and the connections.

3. Of the dynamic tests that have been conducted, relatively few have investigated dynamic shear [34, 36, 59]. No tests have been developed to generate a characteristic blast

loading on bolts loaded in shear to characterize the resulting damage to the bolt and/or the connection from varied input energies.

4. The effects of an impulsive load on slip-critical connections have not been investigated. Additionally, the effect of bolt pretension with structural bolts at specified levels has not been investigated to determine the amount of energy dissipation provided by the slip-critical joint. When preloading bolts in related studies, previous researchers have used inconsistent methods (i.e., torque control) [49, 78] or improper materials (i.e., mild carbon steel) [34, 36, 59].

5. Several different bolted joint configurations have been tested under shock loads. However, little is known about the more generalized behavior of bolts and bolted joints – both bearing and slip-critical – during extreme loading that would facilitate full structural modeling of the dynamic event. Experiments of simplified connections are needed to be able to characterize bolt and joint behavior under impulsive loads.

6. The residual capacity of structural bolts and steel bolted connections after an extreme loading event is not well understood. No studies to date have investigated the static capacity of a structural bolt or connection after damage due to an impulsive load.

2.7 References

[1] Unifed Facilities Criteria, *Structures to Resist the Effects of Accidental Explosions*, 3-340-02, 2008.

[2] American Society of Civil Engineers, *Blast Protection of Buildings*, 59-11, 2011.

[3] American Institute of Steel Construction, *Steel Construction Manual, 14th ed.*, 2011.

[4] American Society for Testing and Materials, *Standard Specifications for Carbon Steel Bolts, Studs, and Threaded Rod 60 000 PSI Tensile Strength*, ASTM A307-14, 2014.

[5] American Society for Testing and Materials, *Standard Specification for High Strength Structural Bolts, Steel and Alloy Steel, Heat Treated, 120 ksi (830 MPa) and 150 ksi (1040 MPa) Minimum Tensile Strength, Inch and Metric Dimensions*, ASTM F3125-15A, 2015.

[6] Allan, R. N. and J. W. Fisher, "Bolted joints with oversize or slotted holes," *Journal of the Structural Division*, vol. 94, no. 9, pp. 2061-2080, 1968.

[7] Bao, X. and B. Li, "Residual strength of blast damaged reinforced concrete columns," *International Journal of Impact Engineering*, vol. 37, no. 3, pp. 295-308, 2010.

[8] Batho, C. and E. H. Bateman, "Investigations on Bolts and Bolted Joints," in "Second Report of the Steel Structures Research Committee," His Majesty's Stationary Office, London, 1934.

[9] Bendigo, R., J. Fisher, and J. Rumpf, "Static tension tests of bolted lap joints, August 1962," Fritz Laboratory Reports, Paper 1741, 1962, Available: http://preserve.lehigh.edu/engr-civil-environmental-fritz-lab-reports/1741.

[10] Bendigo, R. A., R. M. Hansen, and J. L. Rumpf, "Long bolted joints," *Journal of the Structural Division*, vol. 89, no. 6, pp. 187-214, 1963.

[11] Bickford, J. and S. Nassar, *Handbook of Bolts and Bolted Joints*. New York: Marcel Dekker, 1998.

[12] Bickford, J. H., *An Introduction to the Design and Bahavior of Bolted Joints*, 4 ed. Boca Raton, FL: CRC Press, 2007.

[13] Cadoni, E., D. Asprone, and A. Prota, "High strain-rate testing of concrete and steel for the assessment of the Tenza Bridge under blast loading," *New trends in fractures mechanics of concrete,* pp. 627-635, 2007.

[14] Chen, S.-J., C. Yeh, and J. Chu, "Ductile steel beam-to-column connections for seismic resistance," *Journal of Structural Engineering,* vol. 122, no. 11, pp. 1292-1299, 1996.

[15] Chen, W. and B. Song, *Split Hopkinson (Kolsky) Bar*. New York: Springer, 2011.

[16] Chesson, E., N. L. Faustino, and W. H. Munse, "High-strength bolts subjected to tension and shear," *Journal of the Structural Division,* vol. 91, no. 5, pp. 155-180, 1965.

[17] Christopher, R., G. Kulak, and J. Fisher, "Calibration of alloy steel bolts, Proc. ASCE, Vol 92, ST2, April 1966, Publication No. 296," Fritz Laboratory Reports, Paper 162, 1966, Available: http://preserve.lehigh.edu/engr-civil-environmental-fritz-lab-reports/162.

[18] Citipitioglu, A., R. Haj-Ali, and D. White, "Refined 3D finite element modeling of partially-restrained connections including slip," *Journal of Constructional Steel Research,* vol. 58, no. 5, pp. 995-1013, 2002.

[19] Clements, E., "Properties of bolts under shock loading," Naval Research Laboratory, Washington, D.C., 1956.

[20] Durrant, B., "Shock Environment Characterization: Experimental and Numerical Methods," Masters Thesis, University of California, San Diego, 2013.

[21] Dusenberry, D. O., "General Considerations for Blast-Resistant Design," in *Handbook for Blast Resistant Design of Buildings*, D. O. Dusenberry, Ed. Hoboken, NJ: Wiley & Sons, 2010.

[22] Engelhardt, M. and A. Husain, "Cyclic-loading performance of welded flange-bolted web connections," *Journal of Structural Engineering,* vol. 119, no. 12, pp. 3537-3550, 1993.

[23] Fisher, J., P. Ramseier, and L. Beedle, "Strength of A440 steel joints connected with A325 bolts, Publication IABSE, Vol. 23, 1963, Reprint 245 (63-24)," Fritz Laboratory Reports, Paper 1830, 1963, Available: http://preserve.lehigh.edu/engr-civil-environmental-fritz-lab-reports/1830.

[24] Fitzgerald, T., T. Anagnos, M. Goodson, and T. Zsutty, "Slotted bolted connections in a seismic design for concentrically braced connections," *Earthquake Spectra,* vol. 5, no. 2, pp. 383-391, 1989.

[25] Foreman, R. T. and J. L. Rumpf, "Static tension tests of compact bolted joints," *Transactions of the American Society of Civil Engineers,* vol. 126, no. 2, pp. 228-254, 1961.

[26] Frank, K. H. and J. A. Yura, "An experimental study of bolted shear connections," Federal Highway Administration, FHWA-RD-81-148, 1981.

[27] Fransplass, H., M. Langseth, and O. S. Hopperstad, "Tensile behaviour of threaded steel fasteners at elevated rates of strain," *International Journal of Mechanical Sciences,* vol. 53, no. 11, pp. 946-957, 2011.

[28] Fransplass, H., M. Langseth, and O. S. Hopperstad, "Experimental and numerical study of threaded steel fasteners under combined tension and shear at elevated loading rates," *International Journal of Impact Engineering,* vol. 76, pp. 118-125, 2015.

[29] Freidenberg, A., "Advancements in Blast Simulator Analysis Demonstrated on a Prototype Wall Structure," Doctoral Thesis, University of California, San Diego 2013.

[30] Freidenberg, A., A. Aviram, L. K. Stewart, D. Whisler, H. Kim, and G. A. Hegemier, "Demonstration of tailored impact to achieve blast-like loading," *International Journal of Impact Engineering,* vol. 71, pp. 97-105, 2014.

[31] Freidenberg, A., C. W. Lee, B. Durant, V. F. Nesterenko, L. K. Stewart, and G. A. Hegemier, "Characterization of the blast simulator elastomer material using a pseudo-elastic rubber model," *International Journal of Impact Engineering,* vol. 60, pp. 58-66, 2013.

[32] Gram, M., A. Clark, G. Hegemier, and F. Seible, "Laboratory simulation of blast loading on building and bridge structures," *WIT Transactions on State-of-the-art in Science and Engineering,* vol. 60, 2012.

[33] Grimsmo, E. L., A. H. Clausen, M. Langseth, and A. Aalberg, "An experimental study of static and dynamic behaviour of bolted end-plate joints of steel," *International Journal of Impact Engineering,* vol. 85, pp. 132-145, 2015.

[34] Hadjioannou, M., D. Stevens, and M. Barsotti, "Development and Validation of Bolted Connection Modeling in LS-DYNA® for Large Vehicle Models," in *14th International LS-DYNA Users Conference,* Dearborn, MI, 2016.

[35] Harding, J., "The Effect of High Strain Rate on Material Properties," in *Materials at High Strain Rates,* T. Z. Blazynski, Ed. New York: Elsevier Applied Science, 1987, pp. 133-186.

[36] Horsfall, I., B. Hansen, and D. Carr, "Security of bolted joints during explosive loading," *International Journal of Vehicle Structures & Systems (IJVSS),* vol. 3, no. 2, pp. 107-112, 2011.

[37] Ibrahim, R. A. and C. L. Pettit, "Uncertainties and dynamic problems of bolted joints and other fasteners," *Journal of Sound and Vibration,* vol. 279, no. 3, pp. 857-936, 2005.

[38] Jayasooriya, R., D. P. Thambiratnam, N. J. Perera, and V. Kosse, "Blast and residual capacity analysis of reinforced concrete framed buildings," *Engineering Structures,* vol. 33, no. 12, pp. 3483-3495, 2011.

[39] Karpanan Nakalswamy, K., "Experimental and numerical analysis of structures with bolted joints subjected to impact load," Doctoral Thesis, University of Nevada, Las Vegas, 3412376, 2010.

[40] Kelliher, D. and K. Sutton-Swaby, "Stochastic representation of blast load damage in a reinforced concrete building," *Structural Safety,* vol. 34, no. 1, pp. 407-417, 2012.

[41] Kimball, D. S. and J. H. Barr, *Elements of Machine Design,* 3d ed. New York: J. Wiley & Sons, 1935.

[42] King, W. R., "Experiments with bolts and screw threads," *Transactions of the American Institute of Mining Engineers,* vol. 14, pp. 90-98, 1885.

[43] Krauthammer, T., "Blast-resistant structural concrete and steel connections," *International Journal of Impact Engineering,* vol. 22, no. 9, pp. 887-910, 1999.

[44] Kulak, G. L., J. W. Fisher, and J. H. Struik, *Guide to Design Criteria for Bolted and Riveted Joints, 2nd ed.* Chicago: American Institute of Steel Construction, 2001.

[45] Magallanes, J. M., R. Martinez, and J. W. Koenig, "Experimental results of the AISC full-scale column blast test," *Rep. TR-06,* vol. 20, 2006.

[46] Mlakar, P. F. and D. Barker, "Blast Phenomena," in *Handbook for Blast Resistant Design of Buildings,* D. O. Dusenberry, Ed. Hoboken, NJ: Wiley & Sons, 2010.

[47] Mlakar, P. F. and W. Bounds, "Blast Loading," in *Handbook for Blast Resistant Design of Buildings,* D. O. Dusenberry, Ed. Hoboken, NJ: Wiley & Sons, 2010.

[48] Morrill, K. B., J. E. Crawford, J. M. Magallanes, and H. J. Choi, "Development of simplified tools to predict blast response of steel beam-column connections," in *Structural Engineering Research Frontiers*, 2007, pp. 1-10.

[49] Mouritz, A. P., "Failure mechanisms of mild steel bolts under different tensile loading rates," *International Journal of Impact Engineering,* vol. 15, no. 3, pp. 311-324, 1994.

[50] Munoz-Garcia, E., J. Davison, and A. Tyas, "Analysis of the response of structural bolts subjected to rapid rates of loading," in *4th European Conference on Steel and Composite Structures (EUROSTEEL)*, 2005, vol. 100, p. 4.10.

[51] Munse, W. H., "Research on bolted connections," *Transactions of the American Society of Civil Engineers,* vol. 121, no. 1, pp. 1255-1266, 1956.

[52] Nah, H.-S., H.-J. Lee, K.-S. Kim, W.-B. Kim, and W. Kim, "Evaluation of slip coefficient of slip critical joints with high strength bolts," *Structural Engineering and Mechanics,* vol. 32, no. 4, pp. 000-000, 2009.

[53] Neubert, V. H. and D. F. Poeth, "Shock response of a preloaded connection," *Experimental Mechanics,* vol. 7, no. 2, pp. 75-81, 1967.

[54] Ngo, T., P. Mendis, A. Gupta, and J. Ramsay, "Blast loading and blast effects on structures–an overview," *Electronic Journal of Structural Engineering,* vol. 7, no. S1, pp. 76-91, 2007.

[55] Oberg, E., F. D. Jones, H. L. Horton, H. H. Ryffel, and J. H. Geronimo, *Machinery's handbook*. Industrial Press, Incorporated, 2016.

[56] Orton, S. L., V. P. Chiarito, C. Rabalais, M. Wombacher, and S. P. Rowell, "Strain rate effects in CFRP used for blast mitigation," *Polymers,* vol. 6, no. 4, pp. 1026-1039, 2014.

[57] Pai, N. G. and D. P. Hess, "Three-dimensional finite element analysis of threaded fastener loosening due to dynamic shear load," *Engineering Failure Analysis,* vol. 9, no. 4, pp. 383-402, 2002.

[58] Pekelnicky, R. G. *et al.*, "Blast-Resistance Benefits of Seismic Design, Phase 2 Study: Performance Analysis of Structural Steel Strengthening Systems," Federal Emergency Management Agency, 2010.

[59] Rabalais, C. P., "Analysis of bolt and rivet structural fasteners subjected to dynamic and quasi-static shear loadings," Masters Thesis, Texas A&M University, 2015.

[60] Renner, A. and J. Lange, "Load-bearing behaviour of high-strength bolts in combined tension and shear," *Steel Construction,* vol. 5, no. 3, pp. 151-157, 2012.

[61] Richard, R. M., J. D. Kriegh, and D. E. Hormby, "Design of single plate framing connections with A307 bolts," *AISC Engineering Journal,* vol. 19, no. 4, pp. 209-213, 1982.

[62] Rumpf, J. and J. Fisher, "Calibration of A325 bolts," *Proc. ASCE,* vol. Vol. 89 (ST6), no. December 1963, Reprint No. 232 (63-18), 1963.

[63] Sabuwala, T., D. Linzell, and T. Krauthammer, "Finite element analysis of steel beam to column connections subjected to blast loads," *International Journal of Impact Engineering,* vol. 31, no. 7, pp. 861-876, 2005.

[64] Salih, N., J. Smith, H. M. Aktan, and M. Usmen, "An experimental appraisal of the load-deformation properties of A325 high-strength bolts," *Journal of Testing and Evaluation,* vol. 20, no. 6, pp. 440-448, 1992.

[65] Salmon, C. G., J. E. Johnson, and F. A. Malhas, *Steel Structures: Design and Behavior*, 5th ed. Upper Saddle River, NJ: Pearson Prentice Hall, 2009.

[66] Sierakowski, R. L., "Strain Rate Behavior of Metals and Composites," in *Convegno IGF XIII Cassino 1997*, 1997.

[67] Sterling, G., E. Troup, E. Chesson Jr, and J. Fisher, "Calibration tests of A490 high-strength bolts, Proc, ASCE, Vol. 91, ST5, 1965, Publication No. 273," Fritz Laboratory Reports, Paper 164, 1965, Available: http://preserve.lehigh.edu/engr-civil-environmental-fritz-lab-reports/164.

[68] Sterling, G., J. Wallaert, and J. Fisher, "What happens to bolt tension in large joints?," *Fasteners*, vol. 20, no. 3, 1965.

[69] Stewart, L. and K. Morrill, "Residual capacity prediction of blast-loaded steel columns using physics-based fast running models," *International Journal of Safety and Security Engineering*, vol. 5, no. 4, pp. 289-303, 2015.

[70] Stewart, L. K., "Course Notes, CEE 8813: Multi-hazard Analysis and Design," 2015.

[71] Stewart, L. K., B. Durant, J. Wolfson, and G. A. Hegemier, "Experimentally generated high-g shock loads using Hydraulic Blast Simulator," *International Journal of Impact Engineering*, vol. 69, pp. 86-94, 2014.

[72] Stewart, L. K. *et al.*, "Methodology and validation for blast and shock testing of structures using high-speed hydraulic actuators," *Engineering Structures*, vol. 70, pp. 168-180, 2014.

[73] Stewart, L. K. *et al.*, "Georgia Institute of Technology Laboratory for Blast, Shock, and Impact," in *Proc. 7th International Conference on Advances in Experimental Structural Engineering (AESE)*, Pavia, Italy, 2017.

[74] Stoddart, E., M. Byfield, and A. Tyas, "Blast modeling of steel frames with simple connections," *Journal of Structural Engineering*, vol. 140, no. 1, p. 04013027, 2012.

[75] Stoddart, E. P., "Development of component-based connection modelling for steel framed structures subjected to blast or progressive collapse," University of Southampton, 2012.

[76] Swanson, J. A. and R. T. Leon, "Bolted steel connections: tests on T-stub components," *Journal of Structural Engineering*, vol. 126, no. 1, pp. 50-56, 2000.

[77] Szuladzinski, G., *Formulas for Mechanical and Structural Shock and Impact*. Boca Raton, FL: CRC Press, 2009.

[78] Vigness, I., E. Seibert, and H. Forkois, "Effect of chamfered holes on the resistance of bolts and dowels to shock loads in shear," Naval Research Lab, Washington, DC, 1962.

[79] Wallaert, J. J. and J. W. Fisher, "Shear strength of high-strength bolts," Fritz Laboratory Reports, Paper 1822, 1964, Available: http://preserve.lehigh.edu/engr-civil-environmental-fritz-lab-reports/1822.

[80] Whittemore, H. L., E. O. Seaquist, and G. W. Nusbaum, "Impact and Static Tensile Properties of Bolts," *U.S. Bureau of Standards, Journal of Research*, vol. 14, no. 2, pp. 139-188, 1935.

[81] Wilson, W. M. and F. P. Thomas, "Fatigue Tests on Riveted Joints," University of Illinois, Engineering Experiment Station, Urbana, IL, Bulletin 302, 1938.

[82] Wu, K.-C., B. Li, and K.-C. Tsai, "Residual axial compression capacity of localized blast-damaged RC columns," *International Journal of Impact Engineering*, vol. 38, no. 1, pp. 29-40, 2011.

[83] Zukas, J. A., T. Nicholas, H. F. Swift, L. B. Greszczuk, and D. R. Curran, *Impact Dynamics*. New York: John Wiley & Sons, 1982.

CHAPTER 3

RESEARCH OBJECTIVES

3.1 Research Objectives

The research conducted for this thesis focuses on developing a better understanding of the behavior of structural bolts and bolted connections under blast or impulsive loading conditions and their residual capacity after such an event. This understanding is crucial in being able to more accurately model and predict the behavior of structures under these loading conditions and prevent progressive collapse failures [2].

The overarching objective of the research was to demonstrate and validate the use of a modified high-speed hydraulic actuator (blast simulator) to investigate the response and residual capacity of bolted structural steel connections. Previous researchers [4, 10, 11] have investigated full-scale bolted steel structural connections under blast loadings. In these connections, bolts are loaded in combined tension and shear and the connected components influence behavior. Because of the complex stress states that develop in such connections, it can be difficult to develop a more generalized understanding of the behavior based on these experiments. The objective of this research was therefore to reduce the complexity of the problem by examining a single bolt with a shear load applied through a single lap joint configuration. A final objective of the research was to compare current, commonly used modeling methods to determine how accurately these methods predict the response and residual capacity of structural bolts subjected to an impulsive load.

3.2 Research Questions

The research sought to answer four questions regarding the behavior of bolts and bolted joints during and after an impulsive event. The specific research questions (*RQ*), hypotheses (*H*), and specific aims (*SA*) this project investigated were:

RQ1: What is the relationship between an applied shear impulse to a bolt and the subsequent damage to the bolt in terms of permanent shear deformation?

H1: The permanent shear deformation will increase as the applied load increases. Based on previous dynamic tensile strength investigations [7], the increase will be linear until the fracture impulse is reached.

SA1: Conduct a rigorous experimental test program consisting of different types of structural bolts under varying impulsive loads and quantify the permanent deformation in the bolt after the impulsive loading event.

RQ2: What is the relationship between an applied shear impulse to a structural bolt and the residual shear capacity of the bolt?

H2: The residual load capacity of the damaged bolt will be similar to the load capacity of undamaged bolts. However, the residual ductility will be less than the ductility of undamaged bolts [9]. As the applied impulse increases, the residual ductility of the bolt will decrease.

SA2: Conduct a rigorous experimental test program consisting of different types of structural bolts under varying impulsive loads and quantify the residual static capacity of the bolt in terms of load and displacement. Compare the residual static capacity of the bolt to bolts that have not experienced an impulsive load.

RQ3: What is the relationship between an applied impulse and energy dissipation in preloaded structural bolts in slip-critical connections?

H3: As the applied impulse increases, the residual load required to generate major slip will decrease due to energy dissipation in the connection.

SA3: Conduct a rigorous experimental test program consisting of high-strength bolts preloaded to current specifications and subjected to varying impulsive loads. Quantify the force required to generate major slip in the connection and compare it to the force required to generate major slip in connections that have not experienced an impulsive load.

RQ4: Do current, standard modeling practices accurately capture damage and residual capacity of bolts and bolted connections subjected to impulsive loadings?

H4: Current modeling practices do not accurately capture the damage or residual capacity of bolts and bolted connections subjected to impulsive loadings.

SA4: Conduct a rigorous investigation of current modeling practices for bolts and bolted connection subjected to impulsive loadings. Compare the results from these models to data collected through the experimental test program previously described to determine accuracy of current modeling practices.

3.3 Project Scope

A large number of variables influence the behavior of bolts and bolted connections [6]. These variables include bolt type, bolt diameter, the inclusion or exclusion of threads in the shear plane, material of connected members, surface treatments of connected members, pretension in the bolt, and the diameter of the bolt hole, among many other variables. Given unlimited resources, each of these variables would have been investigated using an analysis of variance (ANOVA) methodology. Time and resource constraints limited the scope of the project to the variables most likely to best describe the behavior and residual capacity of structural bolts and connections.

Overall, the research tested four parameters: 1) the applied impulse; 2) the type of structural bolt; 3) the clamping force or bolt pretension in the connection; and 4) the connected plate material. The applied impulse was varied by changing the impact energy of the high-speed hydraulic actuator, ensuring that plastic deformation occurred in the bolt. Two types of structural bolts were tested, ASTM A307 and A325, because of their significantly different mechanical properties. ASTM A325 high-strength bolts are most commonly used in steel structures whereas ASTM A307 bolts are used in more general applications, both structural and non-structural [6]. Bolts were either installed loosely or tightened to current specifications depending on the type of test conducted. Bolt pretension is highly variable but significantly influences the behavior of connections and is important to understanding the behavior of connections under impulsive loads. Finally, the material of the connected plates varied between tests to investigate bolt residual capacity and tests to investigate slip-critical connections. When investigating bolt residual capacity, ASTM

A514A steel was used due to its high yield strength and likelihood of not exhibiting localized bearing failure. In slip-critical connection testing, ASTM A572 Grade 50 steel was used because it is more prevalent in steel structures than ASTM A514A steel.

Likewise, several important parameters were held constant. First, only 7/8 inch (2.22 cm) diameter bolts were tested apart from validation of the experimental setup in which 3/4 inch (1.91 cm) bolts were used. The most common diameters for steel structures are 3/4 inch (1.91 cm) and 7/8 inch (2.22 cm) while the most common diameters for steel bridges are 7/8 inch (2.22 cm) and 1 inch (2.54 cm) [8]. Additionally, previous research has focused on using 7/8 inch (2.22 cm) structural bolts for static testing [6, 8]. The length of bolts tested was 3.50 inch (8.89 cm) for bolt impulsive and residual capacity tests and 3.00 inches (7.62 cm) for slip critical connection tests to ensure full grip of the connected plates. All bolts had a gauge length of 2.0 inches (5.08 cm) with threads excluded from the shear plane. Specimen bolts were from randomly selected lots and manufacturers.

Finally, numerical simulation techniques were limited to common methods included in the commercially available software package, LS-DYNA [1]. While advanced methods to model fastener behavior have been posited [3, 5, 10], investigation of these techniques was beyond the scope of this project. Additionally, the numerical investigations in this research were focused on assessing the current state of the art and comparing it to experimentally determined data, and therefore development of a new modeling technique was beyond the scope of this project.

3.4 References

[1] Livermore Software Technology Corporation, *LS-DYNA Keyword User's Manual*, 2007.

[2] Ellingwood, B. R. and D. O. Dusenberry, "Building design for abnormal loads and progressive collapse," *Computer-Aided Civil and Infrastructure Engineering,* vol. 20, no. 3, pp. 194-205, 2005.

[3] Fransplass, H., M. Langseth, and O. S. Hopperstad, "Experimental and numerical study of threaded steel fasteners under combined tension and shear at elevated loading rates," *International Journal of Impact Engineering,* vol. 76, pp. 118-125, 2015.

[4] Grimsmo, E. L., A. H. Clausen, M. Langseth, and A. Aalberg, "An experimental study of static and dynamic behaviour of bolted end-plate joints of steel," *International Journal of Impact Engineering,* vol. 85, pp. 132-145, 2015.

[5] Hadjioannou, M., D. Stevens, and M. Barsotti, "Development and Validation of Bolted Connection Modeling in LS-DYNA® for Large Vehicle Models," in *14th International LS-DYNA Users Conference*, Dearborn, MI, 2016.

[6] Kulak, G. L., J. W. Fisher, and J. H. Struik, *Guide to Design Criteria for Bolted and Riveted Joints, 2nd ed.* Chicago: American Institute of Steel Construction, 2001.

[7] Munoz-Garcia, E., J. Davison, and A. Tyas, "Analysis of the response of structural bolts subjected to rapid rates of loading," in *4th European Conference on Steel and Composite Structures (EUROSTEEL)*, 2005, vol. 100, p. 4.10.

[8] Salih, N., J. Smith, H. M. Aktan, and M. Usmen, "An experimental appraisal of the load-deformation properties of A325 high-strength bolts," *Journal of Testing and Evaluation,* vol. 20, no. 6, pp. 440-448, 1992.

[9] Smith, P., M. Byfield, and D. Goode, "Building robustness research during World War II," *Journal of Performance of Constructed Facilities,* vol. 24, no. 6, pp. 529-535, 2010.

[10] Stoddart, E., M. Byfield, and A. Tyas, "Blast modeling of steel frames with simple connections," *Journal of Structural Engineering,* vol. 140, no. 1, p. 04013027, 2012.

[11] Stoddart, E. P., "Development of component-based connection modelling for steel framed structures subjected to blast or progressive collapse," University of Southampton, 2012.

CHAPTER 4

BOLT SHEAR RESIDUAL CAPACITY TEST SYSTEM

A novel bolt shear residual capacity system was developed to experimentally investigate the behavior of structural bolts and steel bolted connections under impulsive loading events with the objective of being able to answer the research questions discussed in Chapter 3. This chapter discusses the design, fabrication, validation, and calibration of a bolt shear residual capacity experimental test system. Additionally, the results of initial residual capacity tests and subsequent improvements to the test system are presented.

4.1 Design of a Bolt Shear Residual Capacity Experimental Test System

The bolt shear residual capacity experimental test system consists of two main components: 1) a dynamic shear experimental test system; and 2) a static shear experimental test system. The system is designed such that the blast generator high-speed hydraulic actuator applies a dynamic impact to the specimen bolt or connection short of the impulse required to fracture the bolt. A quasi-static test jig is then installed to test the static capacity of the damaged bolt in-situ without manipulating the bolt or connection.

Figure 4.1 shows the design methodology used to develop the bolt shear residual capacity experimental test system. In general, the dynamic test system was the primary driver of the design with the static test system designed to work in conjunction with the dynamic test system.

A finite element (FE) model of the dynamic test system was developed to initially investigate the experiment. Simultaneously, design and fabrication drawings were drafted with an emphasis on constructability and testing efficiency. Results and changes from the FE model analysis were incorporated into the design drawings and vice versa until a satisfactory design was reached.

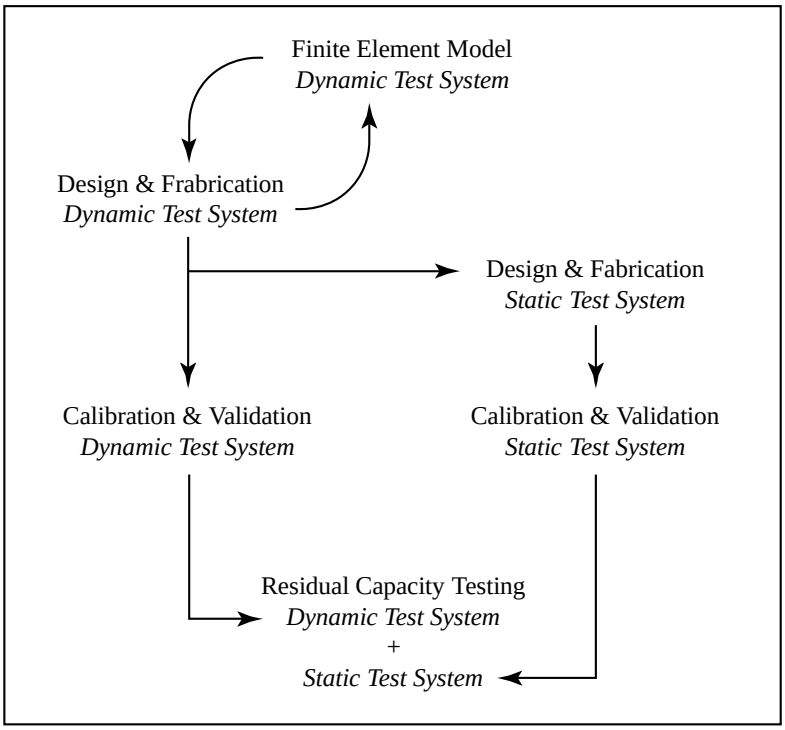

Figure 4.1: Design methodology for the residual capacity experimental test system.

Once the design of the dynamic test system was finalized, the static test system was designed to work with the dynamic test system and within the physical constraints of the BG apparatus. The dynamic and static test systems were then validated independently. Finally, the entire test system was validated for residual capacity tests involving an impact

on the specimen followed by an in-situ static test. The following subsections discuss the design of the experimental test system in detail.

4.1.1 Test System Concept and Theory

4.1.1.1 Test System Concept

The experimental test system is a simple lap joint in a compression jig configuration to capitalize on the inherent compressive nature of the BG. Figure 4.2 shows a schematic of the test concept. A flyer mass with an attached programmer is accelerated to an impact velocity, v_0, by the BG. Load cells measure the input impulse on the impact T-section as energy from the flyer is transferred to the impact T-section. The energy is transferred from the impact T-section to the reaction T-section through the specimen bolt. The reaction T-section is affixed to a rigid plate with load cells in between to measure the reaction impulse.

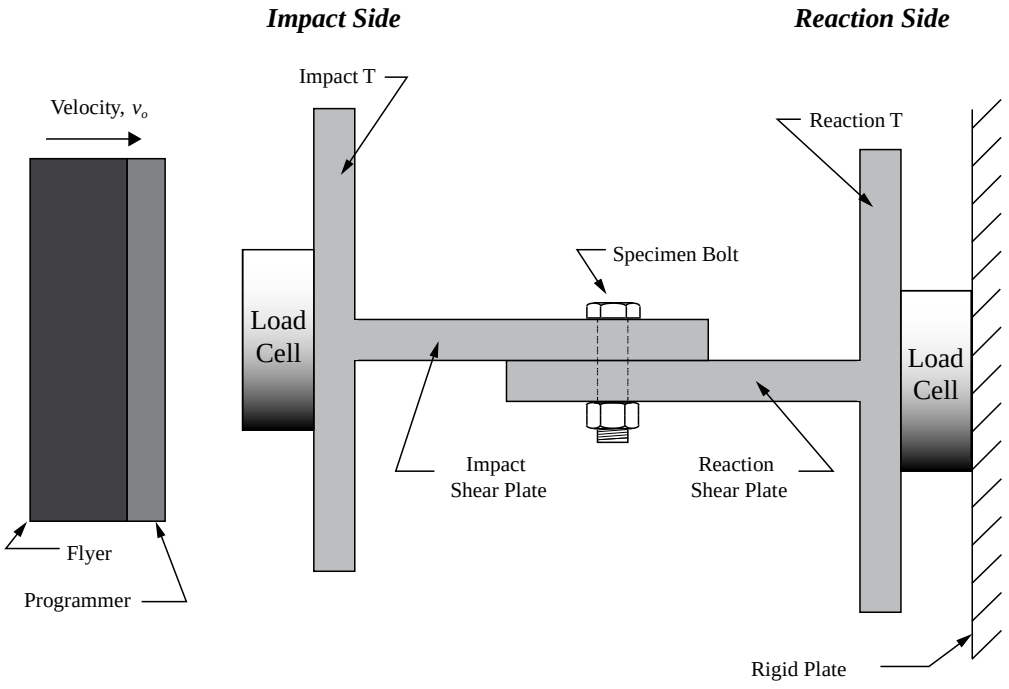

Figure 4.2: Test system concept schematic.

4.1.1.2 Theoretical Impulse

The system can be modeled as a multiple degree of freedom (MDOF) system. Figure 4.3 shows the MDOF model for the experimental test system. Represented are the three states of motion: 1) prior to impact; 2) at impact; and 3) after impact. The mass of the flyer, impact T-section, and reaction T-section are represented by m_1, m_2, and m_3, respectively. The programmer is represented by a non-linear spring, k_P. Similarly, the specimen bolt is also represented by a non-linear inelastic spring, k_B.

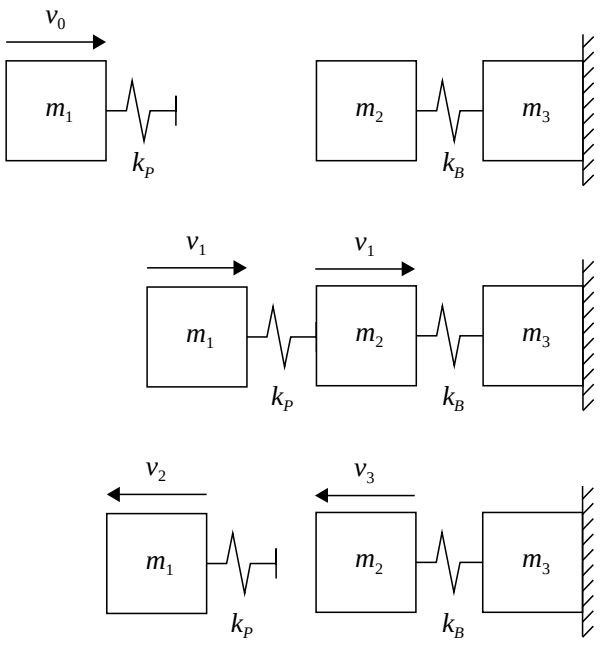

Figure 4.3: States of motion for MDOF model of the test system.

The flyer mass has an initial velocity, v_0, imparted by the high-speed actuator. Upon impact of the flyer and the impact T-section, the programmer compresses and the flyer and impact T-section move at a new velocity, v_1. The bolt resists the displacement of the flyer and

impact T-section and both elements rebound in the opposite direction at velocities, v_2, and v_3, respectively.

Assuming an ideal system, momentum must be conserved for the system to be in equilibrium. Therefore, the magnitude of the change in momentum – or impulse, S – of the flyer mass must equal the impulse on the impact side of the system and the impulse of the reaction side of the system,

$$S_{system} = S_{flyer} = S_{impact} = S_{reaction} \tag{4.1}$$

Recalling that impulse is defined as,

$$S = m\Delta v = \int F(t)dt \tag{4.2}$$

then in terms of this system, Equation 4.1 can be rewritten,

$$S_{sys} = m_1(v_2 - v_0) = \int F_I(t)dt = \int F_R(t)dt \tag{4.3}$$

where $F_I(t)$ and $F_R(t)$ are the force-time histories measured by the respective load cells.

The system, however, is not ideal and so there will be some loss of momentum, primarily from friction in the system. Assuming some friction loss on the impact side, $S_{f,I}$, and some friction loss on the reaction side, $S_{f,R}$, Equation 4.3 becomes,

$$S_{sys} = m_1(v_3 - v_0) = \int F_I(t)dt + S_{f,I} = \int F_R(t)dt + S_{f,I} + S_{f,R} \tag{4.4}$$

Because the reaction side captures all of the loss of momentum in the system, the reaction side directly measures the impulse on the bolt.

4.1.1.3 Effects of Prying Action in Lap Joints

As previously noted in Chapter 2, lap joints are generally less preferred than butt joints due to the unbalanced loading condition inherent in a lap joint [8]. However, previous researchers have used lap joints to investigate dynamic shear in bolts [7, 10] with

success. Figure 4.4(a) shows the theoretical loads and lines of action for the forces applied to a lap joint, separated by a distance, *d*, based on the thickness of the connected plates. The offset creates a couple in the system and, combined with the rotation of the bolt due to the 1/16 in (1.59 mm) gap from the bolt hole, has a tendency to cause rotation in the plate as shown in Figure 4.4(b), where the plate rotation is exaggerated for clarity. The application of the force with the top plate at an angle, θ, causes prying action of the bolt, inducing combined axial tension and shear.

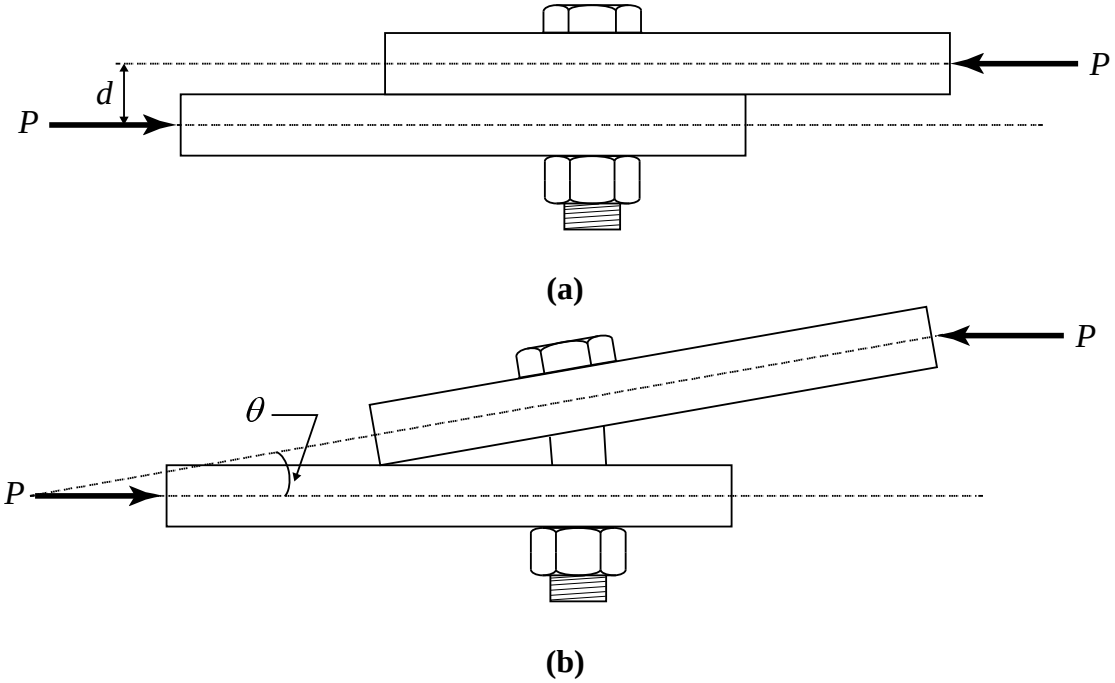

Figure 4.4: Prying action in a lap joint.

Because the test system will inherently introduce both tension and shear into the bolt, it is important to control the amount of tension introduced into a test. Researchers [4, 8] have found that 20 to 30% tensile stress in the bolt has minimal effect on the shear capacity of the bolt. To minimize the tension in the bolt, the test system geometry must be

designed to maintain the tensile stresses in the bolt within the elastic region and below 30% of the ultimate tensile tress.

Using the interaction equation from Figure 2.12, it is possible to estimate the tensile stress in the bolt based on the geometry of the test system and investigate the rotation that would have to occur before the prying action would significantly affect the shear capacity of the bolt. The interaction equation at rupture is,

$$\left(\frac{f_t}{f_{ut}}\right)^2 + \left(\frac{f_v}{0.62 f_{ut}}\right)^2 = 1.0 \tag{4.5}$$

where f_t is the tensile stress in the bolt and f_v is the shear stress in the bolt.

The tensile force in the bolt can be found through equilibrium. Figure 4.5 shows a free body diagram of the top plate and the bolt. The load is applied in the horizontal direction. In this scenario, the tensile stress developed in the bolt is a function of the angle of rotation, θ, of the rigid plate, the thickness of the plate, t_{plate}, the distance from the lead edge of the plate (point A) to the center of the bolt, x_1, and the distance from the trail edge of the plate to the center of the bolt, x_2.

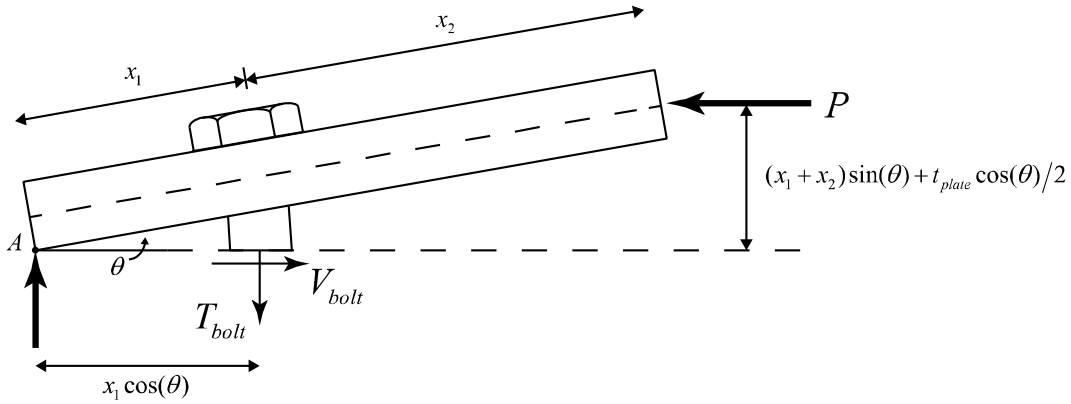

Figure 4.5: Free body diagram of bolt prying action; load applied horizontally.

From equilibrium, the shear force in the bolt, V_{bolt}, and the tensile force in the bolt, T_{bolt}, are,

$$V_{bolt} = P \tag{4.6}$$

$$T_{bolt} = P\left[\frac{t_{plate}}{2x_1} + \left(1 + \frac{x_2}{x_1}\right)\tan(\theta)\right] \tag{4.7}$$

The tensile stress in the bolt due to prying action is therefore,

$$f_t = \frac{T_{bolt}}{A_s} = \frac{P\left[\frac{t_{plate}}{2x_1} + \left(1 + \frac{x_2}{x_1}\right)\tan(\theta)\right]}{A_s} \tag{4.8}$$

where A_s is the stress area of the bolt from Equation 2.3. Likewise, the shear stress in the bolt is,

$$f_v = \frac{P}{A_b} \tag{4.9}$$

where A_b is the nominal area of the bolt, assuming that the threads are excluded from the shear plane. Substituting Equations 4.6 and 4.7 into Equation 4.5 yields,

$$\left(\frac{P\left[\frac{t_{plate}}{2x_1} + \left(1 + \frac{x_2}{x_1}\right)\tan(\theta)\right]}{f_{ut}A_s}\right)^2 + \left(\frac{P}{0.62f_{ut}A_b}\right)^2 = 1.0 \tag{4.10}$$

Equation 4.8 can be solved for P, the load required to fracture the bolt for a given geometry at a given angle of rotation. The tensile stress in the bolt as a percentage of the ultimate tensile stress can be determined by substituting the fracture load, P, into the tension component of the stress,

$$\%\, Tensile\ Stress = \frac{f_t}{f_{ut}}\% = \frac{P\left[\frac{t_{plate}}{2x_1} + \left(1 + \frac{x_2}{x_1}\right)\tan(\theta)\right]}{f_{ut}A_s} \times 100 \tag{4.11}$$

Figure 4.6 shows the tensile stress in the bolt as a percentage of the ultimate tensile stress for different geometries of the test system at varying rotation angles. The thickness of the plate significantly influences the tensile stress in the bolt. With the thickness of the plate equal to double the distance from the lead edge of the plate, nearly 40% tensile stress is introduced into the bolt from test system geometry alone. The location of the bolt in the plate, or ratio of x_2 to x_1, also influences the tensile stress induced in the joint. A larger ratio of x_2 to x_1 increases the rate that the tensile stress in the bolt increases with an increased rotation angle. From this analysis, it is evident that a bolt location more towards the center of the shear plate, combined with shear plates as thin as possible, reduces the tension in the bolt due to the geometry.

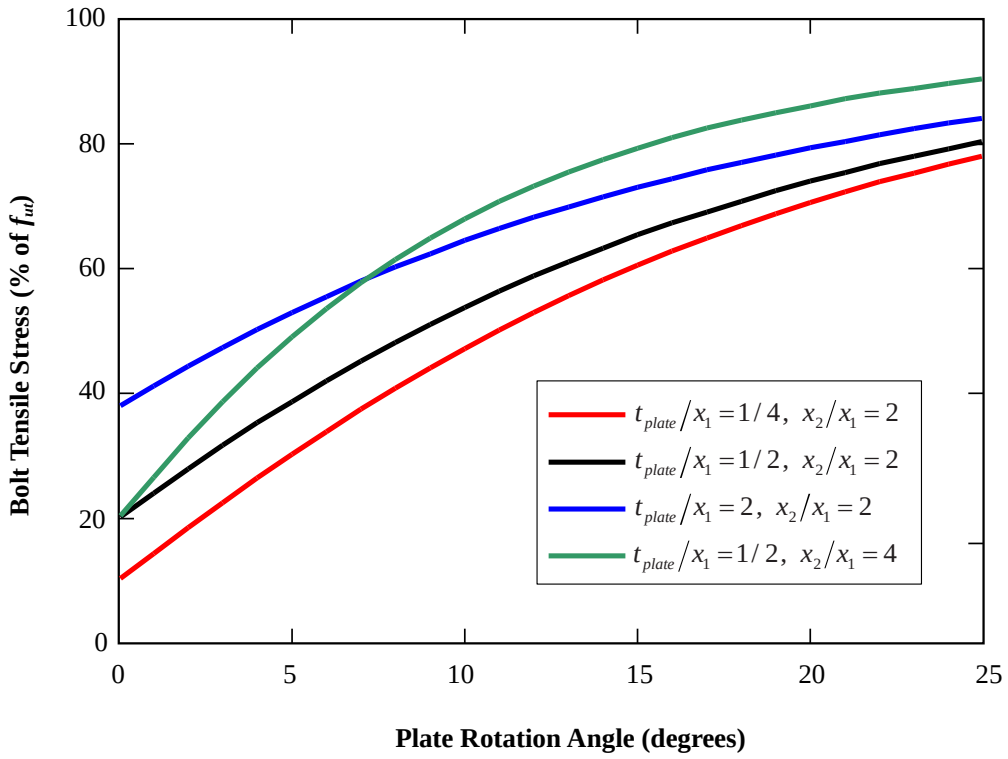

Figure 4.6: Bolt tensile stress versus rotation angle for various system geometries.

In a static test, it is possible to reduce the influence of plate rotation by directing the force along the axis of the plate as shown in Figure 4.7. The introduction of a universal joint directs the load, P_R, along the axis of the plate, generating a vertical and horizontal component of the load. From equilibrium and by inspection, the additional tension in the bolt from the angle of inclination is zero. The tensile force in the bolt is therefore reduced to the first term in Equation 4.7,

$$T_{bolt} = P\left(\frac{t_{plate}}{2x_1}\right) \tag{4.12}$$

In this case, the only tensile stress in the bolt is the stress from the geometry of the test system. However, the actual load on the bolt will be higher than measured depending on the placement of the load cell (in front of or behind the universal joint).

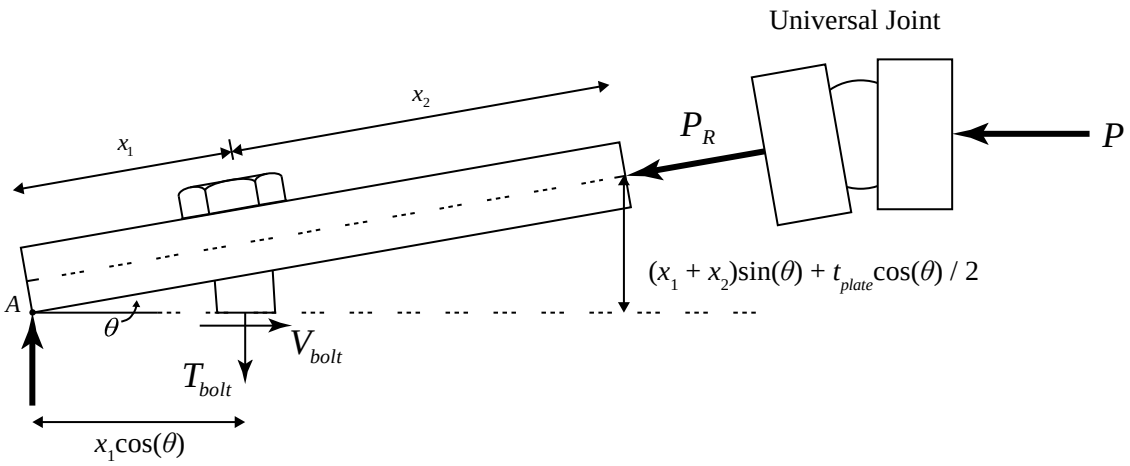

Figure 4.7: Free body diagram of bolt prying action; load applied with universal joint.

Figure 4.7 represents an ideal system and rotation is likely to occur due to eccentricities in the system. Any angle of rotation will introduce additional tensile stresses in the bolt due to the deformation of the bolt. Therefore, for both the dynamic and static

tests, it essential to measure the rotation in the impact shear plate to determine the level of tension in the bolt and how significantly it influences the measured shear capacity.

4.1.2 Finite Element Model of Dynamic Shear Experimental Test System

A finite element model was developed to design and determine the efficacy of the experimental test system. Specifically, the objectives of the finite element model were to: 1) validate the MDOF model of the system and confirm load cell instrumentation scheme; 2) determine the feasibility of the experimental test system to induce the necessary shear impulse to cause permanent deformation in the bolt; and 3) evaluate design decisions, including geometry and materials for the components of the test system.

An initial, simplified model of the setup was used to address the first objective while a more detailed model was used for the second and third objectives. In both the simplified model and the detailed model, the mesh was generated using XYZ Scientific Applications' True*Grid* mesh generation software package [11] and the dynamic analysis was conducted using LS-DYNA's explicit solver [1].

4.1.2.1 Initial Finite Element Model and Results

The initial finite element model geometry was a simplification of the test system. Figure 4.8 shows isometric and elevation views of the mesh as well as the specimen bolt. Major parts in the initial model are the reaction T-section, impact T-section, mounting plate, load cells, and a specimen bolt-nut-washer system. The impact T-section and reaction T-sections also include angle sections on the top and bottom of the shear plates. The use of angles in the T-sections is to allow the shear plates to be changed for different specimens or different materials. Table 4.1 shows the dimensions of the model parts. The

T-sections are symmetrical. Initial dimensions of parts were estimated based on physical constraints of the test area, availability of materials, and engineering judgment.

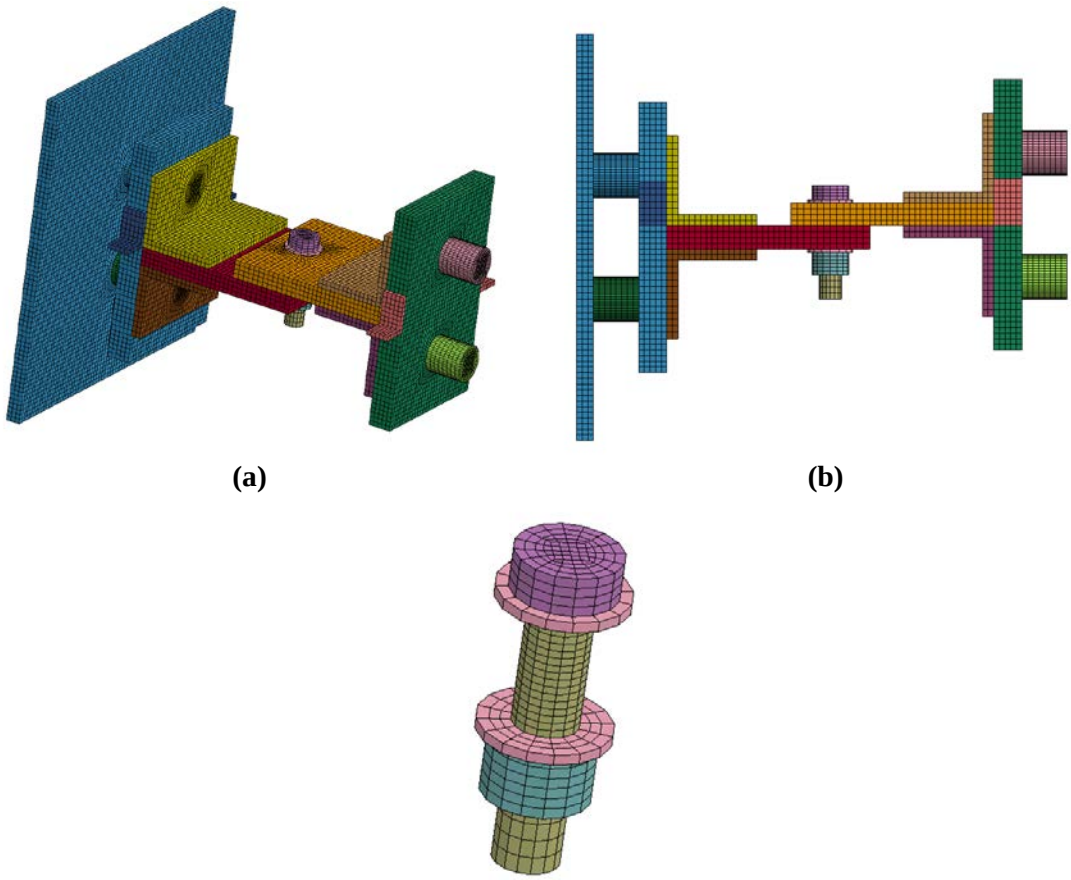

(a) **(b)**

(c)

Figure 4.8: Initial finite element model: **(a)** isometric view; **(b)** elevation view; and **(c)** specimen bolt.

Parameters in the initial model were intentionally simplified as much as possible. All components were modeled with single integration, constant stress solid elements. All nodes between parts were merged to minimize contact surfaces. Contact surfaces were only used between the two shear plates and between the specimen bolt and the shear plates. In the model, *CONTACT_AUTOMATIC_NODES_TO SURFACE was used to separate

those parts in contact. The only boundary condition in the model was the rear face of the mounting plate, in which all nodes were fixed in all degrees of freedom. Friction or any bolt pretension was not considered in the model.

Table 4.1: Initial model part dimensions.

Model Component	**Dimensions** in (cm)	**Mesh Size** in (mm)
Mounting Plate	18 x 18 x 3/4 (45.7 x 45.7 x 1.91)	1/4 (6.35)
T-section Flange	8 x 12 x 1 1/4 (20.3 x 30.5 x 3.18)	1/4 (6.35)
Shear Plate	8 x 9 x 1 (20.3 x 22.9 x 2.54)	1/4 (6.35)
T-section Angle	4 x 4 x 8 x 1/2 (10.2 x 10.2 x 20.3 x 1.27)	1/4 (6.35)
Load Cell	Ø 2 x 2 (5.08 x 5.08)	≥ 1/8 (3.175)
Specimen Bolt	Ø 1 x 4 1/4 (2.54 x 10.8)	≥ 1/8 (3.175)
Bolt Hole Diameter	Ø 1 3/32 (2.78)	-
Bolt Distance from Edge	1 3/4 (4.45)	-

LS-DYNA material model, *MAT_PIECEWISE_LINEAR_PLASTICITY, for A572, Grade 50 steel was used for all parts in the model. This material model is an elastic-plastic material model with strain rate dependency [1] that was developed by Karagozian & Case based on experimental data [9].

Finally, a simplified blast pressure-time history was applied directly to the load cells. The simplified blast pressure-time history consisted of an instantaneous peak pressure followed by a linear decay. Typical loads were approximately 6,000 psi (41.37 MPa) applied over one millisecond. Force in the load cells and in the shear plates was determined by averaging the resulting stresses over the area of a section at the center of either the load cells or the shear plate using *DATABASE_CROSS_SECTION_SET_ID in LS-DYNA. Because multiple load cells were used on both the impact side and the

reaction side of the system, the total force-time history is found by summing the load cells together,

$$F(t) = \sum_{i=1}^{n_{LC}} F_i(t) \tag{4.13}$$

where n_{LC} is the total number of load cells on either the impact side or the reaction side of the system.

Figure 4.9 shows the results from a typical simulation of the test system using the initial model. In the simulation, a blast pressure of 6,366 psi (43.89 MPa) peak pressure applied over an area of 6.3 in^2 (40.6 cm^2), equivalent to the area of two load cells, decaying over 0.8 msec was applied to the system. The resulting force time histories are plotted on the left, and the velocity of the impact T-section, the only part free to move in the system, is plotted on the right.

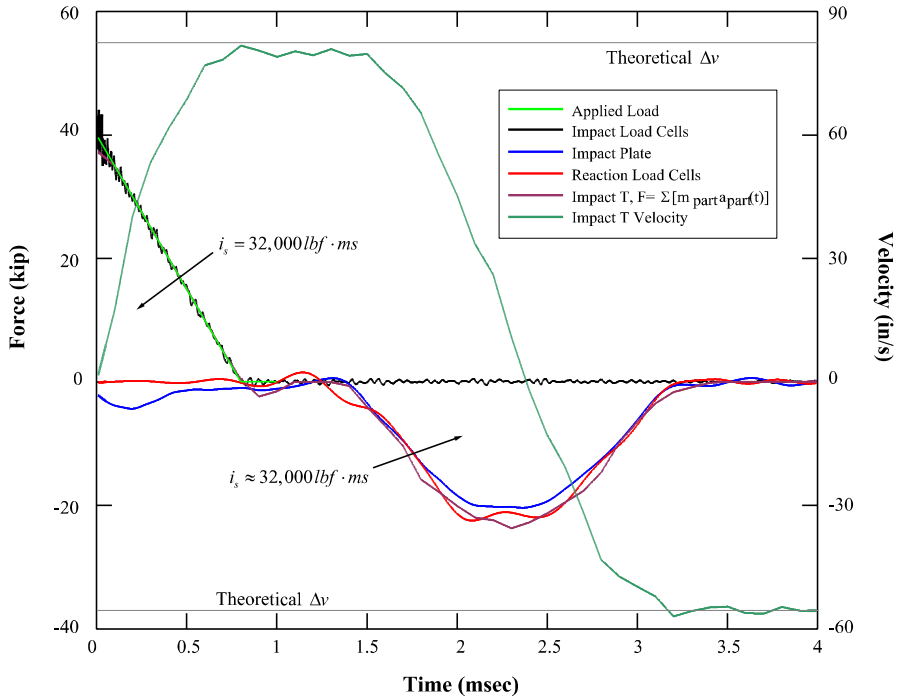

Figure 4.9: Initial model simulation results.

As the blast load is applied to the setup, the impact T-section is accelerated it reaches a constant velocity. At this point the impact T-section is in "free flight" as it is not in contact with the bolt due to the tolerance in the bolt hole. The theoretical change in velocity can be determined by,

$$\Delta v = \frac{1}{m}\int_0^{t_D} F(t)dt \tag{4.14}$$

where m is the mass of the impact T-section, t_D is the duration of the load, and $F(t)$ is the force time history of the applied load. The impact T-Section engages the bolt, decreasing in velocity, and rebounds in the opposite direction. The change in velocity can again be calculated using Equation 4.14, but where $F(t)$ is the force-time history of the reaction load cells. Based on this analysis it was found that the simulation results very closely matched the theoretical changes in velocity, thereby confirming the SDOF model of the system.

The model also confirmed that the impact and reaction load cells measure the applied force-time history and the resulting force-time history on the bolt. From Figure 4.9, it can be seen that the impact load cells directly measure the applied impulse. In the simulation, the force of the impact T-section can be found by multiplying the acceleration-time history, $a_{part}(t)$, of each part by the mass of the part, m_{part}, and summing the resulting force-time history for all of the parts:

$$F(t) = \sum_{i=1}^{n}\left[\left(m_{part_i}\right)\left(a_{part_i}(t)\right)\right] \tag{4.15}$$

The results of this analysis match the impact load cell curve and the applied force curve. Similarly, the force-time history of the reaction load cells match the force-time history in the impact shear plate, the reaction shear plate, and the force-time history of the impact-T section. Therefore, the reaction load cells capture the impulse applied to the bolt.

Finally, the impulse measured by the impact load cells must be equal to the reaction load cells minus any losses in the system. Because of the approximated blast load applied in the simulation, the impulse measured by the impact load cells is the same as the area of a triangle. Therefore, for this simulation the following must be true:

$$i_{s,Impact} = i_{s,reaction} \tag{4.16}$$

$$\frac{1}{2} F_{peak,I} t_{D,I} = \int_{t_{A,R}}^{t_A + t_{D,R}} F_R(t) dt \tag{4.17}$$

where $F_{peak,I}$ is the peak force measured by the impact load cells, $t_{D,I}$ is the duration of the impulse measured by the impact load cells, t_A is the arrival time of impulse on the reaction load cells, $t_{D,R}$ is the duration of the impulse measured by the reaction load cells, an $F_R(t)$ is the force-time history measured by the reaction load cells. In the simulation, the impulse measured by the impact load cells is approximately equal to impulse measured by the reaction load cells.

4.1.2.2 Detailed Finite Element Model and Results

Refinement of the design of the test system occurred concurrently with the development of the initial finite element model. Once the conceptual model and the instrumentation scheme was confirmed by the initial model, a more detailed model of the test system was developed to evaluate design decisions. Figure 4.10 shows the refined concept for the experimental test system and the corresponding detailed finite element model. Details of the physical setup of the experimental test system will be further discussed in Section 4.1.3

There are several key differences between the initial model and the detailed model. The detailed model uses a flyer mass to impact the test system instead of a blast pressure loading. The detailed model includes an impact plate in front of the impact load cells to

prevent the flyer from impacting the load cells directly. Bolts designed to clamp the shear plates and to the T-section flanges are also included. Finally, shoulder bolts that support the impact plate and secure the reaction T-section to the mounting plate were added to the model.

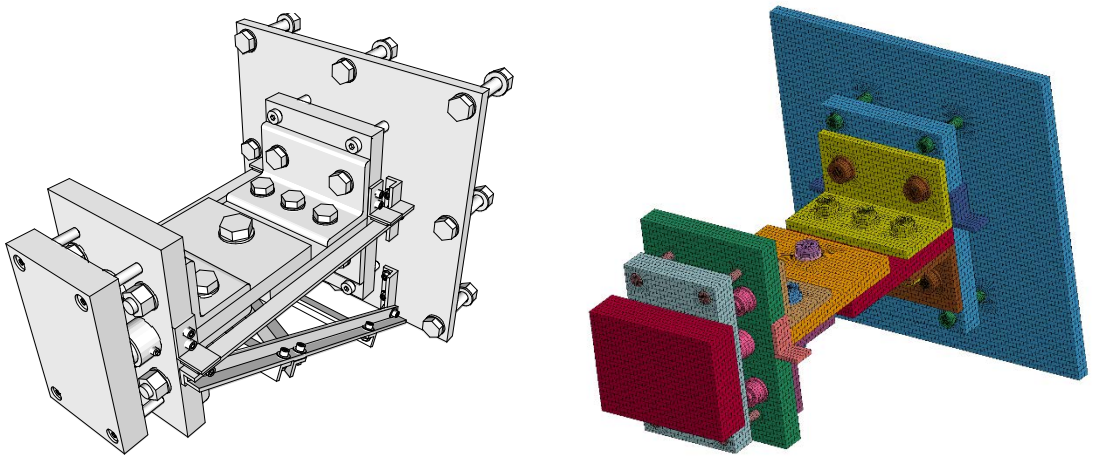

(a) **(b)**

Figure 4.10: Detailed model of test system: **(a)** test system concept; and **(b)** detailed finite element model.

The detailed model continued to use constant stress solid elements, but several more contact surfaces were added using the same methods as the initial model. In addition to the contact surfaces in the initial model, contact surfaces were added between the reaction load cells and the mounting plate, the impact load cells and the impact plate, the impact shoulder bolts and the impact plate, and the reaction shoulder bolts and the reaction T-section flange. Finally, contact surfaces were added between each of the T-section flanges and the angles. Because of the influence of the circular load cells on the mesh and the intersection of several parts with the T-section flanges, contact surfaces provided a more realistic model than trying to merge nodes. As with the initial model, friction and any

preload on the bolts were not considered. Where possible, fabrication bolts were merged with the connected components since they would be preloaded and, in theory, act as a single component.

The most significant difference between the initial model and the detailed model was the material models. In the detailed model, A572 Grade 50 steel was only used in the shear plates. Figure 4.11 shows the additional steel material models used in the detailed model. A material model was developed for the other major steel components to evaluate their performance using ASTM A36 steel, which was more economical than ASTM A572, Grade 50. LS-DYNA material model *MAT_003 (*MAT_PLASTIC_KINEMATIC) was used to model the ASTM A36 steel. This material is an elastic-plastic model with strain hardening. A static increase factor (SIF = 1.1) and a dynamic increase factor (DIF = 1.1) were included in the material model.

An attempt was made to more accurately model the bolt and bolt material. Based on load-displacement data from direct tension tests conducted by previous researchers [12, 13], a material model was developed for A325 bolts. The load and displacement data were converted to stress and strain based on information available in the literature. The LS-DYNA material model used for the A325 bolts was *MAT_024 (*MAT_PIECEWISE_LINEAR_PLASTICITY) though strain-rate effects were not considered in the material model. A conservative dynamic increase factor (DIF = 1.1) was included in the A325 bolt material model. Finally, the programmer was modeled using LS-DYNA material model *MAT_SIMPLIFIED_RUBBER_WITH_DAMAGE. This material model was developed by Friedenberg [5] and is based on experimental data.

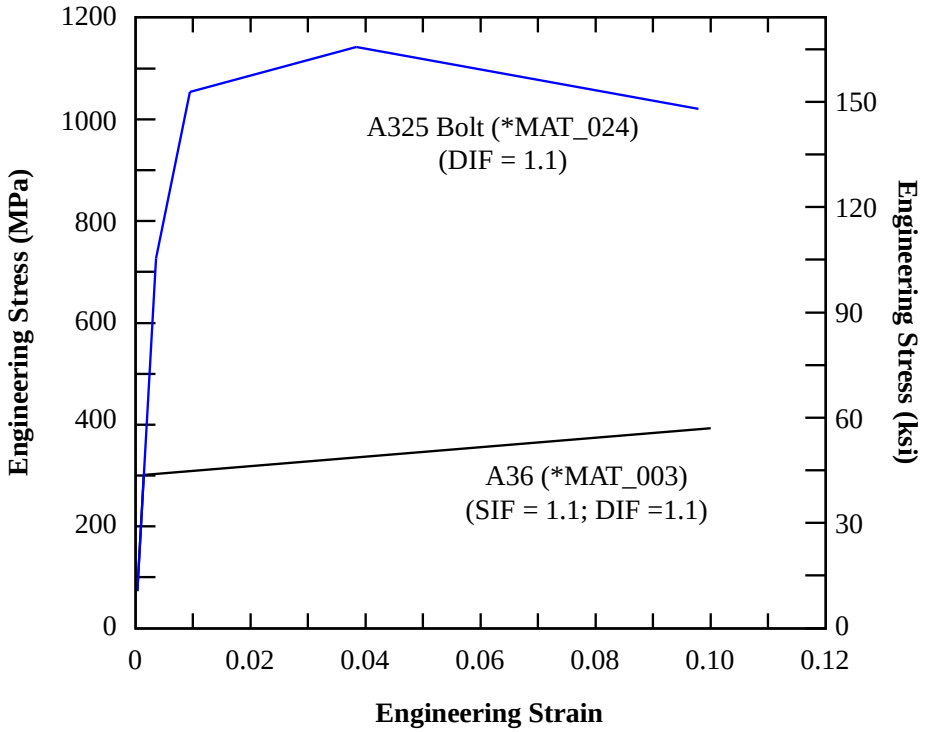

Figure 4.11: Steel material models.

Typical load cell results from simulations with the detailed model are shown in Figure 4.12(a). As in the initial model, the impact load cells measure the input impulse from the flyer mass moving at a constant velocity and the reaction load cells measure the corresponding impulse on the bolt. The impact side impulse is approximately equal to the reaction side impulse. The input impulse is characterized by a rapid peak followed by a decay. The reaction impulse is much lower in magnitude but occurs over a much longer duration.

Figure 4.12(b) shows the typical damage to the specimen bolt in the simulation. While not expected to accurately model the bolt damage, the results were used to determine the appropriate size of the flyer mass that could cause damage to or fracture the bolt and still be operated safely within the limits of the BG. Based on these results, it was

determined that a flyer mass of approximately 40 pounds (178 N) would be appropriate for bolts up to 1 1/4 inches (3.175 cm) in diameter. Hourglassing was observed in the bolt model during the simulation, however, because the model was not intended to produce precise results, hourglass controls were not included in the model.

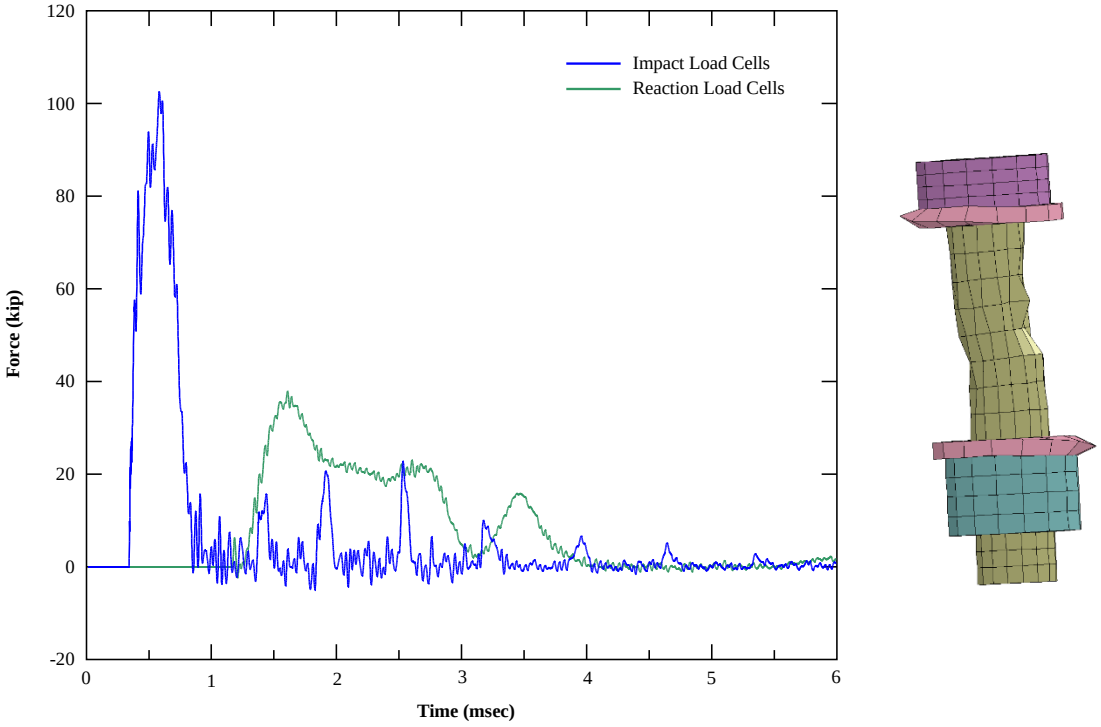

Figure 4.12: Detailed model simulation results **(a)** load cell force-time history; and **(b)** bolt damage.

Several other important design decisions resulted from the detailed model simulations. First, simulations at varying velocities indicated that higher velocities would be needed to cause damage in larger specimen bolts. Since the higher velocities generated more force in the load cells, there was concern that the capacity of the load cells would be

exceeded in testing. As a result, four additional load cells were added to the design – two on each side of the system.

Different material types and thickness were evaluated for use as the impact plate. Initial concepts intended to use steel for the impact plate, but after several simulations, it was observed that the large mass of a steel impact plate that would be stiff enough to absorb the impact of the flyer created inertial effects on the impact load cells that resulted in dissimilar readings from other tests. As a result, the material was changed to a machine grade polycarbonate that offered the necessary protection to the load cells but was significantly lighter and so did not produce the same inertial effects. The polycarbonate was modeled using *MAT_003 (*MAT_PLASTIC_KINEMATIC) based on the manufacturer's mechanical properties data sheet with static and dynamic increase factors of 1.1 each.

Finally, different materials were evaluated for the shear plates. Simulations of the A572, Grade 50 material indicated the potential for bearing failure of the plates. Results showed slight localized yielding of the shear plates with larger bolts at higher velocities. To prevent the localized yielding, other materials were considered, including A514 steel (f_y = 100 ksi), hardened tool steels, and inserts of high-strength materials into the bolt hole. However, based on the uncertainty in the bolt material model and the relative certainty of the calibrated A572 Grade 50 model, it was decided to continue with A572 Grade 50 steel for validation and calibration testing.

The detailed model was also used to investigate prying action in the bolt. Figure 4.13 shows the tensile stretch of the bolt shank, the contributions of geometry and plate rotation to the tensile stretch, and the shear displacement. Relative displacements are

shown rather than strains due to the uncertainty in the material models and the fact that the tensile stretch would actually occur in the threads and not in the shank of the bolt, which are not included in the model. Tensile displacement during the early part of the impulse is a result of the geometry of the system. Towards the end of the impulse, as the impact T-section slows, rotation of the impact T-section contributes more to the tensile displacement. From Figure 4.13 it is evident that the tensile stretch in the bolt has little influence on the shear behavior of the bolt as the displacement is relatively low when shear is at its maximum. During the rebound, when the tensile displacement is greatest, there is no longer significant shear stress on the bolt.

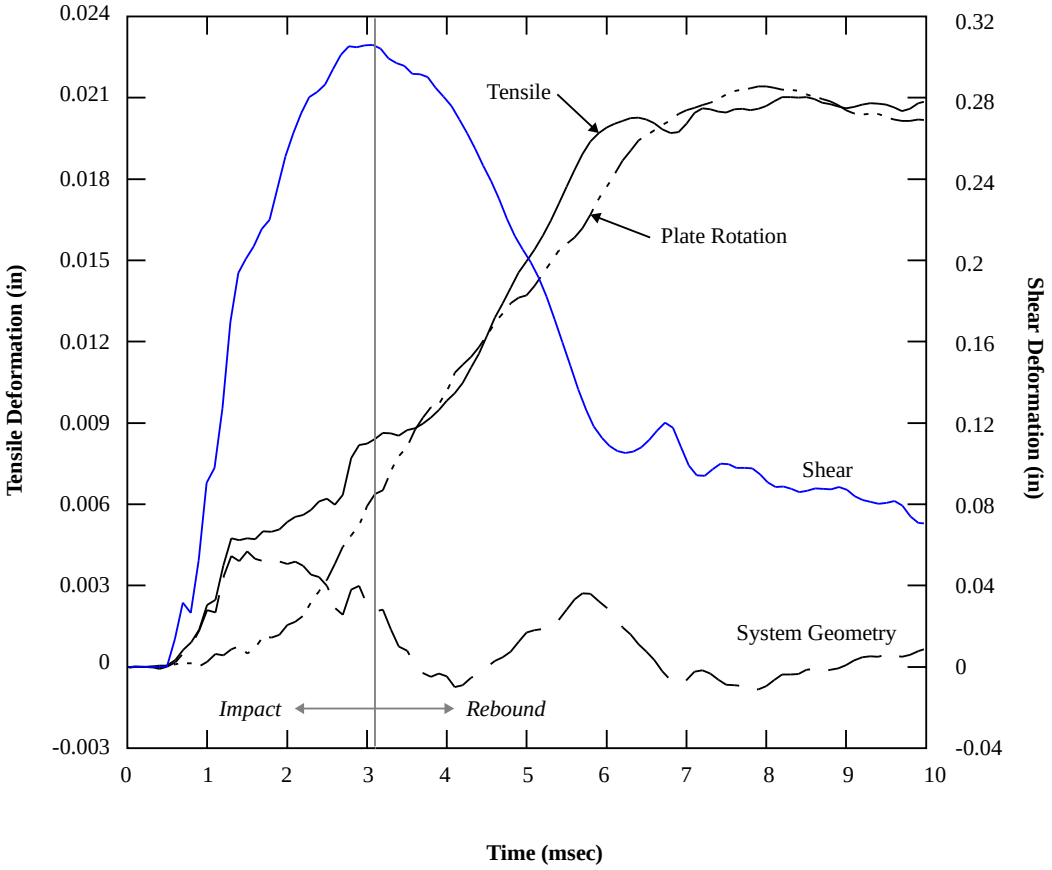

Figure 4.13: Tensile and shear deformation in specimen bolt.

4.1.3 Dynamic Shear Experimental Test System

4.1.3.1 Testing System and Components

The dynamic shear experimental test system consists of three main components: 1) the blast generator setup used to accelerate the flyer mass to a constant velocity and provide a rigid reaction to the impulse; 2) the flyer mass to impact and generate the impulse on the shear system; and 3) the shear system itself. The blast generator system is part of the Georgia Tech Blast, Impact, and Shock Laboratory while the dynamic shear system and the flyer mass were custom fabricated based on the design process previously discussed.

The blast generator system consists of a reaction wall, the BG, a custom fabricated frame and rail system, reaction blocks, and a reaction plate. Figure 4.14 shows the blast generator setup. The blast generator is mounted to a 3 feet (0.914 m) thick reinforced concrete reaction wall that is post tensioned to the laboratory strong floor and strong wall that absorbs the recoil of the BG when it is fired. The pusher plate of the blast generator is supported by a steel frame and rail system. The rail systems also serve to guide the flyer mass towards the specimen. The dynamic shear system is mounted to a 4 feet by 4 feet by 3 inches thick (122.9 x 122.9 x 7.6 cm) ASTM A36 steel reaction plate. The plate has various bolt holes to allow mounting different specimens to the plate. The reaction plate is in turn mounted to four or five reinforced concrete reaction blocks by 1 1/4 inch (3.2 cm) DYWIDAG post-tensioning bars. Each reaction block is 10 feet long, 6 feet deep, and 2 feet thick (3.1 x 1.8 x 0.61 m) and weighs approximately 18,000 lbs (8,200 kg). The reaction blocks are post-tensioned to laboratory's strong floor system using a DYWIDAG post-tensioning system.

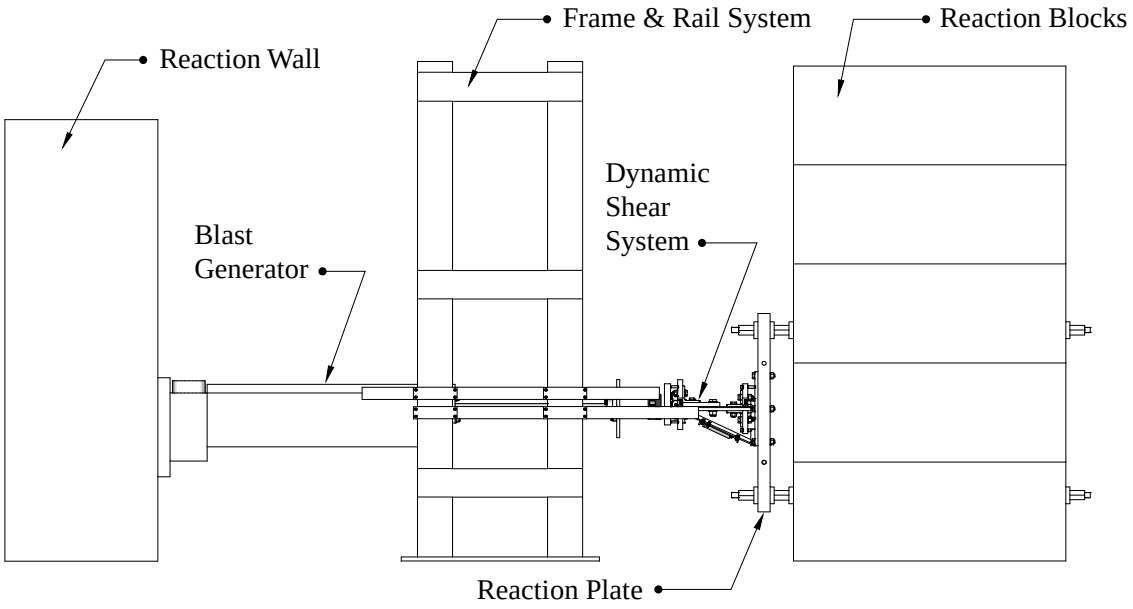

Figure 4.14: Blast generator setup schematic.

The flyer mass is a custom designed and fabricated impactor, consisting of an 8 inch by 6 inch by 2 inch thick (20.3 x 15.2 x 5.1 cm) ASTM A36 steel plate. Figure 4.15 shows a schematic of the flyer system. The total mass of the flyer is 38.0 pounds (17.2 kg). Fabrication drawings for the flyer mass can be found in Appendix A. The flyer mass is designed to move along the BG rail system. Welded to sides of the flyer are hollow square tube wings that enable the flyer to rest on the BG rail system at the appropriate level to impact the dynamic shear test system at the impact T-section center of mass. Steel C-channel rail guides that provide stability to the flyer as it is accelerated are bolted to the end of the flyer wings. Commercially available 1/8 inch (3.2 mm) thick phenolic is used to reduce friction along the rails.

A bumper plate is attached to the rear of the flyer with self-locking mushroom head fasteners. Made of abrasion resistant polyurethane rubber with a durometer of 95A, the bumper plate allows the flyer to be mounted flush to the pusher plate prior to testing.

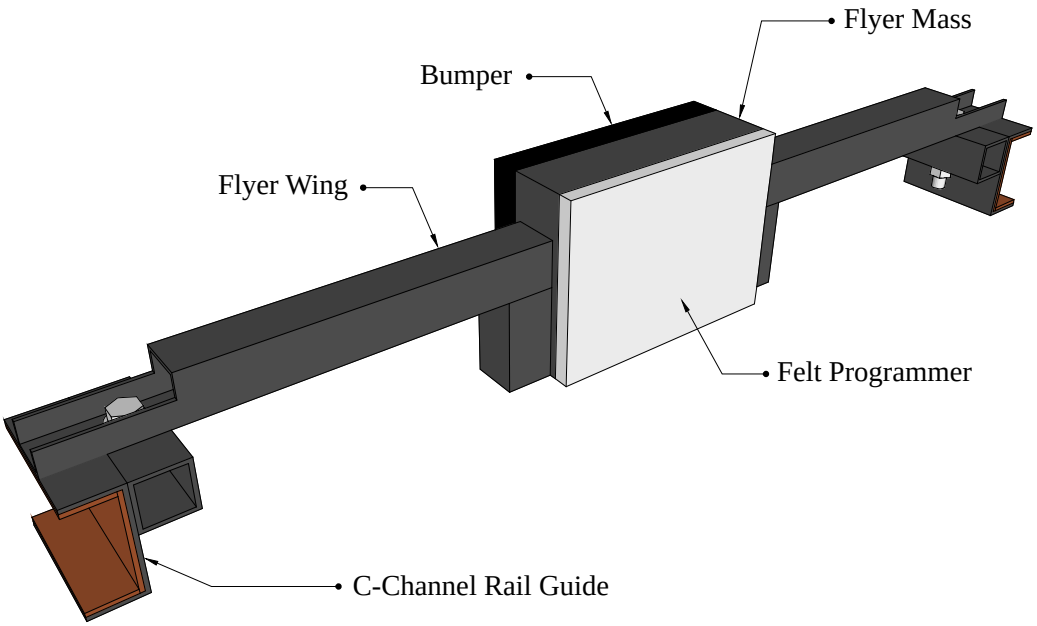

Figure 4.15: Dynamic shear flyer mass schematic.

On the front of the flyer is a programmer consisting of 1/2 inch (12.7 mm) thick, medium density, F5 pressed felt with a durometer of 25A. Through experimentation with different types of programmers, it was found that F5 felt provided the best pulse shaping characteristics.

The dynamic shear test system is comprised of a mounting plate, an impact T-section, reaction T-section, rail system, and the specimen. The impact T-section and the reaction T-section are symmetrical. Figure 4.16 shows a schematic of the dynamic shear test system in isometric and elevation views. Figure 4.17 shows the fabricated and assembled dynamic shear test system with the flyer mass just prior to testing. Detailed fabrication drawings can be found in Appendix A. Table 4.2 shows the mass of the various components of the experimental setup after all machining and fabrication was complete. Components were weighed on a calibrated Ohaus CD-11 industrial scale with a precision of 0.01 lbm (4.5 g).

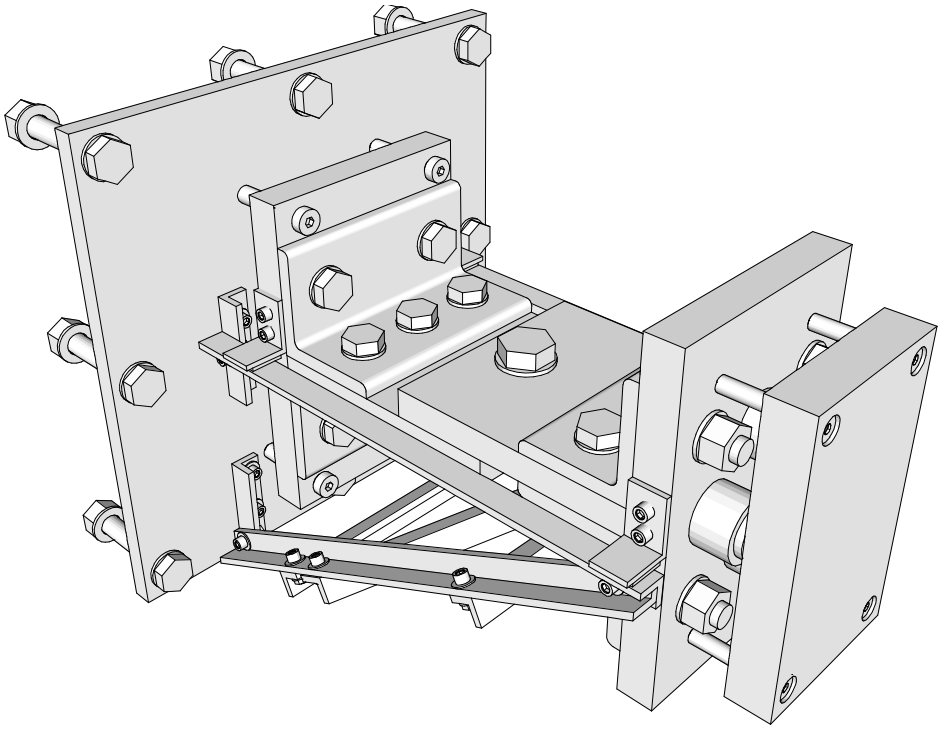

(a)

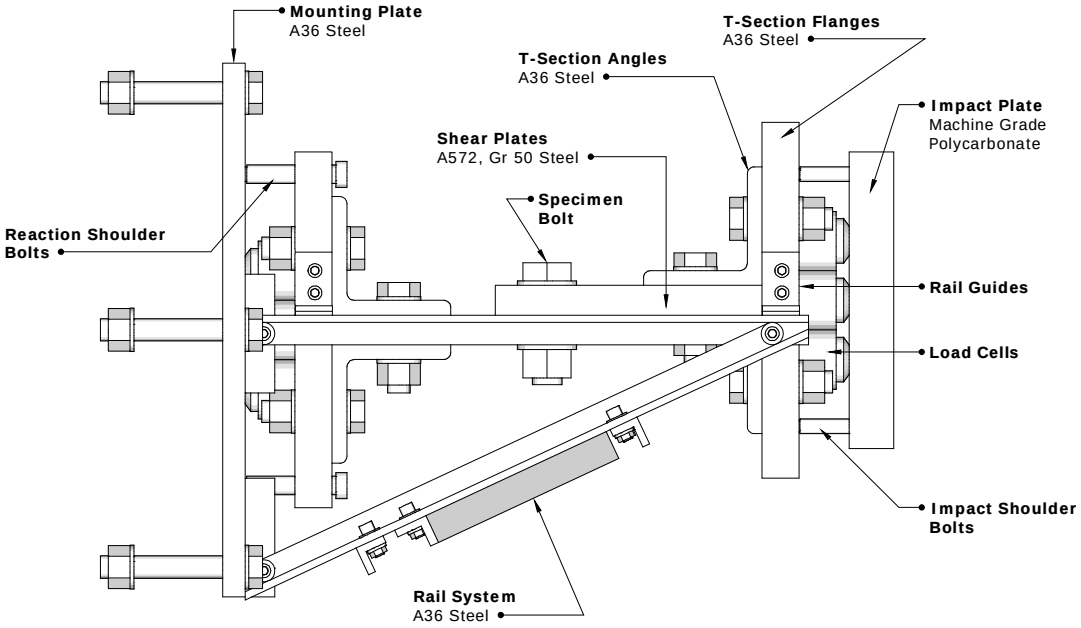

(b)

Figure 4.16: Dynamic shear test system detail **(a)** isometric; and **(b)** elevation.

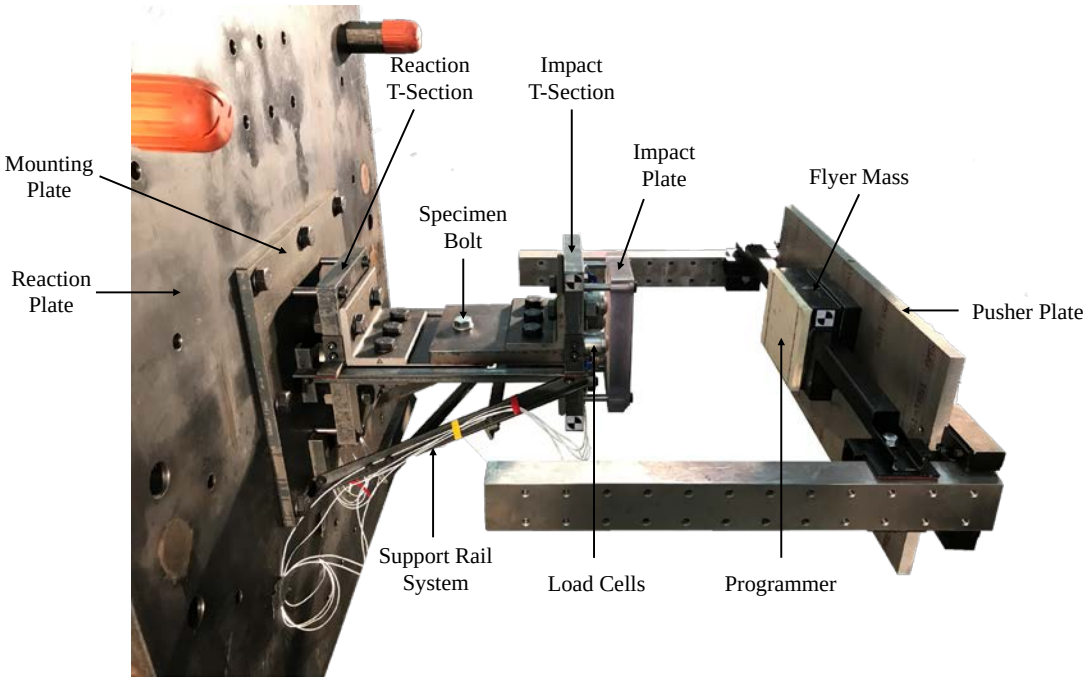

Figure 4.17: Dynamic shear test system setup prior to testing.

Table 4.2: Mass of setup components.

	Mass (lbm)	**Mass (lbf·s^2/in)**	**Mass (kg)**
Flyer Mass†	39.35	0.102	17.85
Impact T-Section	74.65	0.193	33.86
Load Cell (each)	1.2	0.003	0.54
Impact Plate	3.9	0.010	1.77
Shoulder Bolts	0.2	0.001	0.09
Reaction T-Section	74.55	0.193	33.81

†Includes flyer, programmer, flyer wings, and C-channel rail guides.

The impact plate provides a surface for the flyer mass to make contact with the load cells on the impact side of the system. It is a 1 1/2 inch (3.81 cm) thick machine grade

polycarbonate plate that provides high-strength, stiffness, and impact resistance. The impact plate is attached to the impact T-section by four 1/2 inch (12.7 mm) steel shoulder bolts. The shoulder bolts attach the impact plate to the impact T-section and allow the plate to freely translate in the direction of the impulse. The translation of the impact plate along the shoulder bolts enables the load cells to measure the force-time history. On the reaction side, 5/8 inch (15.8 mm) shoulder bolts secure the reaction T-section directly to the mounting plate. Synthetic grease was applied to all shoulder bolts to reduce friction. The mounting plate is attached to the reaction plate of the BG system with 3/4 inch (19.1 mm) A325 bolts.

Both T-sections consist of four main components: 1) a T-section flange; 2) two T-section angles; 3) a shear plate; and 4) two rail guides. The T-section flange is a 1 1/4 inch (3.18 cm) thick ASTM A36 steel plate. The 1 inch (12.7 mm) thick ASTM A572, Grade 50 shear plate is attached to the T-section flange by two 1/2 inch (12.7 mm) thick ASTM A36 steel angles. Three 3/4 inch (19.1 mm), A325 bolts secure the shear plate to the angles and two 3/4 inch (19.1 mm), A325 bolts secure the angle to the flange. All of the bolts were tightened to 70% of the proof load to ensure full contact and slip resistance. Contact surfaces between the shear plates were treated with synthetic grease to reduce friction. Rail guides on each side of the T-section flange help support the weight of the T-sections. Each rail guide is fabricated from 1/4 inch (6.35 mm) thick ASTM A36 steel angle and has a phenolic pad on the bottom to reduce friction.

The rail guides attached to the T-sections rest on a support rail system fabricated from 1 inch by 1 inch by 1/4 inch (2.54 x 2.54 x 0.64 cm) thick ASTM A36 angles. The components of the rail system are bolted together and then bolted to the mounting plate.

The support rail system is a simple truss and is designed to ensure the system remains level throughout the test. To reduce friction, the top rail surface was sanded, cleaned and coated with a commercially available Teflon spray. Synthetic grease was then applied to the surface in an effort to further reduce friction.

Specimens for the first series of dynamic shear test consisted of 3/4 inch (19.1 mm) A307 and A325 bolts. While bolts were initially used in the test system, the system is designed with bolted shear plates such that they can be quickly removed and replaced with shear plates of different materials or with different diameter holes to allow for testing of other types of specimen. The system can be used to test dynamic shear for any bolt, pin, rod, or dowel.

The system geometry was found to be adequate in terms of reducing the amount of tension into the specimen bolt. The 1 inch (2.54 cm) shear plates (t_{plate}) are 9 inches (22.9 cm) long ($x_1 + x_2$) and the distance from the lead edge of the impact shear plate to the center of the bolt hole is 1 3/4 inches (4.45 cm) (x_1). Substituting these values into Equation 4.10 yields 22% tensile stress (f_t/f_{ut}) with no rotation in the plate. Rotations of up to 1.1 degrees are allowed before the tensile stress exceeds levels that will significantly reduce the measured shear capacity of the bolt.

4.1.3.2 Instrumentation

The main instrumentation scheme for the dynamic shear test system consists of dynamic load cells and high-speed video. A total of eight Dytran 1061V6 piezoelectric dynamic force sensors are used to measure the force-time history of the event. Each load cell has a maximum compressive capacity of 50,000 lbf (222 kN) and 10,000 lbf (44 kN) in tension and is equipped with a Dytran 6217 steel impact cap. Four of the load cells are

attached to each T-section flange using supplied 1/2 inch (12.7 mm) long, 3/8 inch (9.53 mm) diameter mounting studs. Figure 4.18 shows the typical installation of the load cells on the T-section flange. The load cells are arranged in a diamond pattern at the 12, 3, 6, and 9 o'clock positions. The loads cells are installed on their respective center of mass axis of the T-section.

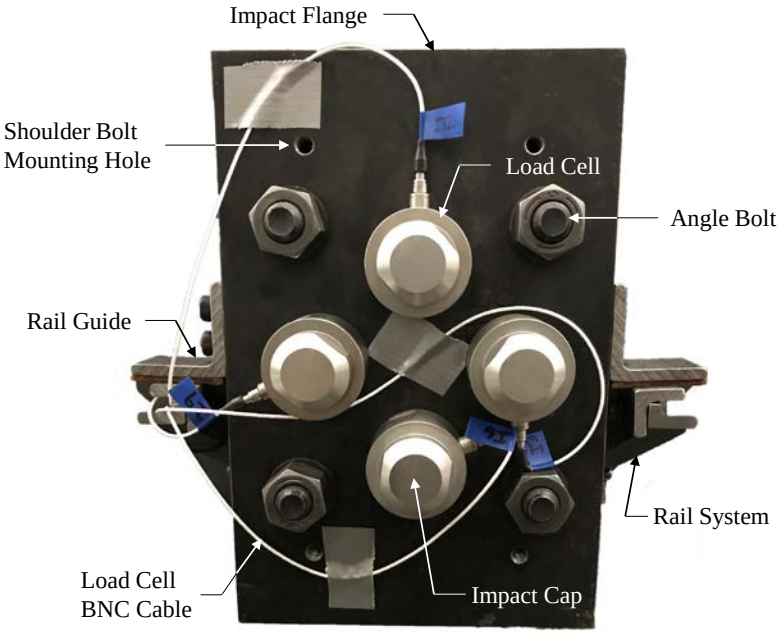

Figure 4.18: Typical load cell installation.

To obtain the total force-time history, the measurements from the load cells on each side of the system are combined,

$$F(t) = \sum_{i=1}^{4} F_i(t) \tag{4.16}$$

where $F_i(t)$ is the individual load cell data on either the impact or the reaction side. The impact side load cells measure the force-time history of the input impulse and the reaction

side load cells measure the force-time history of the impulse on the specimen bolt. The load cells are connected by standard BNC cables to the data acquisition system.

Two high-speed video cameras are used to capture the dynamic event. One camera is used to capture the motion and impact of the flyer and the other camera captures the dynamic event at the bolt. A Phantom Miro M310 high-speed camera is used to capture the motion of the flyer. This camera is capable of recording at 3,200 frames per second at a resolution of 1280 x 800. A Phantom Miro C110 capable of 1,200 frames per second at a resolution of 1280 x 720 is used to capture the dynamic impact at the bolt. Settings for the cameras are controlled through the Phantom Camera Control application (PCC v2.8) [2]. Custom targets are used to track the motion of key aspects of the test system throughout the dynamic event, which are then analyzed using Xcitex's ProAnalyst software package [3].

Though not directly part of the system's instrumentation scheme, the blast generator's internal system also records various aspects of the system, including displacement-time history of the pusher plate and various pressures within the system. The displacement-time history is used to validate the velocity of the flyer measured by the Phantom Miro M310 and confirm the predicted performance of the blast generator.

4.1.3.3 Data Acquisition

Data from the load cells are recorded using a Synergy Hi-Techniques data acquisition system (DAQ). The DAQ is a self-contained, standalone chassis capable of recording data for up to 16 input channels at 2 million sweeps per second on each channel. The DAQ features a 200-kHz analogue filter for each channel. For this system, data were recorded at 1 million sweeps per second with a total sweep length of 200 msec.

Data from the Phantom cameras are recorded directly to the camera's internal memory. The data are then saved for analysis through the PCC application. For this system, data were recorded at the highest possible rates and resolution. The flyer motion was captured at 3,200 frames per second with a resolution of 1280 x 800 and the specimen bolt was captured at 1,200 frames per second with a resolution of 1280 x 720.

Both the DAQ and the Phantom cameras begin recording data based on a trigger from the BG controller. Upon firing the BG, a voltage trigger signal is sent to the DAQ and to each camera via standard BNC cables. The DAQ records 5% pre-trigger data and the camera begins recording upon receiving the trigger signal.

For tests where the bolt's residual capacity was not being tested, the bolt was removed from the setup and still photographs taken to characterize any bolt damage. For tests involving the residual capacity, still photographs of the test system were taken.

4.1.3.4 Test Procedure

Proper alignment of the dynamic shear test system with the blast generator setup and the flyer mass is critical to a successful test. The following test procedure is used to conduct a test with the dynamic shear test system:

1. Prepare dynamic shear test specimen and setup by applying synthetic grease to appropriate contact surfaces and installing specimen bolt to desired pretension level.

2. Align dynamic shear test system with blast generator rail system. Impact plate face should be perpendicular to the rail system.

3. Install flyer mass flush and center with the impact plate; tighten C-channel bolts.

4. Conduct blast generator safety protocols, inspections, and warmup sequence [14]. Move blast generator pusher plate to initial starting position.

5. Push flyer mass way from dynamic shear test system until flush with the pusher plate. Loosen C-channel bolts. Verify alignment of the pusher plate with the blast generator rail system.

6. Verify instrumentation settings and trigger status.

7. Execute blast generator firing sequence [14].

4.1.4 Static Experimental Test System

4.1.4.1 Testing System and Components

The static experimental test system uses the dynamic shear test rig with minor modifications to apply a quasi-static load to the bolt. To protect the dynamic load cells on the impact side, they are removed along with the impact plate and impact shoulder bolts. Additionally, ASTM A36 steel bearing blocks are inserted in between the reaction T-section flange and the mounting plate to protect the reaction load cells during the static test.

Figure 4.19 shows the details of the test rig. A W12x65 steel beam is affixed to the strong floor in the center of the blast generator's frame and rail system using DWYIDAG post-tensioning bars. This beam is installed and remains in place throughout the dynamic test. The beam 6 foot (1.83 m) beam has 1/2 inch (12.7 mm) stiffeners every 2 feet (0.61 m) along its length.

A 31 1/2 inch (0.8 m) tall steel W14x145 column that has been welded to a 1 1/2 inch (3.81 cm) thick steel baseplate is bolted to the base beam using ten 3/4 inch (19.1 mm) A325 bolts and tightened to the snug tight condition. The column has 1/2 inch (12.7 mm) stiffeners every 8 3/4 inches (22.2 cm). The column supports a 7 inch (201 cm) diameter hydraulic actuator that is controlled with a manual pump. Figure 4.20 shows the manual

pump used to operate the actuator and load the setup. Attached to the actuator is a load cell. After a dynamic test, the column, actuator, and load cell are moved into position as a single unit using a 30 ton overhead crane.

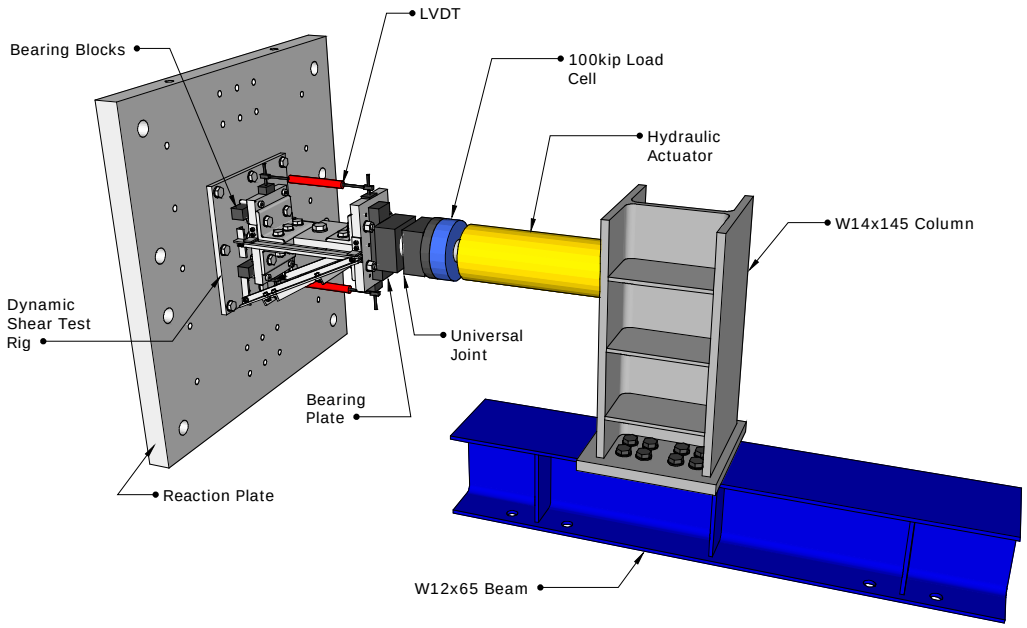

Figure 4.19: Static test system detail.

Figure 4.20: Manual hydraulic pump for quasi-static loading.

A universal joint is installed between the load cell and a bearing plate to protect the actuator piston from bending due to eccentricities and to direct the force along the plate if any plate rotation occurs. The bearing plate is a 1 1/2 inch (3.81 cm) thick by 3 inches (7.62 cm) wide ASTM A36 steel bar that allows the universal joint to apply the load directly to impact T-section flange, otherwise the T-section angle bolts would interfere with the application of the load (see Figure 4.18). The universal joint and bearing plate are installed into position by means of a small hydraulic jack. Figure 4.21 shows the completed setup with the bearing plate and universal joint being supported by the jack. The height of the jack can be adjusted so that the load is applied directly at the shear plane. Once the universal joint and bearing plate are in position, approximately 1,000 pounds (4.5 kN) of force are applied to the setup such that the universal joint and the bearing plate are held in position by the compressive force of the actuator. The jack is then lowered for the remainder of the test.

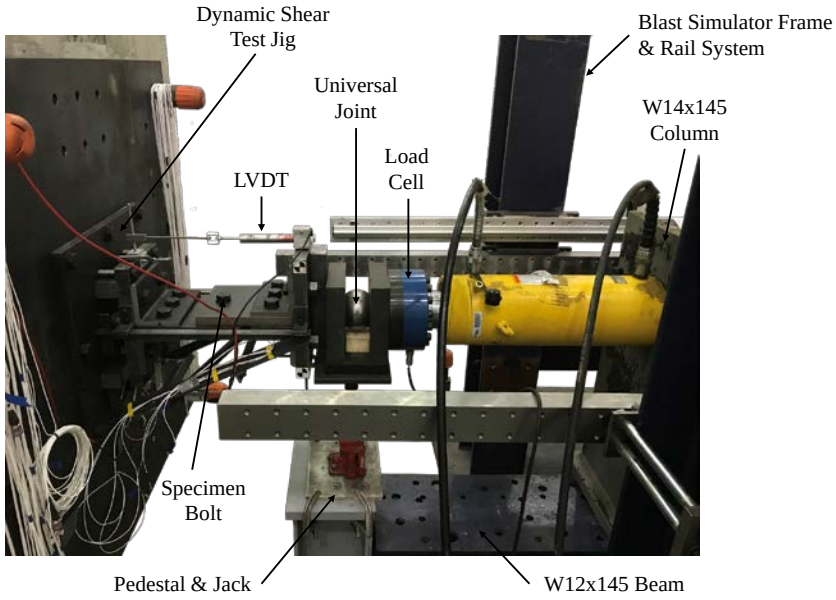

Figure 4.21: Installation of universal joint and bearing plate using a hydraulic jack.

4.1.4.2 Instrumentation

Instrumentation for the static experimental test system includes a load cell to measure the shear force applied to the bolt and two linear variable displacement transducers (LVDT) to measure the displacement of the impact T-section. The load cell is an Interface (model 1232-AF) load cell rated at 100,000 lbf (445 kN). The load cell was calibrated using the manufacturer's calibration certificate.

Two LVDTs were used to measure the displacement of the impact T-section. One was placed on the top of the impact T-section and one on the bottom. The LVDTs were aligned centerline of the T-sections. Figure 4.22 shows the installation of the LVDTs on the T-section flanges. Sheet metal U-shaped sections were fabricated to mount the LVDTs. The LVDT components were affixed to the U-shaped sections using double sided very-high-bond (VHB) tape. The U-shaped sections were then clamped to the T-section flanges using C-clamps. The required 24 VDC to power the LVDTs was provided by a BK Precision DC Power Supply, model 1711. The LVDTs were calibrated using precision gauge blocks and verified prior to each test.

4.1.4.3 Data Acquisition

Data were acquired through the National Instruments cDAQ-9178 compact data acquisition system with an NI 9237 bridge module for the load cell and a NI 9219 universal module for the two LVDTs. Figure 4.23 shows the data acquisition system and modules used in static testing. A sample of rate of 1,000S/s was used for all quasi-static tests using the arithmetic mean of the acquired signals. Incorporated into the closed loop data acquisition system was a baseline function. Initial readings were recorded and then those initial readings were subtracted from subsequent data points to provide a zeroed data set.

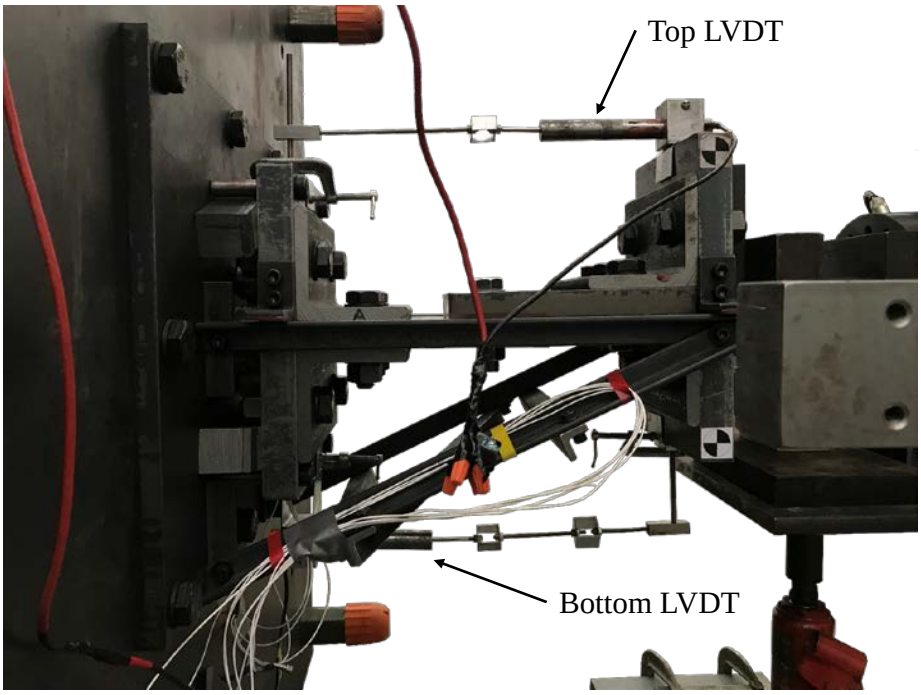

Figure 4.22: Typical LVDT installation.

Figure 4.23: Static test data acquisition system.

4.1.4.4 Test Procedure

The following test procedure is used for the static experimental test system:

1. Reconfigure dynamic experimental test system by removing the impact plate and impact load cells; install bearing blocks behind reaction T-section flange.

2. Install W14x145 column with hydraulic actuator and load cell attached. Secure to base beam with ten 7/8 in (22.2 mm) A325 bolts. Connect hydraulic pump to the actuator.

3. Install hydraulic jack and place universal joint and bearing plate in between load cell and the impact T-section flange. Raise height of jack until universal joint is at desired level.

4. Advance the actuator until the universal joint is approximately 1/8 to 1/4 inches (3.2 to 6.4 mm) from the impact T-section flange.

5. Install LVDTs, LVDT cabling, and load cell cabling.

6. Load the test system until approximately 1,000 pounds (4.5 kN). Confirm the bearing plate and universal joint are secured by the load from the actuator and lower the jack.

7. Begin testing by slowly pumping the manual hydraulic pump. Confirm readings from LVDTs and load cells. Continue applying load until bolt fractures.

4.2 Dynamic Experimental Test System Validation

A series of 27 dynamic tests were conducted to validate the dynamic experimental test system. Validation of the test system centered on achieving consistent, repeatable direct hits with the flyer mass, selection of a programmer material that provided an impulsive load curve with similar characteristics to a blast loading, and validation of the instrumentation and data collection scheme.

Table 4.3 provides a summary of the dynamic tests conducted. Nearly all of the tests were conducted with non-pretensioned, 3/4 inch (19.1 mm) A325 bolts. The last validation test was conducted with a 3/4 inch (19.1 mm) A307 bolt. Velocities varied from 5 m/s (197 in/s) to 15 m/s (591 in/s) with the majority of tests conducted in the 8 to 10 m/s (315 to 394 in/s) range. The configuration of the flyer, type of bumper, programmer and actuator initial starting position were all recorded. For each test, a qualitative observation of the impact based on high-speed video data was noted as well as any subsequent modifications to the system in preparation for the next test.

Table 4.3: Validation test summary.

Test #	Test Bolt Ø (in)	Bolt Type	Velocity (mps)	Flyer Type	Bumper	Programmer	Initial Posn. (in)	Impact	System Modification
1-01	3/4	A325	5.288	Plate	None	Neoprene (70A)	10.0	Low, near miss	Initial position forward
1-02	3/4	A325	5.700	Plate	None	Neoprene (70A)	20.0	Low	Align flyer guides
1-03	3/4	A325	5.732	Plate	None	Neoprene (70A)	26.0	Low	Higher velocity (BG stutter)
1-04	3/4	A325	10.041	Plate	None	Neoprene (70A)	22.0	Forward tilt, rolling	Flyer wing fabrication (rail mount)
1-05	3/4	A325	5.732	Rail	Center	Neoprene (70A)	26.0	Forward tilt, rolling	Move bumper down to bottom edge
1-06	3/4	A325	10.261	Rail	Bot. Edge	Neoprene (70A)	22.0	High	Move bumper up 1/2 in
1-07	3/4	A325	10.141	Rail	Bot Third	Neoprene (70A)	22.0	Slight forward tilt	Move bumper down 1/4 in
1-08	3/4	A325	10.141	Rail	Bot Third	Neoprene (70A)	28.0	Near direct hit	None
1-09	3/4	A325	10.141	Rail	Bot Third	Neoprene (70A)	28.0	Direct hit	None
1-10	3/4	A325	14.958	Rail	Bot Third	Neoprene (70A)	24.0	Direct hit	Bolt fracture; rebuild setup
1-11	3/4	A325	8.080	Rail	Bot Third	Neoprene (70A)	30.0	Forward tilt, rolling	None
1-12	3/4	A325	9.058	Rail	Bot Third	Neoprene (70A)	29.0	Forward tilt, rolling	Full bumper installation
1-13	3/4	A325	7.980	Rail	Full	Neoprene (70A)	32.0	Backward tilt, rolling	Move starting position back
1-14	3/4	A325	7.980	Rail	Full	Neoprene (70A)	30.0	Backward tilt, rolling	Move starting position forward
1-15	3/4	A325	7.980	Rail	Full	Neoprene (70A)	32.0	Backward tilt, rolling	Move starting position forward
1-16	3/4	A325	8.351	Rail	Full	Neoprene (70A)	34.0	Slight backward tilt	Install C-guides
1-17	3/4	A325	7.086	Rail w/ C	Full	Neoprene (70A)	34.0	Direct hit, mult. peaks	Shorter impact shoulder bolts
1-18	3/4	A325	7.086	Rail w/ C	Full	Neoprene (70A)	34.0	Direct hit, mult. peaks	None
1-19	3/4	A325	7.086	Rail w/ C	Full	Neoprene (70A)	34.0	Direct hit, mult. peaks	None
1-20	3/4	A325	9.963	Rail w/ C	Full	Neoprene (70A)	30.0	Direct hit, mult. peaks	None
1-21	3/4	A325	9.963	Rail w/ C	Full	Neoprene (70A)	30.0	Direct hit, mult. peaks	None
1-22	3/4	A325	7.125	Rail w/ C	Full	Neoprene (70A)	34.0	Direct hit, mult. peaks	Longer impact shoulder bolts
1-23	3/4	A325	9.963	Rail w/ C	Full	Neoprene (70A)	30.0	Direct hit, mult. peaks	Remove programmer
1-24	3/4	A325	7.125	Rail w/ C	Full	None	34.0	Uneven hit (L/R)	New programmer; verify alignment
1-25	3/4	A325	7.185	Rail w/ C	Full	Felt (25A)	34.0	Direct hit	None
1-26	3/4	A325	7.185	Rail w/ C	Full	Felt (25A)	34.0	Direct hit	Change bolt
1-27	3/4	A307	5.010	Rail w/ C	Full	Felt (25A)	34.0	Direct hit	Move to residual capacity tests

4.2.1 Development of Consistent Direct Impacts

The flyer configuration had the most influence on achieving consistent direct impacts on the system. The original design of the flyer called for the flyer to be mounted directly on the pusher plate. Structural steel angles, 1/4 inch (6.35 mm) thick with phenolic pads, were bolted to the flyer and were to rest on top of 1/4 inch (6.35 mm) thick structural steel angles with phenolic pads bolted to the pusher plate. The theory was that when the actuator decelerated, the flyer would continue at the peak velocity and impact the dynamic shear test jig. Figure 4.24 shows the original flyer design and the subsequent typical resulting impact. The flyer had a tendency to move with a downward trajectory and therefore impact the test jig low. Attempts were made to move the starting position forward, adjust the alignment of the angle mounts, and increase the velocity. Based on consistently poor results, the decision was made to use the blast generator rail system to guide the flyer to the test jig.

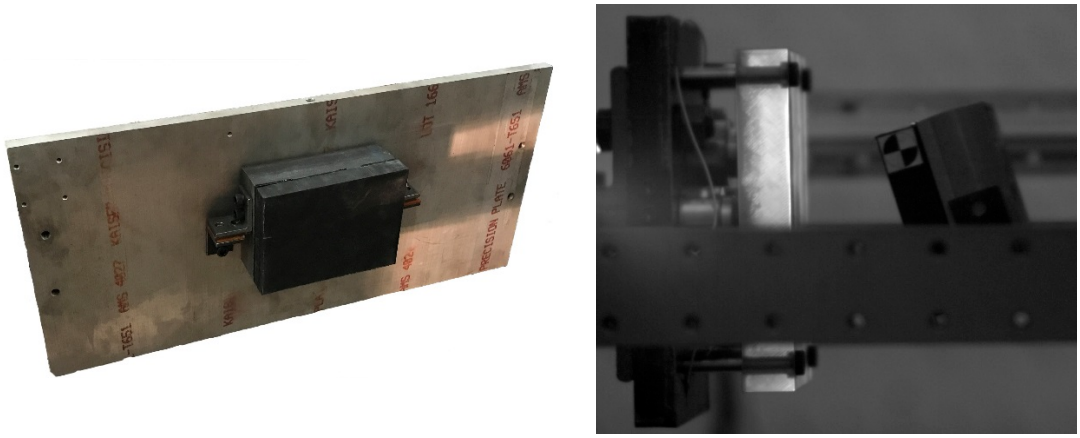

(a) **(b)**

Figure 4.24: Plate mounted flyer configuration **(a)** flyer and **(b)** typical impact.

The flyer was redesigned with the flyer wings discussed in Section 4.1.3.1. The redesign was based on development of flyers for previous, unrelated tests. The flyer wings were made from steel hollow square tube sections with guides to prevent rotation of the plate within the plane of the blast generator rail system. In order to set the flyer flush with the pusher plate at the start of the test, a 1 inch bumper was added to the back of the flyer. The bumper material was neoprene with a durometer of 70A, the same material as the programmer. Figure 4.25 shows the modified flyer with bumper plate installed.

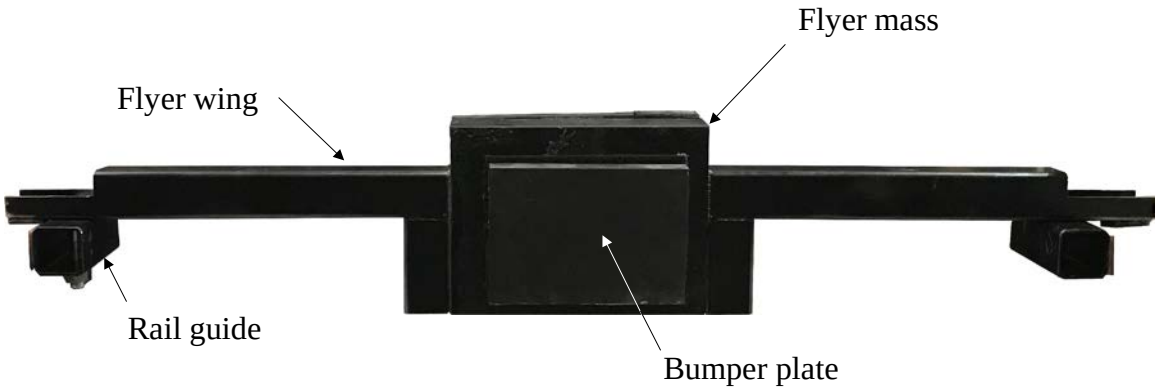

Figure 4.25: Rail mounted flyer configuration.

While this modified flyer was much improved from the plate-mounted flyer, the flyer had a tendency to rotate about the flyer wings. Figure 4.26 shows the typical rotation from the modified flyer. The rotation caused a rolling impact on the face of the impact plate, resulting in a long duration impulse that had none of the characteristics of a blast load.

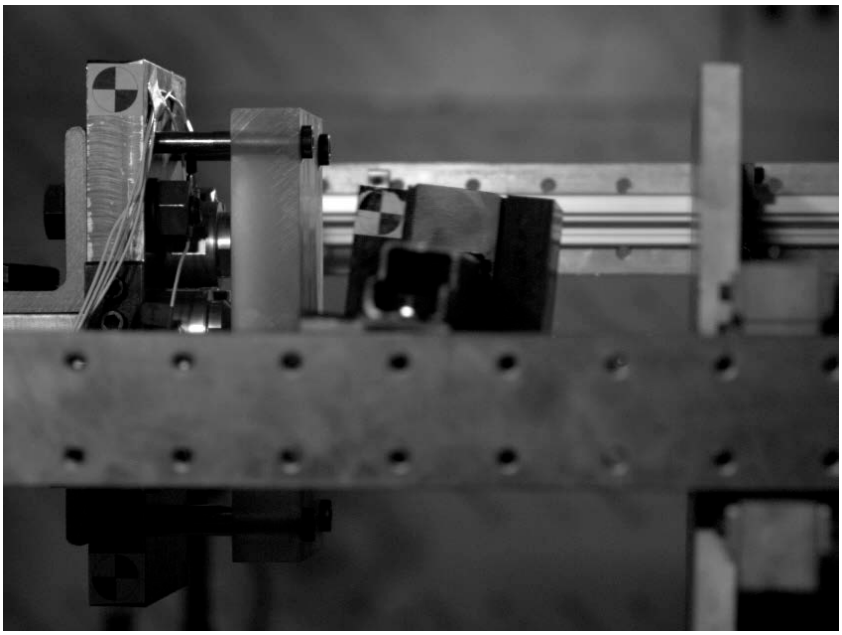

Figure 4.26: Typical flyer rotation about wings prior to impact.

It was observed that the vertical placement of the bumper plate, which was not the full face of the flyer, significantly influenced the rotation of the plate and if placed low enough, would cause the flyer to impact at an upward trajectory. By adjusting the height of the bumper, direct impacts were achieved on several tests. However, the location of the bumper needed to be adjusted for each velocity, and so it was deemed unacceptable for repeatability of the test. The replacement of the initial bumper with a full sized bumper did not prevent rotation from happening (see Figure 4.26), which was a result of an insufficient width of the flyer wings on the blast generator rails to prevent rotation. However, the addition of the C-channel rail guides prevented any further rotation and resulted in consistent, direct impacts. Additionally, the neoprene bumper was replaced with a polyurethane rubber bumper to increase the stiffness of the bumper, but no

significant difference in the impact behavior of the flyer was observed as a result of this change.

4.2.2 Programmer Material Selection and System Alignment

The shape and duration of the impulse is significantly influenced by the material and thickness of the programmer. Figure 4.27 shows the impact load cell data for three tests conducted at approximately 7 m/s with different programmer materials. All tests were conducted with 3/4 inch (19.1 mm) A325 bolts. Test 1-22 used a 1 inch (2.54 cm), neoprene programmer with a durometer of 70A. Test 1-24 removed the programmer completely and the flyer mass impacted the dynamic shear system directly. Test 1-26 used a 1/2 inch (12.7 mm) F5 felt programmer with a durometer of 25A. The data shown in Figure 4.27 was not filtered.

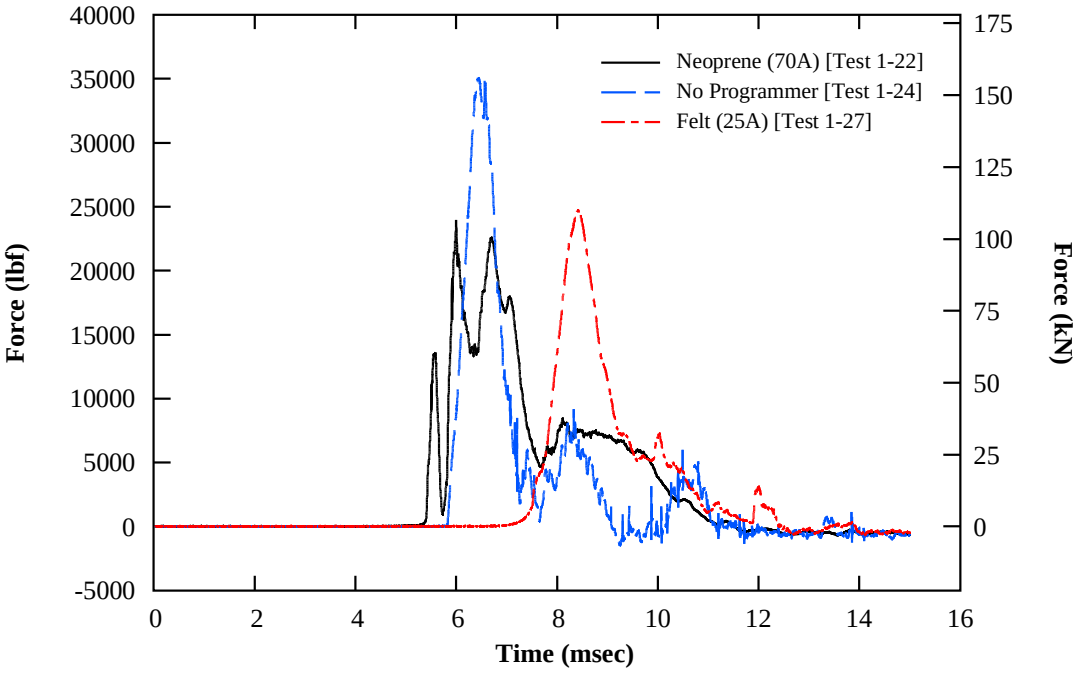

Figure 4.27: Influence of programmer material on impact impulse.

A characteristic blast curve has an instantaneous rise followed by an exponential decay. The neoprene programmer results in an impulse with multiple peaks during the rise due to the non-linear stiffness of the neoprene. When the neoprene programmer was removed, a smooth, near instantaneous rise was observed. The complete removal of the programmer for subsequent tests was not feasible as removing the programmer resulted in damage to the impact plate. Therefore, a less stiff programmer that would absorb some of the initial energy but still produce a smooth rise was needed. The felt programmer provided a near instantaneous rise without damage to the system.

Tests 1-22 and 1-24 did not exhibit an exponential decay. The exponential decay in Test 1-26 was a result of a change to the system alignment. In previous tests, the impact T-section was pulled back from the reaction T-section to allow for free flight of the impact T-section. This had the effect of reducing the bolt stiffness, k_b (discussed in Section 4.1.1.2), in the system. This resulted in a second, lower peak in the impact load cells once the bolt was fully engaged in shear. By aligning the impact T-section towards the reaction side of the system such that the test started with bolt fully engaged in bearing between the two shear plates, an exponential decay of the load curve was achieved. In Figure 4.27, this can also be observed by the time shift of Test 1-26 from Tests 1-22 and 1-24.

4.2.3 Repeatability and Instrumentation Validation

The results of Tests 1-25 and 1-26 were used to verify the repeatability of the experimental method as well as to validate the instrumentation scheme. Repeatability of the test was validated by conducting two tests on 3/4 inch (19.1 mm) A325 bolts at the same target velocity and comparing the resulting impact load cell curves and reaction load

cell curves. Figure 4.28 shows the impact and reaction load cell curves measured from Tests 1-25 and 1-26. The curves generally show good agreement in peak force measured and duration of both the input impulse to the system and the reaction.

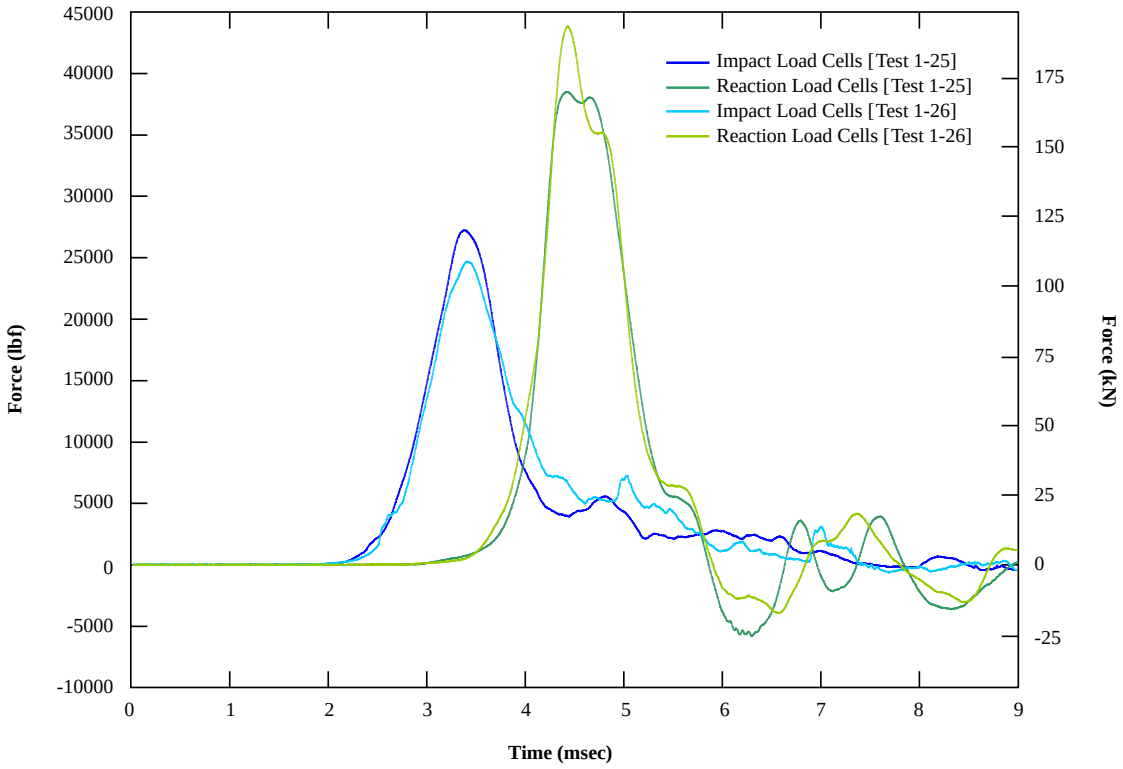

Figure 4.28: Test repeatability, Test 1-25 and Test 1-26.

The curves show that the reaction impulse is characterized by a shorter duration but higher peak force. From Equation 4.4, the following must be true for each test:

$$m_{flyer}(v_r - v_i) = \int F_I(t)dt + S_{f,I} = \int F_R(t)dt + S_{f,I} + S_{f,R} \qquad (4.18)$$

where m_{flyer} is the mass of the flyer, v_i is the initial impact velocity of the flyer, and v_r is the rebound velocity of the flyer. The test instrumentation measures the initial and rebound velocities of the flyer, the impact force time history. $F_I(t)$, and the reaction force time

history, $F_R(t)$. The mass of the flyer is recorded prior to the test. Therefore, the losses in the system due to friction or otherwise can be deduced from Equation 4.18. Table 4.4 shows the results from validation Tests 1-25 and 1-26. These tests were conducted on 3/4 inch (19.1 mm) A325 bolts with threads excluded from the shear plane. The results showed a consistent impact velocity and generally consistent behavior between the two tests. However, these tests indicated a larger impulse on the reaction side of the system than was generated by the flyer mass and was recorded by the impact load cells. Since this would indicate that energy was created in the system, this indicates the fidelity of the test measurements.

Table 4.4: Impulse measurements from Tests 1-25 and 1-26.

		Test 1-25	**Test 1-26**
Flyer Mass	Target velocity, *m/s* (*in/s*)	7.19 (282.9)	7.19 (282.9)
	Impact velocity, *m/s* (*in/s*)	7.08 (278.8)	7.09 (279.2)
	Rebound velocity, *m/s* (*in/s*)	-2.46 (-97.0)	-3.06 (-120.3)
	Measured impulse, *lbf·ms* (*kN·ms*)	37,000 (164.6)	39,350 (175.04)
Impact Load Cells	Total duration, *msec*	6.093	5.885
	Peak force, *lbf* (*kN*)	27,278 (121.3)	24,714 (109.9)
	Measured impulse, *lbf·ms* (*kN·ms*)	33,313 (148.2)	34,683 (154.3)
	% Difference from Flyer	-9.9	-11.8
Reaction Load Cells	Total duration, *msec*	2.966	3.135
	Peak force, *lbf* (*kN*)	38,519 (171.3)	43,895 (195.3)
	Measured impulse, *lbf·ms* (*kN·ms*)	40,311 (179.3)	41,963 (186.7)
	% Difference from flyer	+8.9	+6.6

The target velocity was based on a validated prediction tool for the blast generator performance. The velocity was chosen such that the specimen bolt would remain elastic. The velocity of the flyer mass before and after impact was determined using Xcitex's ProAnalyst software [3]. The user selects a feature on the video that the software processor can identify through contrasting pixels and calibrates the video with a known distance. The displacement of the feature is tracked and recorded for each time step of the video. The displacement-time history of the feature is then used to determine the velocity of the feature through direct differentiation. Figure 4.29 shows the velocity of the flyer for Tests 1-25 and 1-26. An average of the data points was determined by a linear curve fit for the impact velocity and a second order curve fit for the rebound velocity. In general, a trend in the data characterized by three to four data points at the same velocity can be seen. This velocity has been shown to agree with the predicted and measured velocity from the blast generator.

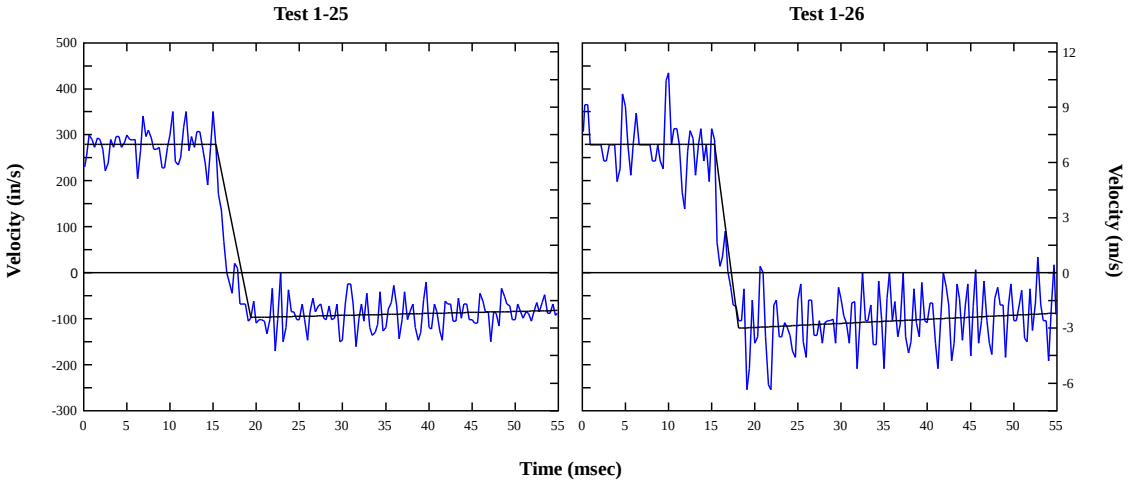

(a) **(b)**

Figure 4.29: Flyer mass velocity time history **(a)** Test 1-25 and **(b)** Test 1-26.

The impulse at the impact load cells and the reaction load cells were found through direct integration of the respective force-time histories. The duration was taken from the first non-zero point of the impulse to where the impulse leveled off, indicating no more area of force-time history curve. The impulse was taken as the maximum point of the curve. Figure 4.30 shows the force-time histories and impulses for the load cells from Tests 1-25 and 1-26.

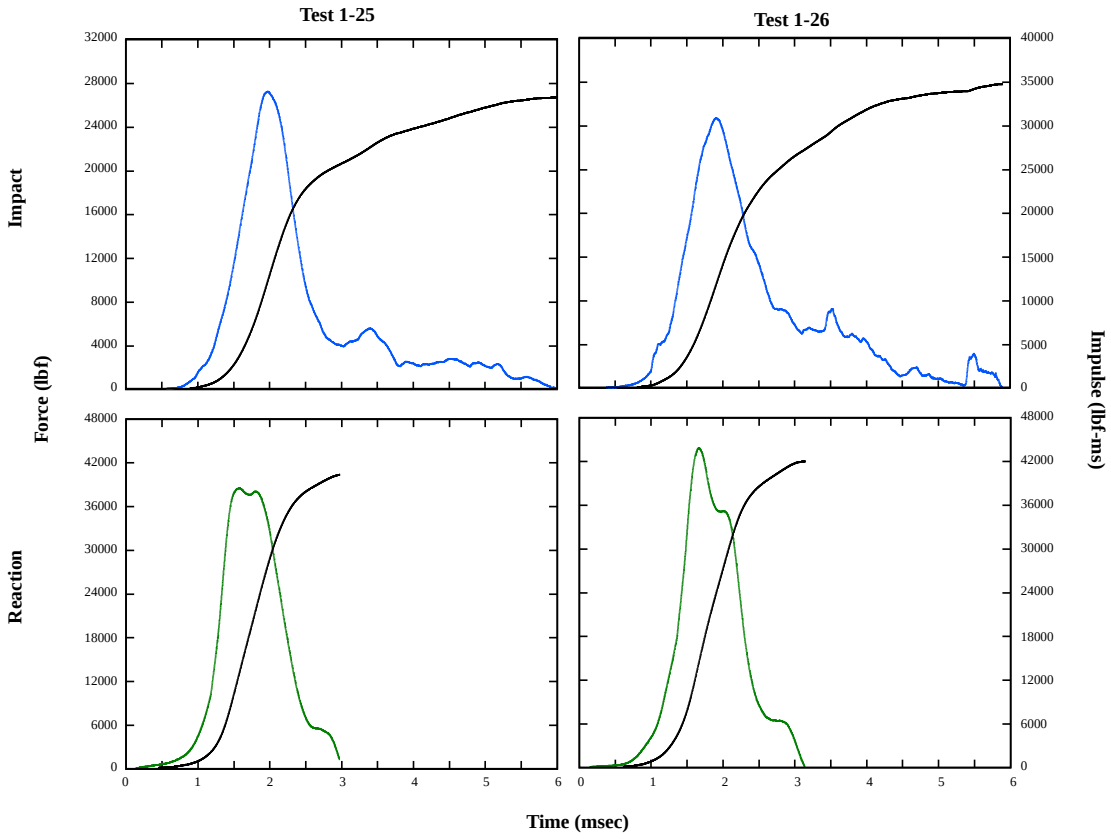

(a) **(b)**

Figure 4.30: Force-time history and impulse **(a)** Test 1-25 and **(b)** Test 1-26.

Issues identified with the conduct of the validation tests serve to explain some of the problems with the results. Improper lighting and targets on the flyer mass rendered it

difficult for the ProAnalyst software to track the location of the flyer. Reflection off of the steel blast generator rails from external lighting washed out much of the camera image and the targets did not provide sufficient contrast. Additionally, the shear plates used during this test had been used in fourteen previous dynamic tests with A325 bolts, five static tests with A325 bolts, and three static tests with A307 bolts. As will be discussed in Section 4.3, the plates showed significant signs of localized bearing failure.

Yielding of the plates during impact would explain the lower rebound velocity, lower impact load cell force levels, and higher reaction load cell force levels. Because the shear plates would absorb energy through plastic deformation, there would be less energy for the flyer mass to rebound and the impact load cells would measure lower force levels as the plate continued to translate. Therefore, the reaction load cells would measure not only the impulse from the flyer but the inertial effects of the impact T-section as well. The localized bearing failure in the plates has been noted is previous research [6].

Thus, in the validation tests, the impact load cells under measured the impulse and the reaction load cells over measured the impulse. However, the results were deemed sufficient to transition to residual capacity testing. Because of the differences in strengths of the A572 Grade 50 plates and the A325 bolts, the decision was made to conduct residual capacity testing of A307 bolts in lieu of A325 bolts. Finally, new shear plates that had not been impacted or used in static tests were used for residual capacity testing.

4.3 Static Experimental Test System Validation

Significantly fewer tests were conducted to validate the static experimental system. Validation of the static experimental system focused on overall performance of the system and achieving repeatable results. A total of six validation tests were conducted. Three tests were conducted with 3/4 inch (19.1 mm) A325 bolts and three tests were conducted with 3/4 inch (19.1 mm) A307 bolts. Figure 4.31 shows the load-displacement curves for one of the A325 tests, all of the A307 tests, and the average of the A307 tests. In all tests, threads were excluded from the shear plane and the bolts were hand tight. Only the last A325 curve is shown because systemic problems were resolved during the testing of the first two bolts resulting in unusable data. Systemic problems included proper vertical alignment of the universal joint to prevent rotation of the impact T-section and proper post tensioning of the reaction blocks to prevent slipping under load.

The objective of the validation tests was to achieve peak force values within 5% of each other to demonstrate repeatability. The results were also compared to the theoretical shear capacity of the bolt. Table 4.5 shows the results of the static validation tests. The largest difference in peak force between A307 tests was 4.3%, within the 5% target. The theoretical peak force was determined by taking 62% of the minimum required tensile stress multiplied by the bolt shank area as threads were excluded from the shear plane:

$$F_v = (0.62) f_{ut} A_b \tag{4.19}$$

The results show a shear capacity of approximately 25% greater than the theoretical shear capacity. These results are consistent with static tensile tests. Researchers [13] have found an 18 to 30% increase in the tensile strength of A325 bolts above their minimum strength.

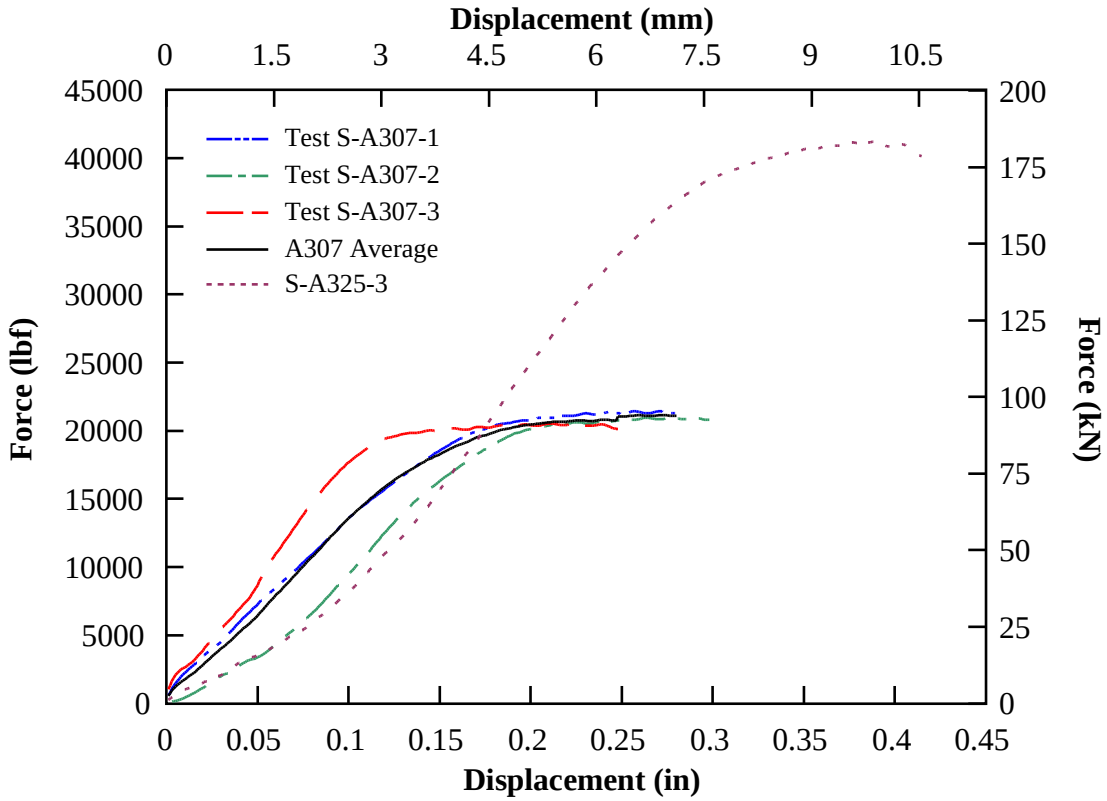

Figure 4.31: Static validation test force-displacement curves.

Table 4.5: Static validation test results.

	Fracture displacement in (mm)	**Ultimate capacity** kip (kN)	**Difference from theoretical capacity** (%)
3/4 in A307 Bolt 1	0.280 (7.112)	21.43 (95.3)	+30.4
3/4 in A307 Bolt 2	0.298 (7.569)	20.95 (93.2)	+27.5
3/4 in A307 Bolt 3	0.248 (6.299)	20.54 (91.4)	+25.0
3/4 in A307 Average	0.276 (7.010)	21.13 (94.7)	+28.6
3/4 in A325 Bolt 3	0.389 (9.88)	41.23 (183.40)	+25.4

The static tests of the A325 bolts revealed the unsuitability of A572, Grade 50 steel shear plates for testing of A325 bolts. Because the bolts have a much higher tensile strength

than the shear plates, localized yielding and deformation occurs around the bolt hole. Figure 4.32 shows the deformation that occurred in the shear plates with A325 bolts. Bolt holes were measured using standard calipers before and after testing. The elongation in the bolt hole was measured to be 0.071 inches (1.8 mm). Elongation occurred on one side of each plate where the bolt rotated to the tolerance gap in the bolt hole. As a result, A307 bolts were used for the remaining validation tests due to their lower strength compared to A325 bolts. However, after several tests with new plates, it was observed that even A307 bolts caused up to 0.02 inches (0.5 mm) in elongation of the bolt hole due to the stress concentrations at the edge of the bolt hole.

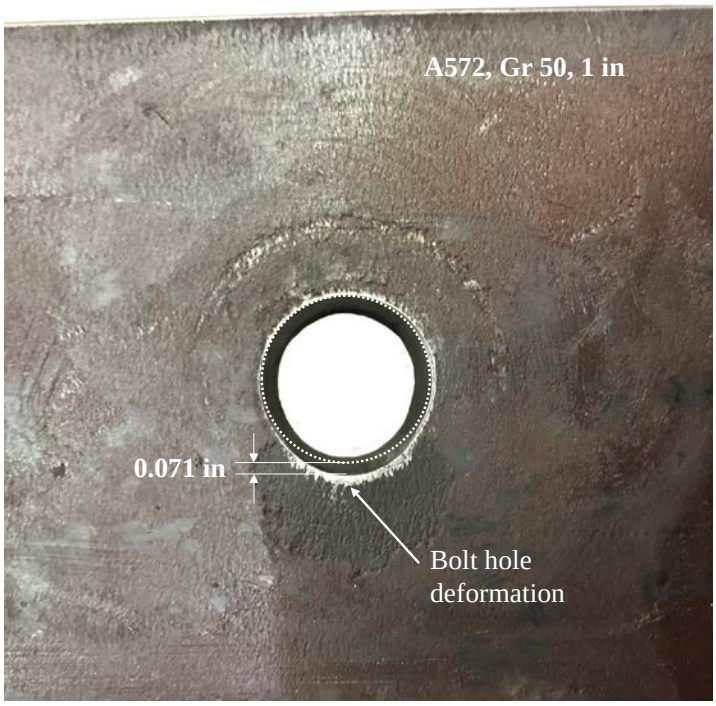

Figure 4.32: Bolt hole elongation from static tests with A325 bolts.

4.4 Initial Residual Capacity Testing of A307 Bolts

To validate the combined system of the dynamic experimental test system and the static experimental test system, residual capacity tests were conducted on 3/4 inch (19.1 mm) A307 bolts with threads excluded from the shear plane. A307 bolts were used in lieu of A325 bolts due to the relative strengths of the shear plates and the bolt materials. New A572, Grade 50 shear plates were installed in the setup for these tests. The tests compared two different velocities with all other variables held constant. Prior to a full residual capacity test consisting of a dynamic test followed immediately by a static test of the same bolt in its post-dynamic event state, a dynamic test was conducted at the same velocity to characterize the bolt damage. The bolt was removed and replaced with a new bolt and the new bolt was subjected to a residual capacity test. Tests 2-03 (dynamic only) and 2-04 (residual capacity) were conducted at approximately 6 m/s (236 in/s) with a corresponding kinetic energy of 310 J. Tests 2-05 (dynamic only) and Test 2-06 (residual capacity) were conducted at 7.5 m/s (295 in/s) with a corresponding kinetic energy of 485 J. Figure 4.33 shows the force-time histories of the dynamic portion of Tests 2-04 and 2-06.

The results of the residual capacity tests are tabulated in Table 4.6. In these tests, the measured impulse from the flyer mass, the impulse from the load cells, and the impulse measured by the reaction load cells are generally equal, with the impact load cells and reaction load cells slightly lower than the flyer mass impulse. These results indicate that the instrumentation is capturing the losses in the system. Figure 4.34 shows the flyer mass velocity-time history for the two tests while Figure 4.35 shows the impulse and force-time

histories of the load cells. The same methods discussed in Section 4.2.3 were used to conduct this analysis.

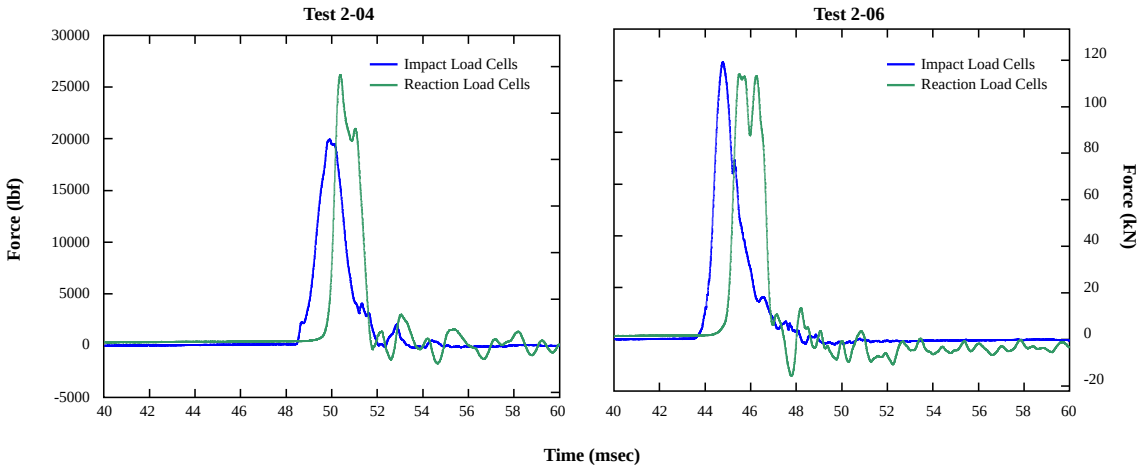

Figure 4.33: Residual capacity test dynamic event force-time histories **(a)** Test 2-04, and **(b)** Test 2-06.

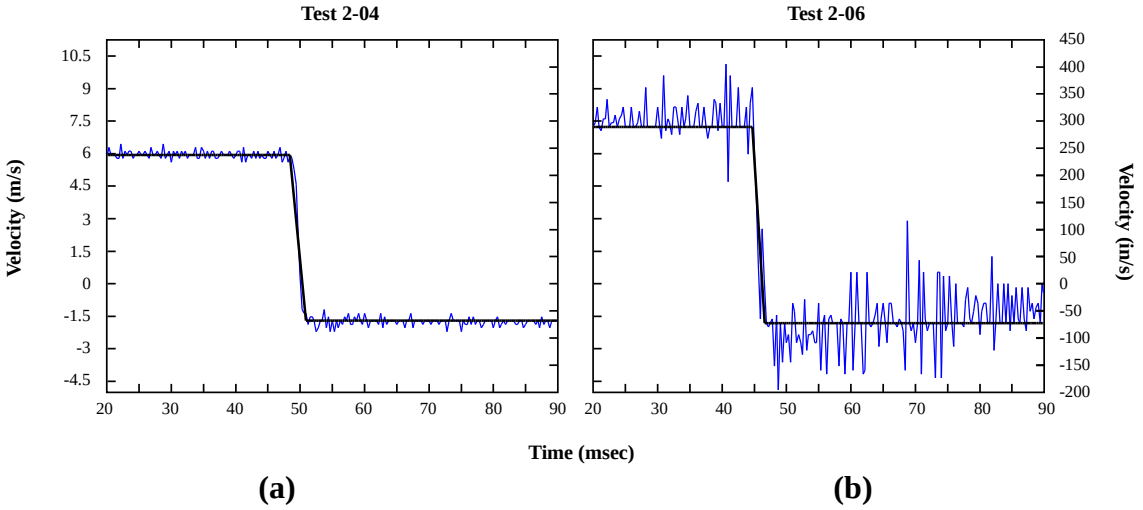

Figure 4.34: Flyer mass velocity time history **(a)** Test 2-04 and **(b)** Test 2-06.

Table 4.6: Residual capacity dynamic event test results.

		Test 2-04	Test 2-06
Flyer Mass	Target velocity, *m/s* (*in/s*)	6.195 (243.9)	7.465 (293.9)
	Impact velocity, *m/s* (*in/s*)	6.040 (237.8)	7.356 (289.6)
	Rebound velocity, *m/s* (*in/s*)	-1.727 (68.0)	-1.839 (72.4)
	Measured impulse, *lbf·ms* (*kN·ms*)	30,087 (133.8)	35,625 (158.5)
Impact Load Cells	Total duration, *msec*	3.552	4.694
	Peak force, *lbf* (*kN*)	19,819 (88.2)	26,740 (118.9)
	Measured impulse, *lbf·ms* (*kN·ms*)	29,366 (130.6)	35,388 (157.4)
	% Difference from Flyer	-2.4	-0.7
Reaction Load Cells	Total duration, *msec*	2.681	2.866
	Peak force, *lbf* (*kN*)	25,732 (114.5)	25,265 (112.4)
	Measured impulse, *lbf·ms* (*kN·ms*)	29,207 (129.9)	35,368 (157.3)
	% Difference from flyer	-2.9	-0.7

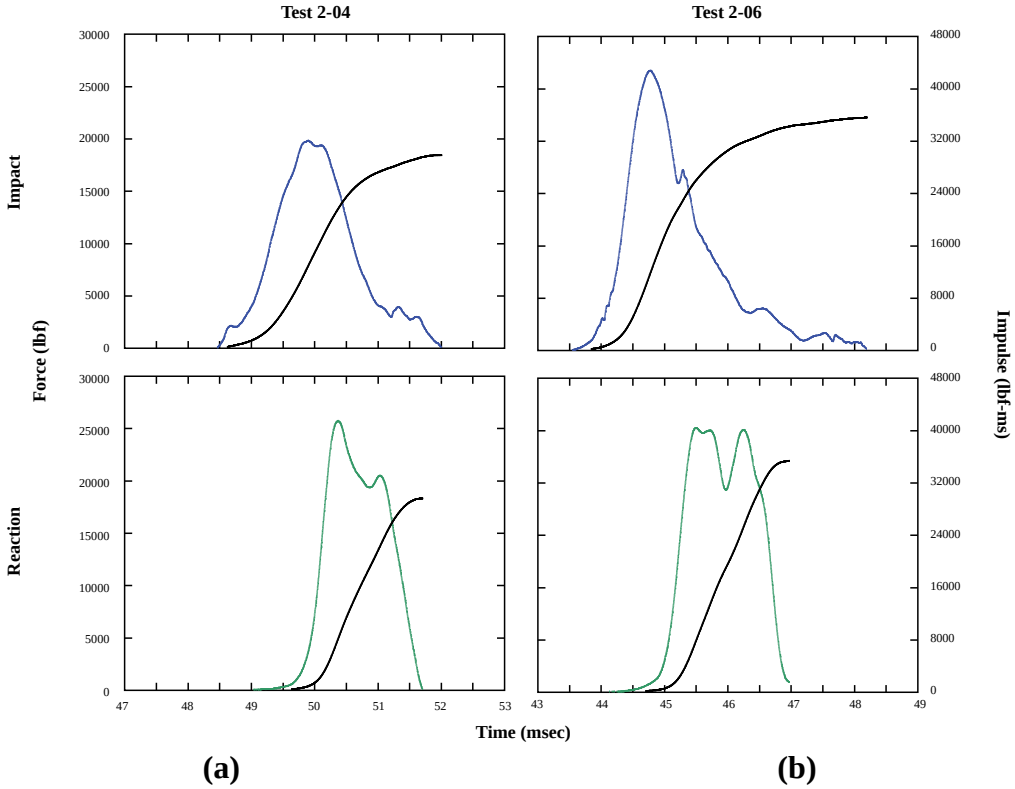

Figure 4.35: Force-time history and impulse **(a)** Test 2-04 and **(b)** Test 2-06.

The bolt damage from the impulses in Tests 2-04 and 2-06 can be inferred from Tests 2-03 and 2-05, which were conducted at the same velocities. Figure 4.36 shows the bolt damage resulting for the impulse. The shear plane and rotation of the bolt due to the tolerances in the bolt hole are clearly visible. Due to its lower impulse, the damage to the bolt in Test 2-03 is significantly less than the damage in Test 2-05. For the purposes of these tests, the actual damage was not quantified but qualitatively measured. Higher velocities for these bolts were not attempted due to the significant visible damage to the bolt from Test 2-05. Based on previous bolt failures, it was assessed that higher velocities might result in bolt fracture during the dynamic test, which was to be avoided.

(a) **(b)**

Figure 4.36: Bolt damage **(a)** Test 2-03, and **(b)** Test 2-05.

Following the dynamic tests, static tests were conducted to determine the residual capacity of the A307 bolts. Figure 4.37 shows the results of the residual capacity tests. The results are compared to the average of the three static tests conducted during the

validation of the static system. In general, it appears that the residual capacity of the bolts in terms of strength are approximately what they were had they not been impacted.

The bolt from Test 2-04 had a residual capacity of 19,900 lbf (88.5 kN) or 5.8% less than the average of the baseline tests and only 1% less than the lowest capacity bolt in the baseline. The bolt from Test 2-06 had a residual capacity of 21,400 lbf (95.2 kN) or 1.2% greater than the average of the baseline tests. The bolt from Test 2-04, which was not appreciably damaged, exhibited behavior very similar to the baseline curve. The behavior of the bolt from Test 2-06 is significantly different, however. The bolt appears to have a higher stiffness once the slack in the system is removed and exhibited less ductility than the other bolts.

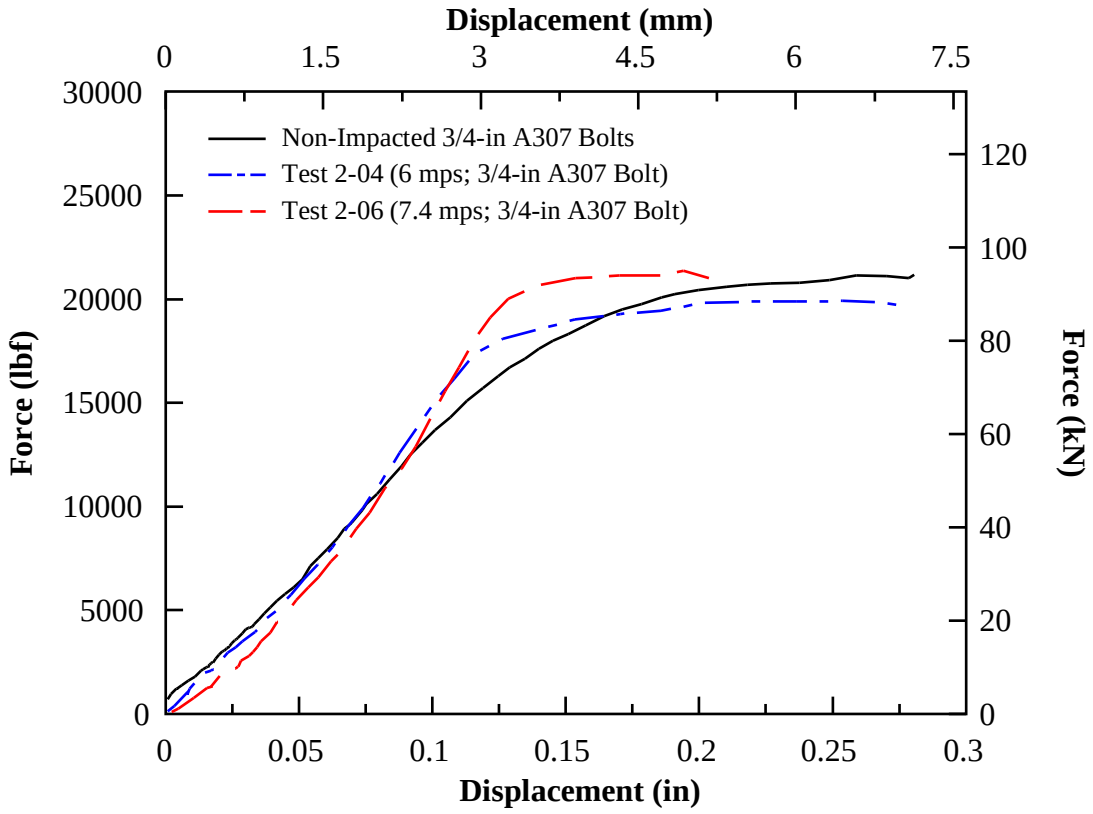

Figure 4.37: Residual capacity of A307 bolts.

The results of the impulsive and residual capacity validation tests demonstrate that the experimental method captures the behavior of structural bolts both during and after an extreme loading event. During the impulsive event, high speed video accurately captures the kinetic energy of the flyer mass and impulse applied to the specimen bolt. Impact load cells measure the force-time history and impulse from the flyer and reaction load cells measure the force-time history and impulse on the bolt. High speed video also captures the shear deformation of the bolt. The impulse can be varied to cause differing amounts of damage to the specimen bolt during the impulsive event. The static experiment test system applies a quasi-static load to the bolt to determine the capacity of a virgin bolt or the residual capacity of the bolt after an impulsive event. As expected, reduced ductility with increased damage was noted during the residual capacity validation tests. Unexpectedly, however, bolts maintained approximately the same residual capacity as virgin bolts after an impulsive event. The results indicate that further investigation of the residual capacity of structural bolts after an impulsive loading event is warranted.

4.5 Improvements to the Bolt Shear Residual Capacity Test System

Based on the results of the preliminary testing, several improvements were made to the dynamic shear experimental test system and the static experimental test system to improve future testing. Improvements focused on the shear plates to improve the performance of both the dynamic and static portions of the test. The shear plate material was changed to a material with a higher yield stress, the bolt hole diameter was adjusted to

increase bearing on the bolt shank, and the rig geometry was adjusted to further reduce prying action.

Yielding of the shear plates can have a significant influence on the results of the test as was seen in Tests 1-25 and 1-26. The ASTM A572 Grade 50 plates should not be used to test A325 or A490 bolts due to the fact that their yield stress is significantly higher than that of the plate. While this was known prior to the initial testing, the impact on the test results was not fully understood. Furthermore, in the testing of A307 bolts, localized yielding of the plate was also noted, although at much lower levels. The yielding problem can be reduced in a combination of two ways: 1) selecting an alternate material for use as the shear plates; and 2) changing the geometry of the bolt hole to reduce stress concentrations on the edge of the bolt hole.

To test the residual shear capacity of A307 bolts, plates made of ASTM A514, Grade A steel should be used. A514 steel has a minimum yield stress of 100 ksi (690 MPa), significantly higher than the minimum tensile strength of A307 bolts at 60 ksi (414 MPa). In addition to A307 bolts, A514 steel may also be used to test A325 bolts. Successful tests were conducted with A307 bolts and A572, Grade 50 steel plates that have a bolt tensile strength to plate yield strength ratio of 1.2. The bolt tensile strength to plate yield strength ratio of A325 bolts to A514 steel would also be 1.2. Minor localized yielding should be expected when testing A325 bolts, however it is unlikely that this would significantly undermine test results.

However, A514 steel plates would be insufficient for A490 bolts with a minimum tensile strength of 150 ksi (1,035 MPa). Although its bolt tensile strength to plate yield strength ratio of 1.5 is less than a ratio of 2.4 that was used in initial validation tests (A325

bolts and A572, Grade 50 steel plates), significant yielding of the plates would likely occur. Instead, specially formulated high hardness, high yield (high hard) steel is most ideal. These steels were developed for military armament applications and are commercially available as ARMOX 500T or ARMOX 600T. ARMOX 500T meets military specification MIL-DTL-46100E and has a 0.2% yield stress of approximately 180 ksi while ARMOX 600T has a 0.2% yield stress of approximately 215 ksi [15]. Higher strength steels for the shear plates would ensure that any energy dissipation occurs in the specimen bolt and not in the plates. While not available for this projects, these specialty steels would be ideal for testing A307, A325, and A490 structural bolts.

The second method to reduce the localized yielding on the bolt hole is to increase the bearing area between the plate and the bolt. This can be achieved by reducing the size of the bolt hole to limit bolt rotation during impact and static testing. Figure 4.37 shows the effects of a bolt hole larger than the actual bolt diameter. In the ideal case, the bolt hole in the plate is the exact same size as the bolt diameter. As a result, the bolt is unable to rotate and so the entire bearing area of the plate engages the bolt. In an actual bolt hole, the diameter of the hole is larger than the diameter of the bolt to allow tolerances for fitting connected members. The bolt is therefore able to rotate and the plates engage the bolt only at the edge of the bearing plate. Stress concentrations result that lead to the localized yielding observed in Section 4.3. Because the experimental test system is not concerned with tolerances due to the testing of a single bolt, the diameter of the bolt hole should be machined as close to the nominal size of the bolt as possible to reduce stress concentrations.

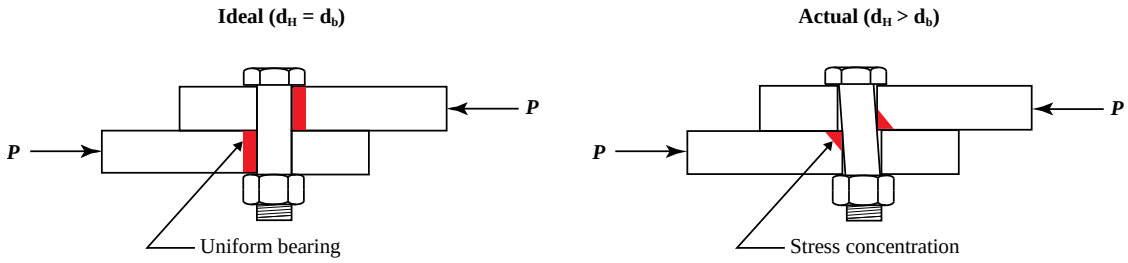

Figure 4.38: Effect of bolt hole diameter on plate bearing stresses.

Finally, in an effort to reduce the tensile stress due to the effects of prying action discussed in Section 4.1.1.3, the geometry of the plates was adjusted slightly. Due to the fabrication of the setup, the thickness of the plates is fixed at 1 inch (2.54 cm). Therefore, to reduce the theoretical prying action, the distance from the lead edge of the plate to the center of the plate, x_1, was increased as much as possible while still allowing the bolt to fracture completely. Because the impact plate and impact load cells extend well beyond the edge of the rail system, any adjustments to the geometry of the plates will not affect the function of the dynamic tests. Figure 4.39 shows the shear plate modifications. Due to the size of the T-section angles, the most that the distance x_1 can increase is 1/4 inch (6.35 mm). However, the 1/4 inch (6.35 mm) increase in x_1 will decrease the theoretical tensile stress due to prying action by an additional 4 to 5%.

Overall, the design, fabrication, and validation of the residual capacity experimental test system was a success. The experimental test system provides a dynamic shear event to a specimen bolt and then is adapted to determine the residual capacity of the specimen after the event. In the dynamic event, instrumentation captures the input energy, the impulse into the system, and the reaction of the system. Subsequent damage to the specimen bolt can be characterized. The static experimental test system allows the

impacted bolt to be tested in situ in order to determine its residual capacity. The static system measures the input force and the resulting shear displacement of bolt.

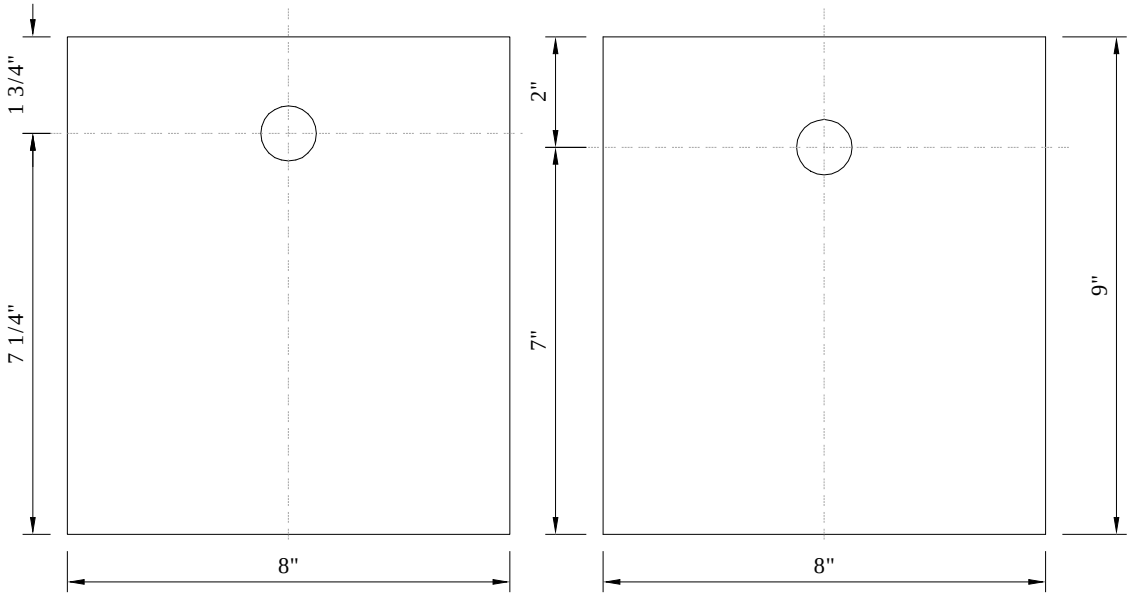

Figure 4.39: Shear plate modification.

4.6 References

[1] Livermore Software Technology Corporation, *LS-DYNA Keyword User's Manual*, 2007.

[2] Vision Research, *PCC 2.6 User Manual*, 2014.

[3] Xcitex, Incorporated, *ProAnalyst User Guide*, 2014.

[4] Chesson, E., N. L. Faustino, and W. H. Munse, "High-strength bolts subjected to tension and shear," *Journal of the Structural Division,* vol. 91, no. 5, pp. 155-180, 1965.

[5] Freidenberg, A., "Advancements in Blast Simulator Analysis Demonstrated on a Prototype Wall Structure," Doctoral Thesis, University of California, San Diego 2013.

[6] Grimsmo, E. L., A. H. Clausen, M. Langseth, and A. Aalberg, "An experimental study of static and dynamic behaviour of bolted end-plate joints of steel," *International Journal of Impact Engineering,* vol. 85, pp. 132-145, 2015.

[7] Horsfall, I., B. Hansen, and D. Carr, "Security of bolted joints during explosive loading," *International Journal of Vehicle Structures & Systems (IJVSS),* vol. 3, no. 2, pp. 107-112, 2011.

[8] Kulak, G. L., J. W. Fisher, and J. H. Struik, *Guide to Design Criteria for Bolted and Riveted Joints, 2nd ed.* Chicago: American Institute of Steel Construction, 2001.

[9] Malvar, L. J., "Review of static and dynamic properties of steel reinforcing bars," *American Concrete Institute Materials Journal,* vol. 95, no. 5, pp. 609-616, 1997.

[10] Rabalais, C. P., "Analysis of bolt and rivet structural fasteners subjected to dynamic and quasi-static shear loadings," Masters Thesis, Texas A&M University, 2015.

[11] Rainsberger, R. (2006). *TrueGrid User's Manual: A Guide and a Reference*. Available: http://www.truegrid.com/pub/TGMAN230.1.pdf

[12] Rumpf, J. and J. Fisher, "Calibration of A325 bolts," *Proc. ASCE,* vol. Vol. 89 (ST6), no. December 1963, Reprint No. 232 (63-18), 1963.

[13] Salih, N., J. Smith, H. M. Aktan, and M. Usmen, "An experimental appraisal of the load-deformation properties of A325 high-strength bolts," *Journal of Testing and Evaluation,* vol. 20, no. 6, pp. 440-448, 1992.

[14] Sanborn, M., "BG-25 Standard Operating Procedure: MTS Single Channel Shock Impactor," Georgia Institute of Technology, 2016.

[15] Showalter, D. D., W. A. Gooch, M. S. Burkins, and R. S. Koch, "Ballistic Testing of SSAB Ultra-High-Hardness Steel for Armor Applications," Army Research Laboratory, ARL-TR-4632, 2008.

CHAPTER 5

BEHAVIOR OF STRUCTURAL BOLTS UNDER IMPULSIVE LOADS

5.1 Introduction

An experimental test series was undertaken to investigate the behavior of structural bolts under impulsive loads. The objective of this test series was to quantify the damage to structural bolts from varied impulses and impact energies. A total of 22 impulsive tests were conducted using the dynamic portion of the residual capacity experimental test system to investigate bolt damage caused by impulsive loads. This chapter describes the materials and methods used in the test series, the theory and calculation methods used to analyze the collected data, presents the significant findings and observations from the test series, and discusses key conclusions from the experiment.

5.2 Materials and Methods

5.2.1 Materials

5.2.1.1 Specimen Bolts

Specimen bolts for this test series consisted of 7/8 inch (22.2 mm) ASTM A307 regular hex head with a minimum tensile strength of 60,000 psi (4,200 MPa) and ASTM A325 heavy hex head structural bolts with a minimum tensile strength of 120,000 psi (8,400 MPa). Corresponding nuts for each bolt were used as specified in ASTM A307-14

and ASTM F1325-15A [1, 2]. Figure 5.1 shows typical specimen bolts of each type. Only 7/8 inch diameter bolts were tested. The most common diameter bolts for steel structures are 3/4 inch (19.1 mm) and 7/8 inch while the most common diameters for bridges are 7/8 inch and 1 inch (25.4 mm) [11]. Additionally, previous research on the static behavior and capacity of structural bolts has focused on using 7/8 inch structural bolts [7, 11]. The length of all bolts tested was 3 1/2 inches (8.89 cm) with a gauge length of 2 inches (5.08 cm). In every test, threads were excluded from the shear plane. Specimen bolts were from randomly selected lots and manufacturers and were purchased from commercial suppliers.

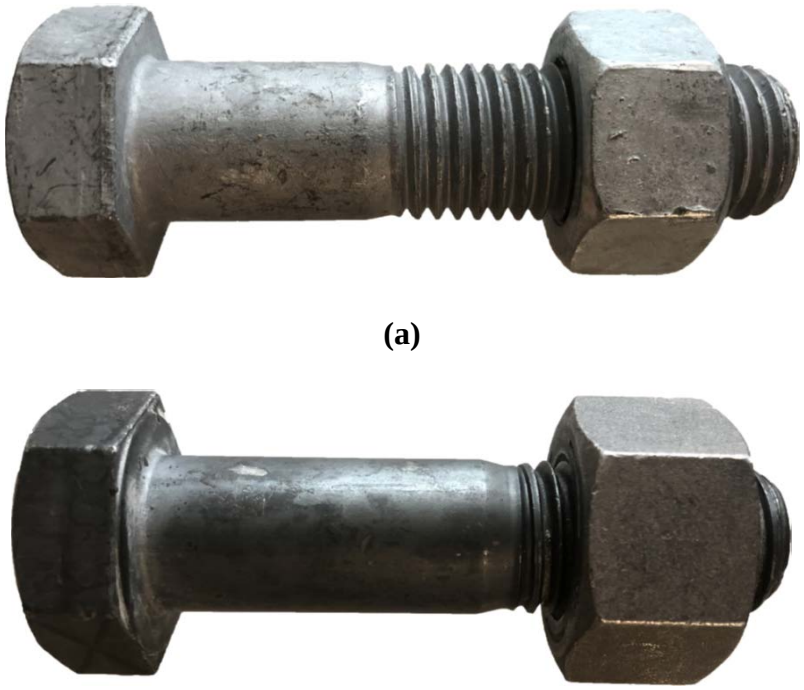

(a)

(b)

Figure 5.1: Typical specimen bolts **(a)** ASTM A307; and **(b)** ASTM A325.

Prior to testing, specimen bolts were inspected for visual defects and signs of corrosion or other damage. Additionally, bolt shank diameters were measured using

calipers under the bolt head, at the shear plane, and above the threaded portion. The measured shank diameter at the shear plane was slightly smaller than the nominal bolt diameter of 0.8750 inches (22.225 mm) for both bolt types. The A325 bolts were consistently 0.8730 inches (22.174 mm) at the shear plane while the A307 bolt shank diameters ranged from 0.8710 inches (22.123 mm) to 0.8735 inches (22.187 mm) with an average diameter of 0.8720 inches (22.149 mm).

5.2.1.2 Shear Plates

To minimize localized yielding in the shear plate in and around the bolt hole, ASTM A514, Grade A (A514A) steel shear plates were used for all tests. Based on previous testing, a higher yield, higher hardness steel would have been more ideal for testing A325 bolts, however, these materials were not readily available. A514A steel is a high yield, quenched and tempered alloy steel with a minimum yield stress of 100 ksi (690 MPa). Shear plates were 1 inch (2.54 cm) thick and measured 8 by 9 inches (20.32 x 22.86 cm).

The shear plates were machined to reduce bolt rotation and further minimize localized yielding in and around the bolt hole as well as to decrease tension in the bolt, which is inherent in the single lap joint design. To reduce bolt rotation, the specimen bolt hole was machined with a much closer tolerance than is normally specified in steel structures. Specimen bolt holes were machined with a tolerance of +1/64 inches (0.4 mm). To further reduce plate rotation, the specimen bolt was machined 2 inches (5.08 cm) from the lead edge of the shear plate.

Finally, to reduce friction between the shear plates the contact surfaces were prepared prior to testing. Mill scale was removed from the plate contact surfaces and the surfaces were then cleaned with acetone and a commercially available Teflon spray was

applied to the surface. The surfaces were then treated with synthetic grease to further minimize friction. Figure 5.2 shows the difference between the prepared and unprepared surfaces of the shear plates. The prepared surface (without synthetic grease applied) is shown in Figure 5.2(a) while the opposite surface (non-contact) is shown in Figure 5.2(b).

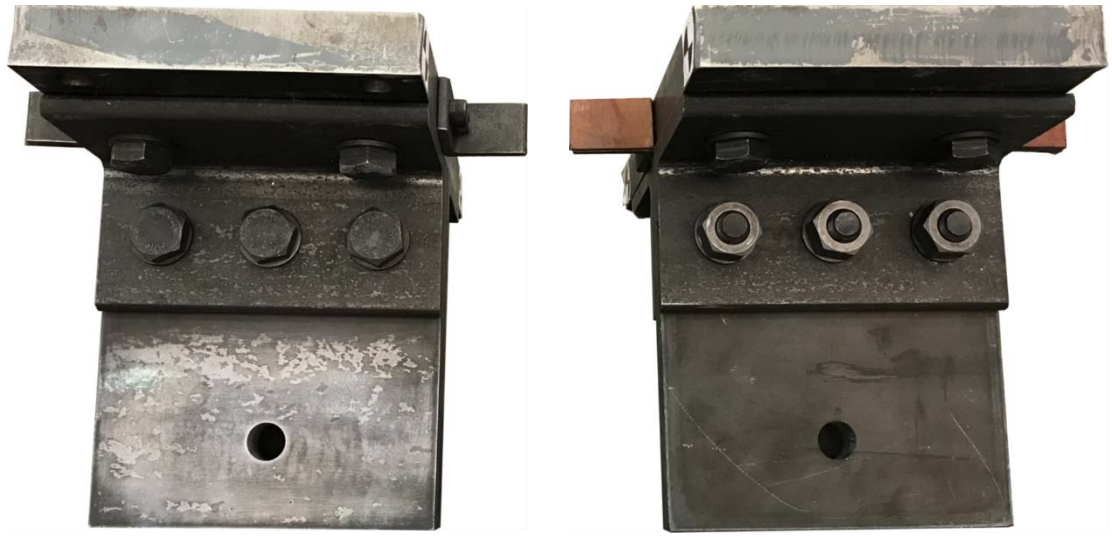

(a) **(b)**

Figure 5.2: Shear plate surface treatment **(a)** contact surface; **(b)** non-contact surface.

5.2.2 Experimental Method

To experimentally investigate the behavior of structural bolts under impulsive loads, the Bolt Shear Dynamic Experimental Test System described in Chapter 4 was used. There were no significant changes to the test system as previously described. However, following the validation tests the apparatus was disassembled and then later reinstalled, realigned, and revalidated. As will be discussed in the results section, changes to the alignment of the test system may have impacted the results as compared to the initial validation tests. Figure 5.3 shows the experimental test system prior to a dynamic test.

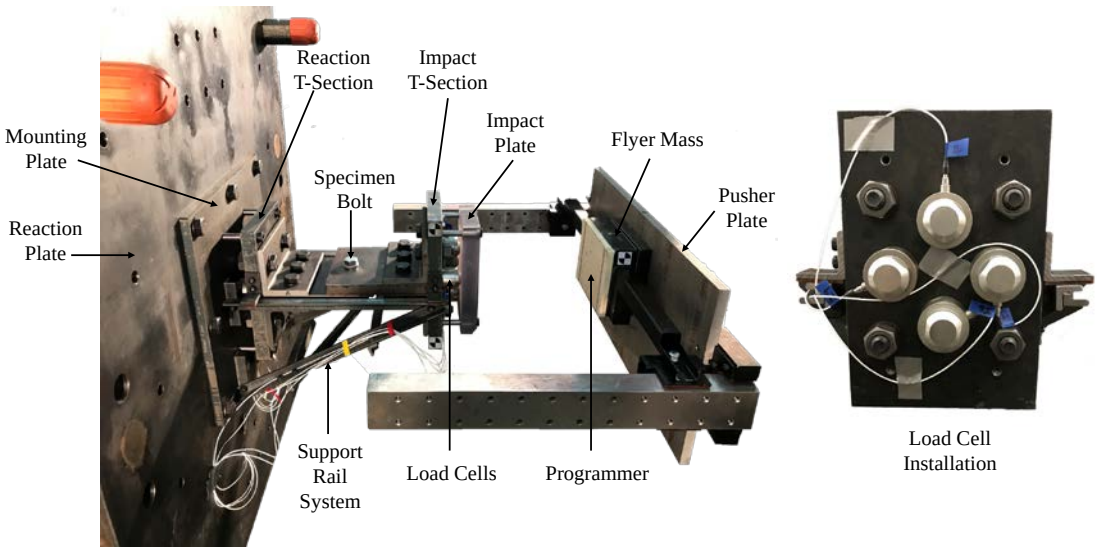

Figure 5.3: Dynamic experimental test system.

A total of 22 impulsive tests were conducted in the experimental test series. Table 5.1 shows the tests conducted as part of the test series. All bolts were 7/8 inches in diameter and were installed loosely such that there was no pretension on the bolt to minimize friction in the system. For each bolt type, impact velocities were selected to increase the expected damage to the bolt from slight damage to fracture. The majority of the tests for each bolt type were in the expected damage range of moderate to heavy damage as the most meaningful data was expected in this range.

For comparative purposes, a total of 12 baseline static tests were conducted on virgin bolts. These tests followed the same method for the residual capacity experimental test system except the bolts were not subjected to an impulsive load prior to testing. Seven tests were conducted on virgin A307 bolts and five tests were conducted on virgin A325 bolts.

Table 5.1: Impulsive event test series.

#	Test #	Bolt Type	Target Flyer Velocity m/s (in/s)	Expected Damage
1	D-307-01	A307	7.0 (276)	Slight
2	D-307-02	A307	7.0 (276)	Slight
3	D-307-03	A307	7.0 (276)	Slight
4	D-307-04	A307	8.0 (315)	Moderate
5	D-307-05	A307	8.0 (315)	Moderate
6	D-307-06	A307	8.0 (315)	Moderate
7	D-307-07	A307	9.0 (354)	Heavy
8	D-307-08	A307	9.0 (354)	Heavy
9	D-307-09	A307	9.0 (354)	Heavy
10	D-307-10	A307	10.0 (394)	Heavy/Fracture
11	D-307-11	A307	11.0 (433)	Heavy/Fracture
12	D-307-12	A307	12.0 (472)	Fracture
13	D-325-01	A325	9.0 (354)	Slight
14	D-325-02	A325	9.0 (354)	Slight
15	D-325-03	A325	9.0 (354)	Slight
16	D-325-04	A325	10.0 (394)	Moderate
17	D-325-05	A325	10.0 (394)	Moderate
18	D-325-06	A325	10.0 (394)	Moderate
19	D-325-07	A325	11.5 (453)	Heavy
20	D-325-08	A325	11.5 (453)	Heavy
21	D-325-09	A325	11.5 (453)	Heavy
22	D-325-10	A325	12.5 (492)	Fracture

5.3 Theory and Calculation

5.3.1 Impulsive Loading

As discussed in Section 4.1 of Chapter 4, conservation of momentum dictates that the impulsive load generated by the flyer mass must be equal to the measured impulse by the impact load cells and equal to the measured impulse by the reaction load cells minus any losses in the system. Equation 5.1 describes the equilibrium of the system in terms of impulse, S_{sys}:

$$S_{sys} = m_1(v_2 - v_0) = \int F_I(t)dt + S_{f,I} = \int F_R(t)dt + S_{f,I} + S_{f,R} \quad (5.1)$$

where m_1 is the flyer mass, v_2 is the rebound velocity of the flyer mass, v_0 is the impact velocity, $F_I(t)$ and $F_R(t)$ are the force time histories of the impact and reaction load cells, respectively, $S_{f,I}$ are the losses on the impact side of the system and $S_{f,R}$ are the losses on the reaction side of the system.

Experimentally, the impact impulse was determined through the use of high speed video capturing both the inbound and rebound displacement by using tracking software. Figure 5.4 shows a representative still shot of the tracking software used to determine the displacement. The tracked data was then used to determine both the impact and rebound velocity of the flyer mass. Figure 5.5 shows a representative plot of the flyer displacement with respect to time. The impact velocity was determined through linear regression of the positive sloped region while the rebound velocity was determined by linear regression of the negative sloped region. In each case, the slope of the regression corresponds to the flyer mass velocity.

From the displacement-time history of the flyer mass, the impact impulse was determined from Equation 5.2:

$$S_{flyer} = m_{flyer}\left(v_{rebound} - v_{impact}\right) \quad (5.2)$$

In addition to the impact impulse, the flyer displacement-time history was used to determine the kinetic energy or impact energy:

$$E_{impact} = E_k = \frac{1}{2} m_{flyer} {v_{impact}}^2 \quad (5.3)$$

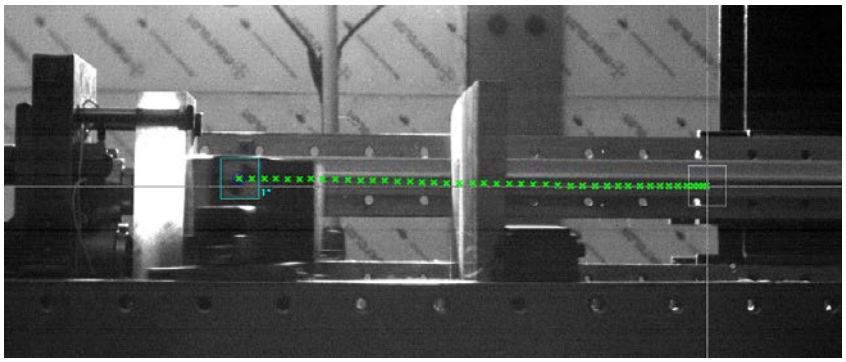

(a)

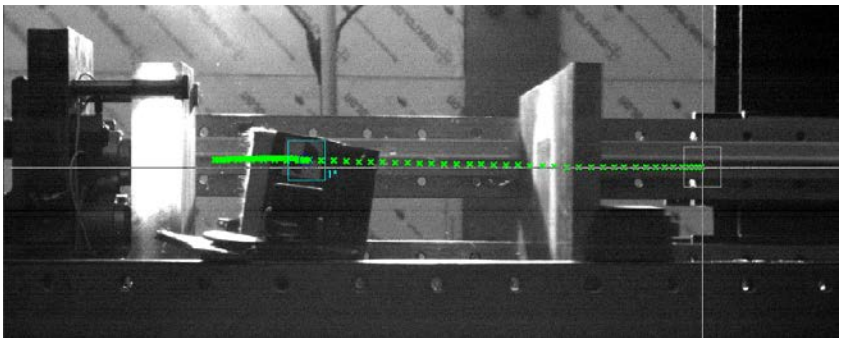

(b)

Figure 5.4: Typical high speed video track of flyer mass **(a)** impact; and **(b)** rebound.

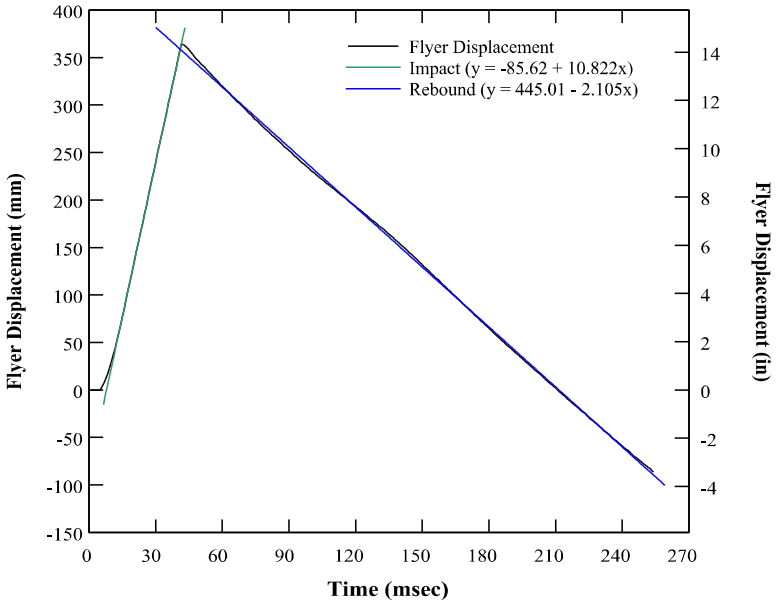

Figure 5.5: Typical flyer mass displacement-time history.

The impact impulse and the reaction impulse were determined by dynamic load cells that captured the force-time history of the dynamic event. The force-time history was then integrated over time to determine the corresponding impulse:

$$S = \int F(t)dt \tag{5.4}$$

Figure 5.6 shows a typical force-time history and corresponding impulse for the impact and reaction load cell measurements.

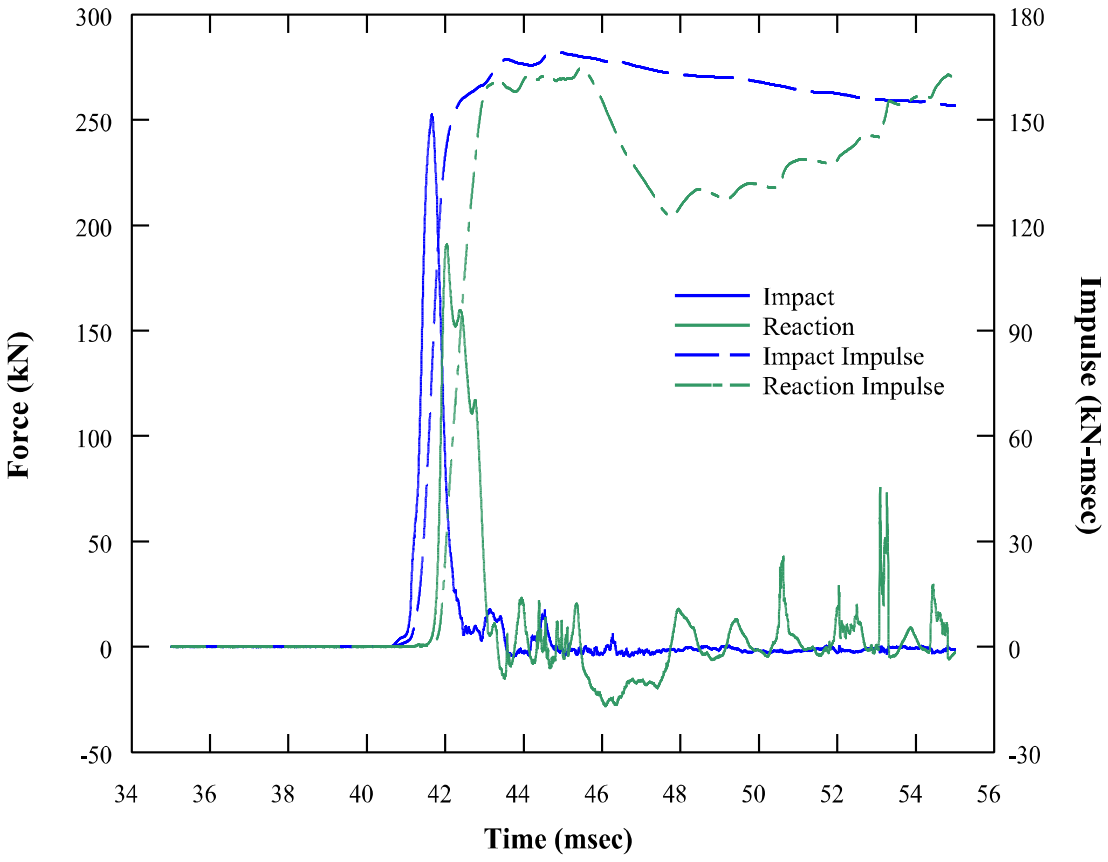

Figure 5.6: Typical force-time history and impulse.

5.3.2 Specimen Bolt Shear Stress and Apparent Shear Strain

For both the impulsive test and the baseline static tests, the load on the bolt was measured in units of force. Because the bolt is in single shear and threads are excluded from the shear plane, the shear stress on the bolt is simply given by:

$$\tau = \frac{V}{A} = \frac{P}{A_b} \tag{5.5}$$

where P is the applied load and A_b is the nominal cross-sectional area of the bolt, 0.601 in^2 (388 mm^2) for a 7/8 inch bolt. For the baseline static tests, P is taken as the measured force from the load cell. For the impulsive tests, P is taken as the force-time history from the reaction load cells since the reaction load cells best represent the actual load on the specimen bolt.

Since strain was not directly measured in the experimental setup, the determination of shear strain from collected data is somewhat subjective. The apparent shear strain in the bolt, γ, is the tangent of the angle formed by the horizontal translation over a given height. Figure 5.7 shows the shear strain for a theoretical stress block subjected to pure shear.

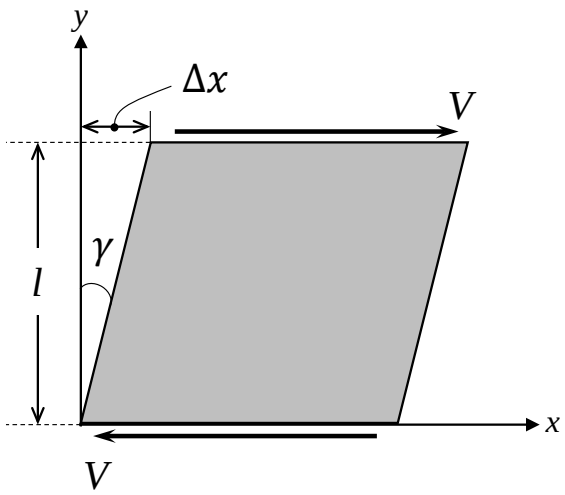

Figure 5.7: Shear strain in a theoretical stress block.

Based on the Figure 5.7, the apparent shear strain is calculated by the following equation:

$$\gamma = \frac{\Delta x}{l} \tag{5.5}$$

where Δx is the horizontal translation and l is the fixed height. In the test series, Δx was measured by high speed video in the impulsive tests and by low voltage displacement transducers (LVDTs) in the baseline static tests. Subjectivity arises in determining a value for the fixed height, l, in calculating shear strain. In the experimental setup, the bottom shear plate is relatively fixed and the top shear plate translates horizontally. Because of the close tolerances between the bolt shank diameter and the bolt hole, translation of the top shear plate is a reasonable approximation of the shear deformation of the bolt underneath the bolt head. The distance from the bolt head to the shear plane corresponds to the thickness of the shear plate, and so a height of 1 inch (2.54 cm) was used for the fixed height, l, in calculating shear strain in the bolt.

5.3.3 Apparent Strain Rate in Specimen Bolt

The strain rate of the specimen bolt under impulsive load was determined from high speed video recording of the impact shear plate displacement. Using the same technique described above to determine the flyer mass displacement-time history, the displacement-time history of the impact shear plate can also be determined from high speed video of the specimen bolt. This analysis again makes the reasonable assumption that the displacement of the impact shear plate corresponds to the shear deformation in the bolt. Figure 5.8 shows the displacement track of the impact shear plate. Because the tracking software tracks individual pixels within the image, the high definition video recording used allowed for displacements of 0.002 inches (0.051 mm) to be tracked. Figure 5.9 shows a typical

displacement-time history of the impact shear plate. The shear plate displacement was converted to a corresponding apparent shear strain in the bolt and then a linear regression was performed on the initial positive slope to determine the average apparent strain rate during the impulsive event.

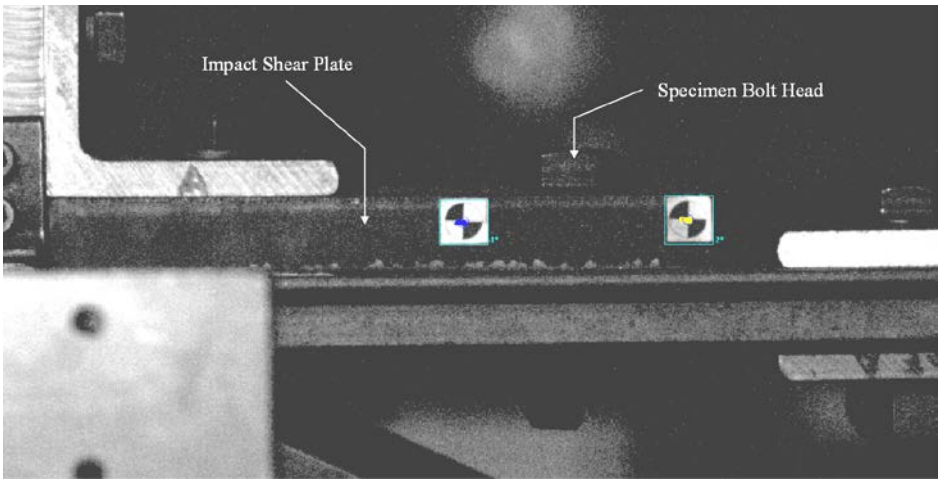

Figure 5.8: Typical high speed video track of impact shear plate.

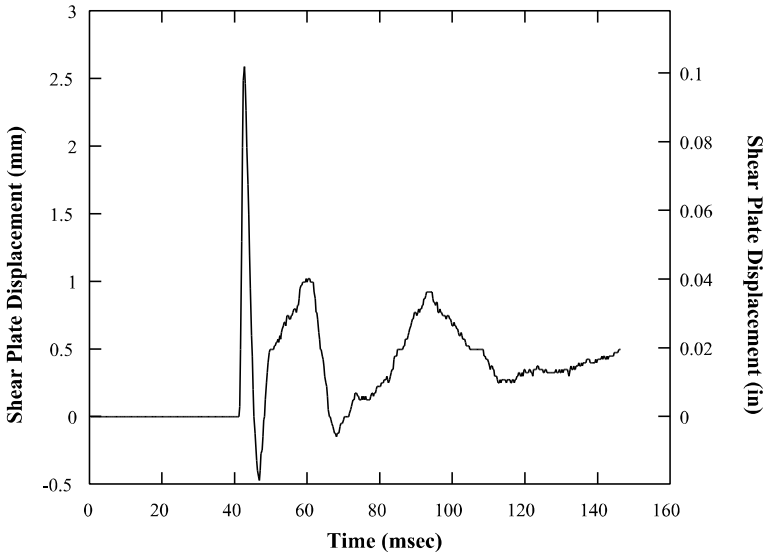

Figure 5.9: Typical impact shear plate displacement-time history.

5.3.4 Impulsive Load – Shear Displacement Curve

To determine to the specimen bolt load-displacement curve during the impulsive event, the force-time history from the reaction load cells were aligned in time with the displacement-time history of the impact shear plate. The reaction load cell data were then plotted against the displacement data at each time interval. Figure 5.10 shows a typical load-displacement curve developed through this analysis. In the figure, the blue curve represents the raw, pre-processed data. The pre-processed data show slack in the system as the bolt becomes fully engaged under load. Similarly, under unload the slack in the system is also visible. On both the load and unload portions of the curve, the data were corrected to remove the slack and produce a corresponding linear load and unload portion of the curve. To correct the data, a representative linear portion of the curve was isolated and a linear curve fit conducted on that portion of the curve. The linear portion was then extended from the y-intercept to the corresponding linear portion of the data. Past researchers have removed system slack from data using a similar procedure [11]. In the figure, these corrections to the data are shown in red.

Finally, to determine the corresponding permanent deformation in the bolt as a result of the impulsive load, the corrected curve was shifted to zero deformation as the load was applied to the bolt, corresponding to the black curve in Figure 5.10. The intersection of the unload portion of the curve with zero stress was taken as the permanent deformation in the bolt. This method of determining the permanent deformation in the bolt was consistent with validation tests where the permanent deformation in the bolt was physically measured after an impulsive test. In this test series, permanent deformation in the bolts

was not physically measured because the bolts could not be physically removed after the impulsive test due to close machining tolerances.

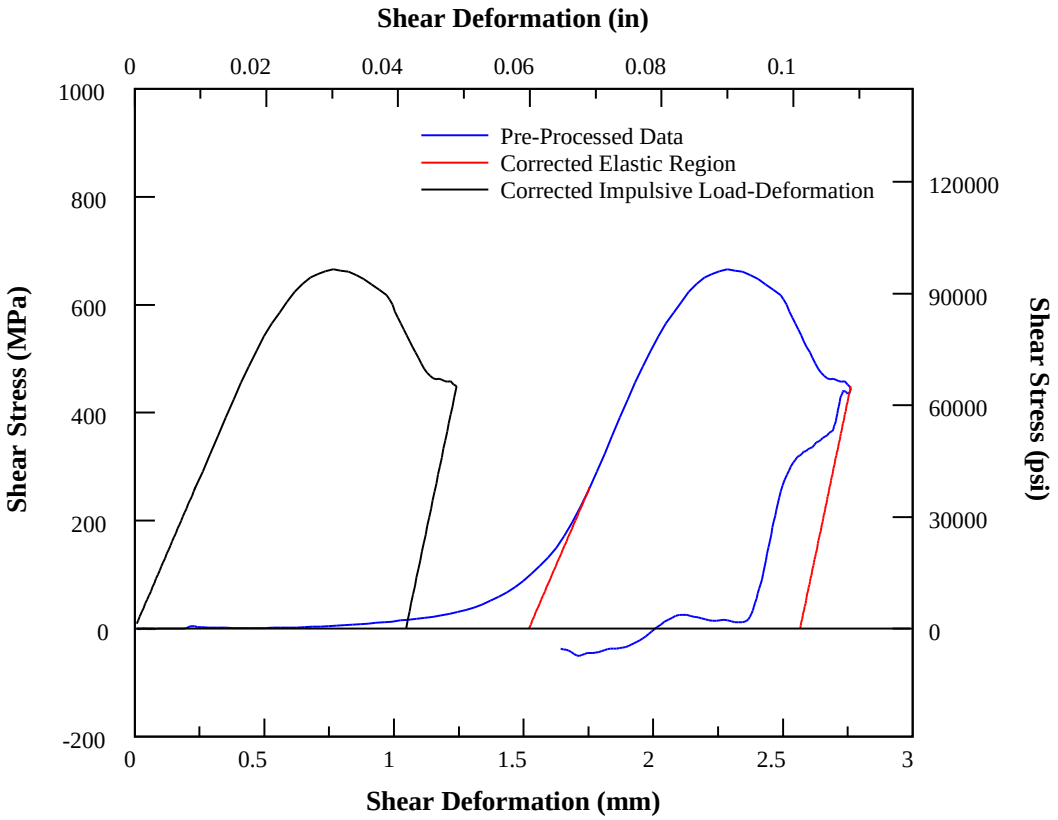

Figure 5.10: Typical specimen bolt impulsive load-displacement curve.

5.4 Results and Discussion

5.4.1 Baseline Static Tests

The results of the baseline static tests were consistent with other reported research on the shear capacity of structural bolts [7]. Figure 5.11 shows the average load-deformation curves for each type of structural bolt. Figure 5.12 shows the corresponding

stress-strain data for the baseline static tests. Bolts were loaded well within the quasi-static range at an average strain rate of $5 \cdot 10^{-3}$ s^{-1}. The data were corrected to remove system slack at the lower end of the load-deformation curve. Table 5.2 shows the average rigidity, ultimate strength, and fracture ductility as well as the range of results observed for each bolt type.

Table 5.2: Baseline static test results.

		7/8-in A307	**7/8-in A325**
Rigidity, *lbf/in* (*kN/mm*)	Average	475,804 (83.3)	719,234 (126.0)
	Minimum	374,037 (65.5)	682,341 (119.5)
	Maximum	592,913 (103.8)	763,787 (133.8)
Ultimate Capacity, *lbf* (*kN*)	Average	26,063 (115.9)	54,121 (240.7)
	Minimum	25,449 (113.2)	53,871 (239.6)
	Maximum	27,683 (123.1)	54,550 (242.7)
Fracture Deformation, *in* (*mm*)	Average	0.24835 (6.308)	0.23214 (5.896)
	Minimum	0.22133 (5.622)	0.20983 (5.330)
	Maximum	0.27026 (6.865)	0.24550 (6.236)

As expected, the A325 bolts exhibited higher stiffness and a significantly higher capacity than the A307 bolts. The A325 bolts fractured at an average capacity of 54,000 lbf (240 kN) while the A307 bolts fractured at an average capacity of 26,000 lbf (116 kN). These capacities were 21% and 16% higher than the expected capacity based on the minimum tensile strength of the bolts. These results are again consistent with previous research conducted on structural bolts [7, 9-12]. Both bolts exhibited similar ductility with an average shear deformation of 0.232 inches (5.893 mm) for A325 bolts and 0.248 inches (6.299 mm) for A325 bolts. The results of the A325 bolts showed much less variability

than the A307 bolts. This is likely due to the more stringent quality standards for the manufacture of A325 bolts as compared to A307 bolts.

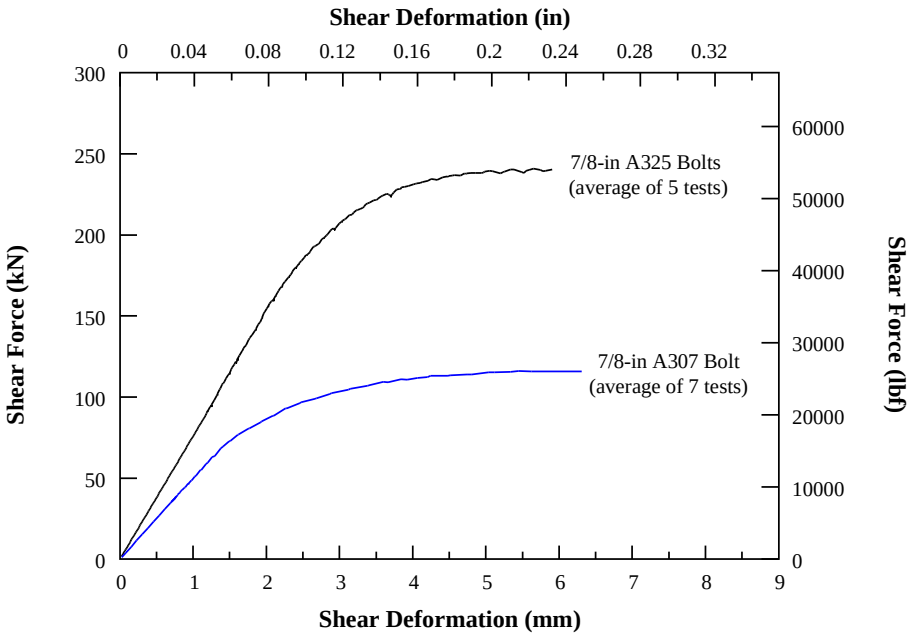

Figure 5.11: Baseline static test results (force-displacement).

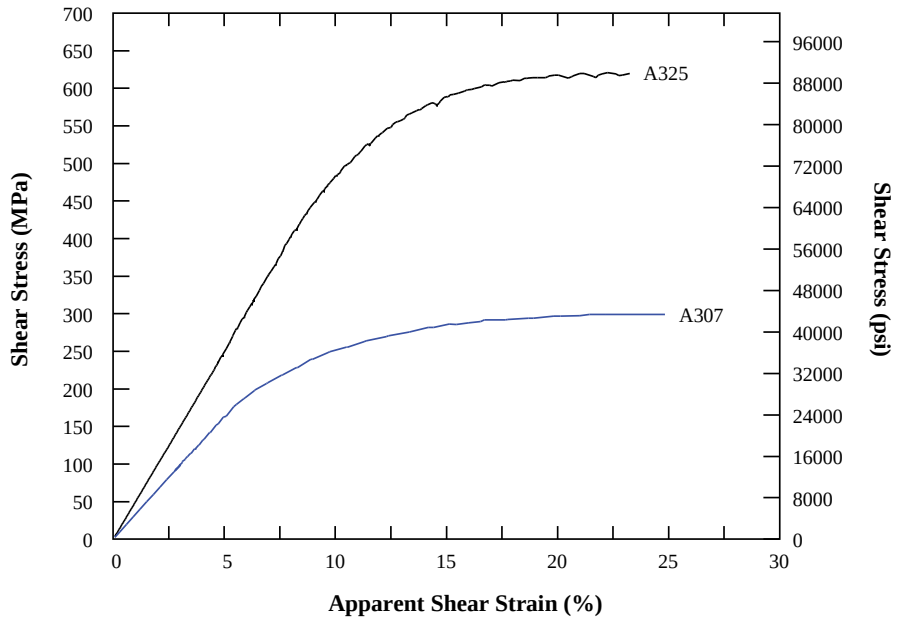

Figure 5.12: Baseline static test results (stress-strain).

5.4.2 Impulsive Loads and Test Efficiency

Comparison of the impulsive load as determined from the flyer mass and the impulsive load determined by both the impact and reaction loads is important to understand the efficiency of the experimental setup. Figure 5.13 shows the calculated flyer impulse as a function of the impact velocity. Variability exists in this calculation due to the tracking of the flyer rebound. During the impulsive event, the flyer exhibited a tendency to rotate during rebound. Because the high speed camera can only measure displacement with respect to a single plane, the rotation of the flyer can skew the determination of the rebound velocity. From Figure 5.13, it is evident that there is a linear relationship between the calculated flyer mass impulse and the impact velocity. As the flyer mass impact velocity increases, the impulse on the specimen bolt increases linearly ($R^2 = 0.914$).

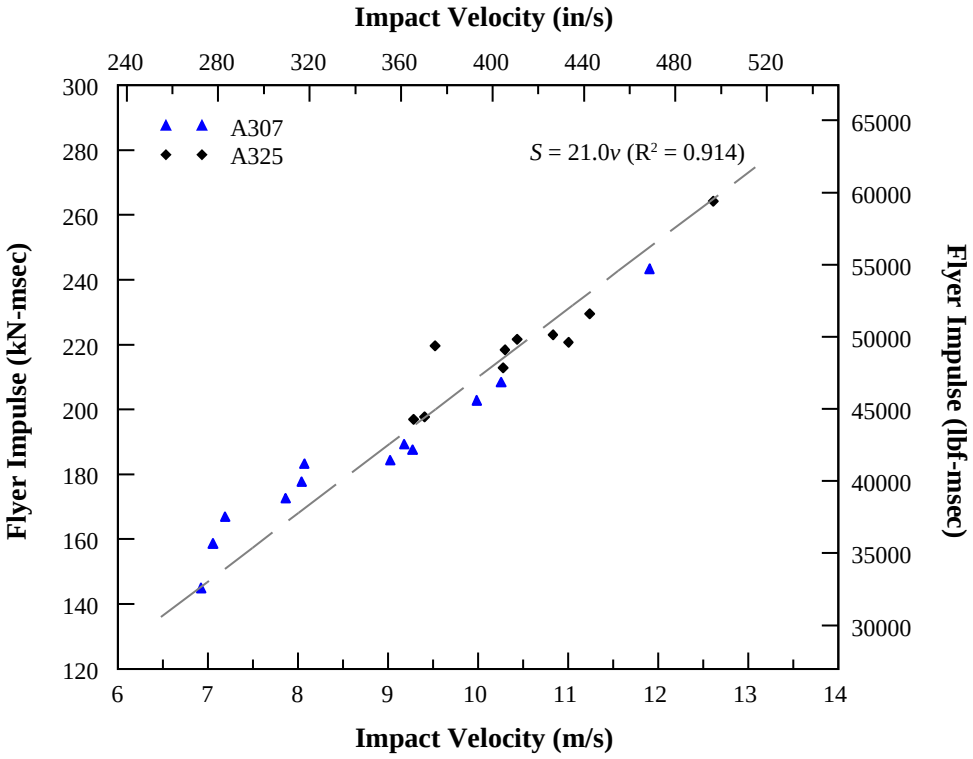

Figure 5.13: Flyer mass impulse.

In an ideal system, the impact and reaction load cells would measure the same impulse as the impulse determined by the flyer mass. However, losses from friction in the system reduce the impulse at each critical point in the system and therefore reduce the load on the bolt. Figure 5.14 shows the relative efficiency of the system at the impact load cells and at the reaction load cells. The figure shows the ratio of the impact and reaction load cell measurements to the flyer mass impulse measurement for each test plotted against the impact velocity. On average, the impact load cells were 83.1% efficient while the reaction load cells were 73% efficient. This efficiency is lower than the validation tests described in Chapter 4 and is likely the result of a combination of losses from friction, inertia, and misalignment introduced into the system when the setup was reinstalled. For future tests, it is recommended to keep assembly in place between validation (shakedown) and other tests. In general, tests were less efficient at lower impact velocities than at higher impact velocities due to the fact that the lower velocity tests operated at the lower end of the dynamic load cell range.

The impulsive load on the bolt results in an increased strain rate on the bolt. Figure 5.15 shows the bolt strain rate with respect to impact energy. As expected, the strain rate on the bolt increases with increased impact energy. The data also show good agreement ($R^2 = 0.93$) of a linear relationship between impact energy and strain rate on the specimen bolt. The figure shows that the bolt experienced strain rates in the intermediate to high strain rate range of 50 s^{-1} to 150 s^{-1}. These strain rates are consistent with actual strain rates that a structure would experience in response to a blast load [4].

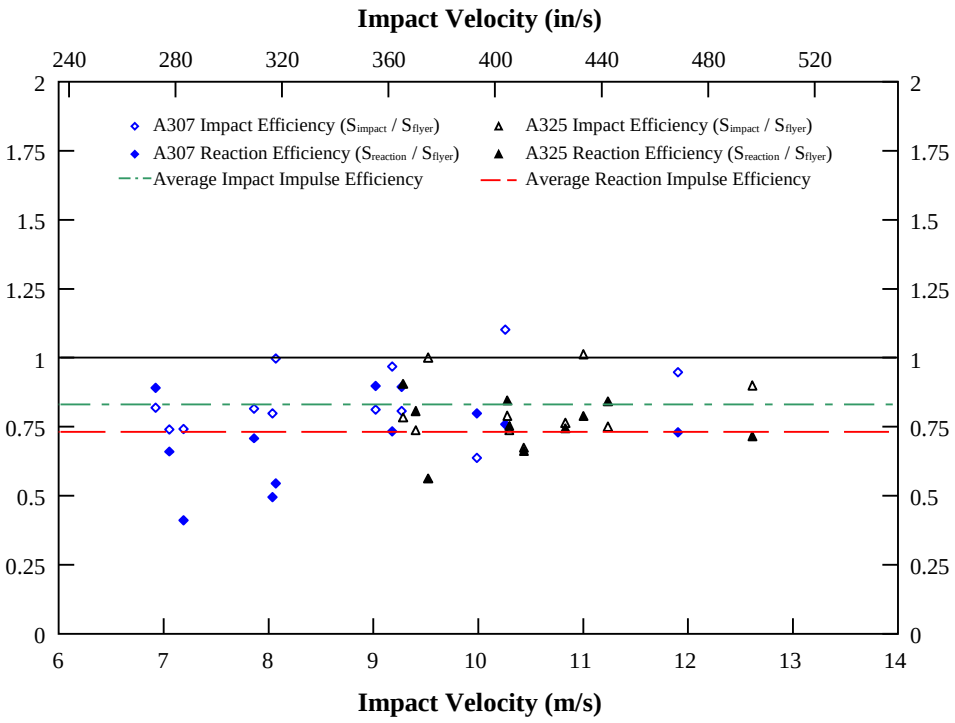

Figure 5.14: Impulsive test efficiency.

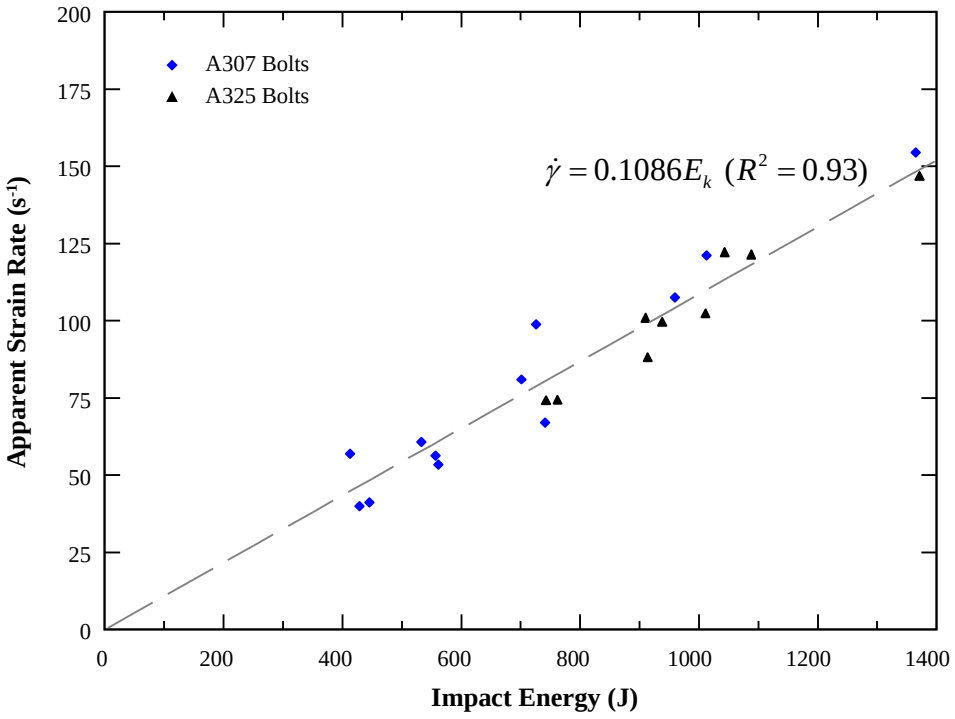

Figure 5.15: Bolt apparent strain rate under impulsive loads.

5.4.3 Behavior of Structural Bolts under Impulsive Loads

Understanding the behavior of structural bolts under impulsive loads focused on three aspects: 1) the rigidity of the bolts under impulsive loads as compared to static loading conditions; 2) the appropriateness of static and dynamic increase factors under impulsive shear loads for structural bolts; and 3) the characterization of bolt damage in terms of permanent shear deformation as the result of an impulsive loading.

5.3.3.1 Rigidity of Structural Bolts under Impulsive Loads

An important characteristic of the response of the structural bolt is the stiffness or rigidity of the bolt. The stiffness or rigidity defines the linear elastic region of the response. When loaded in tension or compression, the modulus of elasticity, *E*, describes the linear elastic stiffness of the bolt. When loaded in shear, the modulus of rigidity, *G*, describes the linear elastic rigidity of the bolt. The modulus of rigidity is related to the modulus of elasticity through Poisson's ratio, *v*:

$$G = \frac{E}{2(1+v)} \tag{5.6}$$

Common design and analysis techniques for blast load response neglect any increase in stiffness or rigidity for metals under high rates. Instead, the static stiffness or rigidity is assumed with an increased yield stress applied to account for strain rate effects. The results of this test series, however, show that the increase in rigidity for structural bolts under impulsive shear loads can be significant. Figure 5.16 shows the ratio of the impulsive modulus of rigidity to the static modulus of rigidity from the baseline static tests for the varying impact energies and corresponding strain rates of the bolts tested. The results show that all tested bolts were at least twice as rigid under the impulsive loads as under static conditions, with an average of four times the rigidity within the tested strain rate range.

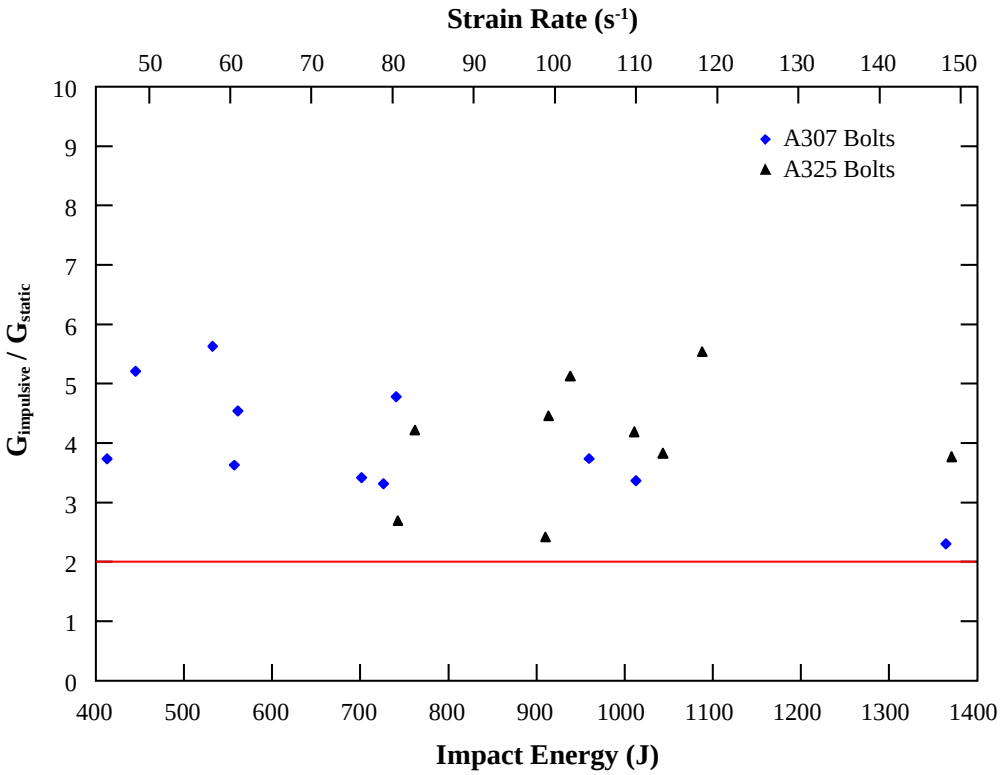

Figure 5.16: Impulsive modulus of rigidity.

5.4.3.2 Static and Dynamic Increase Factors for Structural Bolts

Under impulsive loads, a higher yield strength is expected due to strain rate effects. Typically a dynamic increase factor is taken to be 1.10 and is applied in conjunction with a static increase factor of 1.10 for steel. However, the type of steel significantly effects the dynamic increase that is to be expected. High yield strength steels typically see an increase of 20% at 200 s^{-1} while mild steel will typically see an increase of 200% at the same strain rate [6]. Figure 5.17 shows the ratio of the peak impulsive shear stress to the minimum proof stress for the varying impact energies and strain rates of the bolts tested. The minimum proof stress is defined as 70% of the minimum tensile strength of the bolt [2].

For A325 structural bolts, this corresponds to a strength of 84,000 psi (580 MPa) in tension and 52,080 psi (360 MPa) in shear. Figure 5.17 shows that both types of structural bolts averaged an increased strength of 50% (combined dynamic and static increase factors) above the minimum proof strength.

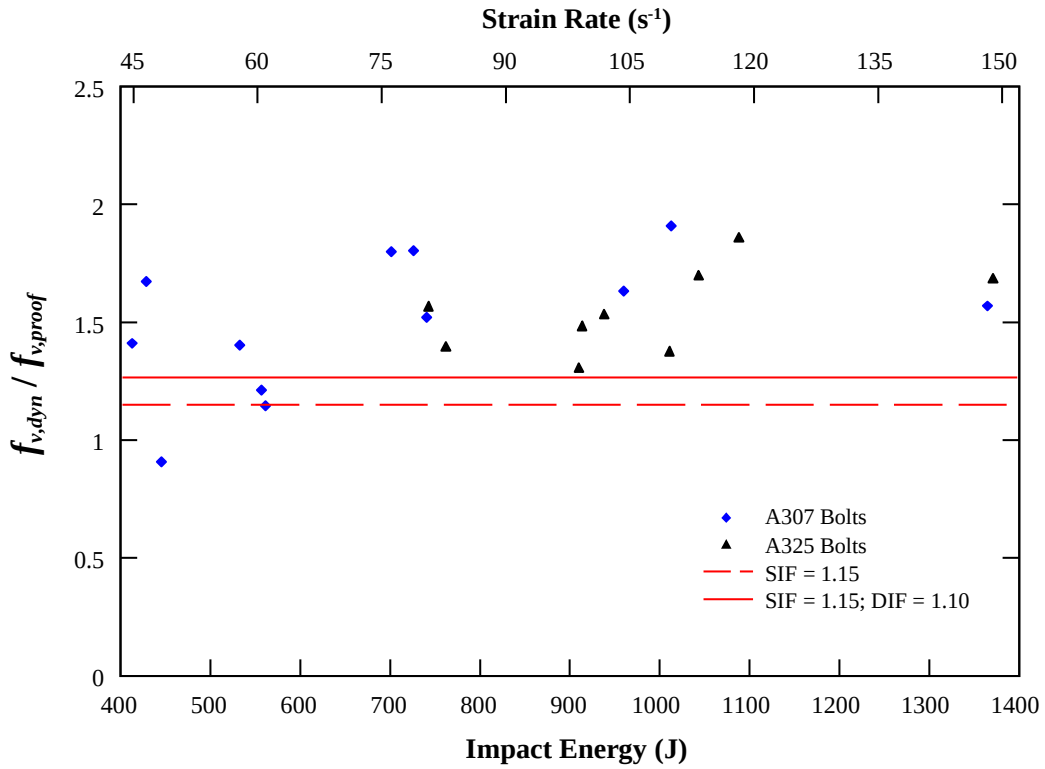

Figure 5.17: Static and dynamic increase factors.

Based on the results of the baseline static tests, a static increase factor (SIF) of 1.15 is recommended for structural bolts. A dynamic increase factor (DIF) of 1.10 is recommended for structural bolts. Combined, these increase factors provide an increased strength of 26.5%. Figure 5.17 shows that in the intermediate strain rate range, these

increase factors are conservative and appropriate. Additionally, within the relatively small tested strain rate range, the increase factor appears to be independent of the strain rate.

5.4.3.3 Characterization of Bolt Damage

The damage to a structural bolt subjected to an impulsive load can be characterized qualitatively in terms of the residual permanent shear deformation or strain. At the tested impact velocities slight, moderate, and heavy bolt damage was observed. Figure 5.18 shows the visible damage to A307 bolts while Figure 5.19 shows the visible damage to A325 bolts due to an impulsive load. Impact velocities for the A307 bolts were 7.0 m/s (274 in/s), 8.0 m/s (315 in/s), and 9.0 m/s (354 in/s) to cause slight, moderate, and heavy damage to the bolts, respectively. Likewise, impact velocities for the A325 bolts were 9.0 m/s (354 in/s), 11.5 m/s (453 in/s) and 12.5 m/s (492 in/s) to cause slight, moderate, and heavy damage, respectively. The visible damage in these figures is representative of the damage by different impulses. The shear plates used to produce the damage in the figures were A572, Grade 50 steel with standard bolt holes so that damaged bolt could be removed from the setup. Because lower strength plates were used, the damage to these bolts is lower than what was observed in bolts impacted with A514 shear plates and low tolerance bolt holes.

Only the A325 bolt fractured during the impulsive event. At the highest impact velocity tested, the A307 bolt did not completely fracture but was heavily damaged. Figure 5.20 shows the reconstructed A325 bolt showing the total deformation in the bolt before fracture as well as the fractured shear plane. The failure plane is visually consistent with the shear failure plane previous researchers have observed in similar tests [3, 5].

(a) **(b)** **(c)**

Figure 5.18: Permanent residual shear deformation in A307 bolts subjected to an impulsive load **(a)** slight damage; **(b)** moderate damage; **(c)** heavy damage.

(a) **(b)** **(c)**

Figure 5.19: Permanent residual shear deformation in A325 bolts subjected to an impulsive load **(a)** slight damage; **(b)** moderate damage; **(c)** heavy damage.

(a) **(b)**

Figure 5.20: A325 bolt fractured during impulsive event **(a)** reconstructed bolt; and **(b)** fracture plane.

The permanent residual shear strain can also be quantified in terms of the impact energy. Figure 5.21 shows the residual permanent shear strain as a function of the impact energy per millimeter of bolt diameter. Based on the results, the permanent residual shear strain increases linearly with increased impact energy ($R^2 = 0.94$ for A307 bolts; $R^2 = 0.87$ for A325 bolts). This result is consistent with research conducted on mild steel bolts in tension [8]. Based on these results, given the bolt type, diameter of the bolt, and impact energy, the residual permanent shear deformation can be predicted for A307 bolts (Eqn. 5.7a) and for A325 bolts (Eqn. 5.7b):

$$\gamma_{p,A307} = -2.377 + 0.301 d_b E_k \quad [\%] \tag{5.7a}$$

$$\gamma_{p,A325} = -5.002 + 0.216 d_b E_k \quad [\%] \tag{5.7b}$$

where ε_p is the percent residual plastic strain, d_b is the bolt diameter in millimeters, and E_k is the impact energy in Joules. Both bolt types exhibited significantly less ductility under impulsive loads than under static loads. The A307 bolts exhibited 50% of their static ductility before fracture while the A325 bolts only exhibited 33% of their static ductility before fracture.

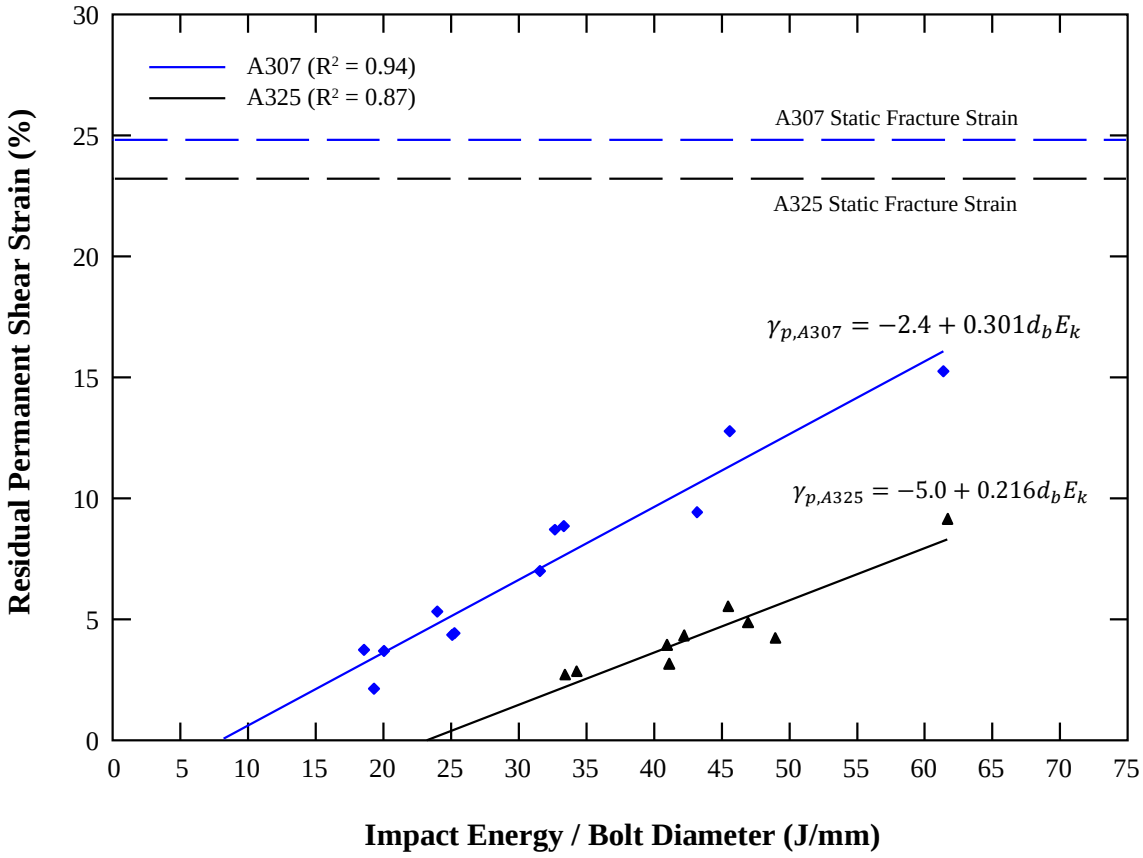

Figure 5.21: Characterization of bolt damage.

From Figure 5.19, it is also evident that both bolts fractured or were near fracture at approximately the same impact energy. The A307 bolts had a much lower resistance to the impact in terms of peak stress but dissipated the same amount of energy through shear

deformation. The much stronger A325 bolts had a much higher stress resistance to the impulsive load but were unable to deform as much as the A307 bolts before fracture. This indicates that when comparing the impulsive resistance of structural bolts (A307 and A325, specifically) the diameter of the bolt is more critical than the bolt material due to the fact that the bolts have approximately the same static ductility.

5.5 Conclusions

An experimental test series was conducted to investigate the behavior of structural bolts under impulsive shear loadings. The bolt shear residual capacity experimental test system was used to conduct the research. Baseline static tests were conducted in the same test rig to compare the static behavior of bolts to the impulsive behavior of bolts under the same conditions. Bolts were tested in the intermediate strain rate range from 40 s^{-1} to 150 s^{-1}. Based on the results of this test series, several important conclusions regarding the behavior of structural bolts subjected to impulsive shear loads can be made:

1. The modulus of rigidity under impulsive loads is a minimum of twice the static modulus of rigidity for strain rates between 40 to 150 s^{-1}. The increase in rigidity was an average of four times greater than the static rigidity. Within this relatively small range, increased strain rate appears to have little influence on the increased rigidity.

2. A static increase factor of 1.15 and a dynamic increase factor of 1.10 are appropriate and conservative increase factors for design and analysis of structural bolts subjected to impulsive loads. These increase factors are appropriate for strain rates within the tested range.

3. There exists a linear relationship between the impact energy and residual permanent shear strain in a structural bolt subjected to an impulsive shear load. Given an applied impact energy, bolt diameter, and bolt material, the residual permanent shear strain in the bolt can be predicted.

4. Bolts subjected to impulsive shear loads are significantly less ductile when compared to their static ductility. Under impulsive loads, A325 structural bolts will fracture at approximately 33% of their static ductility while A307 bolts will fracture at approximately 50% of their static ductility.

5. Both A307 and A325 bolts fractured at nearly the same impact energy indicating that bolt diameter is more critical than bolt material in absorbing energy from impact. A307 bolts result in higher ductility but lower stress resistance while A325 bolts result in less ductility but higher stress resistance.

5.6 References

[1] American Society for Testing and Materials, *Standard Specifications for Carbon Steel Bolts, Studs, and Threaded Rod 60 000 PSI Tensile Strength*, ASTM A307-14, 2014.

[2] American Society for Testing and Materials, *Standard Specification for High Strength Structural Bolts, Steel and Alloy Steel, Heat Treated, 120 ksi (830 MPa) and 150 ksi (1040 MPa) Minimum Tensile Strength, Inch and Metric Dimensions*, ASTM F3125-15A, 2015.

[3] Hadjioannou, M., D. Stevens, and M. Barsotti, "Development and Validation of Bolted Connection Modeling in LS-DYNA® for Large Vehicle Models," in *14th International LS-DYNA Users Conference*, Dearborn, MI, 2016.

[4] Harding, J., "The Effect of High Strain Rate on Material Properties," in *Materials at High Strain Rates*, T. Z. Blazynski, Ed. New York: Elsevier Applied Science, 1987, pp. 133-186.

[5] Horsfall, I., B. Hansen, and D. Carr, "Security of bolted joints during explosive loading," *International Journal of Vehicle Structures & Systems (IJVSS)*, vol. 3, no. 2, pp. 107-112, 2011.

[6] Huh, H., J. Lim, and S. Park, "High speed tensile test of steel sheets for the stress-strain curve at the intermediate strain rate," *International Journal of Automotive Technology*, vol. 10, no. 2, pp. 195-204, 2009.

[7] Kulak, G. L., J. W. Fisher, and J. H. Struik, *Guide to Design Criteria for Bolted and Riveted Joints, 2nd ed.* Chicago: American Institute of Steel Construction, 2001.

[8] Mouritz, A. P., "Failure mechanisms of mild steel bolts under different tensile loading rates," *International Journal of Impact Engineering*, vol. 15, no. 3, pp. 311-324, 1994.

[9] Rabalais, C. P., "Analysis of bolt and rivet structural fasteners subjected to dynamic and quasi-static shear loadings," Masters Thesis, Texas A&M University, 2015.

[10] Rumpf, J. and J. Fisher, "Calibration of A325 bolts," *Proc. ASCE,* vol. Vol. 89 (ST6), no. December 1963, Reprint No. 232 (63-18), 1963.

[11] Salih, N., J. Smith, H. M. Aktan, and M. Usmen, "An experimental appraisal of the load-deformation properties of A325 high-strength bolts," *Journal of Testing and Evaluation,* vol. 20, no. 6, pp. 440-448, 1992.

[12] Wallaert, J. J. and J. W. Fisher, "Shear strength of high-strength bolts," Fritz Laboratory Reports, Paper 1822, 1964, Available: http://preserve.lehigh.edu/engr-civil-environmental-fritz-lab-reports/1822.

CHAPTER 6

RESIDUAL CAPACITY OF STRUCTURAL BOLTS

6.1 Introduction

An experimental test series was developed to investigate the residual capacity of structural bolts after being subjected to an impulsive load. The objective of this test series was to quantify the residual shear capacity and ductility of structural bolts with varied damage levels from an applied impulse. A total of 22 tests were conducted using the residual capacity experimental test system to investigate the residual capacity of structural bolts after being damaged short of fracture. This chapter describes the materials and methods used in the test series, presents the significant findings and observations from the test series, and discusses key conclusions from the experiment.

6.2 Material and Methods

6.2.1 Materials

Impulsively damaged ASTM A307 and ASTM A325 structural bolts served as the specimens for the residual capacity test series. These specimens were the same structural bolts that were tested during the impulsive test series described in Chapter 5 where the structural bolts were subjected to a varied impulsive loads. Following the application of the impulsive load to either the 7/8 inch (22.2 mm) A307 or 7/8 inch A325 structural bolts,

the bolts were loaded to fracture under a quasi-static load. After the impulsive test, the bolts were left unmolested in the test rig while transitioning from the dynamic experimental test system to the static experimental test system. Figure 6.1 shows a typical heavily damaged bolt of each bolt type used in the residual capacity test series. Since the structural bolt was not removed from the test rig after the impulsive event, the same ASTM A514, Grade A shear plates were used for the impulsive tests described in Chapter 5 and the subsequent residual capacity test. However, different sets of identical shear plates were used for each bolt type such that shear plates used to test A325 bolts were not then used to test A307 bolts and vice versa.

(a)

(b)

Figure 6.1: Heavily damaged specimen bolts for residual capacity test series **(a)** ASTM A307 bolt; and **(b)** ASTM A325 bolt.

6.2.2 Experimental Method

The residual capacity of damaged bolts was determined using the static experimental test system of the residual capacity experimental test system described

previously in depth in Chapter 4. In this test series, no significant changes were incorporated into the methodology or experimental procedures. Figure 6.2 shows the static experimental test system used in the testing. Following each impulsive test discussed in Chapter 5, the static experimental test system was installed and the bolt was quasi-statically loaded to fracture to determine the residual capacity of the bolt after being impacted. The average strain rate for the quasi-static tests (baseline and residual capacity) was $5 \cdot 10^{-3}$ s^{-1}. Prior to beginning the impulsive test series, the same experimental system was used to conduct the baseline tests described in Chapter 5. Because both test series involved the same structural bolts, the baseline test results are used for both the impulsive test series and the residual capacity test series.

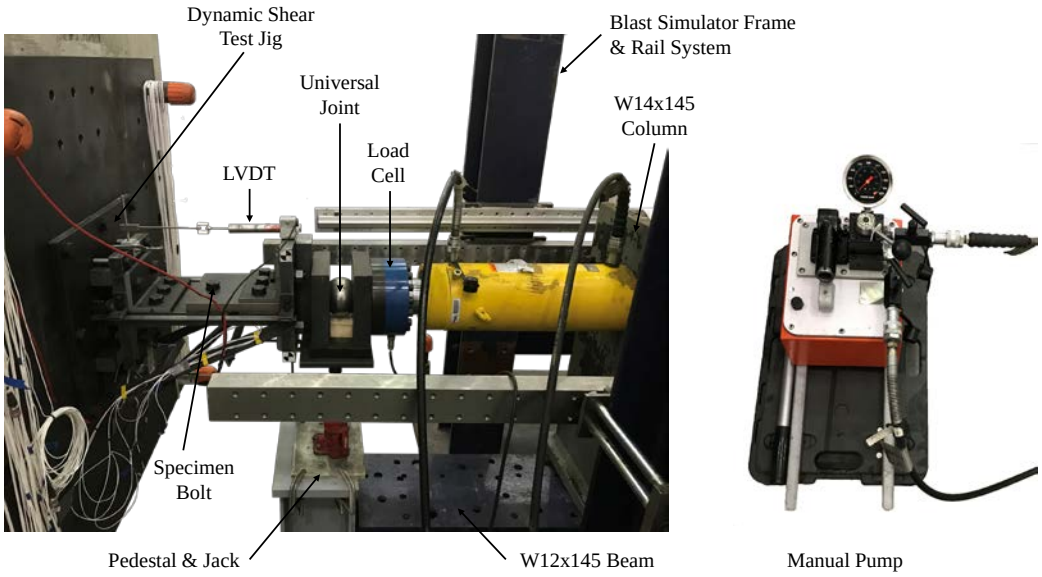

Figure 6.2: Residual capacity experimental test system.

In line with the impulsive tests, a total of 21 residual capacity tests were conducted in this experimental test series. A total of 22 impulsive tests were conducted, however,

one of the bolts fractured during the impulsive event rendering the residual capacity test irrelevant. Table 6.1 shows the tests conducted as part of the test series. All bolts were 7/8 inches in diameter and were initially installed loosely such that there was no pretension on the bolt to minimize friction in the system. For each test, the level of damage was extrapolated from calibration test results where the bolt was removed from the setup after the impulsive event and inspected for damage.

Table 6.1: Residual capacity test series.

#	Test #	Bolt Type	Impact Energy (J)	Bolt Damage Level
1	RC-307-01	A307	412.8	Slight
2	RC-307-02	A307	428.7	Slight
3	RC-307-03	A307	445.2	Slight
4	RC-307-04	A307	556.9	Moderate
5	RC-307-05	A307	532.5	Moderate
6	RC-307-06	A307	561.1	Moderate
7	RC-307-07	A307	726.1	Heavy
8	RC-307-08	A307	740.7	Heavy
9	RC-307-09	A307	701.4	Heavy
10	RC-307-10	A307	959.8	Heavy
11	RC-307-11	A307	1012.8	Heavy
12	RC-307-12	A307	1364.5	Severe
13	RC-325-01	A325	761.9	Very Slight
14	RC-325-02	A325	742.7	Very Slight
15	RC-325-03	A325	781.4	Very Slight
16	RC-325-04	A325	910.1	Moderate
17	RC-325-05	A325	913.7	Moderate
18	RC-325-06	A325	938.2	Moderate
19	RC-325-07	A325	1010.8	Heavy
20	RC-325-08	A325	1043.3	Heavy
21	RC-325-09	A325	1088.1	Heavy
22	N/A	A325	1371.1	Fracture

Finally, the same methods used to calculate shear stress and shear strain in the bolt were the same as those described in Chapter 5. Shear stress, τ, was determined by:

$$\tau = \frac{V}{A} = \frac{P}{A_b} \tag{6.1}$$

where P was the force measured by the load cell in the experimental setup and A_b was the nominal bolt area. The shear strain, γ, was determined by:

$$\gamma = \frac{\Delta x}{l} \tag{6.2}$$

where Δx was the displacement measured by the low voltage displacement transducer (LVDT) and l was taken as the thickness of the shear plate, in this case, 1 inch (2.54 cm).

6.3 Results and Discussion

6.3.1 Residual Properties of Damaged Bolts

The investigation of the residual properties of damaged structural bolts focused on three critical aspects of the bolt shear stress-strain curve: 1) comparison of the residual rigidity to the rigidity of a virgin bolt; 2) comparison of residual capacity or strength to that of a virgin bolt; and 3) comparison of residual ductility to virgin bolt ductility. These aspects of the residual stress-strain curve provide insight into the effect that impulsive damage has on a structural bolts ability to safely transfer load following an extreme event. Figure 6.3 shows a typical residual capacity stress-strain curve compared to the virgin bolt stress-strain curve from the baseline tests.

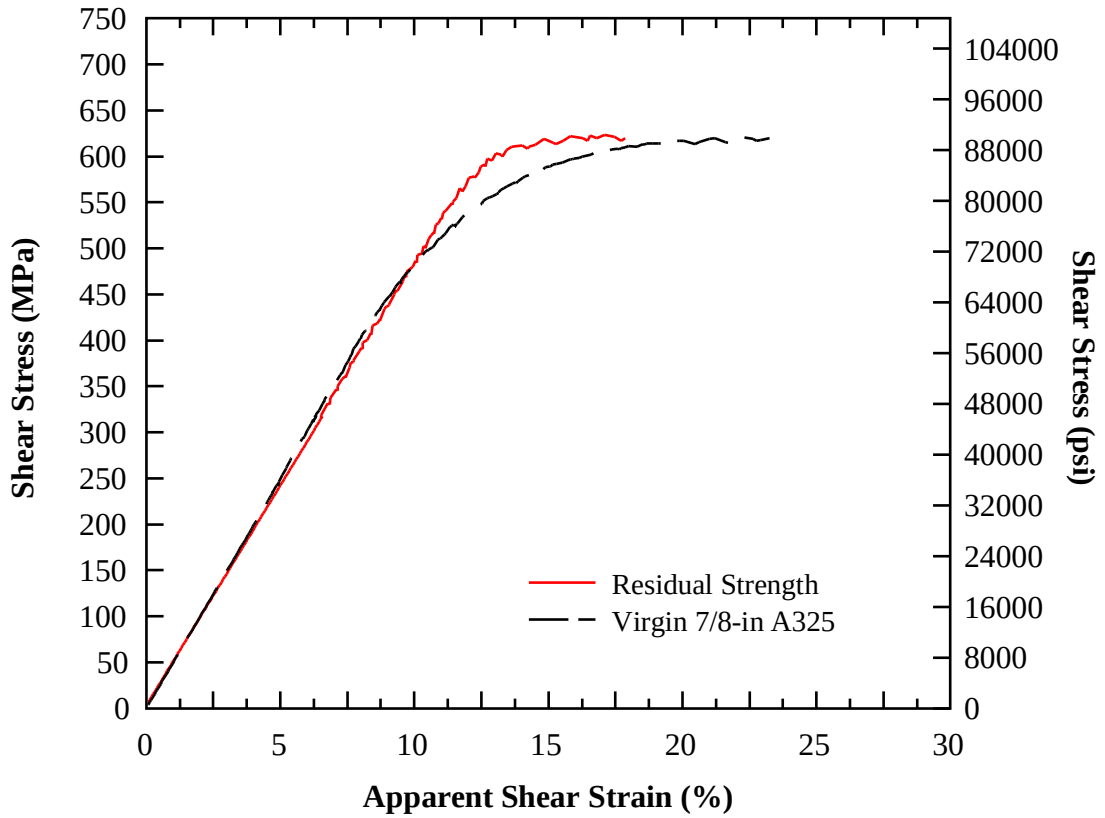

Figure 6.3: Typical residual capacity stress-strain curve.

In Figure 6.3, the rigidity of the bolt is approximately the same as the virgin bolt. This was consistent across all residual capacity tests conducted. Figure 6.4 shows the ratio of the residual rigidity to the average virgin bolt rigidity against the impact energy and strain rate for all tests. The dashed lines for each bolt type show expected ranges based on the variability in the baseline tests. From Figure 6.4, it is evident that residual rigidity of the bolt, regardless of bolt type, is generally equivalent to the virgin bolt rigidity. This appears to be valid regardless of the impact energy or the strain rate in the bolt during the impulsive event.

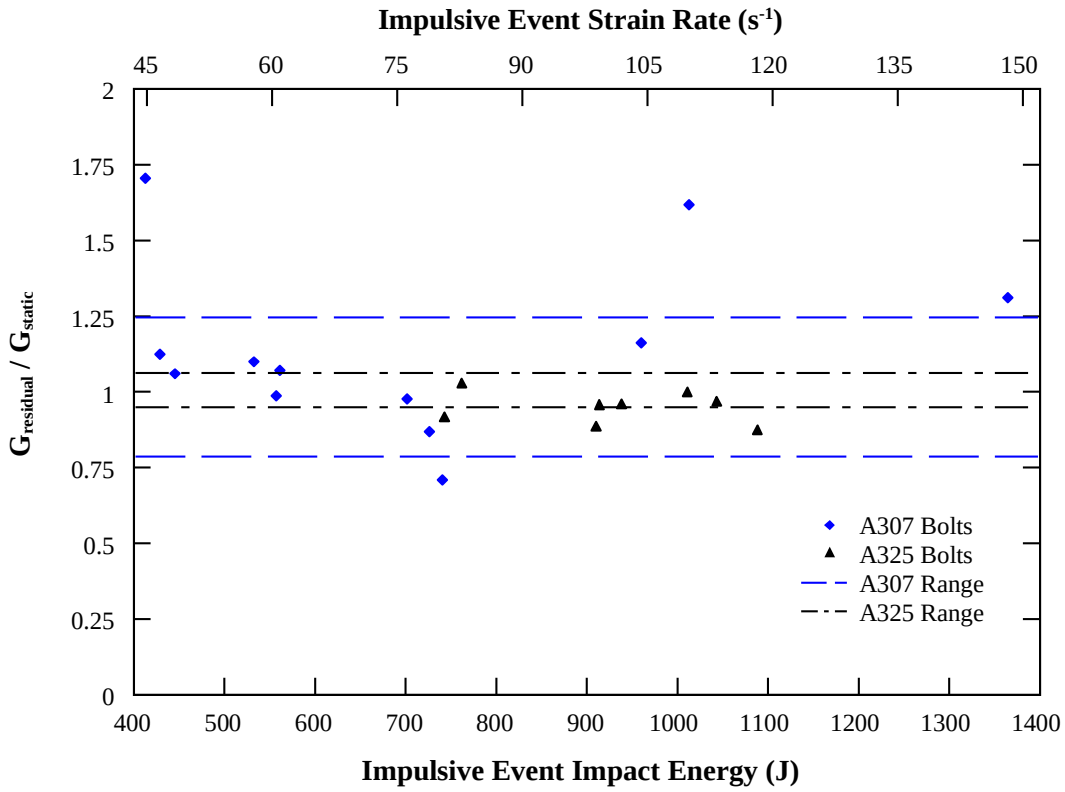

Figure 6.4: Residual rigidity of structural bolts.

The residual strength of the bolt after an impulsive load also appears to be commensurate with the virgin bolt strength. Figure 6.5 shows the residual strength of the bolts tested as a ratio of the residual ultimate strength to the average ultimate strength from the baseline tests. Again, the dashed lines represent the expected range of values based on the variability of the baseline test results. From Figure 6.5 it is evident that from the very slightly damaged range to the heavily damaged range, structural bolts have the equivalent capacity after an impulsive event as though the bolts were never impacted. However, once the bolts become severely damaged – beyond an impact energy of 1100 J for a 7/8 inch (22.2 mm) bolt – the bolts have either reduced capacity or no capacity at all due to fracture during the impulsive event.

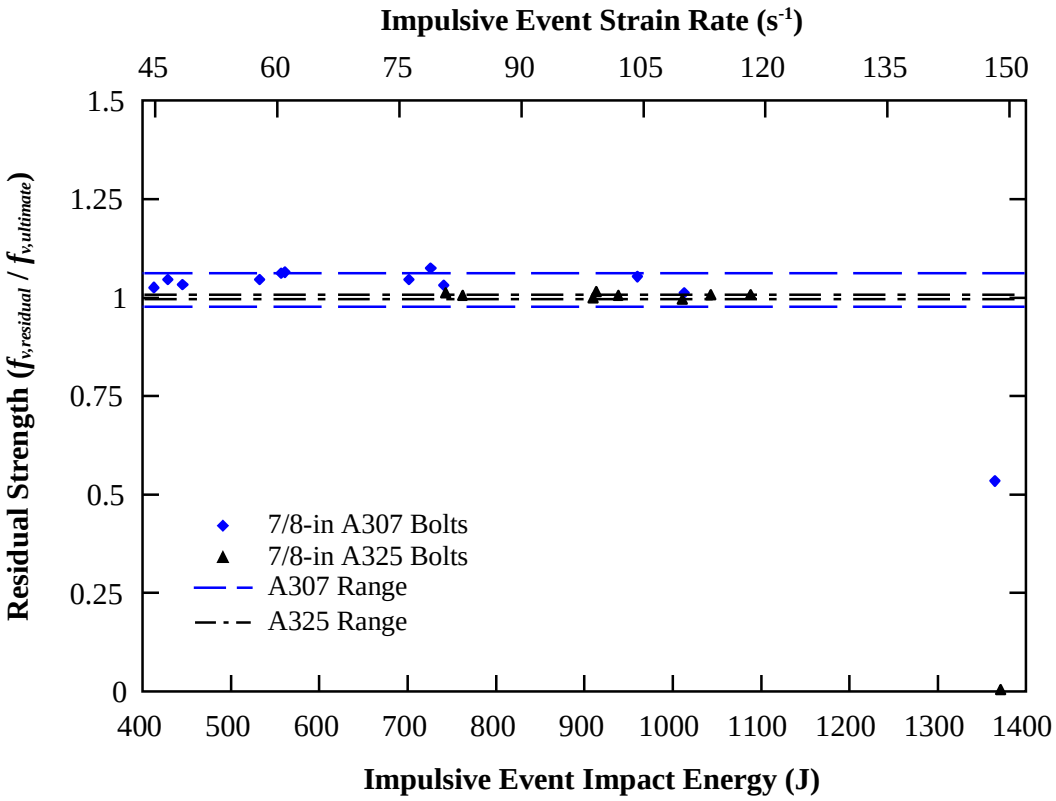

Figure 6.5: Residual strength of structural bolts.

While the residual rigidity and strength are commensurate with that of the virgin bolts, the residual ductility is significantly different than that of a virgin bolt. Figure 6.6 shows the residual ductility of all bolts tested as a ratio of the residual fracture strain to the average fracture strain from the baseline static tests. Figure 6.6 shows that for the majority of tests, the residual ductility is less than the virgin bolt ductility. In one A325 test, RC-325-03, the residual ductility was actually greater than the virgin bolt ductility. However, this test was at the low end of the impact velocities tested and so it is likely that there was actually very little damage to the bolt. For this test, no permanent deformation was noted in the bolt from the impulsive test analysis and so it follows that the bolt would have its full ductility during the residual capacity test.

As expected, the data show that with greater impact energy and therefore more damage to the bolt, there is reduced residual ductility in the bolt. Interestingly, at the lower end of impact energy ranges, the residual ductility is relatively consistent at 78% for A307 bolts and 88% for A325 bolts. These correspond to damage of approximately 33% of the virgin fracture strain in A307 bolts and 20% of the virgin fracture strain in the A325 bolts. At the lower impact energies it is likely that there is not sufficient damage to greatly reduce the residual ductility. Beyond an impact energy of approximately 800 J for A307 bolts and 1,000 J for A325 bolts, the residual ductility of the bolts decreases linearly until there is very little ductility remaining in the bolt and the bolt fractures during the impulsive event.

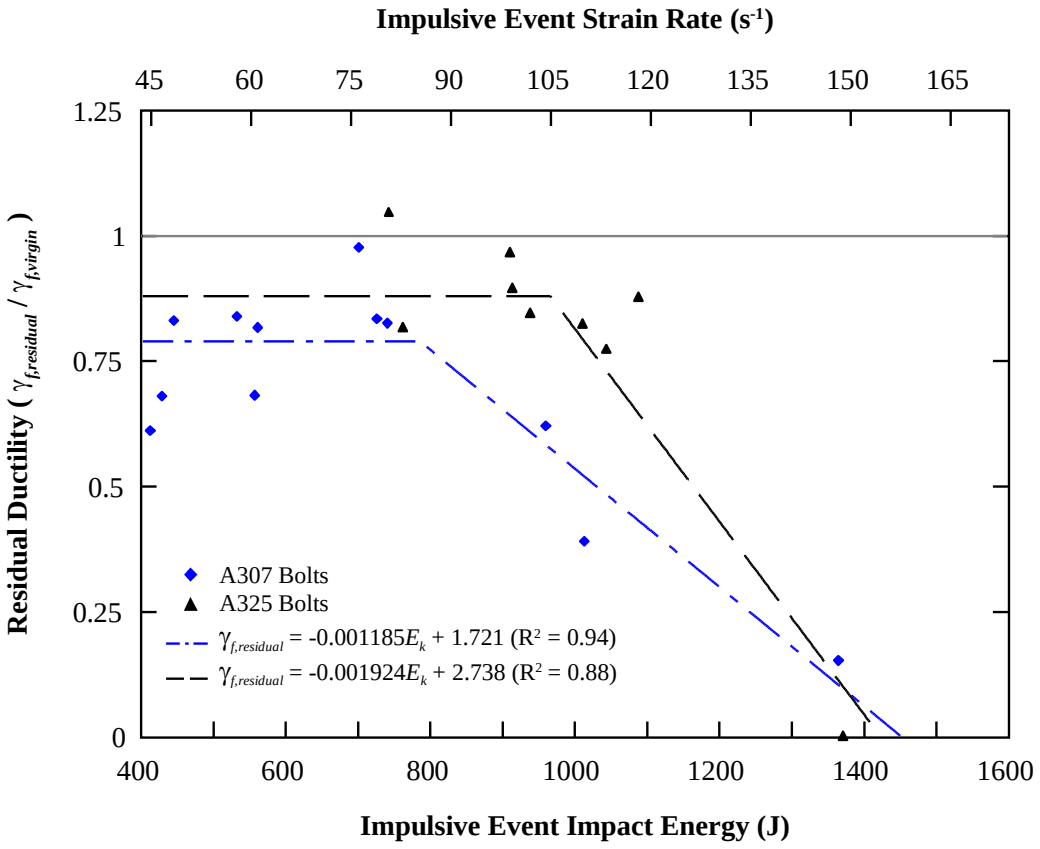

Figure 6.6: Residual ductility of structural bolts.

6.3.2 Composite Event (Impulse + Residual) Behavior

The combination of the residual rigidity, strength, and ductility results indicate that the residual behavior of the bolts after an impulsive event is similar to that of a typical static load-unload-reload behavior observed in ductile materials such as metals. Figure 6.7 illustrates this behavior in a very simple, elastic-perfectly plastic material. If the material is loaded such that plastic deformation occurs and is then unloaded, the material will unload following the modulus of elasticity in tension or rigidity in shear. When the load is completely removed, the material will have residual plastic deformation, $\varepsilon_{p,residual}$. If the material is then subsequently reloaded in the same direction as the initial load, the material will behave elastically until intersecting with the stress-strain curve whereby it will then continue to deform plastically until fracture. Since the load is not reversed, minimal indications of Bauschinger effect will be observed. The total deformation, consisting of the residual plastic deformation from the initial loading and the additional plastic deformation from the reloading are therefore equal to the fracture deformation that would have occurred were the material simply loaded to fracture and not unloaded.

Based on this understanding of material behavior, the bolt shear stress-strain curves developed in Chapter 5 from the impulsive load can be combined with the residual capacity stress-strain curve to determine the overall composite behavior of the structural bolt. Figure 6.8 shows a typical composite curve showing the impulsive stress-strain curve and the residual capacity curve for a single test overlaid with the baseline static tests. In the figure, the residual strength curve was shifted to begin at the measured residual plastic shear deformation from the impulsive event. From Figure 6.8 it is evident that the total ductility of the bolt, when combining the residual plastic deformation from the impulsive

event and the residual ductility, is generally equivalent to the total deformation were the bolt not subjected to an impulsive load.

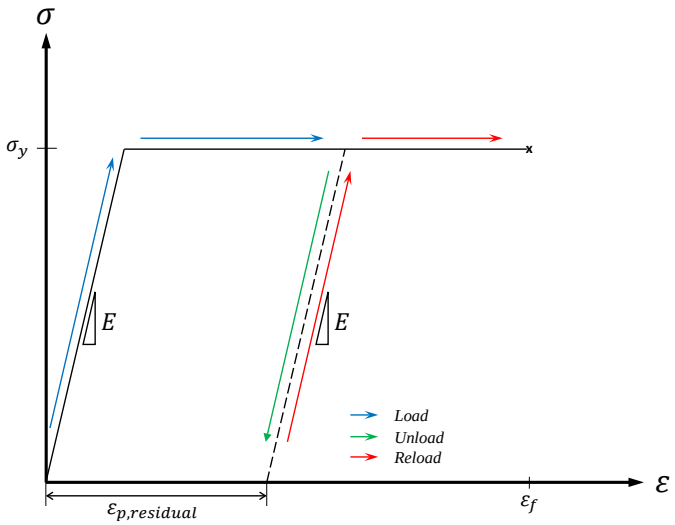

Figure 6.7: Unload-reload behavior model.

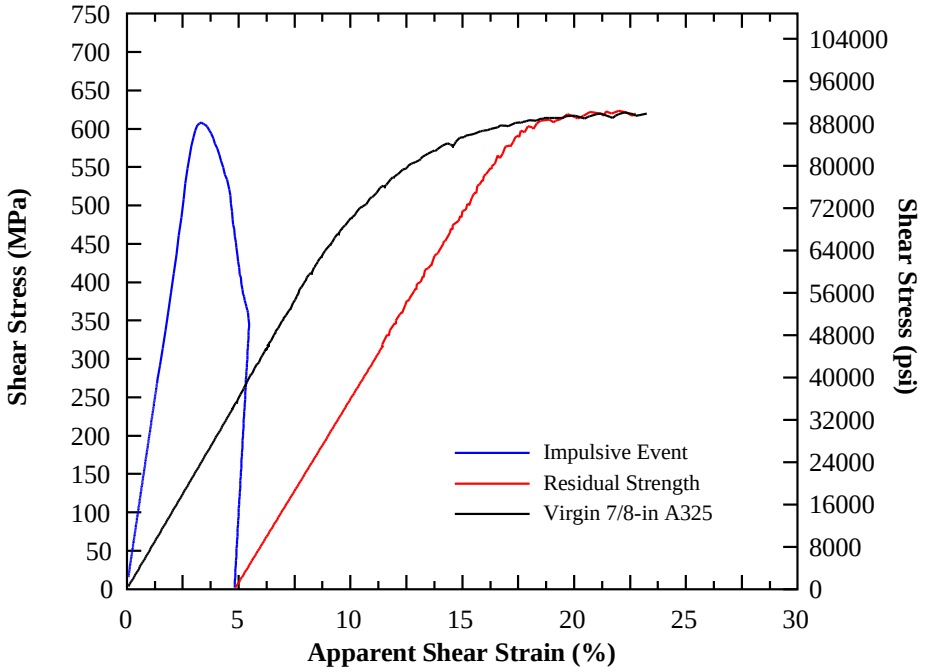

Figure 6.8: Typical composite stress-strain curve.

Across the tests from both types of structural bolt, the total ductility in the bolt was consistent with the ductility of a virgin bolt. Figure 6.9 shows the ratio of total strain to the average fracture strain of the baseline static tests for each test as well as the expected range based on the variability of results in the baseline tests. The majority of tests fall within the expected range with the exception of the severely damaged A307 bolt and the A325 bolt that fractured during the impulsive event. Some outliers exist at lower impact energies but since these tests were A307 bolts manufactured with more imperfections evident in the wider variability in baseline tests, the bolts were likely outside the range of the few baseline static tests conducted.

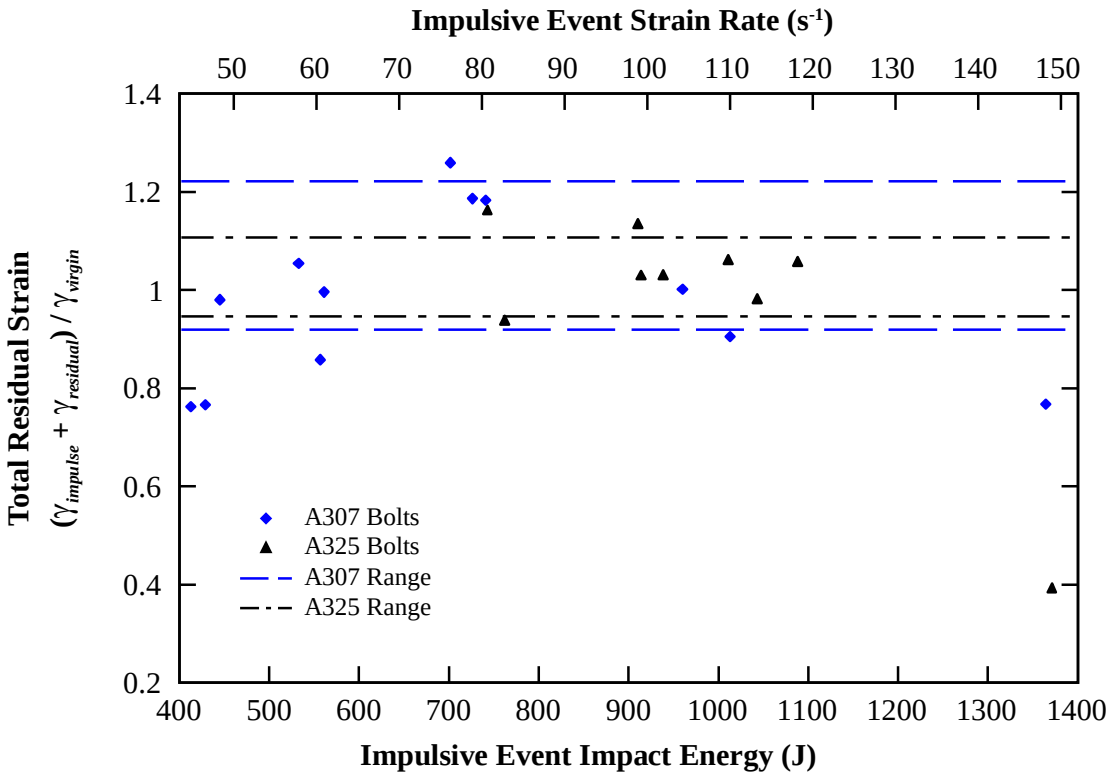

Figure 6.9: Total residual strain.

Closer investigation of the bolts that fractured or had severe damage as a result of the impulsive load present some interesting findings when the impulsive stress-strain curve is compared to the baseline static curve in light of the composite stress-strain curves previously discussed. Figure 6.10 shows the results of test D-325-10 in which the A325 bolt fractured during the impulsive load. While several researchers have conducted dynamic tests on structural bolts, none have compared the performance of the bolts under these loads to their virgin static capacity. From the stress-strain curve in Figure 6.10, the observation can be made that the bolt fractured under the impulsive load at approximately the strain corresponding to the strain at which a virgin bolt was loaded to near fracture and then unloaded. The dashed lines in the figure represent the range of ductility observed in the baseline static tests.

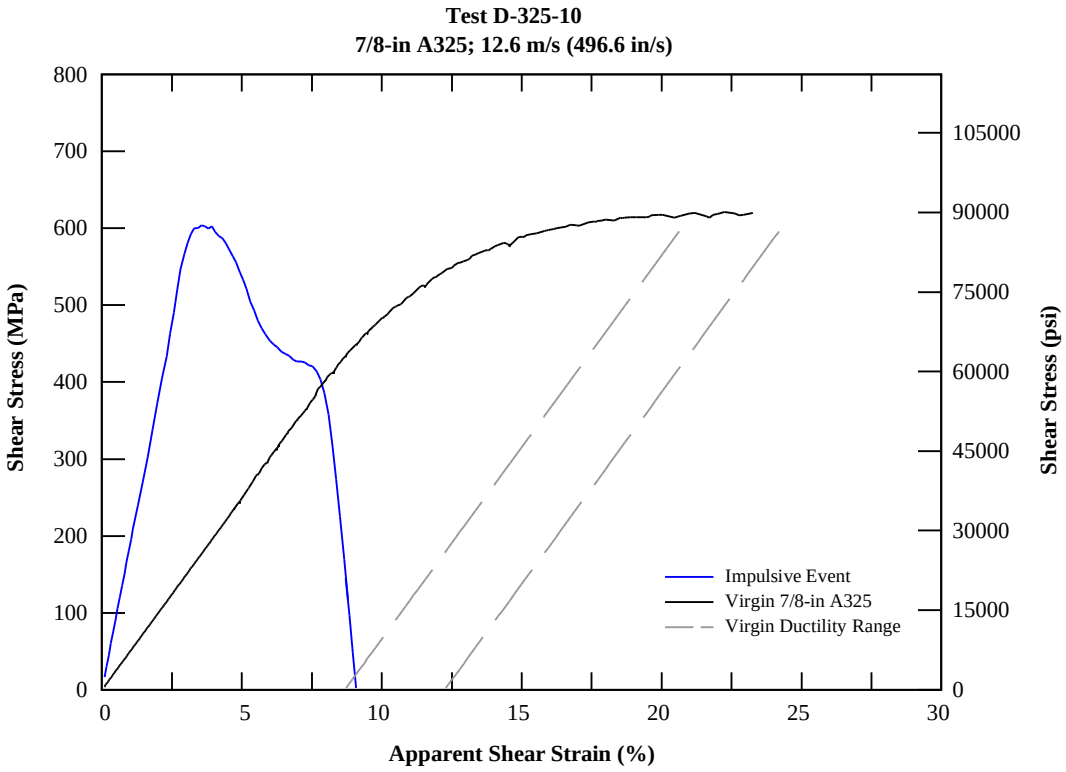

Figure 6.10: Test D-325-10 stress strain curve compared to a virgin A325 bolt.

Test RC-307-12 further supports the observation. During this test the bolt did not fracture during the impulsive event but was severely damaged, and so the bolt was then loaded to fracture using the residual capacity experimental test system. Figure 6.11 shows the composite stress-strain curve for Test RC-307-12. During the residual capacity test, the bolt fractured suddenly while still in the elastic region of the stress-strain curve. In the figure, the residual capacity test results are indicated by the solid red curve. The dashed gray lines again represent the range of ductility observed in the baseline static tests. The dashed red line represents the projected residual capacity from the actual fracture strain. This strain likely represents the maximum strain that the bolt could have experienced before fracture under an impulsive load. These results are significant because they indicate that the fracture strain for structural bolts subjected to impulsive shear loads can be predicted based on the static stress-strain curve.

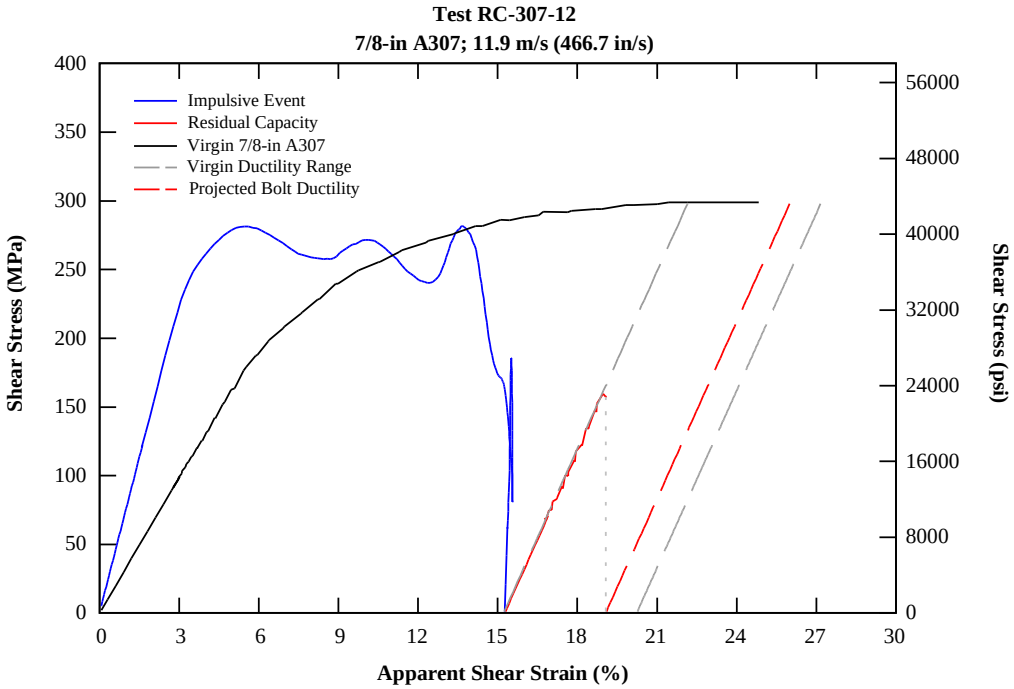

Figure 6.11: Test RC-307-12 stress strain curve compared to a virgin A307 bolt.

The fracture plane of the bolt that fractured under the impulsive load was notably different than those fractured during a residual capacity test and those fractured during the baseline static test. Bolts that fractured in the baseline static test and the residual capacity test exhibited a mixed-mode failure consisting of guillotining and ductile failure observed by other researchers [1]. Figure 6.12 shows the fracture plane from each method of inducing fracture. Both the baseline test and the residual capacity test exhibited a smooth, high sheen surface at the edges indicative of guillotining and a dull, pitted surface in the center, indicative of a ductile failure. The bolt that fractured during impulse, however, showed little evidence of guillotining and was characterized by a shiny, dimpled surface in the center surrounded by dull surface. A full metallographic investigation of the fracture surfaces was beyond the scope of this experimental test series, but the results indicate that the bolts exhibit a ductile failure and that a higher strain rates or impact energies, guillotining in the bolt becomes less pronounced.

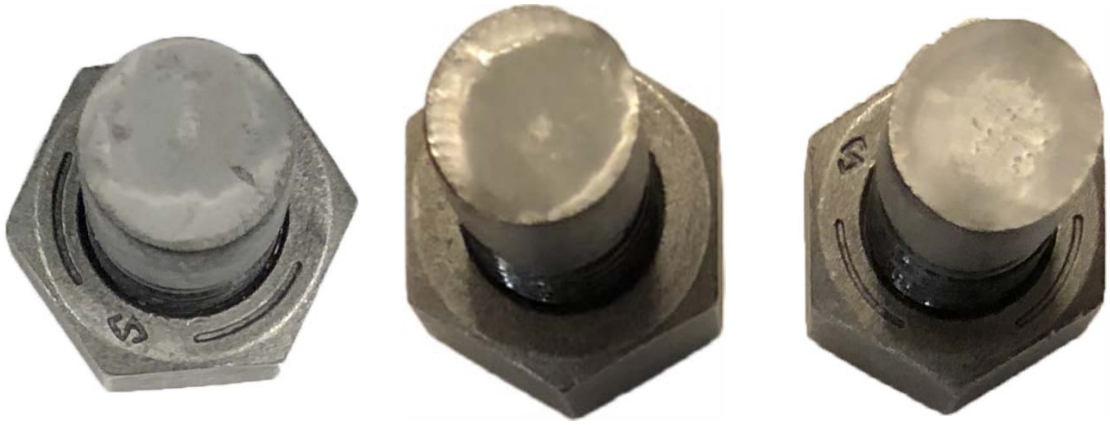

(a) **(b)** **(c)**

Figure 6.12: A325 bolt fracture planes **(a)** baseline test; **(b)** residual capacity test; and **(c)** fracture during impulse.

6.3.3 Residual Capacity of Structural Bolts

Based on the results of the impulsive test series and the residual capacity test series, a general response model of the overall behavior of A307 and A325 structural bolts subjected to impulsive loads can be developed. Figure 6.13 and 6.14 show the models for A307 bolts and A325 bolts, respectively. This model assumes that the impact energy required to cause damage in a structural bolt varies linearly with the bolt diameter. The bolt damage from an impulsive load is reported as the percentage of the residual plastic shear deformation from the impulsive load compared to the static fracture strain of the bolt.

In general, the response model consists of four zones: 1) an elastic response zone; 2) a plastic response zone; 3) a transition zone; and 4) a reduced capacity or bolt fracture zone. At low impact energies the bolt will respond elastically as there will be insufficient energy to cause permanent deformation in the bolt. The largest zone is the plastic response zone. In this zone, the residual strength of the bolt is 100% of the virgin bolt strength, with 40-50% and 20-30% total strain possible without reduced capacity for A307 and A325 bolts, respectively. However, the residual ductility of the bolt in this zone is less than that of a virgin bolt. This ductility decreases linearly with increased impact energy on the bolt.

The fourth zone is the reduced capacity and bolt fracture zone. In this zone, the bolt is severely damaged and will have significantly reduced residual capacity if the bolt does not fracture during impact. The maximum extent of this zone was determined using the range of virgin bolt ductility. Clearly, the one A325 bolt tested in this zone was at the low end of the ductility range tested. The zone between the plastic response zone and reduced capacity zone is a transition zone. Further testing is required to determine the bolt response in this zone as no data were collected in these impact energies. Response in this

zone is likely a combination of reduced capacity and reduced ductility without fracture. Over the spectrum of impact energies that the bolt can absorb, the transition zone is relatively small for both bolt types.

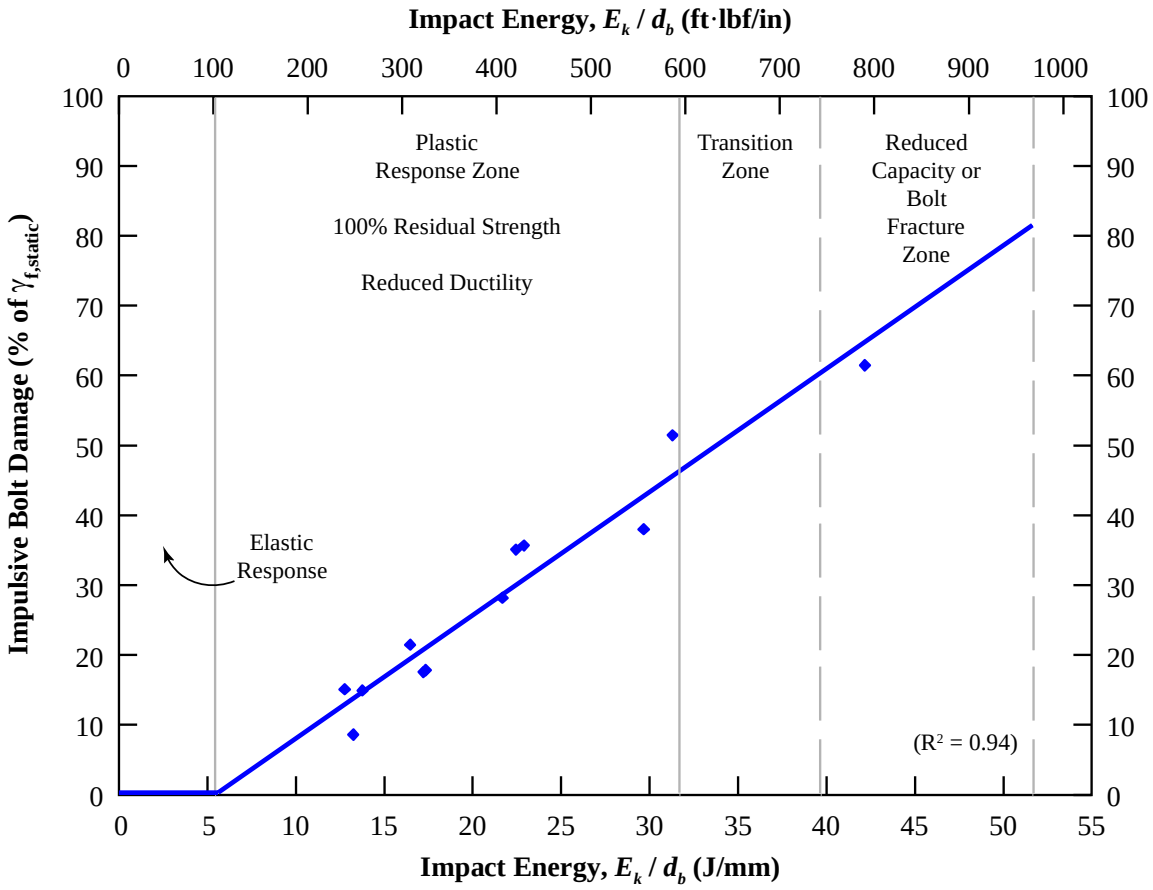

Figure 6.13: A307 bolt damage and residual capacity response model.

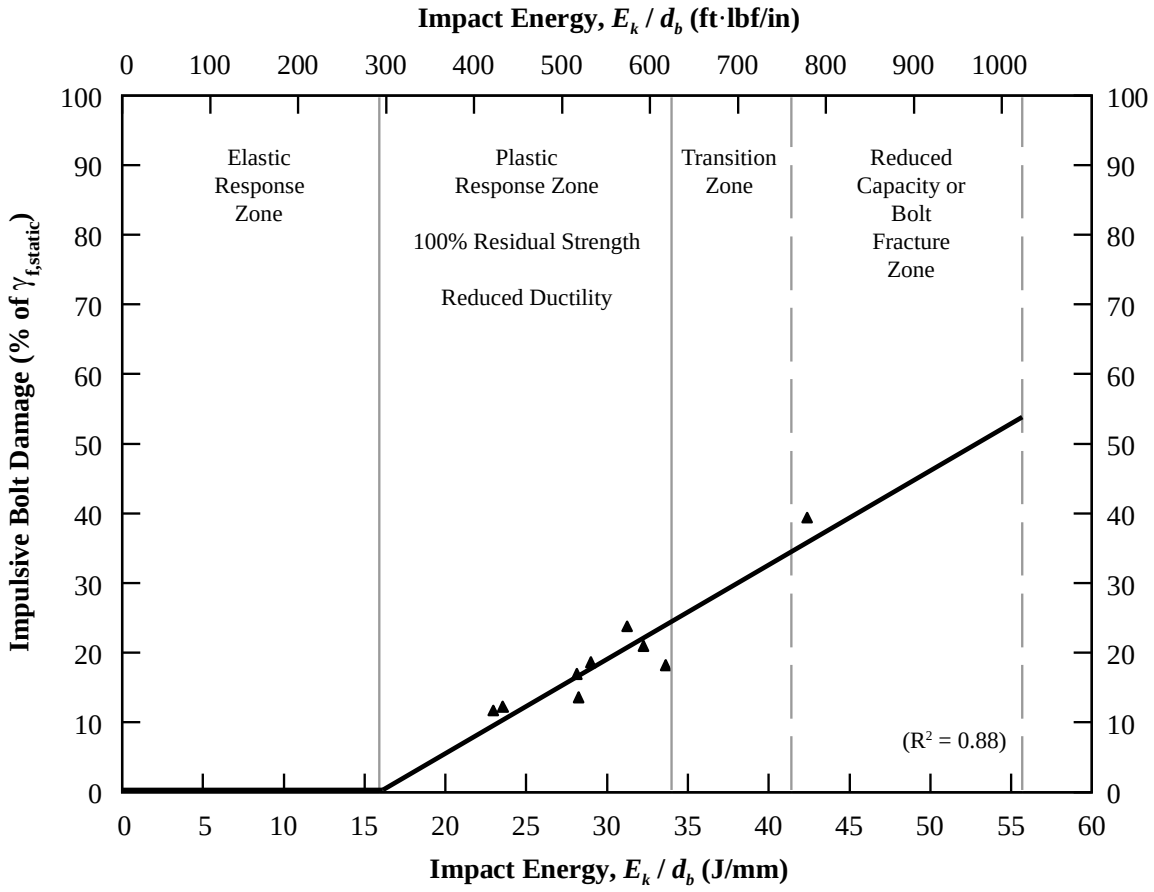

Figure 6.14: A325 bolt damage and residual capacity response model.

6.4 Conclusions

An experimental test series was conducted to investigate the residual capacity behavior of structural bolts after impulsive shear loadings. The bolt shear residual capacity experimental test system was used to conduct the research. Damaged A307 and A325 structural bolts from an impulsive load were subjected to quasi-static tests to determine their residual capacity. Baseline static tests were conducted in the same test rig to compare the static behavior of bolts to the impulsive behavior of bolts under the same conditions. Based on the results of this test series, several important conclusions regarding the residual

capacity behavior of structural bolts after being subjected to an impulsive shear load can be made:

1. Structural bolts' residual modulus of rigidity is not reduced or affected by an impulsive load. In all tests conducted, bolts had the same rigidity in the residual test compared to virgin bolts.

2. For both A307 and A325 7/8 inch (22.2 mm) bolts, an impact energy below approximately 1,100 J (812 ft·lbf) will not reduce the residual strength of the bolt. A307 bolts can deform up to 50% of the bolt's virgin ductility before residual capacity is reduced while A325 bolts can deform up to 30% of the bolt's virgin ductility before residual capacity is reduced.

3. Bolt ductility decreases as the impulsive load on the bolt increases. At lower impact velocities, ductility is reduced 20% from virgin bolt ductility for A307 bolts and 10% for A325 bolts. After impact energies of approximately 800 J (590 ft·lbf), residual ductility decreases linearly in increased impact energy until fracture during the impulsive event occurs.

4. Results indicate that the fracture strain under an impulsive load can be predicted from the virgin bolt stress-strain curve. Bolts appear to fracture at the strain corresponding to a virgin bolt being loaded to near fracture and subsequently unloaded. The fracture plane of bolts that fractured during the impulsive event were significantly different than bolts fractured during residual capacity tests. Guillotining in the bolt appears to decrease as the impact energy increases.

5. A model to predict the residual strain and resulting residual capacity for a bolt subjected to an impulsive shear load was developed. The model accounts for the four

apparent behavior zones based on the impact energy applied to the bolt. At low impact energies, bolts behave elastically. The largest zone is the plastic deformation zone where bolts retain 100% of the virgin bolt strength but have reduced ductility. After a transition where further research is needed, the bolt with either fracture or have significantly reduced capacity.

6.5 References

[1] Horsfall, I., B. Hansen, and D. Carr, "Security of bolted joints during explosive loading," *International Journal of Vehicle Structures & Systems (IJVSS)*, vol. 3, no. 2, pp. 107-112, 2011.

CHAPTER 7

RESIDUAL CAPACITY OF SLIP-CRITICAL CONNECTIONS

7.1 Introduction

Unlike the bolted connections investigated in Chapters 5 and 6, structural bolts are seldom, if ever, installed loosely. Instead, even in bearing-type connections, bolts are pretensioned to varying levels. The pretensioning of the bolt creates a clamping force on the connected members and friction becomes a significant resisting force in the connection to applied loads. The effect of the frictional force on a bolted connection under an impulsive load is not well understood. Further, if the connection survives the impulsive event, the residual bolt tension and residual friction resistance of the connection are even less understood.

An experimental test series was developed to investigate the viability of using the residual capacity experimental test system to investigate the effects of friction in slip-critical connections. The objective of this test series was to quantify the energy dissipation of an impulsive loading through friction and quantify the residual clamping force and force required to initiate slip after such an event. A total of six baseline static tests and six residual capacity tests were conducted using the residual capacity experimental test system. This chapter describes the materials and methods used in the test series, presents the significant findings and observations from the test series, and discusses key conclusions from the experiment.

7.2 Material and Methods

7.2.1 Materials

Materials used in the slip-critical experimental test series were selected to simulate field conditions to the greatest extent possible. Virgin 7/8 inch (22.2 mm) ASTM A325 bolts were used as the structural bolt in the specimen connection. ASTM A307 bolts were not tested because of their inadequacy for use in slip critical connections. In the previous test series the length of the specimen bolts was 3.5 inches (8.89 cm) with a bolt shank length of 2.0 inches (5.08 cm) to ensure that the threaded portion of the bolt did not influence the results. Because the grip length of the bolt for the slip-critical connections was also 2.0 inches, a shorter bolt with a shorter shank was necessary to ensure that the proper bolt tension could be applied to the connection. Therefore, bolts 3.0 inches (7.62 cm) in length were selected for the slip-critical connection tests. Non-standard bolt holes were used in the tests in which the bolt was fractured in bearing. To be more consistent with field conditions and to allow the shear plates additional distance to translate, standard bolt holes oversized by 1/16 inch (1.59 mm) were used in the A572 shear plates for these tests.

Previous experimental tests used ASTM A514, Grade A shear plates to minimize the amount of localized yielding as the specimen bolt was fractured in bearing. Because bearing was not of significant concern in this test series and ASTM A572, Grade 50 steel plates are much more common in steel structures, A572 plates were selected for the shear plates. The surface treatments of the connected plates significantly influence the friction developed between the shear plates. The plates used in this test series were in clean mill

scale condition where loose mill scale was removed by hand with a wire brush and any grease from the manufacturing process was removed with acetone. Steel members are often connected together in this condition given the natural faying surface that the mill scale provides [3].

7.2.2 Experimental Method

The behavior of slip-critical connections during and after an impulsive event was investigated using the residual capacity experimental test system described in Chapters 4 through 6 with slight modification to the bolt installation. Bolts were installed with the nut on top of the impact shear plate as opposed to below the reaction shear plate as was done in previous tests. This was done to facilitate the use of the turn-of-the-nut method, the preferred method for installing high-strength bolts. The *Guide to Design Criteria for Bolted and Riveted Joints* specifies that high-strength bolts should be installed to a preload equivalent to 70% of the minimum ultimate tensile capacity of the bolt. When both connected faces are normal to the bolt axis and the bolt length is up to and including four times the diameter of the bolt, the nut must be rotated 1/3 of a turn from the snug tight condition. The 3.0 inch long, 7/8 inch bolts used in the experiment met this criteria and so the nut was rotated 1/3 of a turn from the snug tight condition to achieve the specified pretension in the bolt.

Achieving the snug tight condition is somewhat vague. The snug tight condition is achieved through either a few impacts from an impact wrench or the full force of an ironworker using an ordinary spud wrench [5]. Figure 7.1 shows the spud wrench used to install the bolts to snug tight. For consistency, the bolt was installed to the snug tight

condition by the same researcher for each test. After the bolt was installed to the snug tight condition, the connection was visually and physically inspected to ensure that the shear plates were in full, firm contact and the impact T-section was unable to move with a light tap of the hand. Prior to and after installing the bolt to the snug tight condition, alignment of the setup was verified so as to ensure a direct hit from the flyer mass to the greatest extent possible.

Figure 7.1: Spud wrench used for snug tight condition.

Once the bolt was installed to the snug tight condition, the bolt was rotated 1/3 of a turn using a Proto Electronic Torque Wrench, Model J6347, with a range of 60 to 600 ft·lbf (81.3 - 813.5 N·m). Figure 7.2 shows the torque wrench used to rotate the nut. The torque wrench was used to measure the torque required to rotate the nut for comparative purposes but was not the primary control for achieving the desired bolt tension. In addition, the torque wrench was also used to measure the torque required to break the bolt after a test. Instead, from the snug tight condition, one of the points of the nut was marked with a grease pencil. At the point corresponding to 1/3 of a turn (the second point from the initial marking since the nut was hexagonal) the shear plate was marked indicating how much rotation in the nut was required. Figure 7.3(a) shows the setup prior to pretensioning the bolt. The nut was then rotated until the mark on the nut was aligned with the mark on the shear plate, as shown in Figure 7.3(b). While specifications allow for a tolerance of

±30°, for consistency between tests, the nut was rotated to as close to 1/3 of a turn as possible.

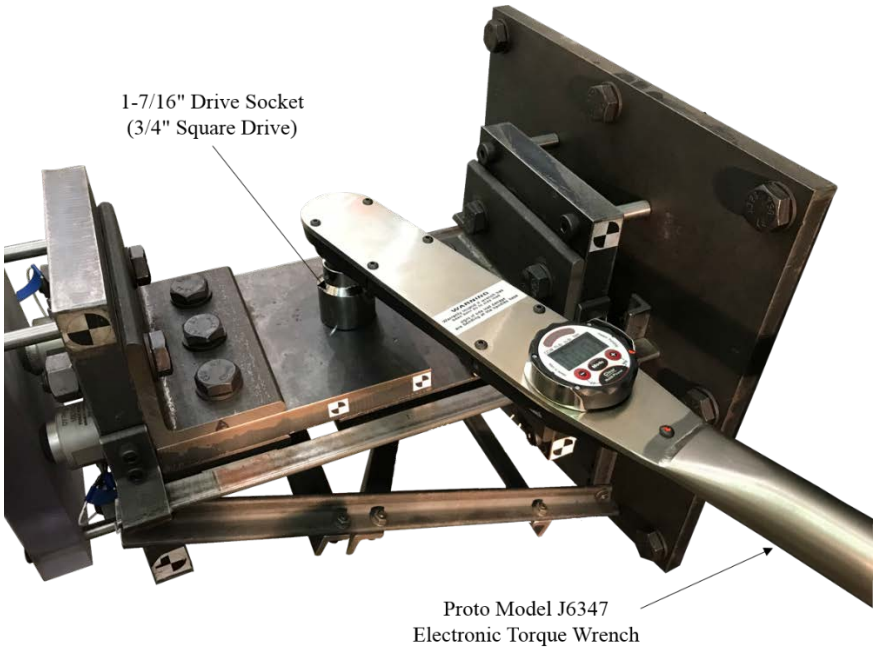

Figure 7.2: Proto Model J6347 used to pretension structural bolt.

Because this test series was conducted as a preliminary investigation into the viability of the use of the residual capacity experimental system to investigate slip critical connections, a limited number of tests were conducted at varying velocities and corresponding impact energies. Table 7.1 shows the six tests that were conducted as part of this test series. Target velocities ranged from the low end of the blast generator's system limits at 5.0 m/s (197 in/s) to velocities that were capable of causing moderate damage to the structural bolt when the bolts were installed loosely at 10.0 m/s (394 in/s). In addition to the residual capacity tests, six baseline tests were conducted. These tests were conducted under the same conditions with the exception of the impulsive event. Virgin bolts were

used for each baseline test and for each residual capacity test. In this test series, bolts were loaded until the first major slip as opposed to being loaded until fracture. Once major slip occurs and the bolt is fully engaged by the shear plates, the test is not fundamentally different than the bearing type tests previously conducted.

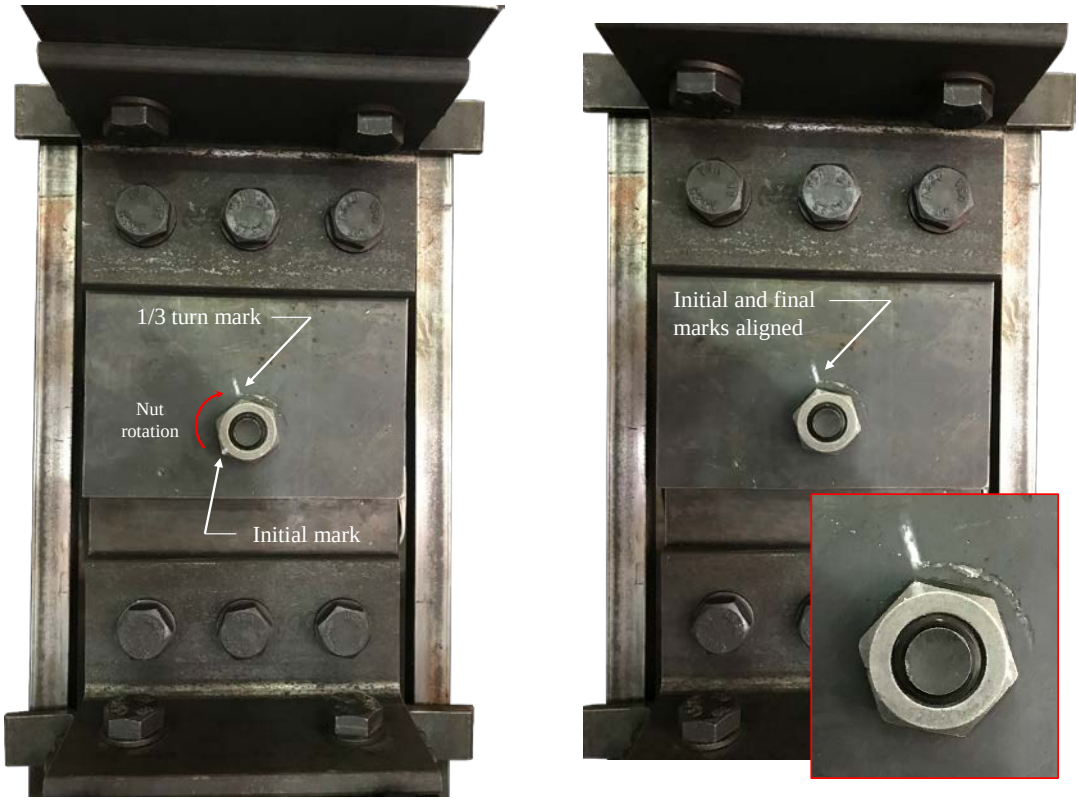

(a) **(b)**

Figure 7.3: Turn-of-the-nut method **(a)** prior to rotating nut; and **(b)** rotated nut.

Table 7.1: Slip-critical test series.

	Test #	Bolt Type	Impact Velocity m/s (in/s)	Target Impact Energy J	Actual Impact Energy J	Shear Plate Relative Velocity m/s (in/s)
1	SC-325-01	A325	5.0	215	196.0	0.62 (24.6)
2	SC-325-01	A325	6.0	310	381.9	1.65 (66.2)
3	SC-325-01	A325	7.0	422	560.8	0.70 (28.2)
4	SC-325-01	A325	8.0	551	708.3	2.18 (87.4)
5	SC-325-01	A325	9.0	698	831.7	2.74 (109.5)
6	SC-325-01	A325	10.0	862	1,022.7	3.00 (119.8)

7.3 Theory and Calculation

7.3.1 Major Slip

As discussed in Section 2.1 of Chapter 2, slip-critical connections rely on friction to resist load. Once the load exceeds the friction resistance developed in the connection due to the clamping force generated by pretensioning the structural bolt and the coefficient of friction between the connected plates, the connected plates will slip past one another. The load that first causes major slip to occur is referred to as the slip load, P_{slip}, and is determined by:

$$P_{slip} = k_s m_s \sum_{i=1}^{n_b} F_{p_i} \tag{7.1}$$

where k_s is the slip coefficient, m_s is the number of shear planes, n_b is the number of bolts in the connection, and F_p is the pretension in each individual bolt. Experimentally this can be observed by a sudden, large displacement with no increase in load. Figure 7.4 shows a

typical force-displacement curve from a baseline static slip-critical test. In Figure 7.4, the slip load corresponds to the plateau at approximately 22,000 lbf (100 kN). The amount of slip, or translation of the shear plate, can also be determined from the force-displacement curve.

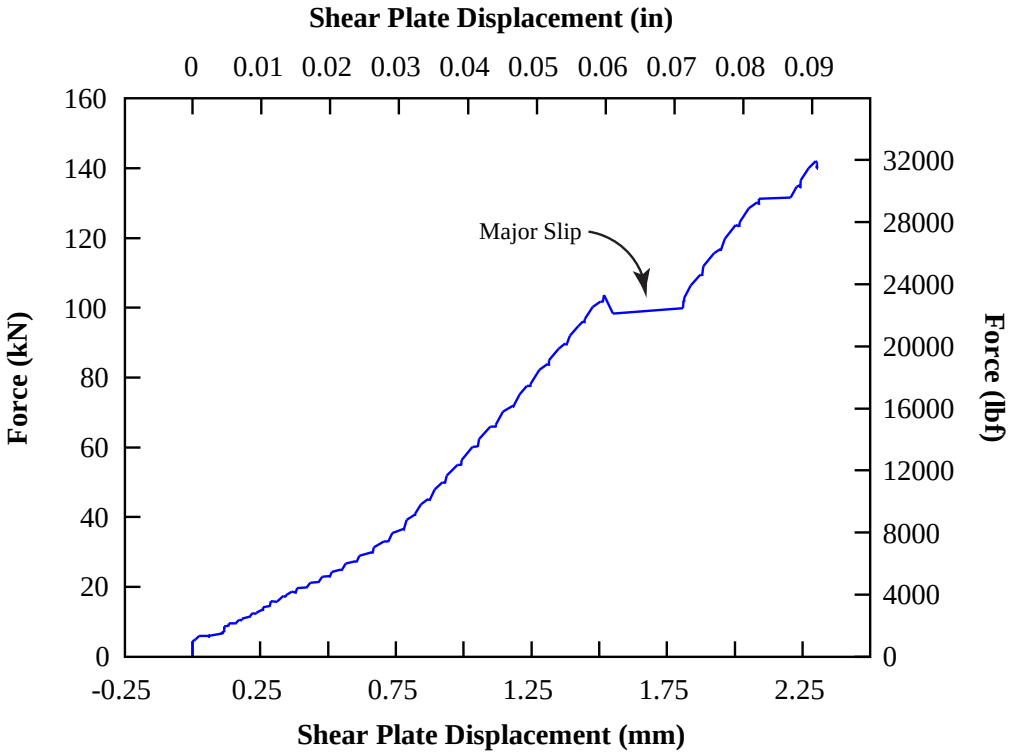

Figure 7.4: Typical static slip-critical test.

7.3.2 Dynamics of Sliding Friction

Despite the well-known, fundamental nature of the physics of friction described by Coulomb's friction law ($F = \mu N$), the nature of sliding friction of a solid body on a substrate is tremendously complex [4]. In reality, multiscale effects contribute to sliding friction behavior, from the macroscale to the subatomic level. As a result, work in tribology – the science of solids moving in contact relative to one another – and friction continue to be

prevalent to further understand the forces at play throughout all levels of interaction. However, the research conducted here is most concerned with the classical physics of sliding friction at the macroscale level where gravitational forces most influence the dynamics of sliding friction. Specifically, the friction interaction and resulting friction force that develops between the two shear plates is of most interest. The critical components of the friction system developed by pretensioning the structural bolt are the fixed reaction shear plate and sliding impact shear plate.

The resulting motion of sliding friction is governed by the sliding velocity of the impact shear plate and the overall system elastic stiffness. The system elastic stiffness results from the elastic properties of the shear plates themselves as well as the elastic properties of the interface between the two plates formed by the surface topography and residual surface contaminants. Figure 7.5 shows a representative kinetic phase diagram describing the interaction between the sliding velocity and the system elastic stiffness. If the system elastic stiffness is large enough, at any sliding velocity the sliding plate's motion will be governed by steady sliding. In steady sliding, frictional forces resist motion until reaching the static friction force at which time the plate will begin move in a steady motion with a constant kinetic friction force developed at the interaction. Likewise, if the sliding velocity is large enough, steady sliding will occur regardless of the system elastic stiffness. However, below a critical sliding velocity and critical system elastic stiffness, stick-slip motion will occur. In stick-slip motion, the sliding plate oscillates between no motion and sliding, resulting in a periodic frictional force between the static friction force and the kinetic friction force. The phase diagram must be ascertained experimentally to determine the critical stiffness and velocity at which steady sliding occurs [4].

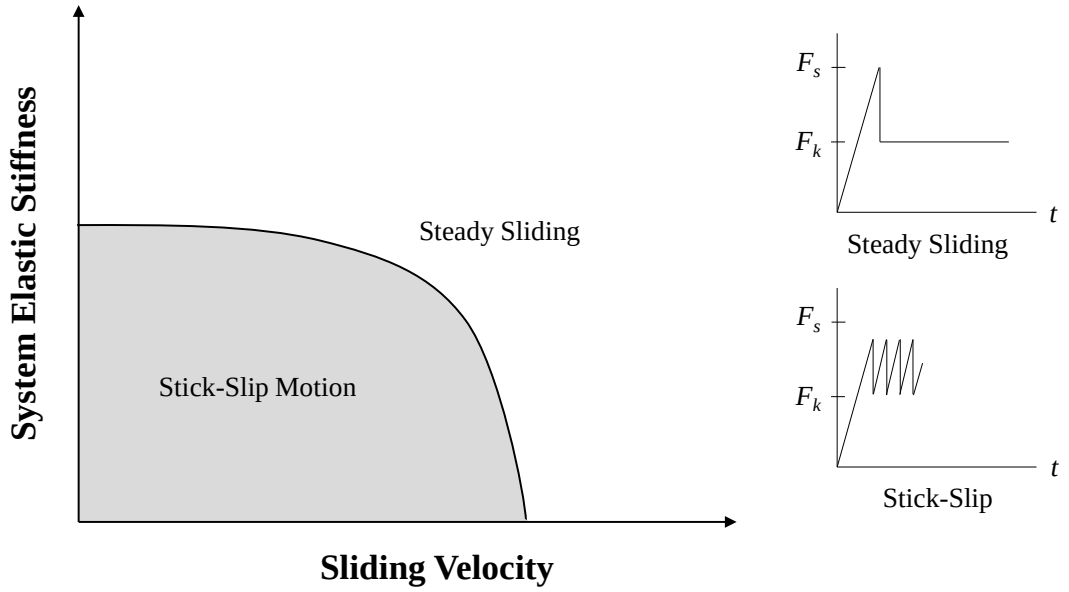

Figure 7.5: Representative kinetic phase diagram for a block sliding on a surface (adapted from [4]).

7.3.3 Impulsive Resistance due to Friction

As discussed in Chapter 5, the reaction load cell data can be used to determine the impulsive resistance of the specimen bolt. Similarly, the reaction load cell data can be used to determine the impulsive friction resistance in a slip critical connection. Figure 7.6 shows a typical low velocity test where the friction resistance in the connection prevented the specimen bolt from becoming fully engaged with the shear plates. In these tests, the friction resistance fully absorbed the impact of the flyer mass through stick-slip motion. As before, the reaction impulse – in this case due to friction – can be determined by integrating the force-time history over time. The peak friction resistance can be taken as the peak reaction force.

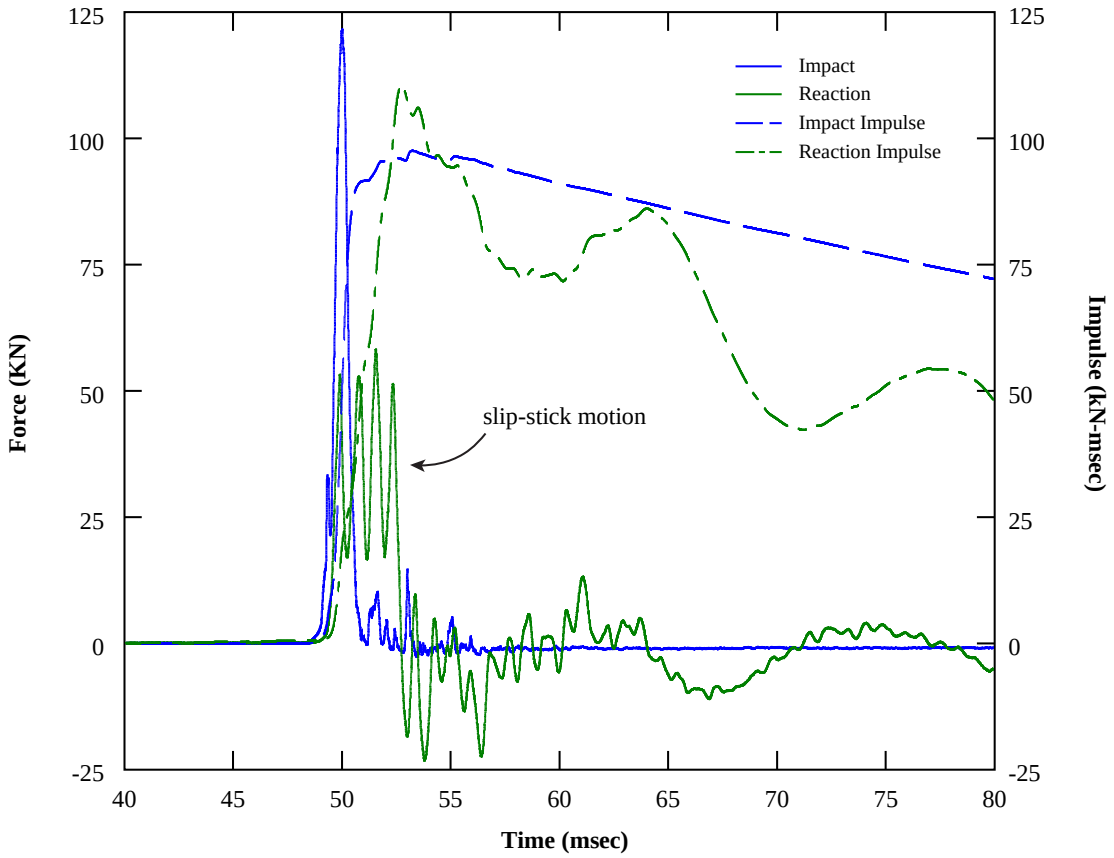

Figure 7.6: Force-time history and impulse for a typical low velocity test.

Even if the impact energy is such that the bolt becomes partially or fully engaged, the reaction load cell data shows two distinct pulses, one for the friction resistance and one for the impact with the bolt. Figure 7.7 shows the force-time history and impulse for a typical higher velocity test. The first pulse, the friction resistance, occurs near simultaneously with the impact and is again characterized by stick-slip behavior. Following the first pulse is a higher, more distinct pulse of the impact with the structural bolt. Again, the impulsive friction resistance can be determined through integration of the force-time history, but in this case, only the initial reaction due to friction is integrated.

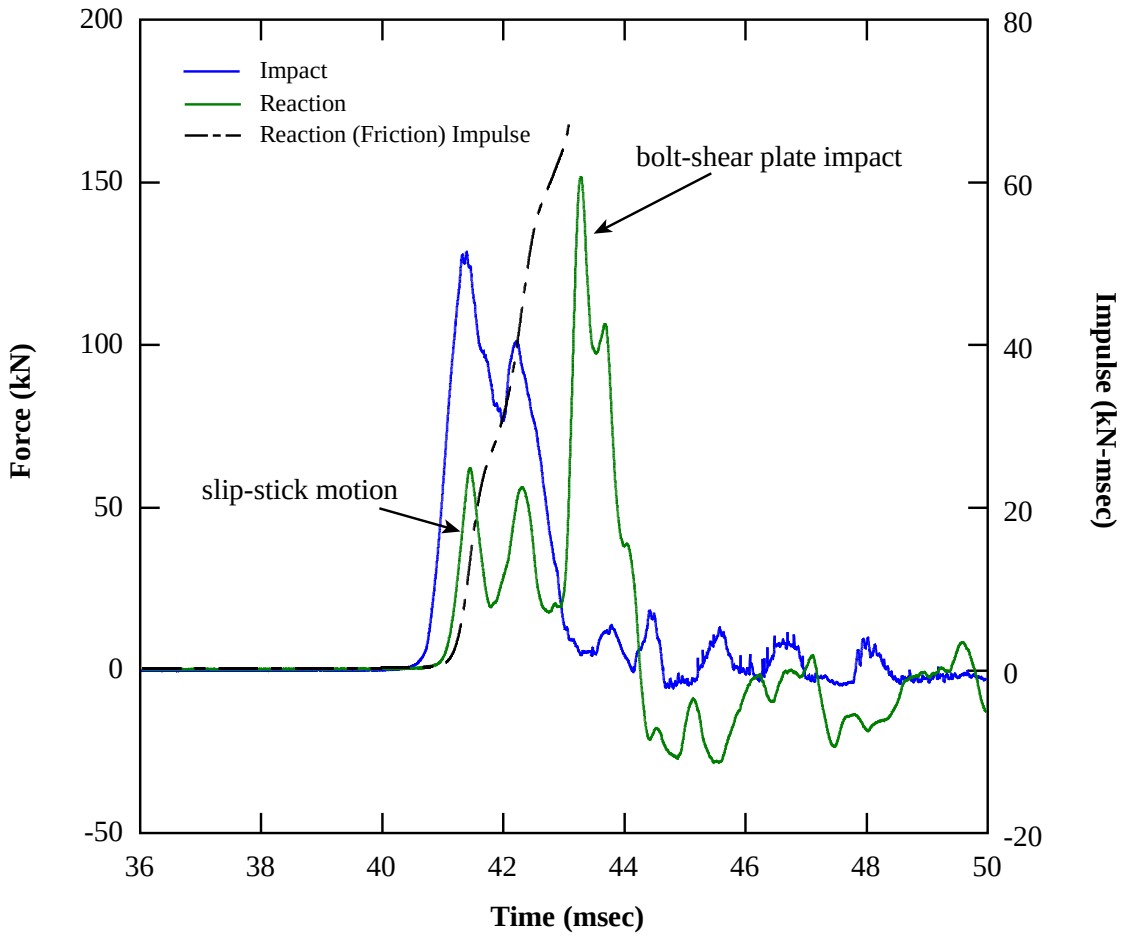

Figure 7.7: Force-time history and impulse for a typical low velocity test.

7.3.4 Shear Plate Displacement

Similar to the procedure discussed in Chapter 5, the high speed video recordings of the slip-critical connection yield valuable data regarding the behavior of the connection during an impulsive event. Figure 7.8 shows the typical displacement-time history of the impact shear plate during the impulsive event. In the figure, x_0 represents the initial displacement, x_1 represents the peak displacement, and x_2 represents the rebound displacement. From this data, the slip due to the impulse, $d_{slip,impulse}$ and the rebound displacement, $d_{rebound}$, can be determined for the event:

$$d_{slip,impulse} = x_1 - x_0 \tag{7.2}$$

$$d_{rebound} = x_2 - x_1 \tag{7.3}$$

Additionally, the average relative velocity, v_{rel}, of the impact T-section during the impulse can be determined by calculating the slope of the initial displacement:

$$v_{rel} = \frac{x_1 - x_0}{t_1 - t_0} \tag{7.4}$$

where t_0 and t_1 are times corresponding to x_0 and x_1, respectively.

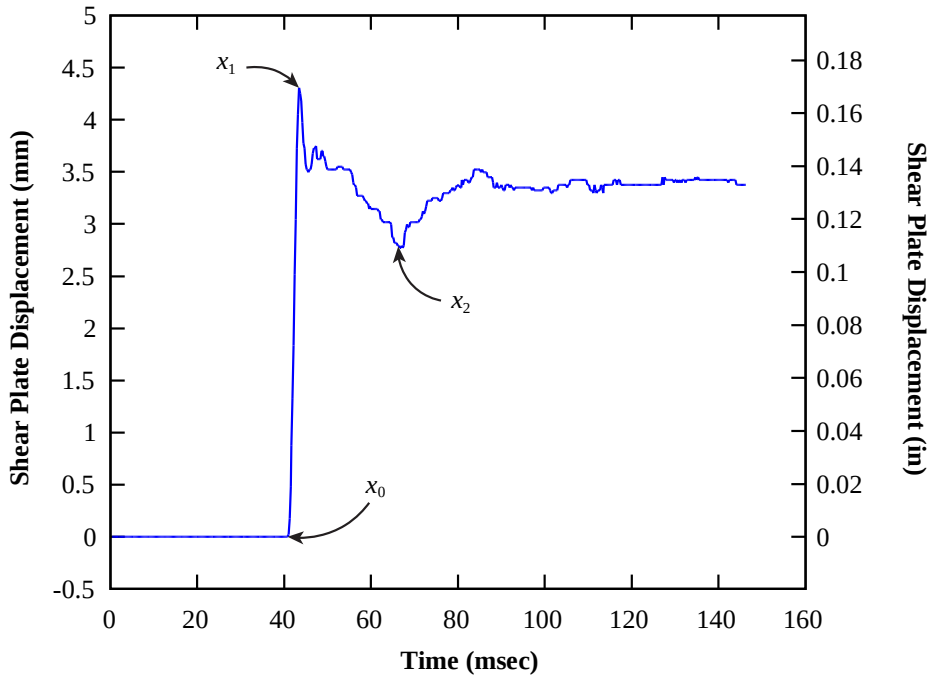

Figure 7.8: Typical high speed video data for a slip-critical test.

7.3.5 Static and Dynamic Friction Parameters

Of particular importance to those modeling slip-critical connections are the coefficients of static friction, μ_s, dynamic friction, μ_d, and the parameters that govern the

transition between the two. The coefficients of static and dynamic friction can be estimated by rearranging Equation 7.1 and solving for the coefficient of friction, k_s, in the equation. In this experimental setup, there is only one shear plane so $m_s = 1$ and there is only one bolt so $n_b = 1$. In the equation, P_{slip} is equal to the force required to cause slip from the baseline static tests while P_{slip} is equal to the peak friction resistance in the impulsive event. Solving for the friction coefficient yields:

$$k_{s,static} = \mu_s = \frac{P_{slip,static}}{F_p} \tag{7.5}$$

$$k_{s,dynamic} = \mu_d = \frac{P_{peak,impulse}}{F_p} \tag{7.6}$$

Some difficulty exists in determining an accurate value for the tensile force in the bolt. Methods such as direct tension indicators would have provided more precise measurements of the tension in the bolt, but the use of these methods was beyond the scope and budget of this project. As a result, multiple methods were used to estimate the tension in the bolt. In the first method, the tension was assumed to be the minimum tension required for a 7/8 inch A325 bolt. The minimum tension for this diameter bolt is 39,000 lbf (173 kN) and was applied to all tests. This method is reasonable, although not entirely accurate, due to the controlled nature in which the bolts were installed. The second method to estimate the tension in the bolt was through the use of the torque data collected during bolt installation. Using this method, the tension in the bolt, F_p, is estimated by [2]:

$$F_p = \frac{T}{K d_b} \tag{7.7}$$

where T is the tightening torque, K is the torque-friction factor, typically taken as 0.20 for steel bolts and nuts, and d_b is the nominal bolt diameter. There were several drawbacks in using this method to estimate the tension in the bolt. First, the torque wrench was only

calibrated to 600 ft·lbf (813.5 N·m) and several of the bolt torque measurements exceeded that value. Second, the method is generally not precise due to the uncertainty in the torque-friction factor. Because neither method was particularly ideal, both methods were used in determining the friction factor and the results compared to one another.

7.3.6 Energy Dissipation due to Friction

Critical to understanding the behavior of a slip-critical connection during an impulsive event is being able to quantify the energy dissipation due to friction. This is important because as more energy is dissipated through friction, there is less energy in the system to cause significant damage to the structural bolt. As was observed in Chapter 6, structural bolts, particularly A325 structural bolts, can absorb a significant amount of energy through impact and still maintain 100% of their strength though some ductility will be lost.

The energy dissipation through friction can be estimated by applying the conservation of energy. Figure 7.9 shows the impulsive event as a series of three phases. In the first phase, the flyer mass, m_{flyer}, is moving at an initial velocity, v_0, from the blast simulator. The impact T section, m_T, is stationary. The second phase represents the events occurring during impact. From the high speed video data of the slip-critical tests, it was observed that the flyer mass maintained contact with the impact T-section throughout the impulse. This is opposite of what was observed during the impulsive tests discussed in Chapter 5, which exhibited immediate rebound due to the reaction shock wave from the stiffer bolt impact. In this model, therefore, the flyer mass and the impact T section move together at some velocity, v_1, during the impulsive event. During this phase, work due to

friction, W_f, dissipates the energy of the flyer mass and the impact T-section. As a result, the velocity, v_1, is significantly lower. Finally, in the third phase, after impact, the flyer mass rebounds and the impact T-section stops translating because it either makes contact with the structural bolt or the friction resistance has caused it to stop displacing.

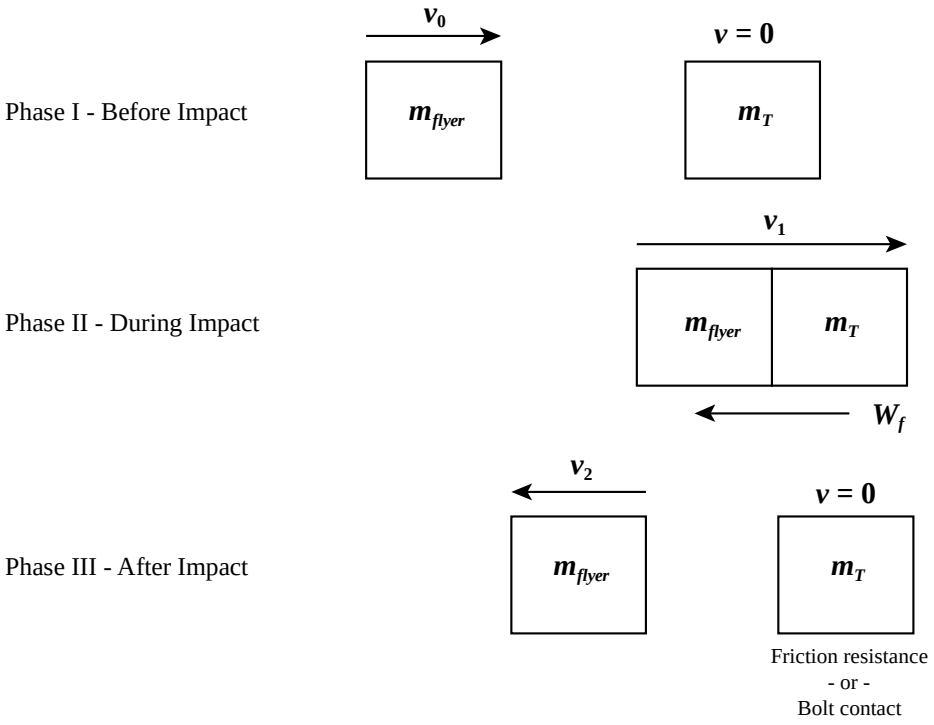

Figure 7.9: Slip-critical event phases.

This investigation was concerned with quantifying the energy dissipation during impact, and so Phases I and II are most relevant. Based on this idealized representation of the impulsive event, the energy equilibrium in the system during impact can be written as:

$$E_{k,flyer} = E_{k,flyer} + E_{k,T} + W_f \tag{7.8}$$

$$\frac{1}{2} m_{flyer} v_0^2 = \frac{1}{2} \left(m_{flyer} + m_T \right) v_1^2 + W_f \tag{7.9}$$

Previous impulsive testing noted that on average there was a 15% loss of energy in the system due to friction present without the additional friction developed by pretensioning the structural bolt. Therefore, the impact energy was reduced by 15% to attempt to account for friction already present in the system. Applying this factor and solving for the work due to friction yields:

$$W_f = (0.85)\left[\frac{1}{2}m_{flyer}v_0^2\right] - \frac{1}{2}\left(m_{flyer} + m_T\right)v_1^2 \tag{7.10}$$

During the experiment, the initial flyer velocity, v_0, and the rebound velocity, v_2, were measured by one of the high speed cameras while the velocity of the impact T-section was captured by the second high speed camera. Masses of all the components were measured prior to testing. Thus, Equation 7.10 was used to estimate the work due to friction in the system or, in other words, the energy dissipation in the system due to friction.

7.4 Results and Discussion

7.4.1 Baseline Tests

The six baseline tests yielded consistent results across all of the data measured and with the expected behavior for slip-critical connections described in Section 2.1 of Chapter 2. Table 7.2 shows the baseline test results, including the tightening torque, T, slip load, P_{slip}, the slip displacement, d_{slip}, the torque required to break the bolt after slipping, T_{break} and the ratio of the break torque to the initial tightening torque. The tightening torque results varied by nearly 20%, likely a result of the variability in friction between the nut and the threads. The tightening torque did not appear to correlate with the resulting slip load, however, as tests with the highest tightening torque had the lowest slip loads and tests

with the lowest tightening torque had the highest slip loads. These results further demonstrate the limitations of using torque control methods to achieve preload in structural bolts.

Table 7.2: Baseline test results

	T ft·lbf (N·m)	P_{slip} lbf (kN)	d_{slip} in (mm)	T_{break} ft·lbf (N·m)	T_{break} / T
B2-325-01	579.8 (786.1)	17,946 (79.8)	0.0407 (1.03)	389.7 (528.4)	0.67
B2-325-02	628.1 (851.6)	16,628 (74.0)	0.0438 (1.11)	402.8 (546.1)	0.64
B2-325-03	600.3 (813.9)	16,416 (73.0)	0.0406 (1.03)	361.9 (490.7)	0.60
B2-325-04	625.7 (848.3)	19,178 (85.3)	0.0389 (0.99)	371.4 (503.6)	0.59
B2-325-05	538.9 (730.6)	19,802 (88.0)	0.0403 (1.02)	335.4 (454.7)	0.62
B2-325-06	534.5 (724.7)	22,068 (98.2)	0.0609 (1.55)	324.6 (440.1)	0.61
Average	584.6 (792.6)	18,673 (83.1)	0.0442 (1.12)	364.3 (493.9)	0.62

A wider range of results than was expected for the slip load was observed in the baseline tests. Because the turn-of-the-nut method was used consistently, results were expected to be within 5 to 10% of each other, however, results varied as much as 25%. This is most likely a result of the difficulty in achieving a more consistent snug tight condition. For example, in test B2-325-06, the bolt may have been significantly tighter at the snug condition compared to test B2-325-03. So while a consistent level of preload was induced in both bolts after the snug tight condition, the total clamping force on the plates

may have been higher in B2-325-06 due to the preload developed in achieving the snug tight condition.

The slip displacement yielded the most consistent results from test to test due to the fact that there was only so much available displacement before the shear plate made contact with the bolt. Test B2-325-06 exhibited a 50% higher slip displacement than the other tests but the same test also had a significantly higher slip load. It appears that the higher slip load resulted in more stored energy in the system up to slip, and so it follows that the displacement would be higher than in other tests.

The break torque and ratio of break torque to the tightening torque yield interesting results. The results indicate that as the connected plates slide past one another, relaxation of the bolt pretension occurs. This relaxation was consistently around 62% for the tests conducted. There are likely many mechanisms at play that cause such relaxation to occur during slip-critical connection failure, but these are beyond the scope of this project. The break torque, however, does present another point of comparison between the static behavior and the dynamic behavior.

7.4.2 Slip-Critical Connections during Impulsive Events

The force required to initiate slip during the impulsive event was compared to the force required to initiate slip in the baseline static tests to determine if the applied impulse had any effect in the behavior of the connection. Figure 7.10 shows the impulsive slip ratio, $P_{peak,impulse} / P_{slip,static}$, as a function of the impact energy. The dashed lines represent the expected range based on the variability in the static slip load. From Figure 7.10, it is evident that the dynamic slip ratio is reasonably consistent across the range of impact

energies tested. On average, the force required to cause slip in the dynamic event was 75% of the static force required to cause slip. These results are consistent with the efficiencies observed in the bolt damage test series described in Chapter 5 and are likely the result of losses in the system previously discussed in Chapter 5.

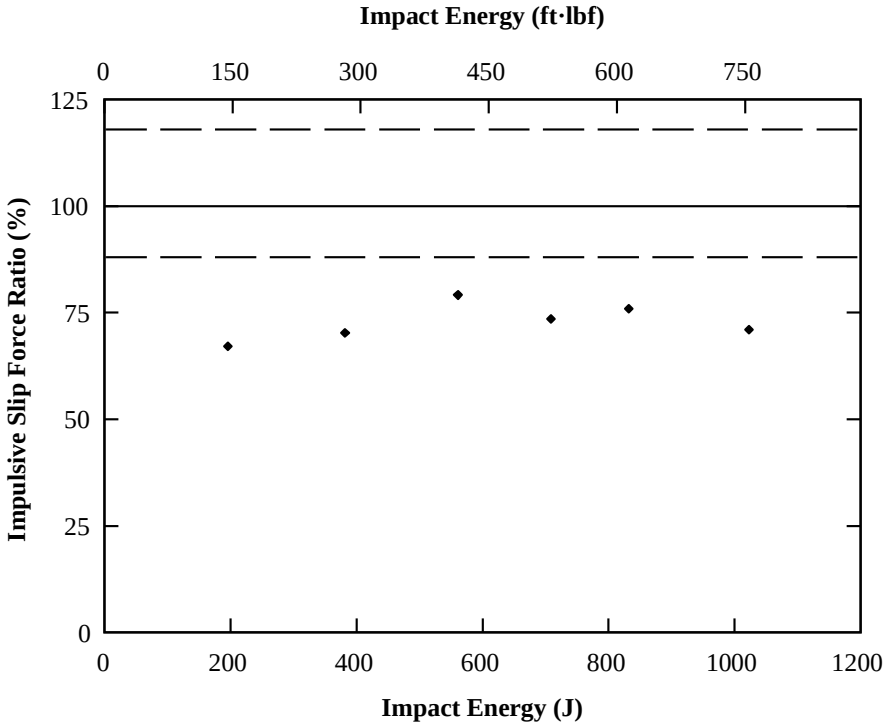

Figure 7.10: Force required to initiate slip during the impulsive event.

The impulsive friction resistance is a measure of how the developed frictional force in the slip-critical connection provides a reaction force to the applied impulse. Figure 7.11 shows the measured impulsive friction resistance for varying impact energies. From the figure, it is apparent that below an impact energy of approximately 600 J (443 ft·lbf), the impulsive friction resistance is relatively constant. After an impact energy of 600 J, however, the impulsive friction resistance drops considerably as the impact energy

increases. These results follow logically from the fact that at the higher impact energies, the impact shear plate travels at a higher velocity and therefore fully engages the bolt more quickly. As a result, there is less time for the friction force to respond and since the impulse is the integral of the friction force over time, there will be less of an impulsive friction resistance.

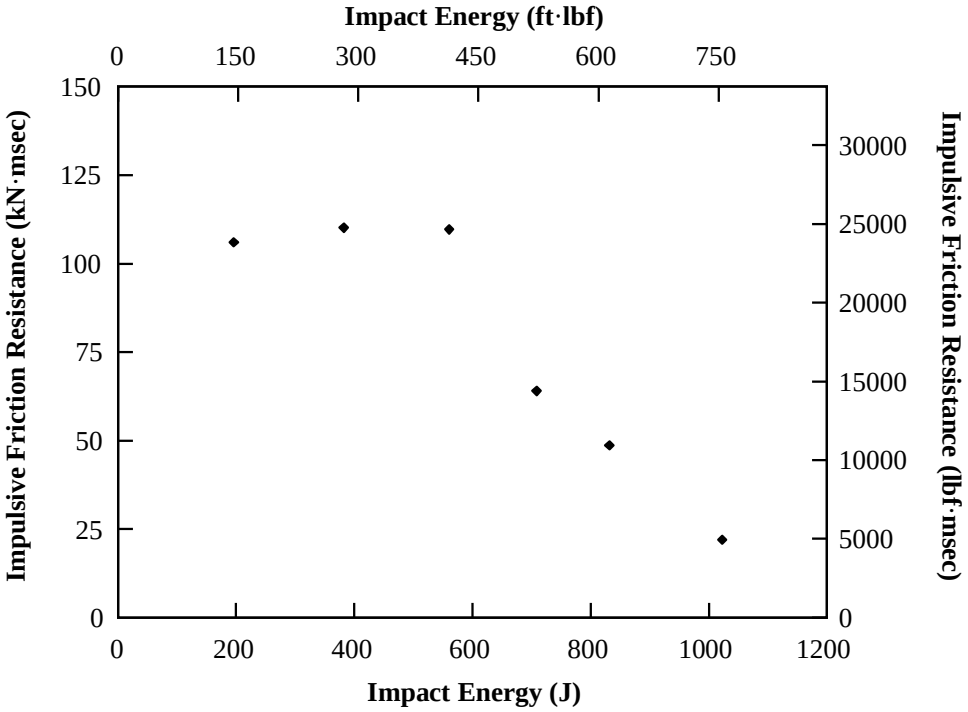

Figure 7.11: Impulsive friction resistance.

The effects of friction during the impulsive event can also be understood by examining the amount that the impact shear plate slips and understanding whether or not the bolt becomes fully engaged during the impulsive. Similarly, the rebound displacement provides an indication of whether or not the friction resistance continues to dissipate energy as the impact shear plate rebounds. Figure 7.12 shows the maximum slip displacement for

each test as a function of the impact energy. The blue dashed line indicates the maximum slip possible with the bolt fully engaged and fully rotated within the bolt hole. The red dashed-dot line indicates the bolt is fully engaged with no bolt rotation.

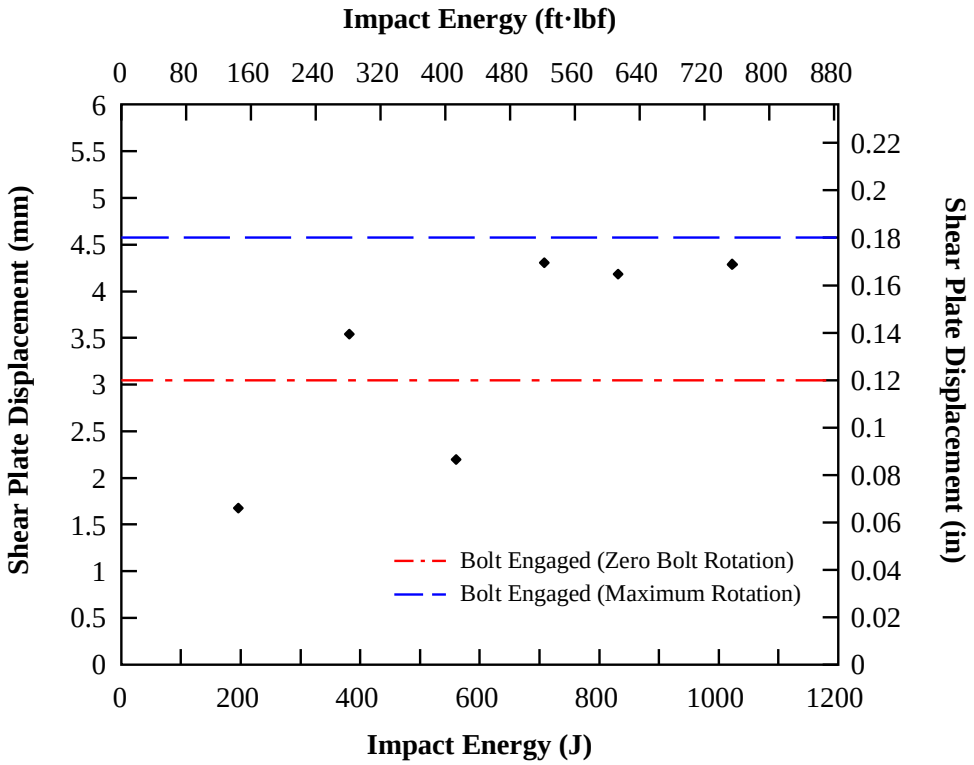

Figure 7.12: Maximum slip displacement.

The results shown in Figure 7.12 indicate again that an impact energy of approximately 600 J (443 ft·lbf) is a threshold for the response of slip-critical connections. Below that threshold, the friction resistance does not appear to be sufficient in preventing the impact shear plate from fully engaging the bolt. It should be noted that SC-325-02 appears to be outlying data point. The measured relative velocity of the impact T-section was significantly higher than expected (see Table 7.1) based on the tests immediately preceding and following. It is likely that the minimum pretension in the bolt was not

achieved for this test and as a result, the clamping force was significantly lower. This would explain the higher level of displacement in this test.

Figure 7.13 shows the maximum rebound displacement as a function of the impact energy. The results show that the amount of rebound is a linear function of the impact energy:

$$d_{rebound} = 0.002073E_k \quad \text{[mm, J]} \tag{7.12}$$

$$d_{rebound} = 0.000153E_k \quad \text{[in, ft·lbf]} \tag{7.13}$$

The results show a good correlation with an R^2 value of 0.92. As the impact energy increases, the amount of rebound displacement increases. However, the results and observations showed that the impact T-section did not rebound to its initial starting position, which indicates that the clamping force continues to dissipate energy throughout the event.

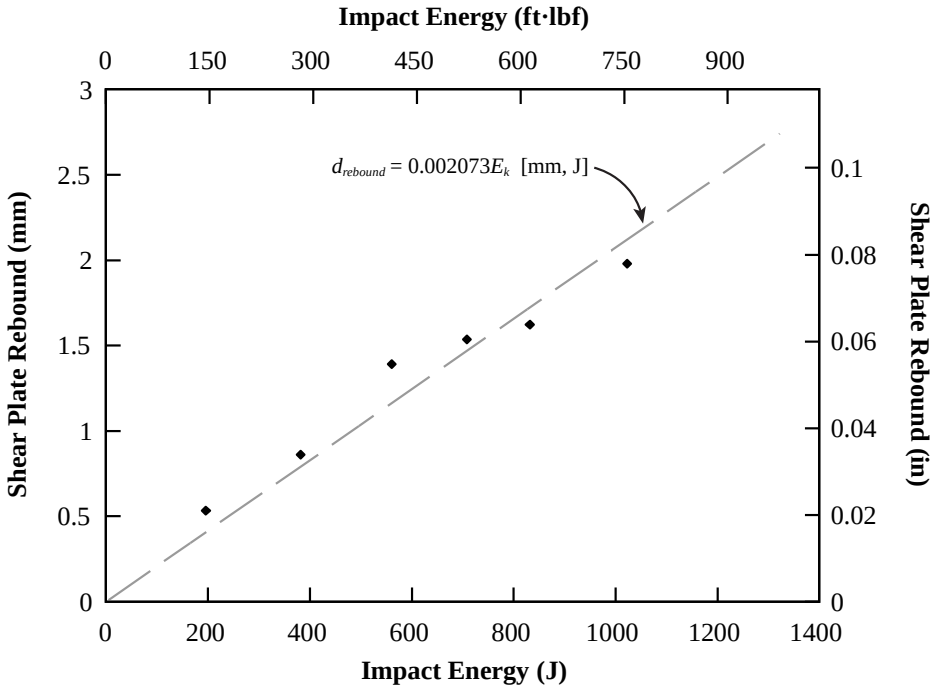

Figure 7.13: Maximum rebound displacement.

An understanding of the energy dissipated through friction is critical in understanding the net impact on the structural bolt in bearing and the resulting survivability of the bolt to the impulsive event. Figure 7.14 shows the friction energy dissipation, estimated as described in Section 7.3.5, as a function of the applied impact energy on the connection. From the results, it is apparent that the amount of energy dissipated through friction increases linearly ($R^2 = 0.91$) with impact energy for the range of impact energies tested:

$$W_f = 0.6479E_k \quad \text{[mm, J]} \tag{7.14}$$

$$W_f = 0.4782E_k \quad \text{[in, ft·lbf]} \tag{7.15}$$

This follows logically from the fact that as the impact energy increases, the velocity of the impact T-section increases with it. Because the energy dissipated by friction is a function of the velocity of the impact-T section, the work done by friction must also increase.

Based on this understanding of friction energy dissipation in the connection, the net impact energy on the bolt in bearing can be estimated. Figure 7.15 shows the friction energy dissipation as a percentage of the impact energy and the resulting net impact energy on the bolt. At impact energies where full slip did not occur and the bolt was not fully engaged, all of the impact energy is dissipated through friction. The results for these tests are slightly below 100% most likely due to minor losses in the programmer and the impact plate. SC-325-02 is also skewed for reasons previously discussed. At impact energies where the bolt was fully engaged, only 20 to 30% of the initial impact energy of the flyer was transferred to bolt. The net impact energy is substantially lower than the impact energy required to cause permanent bolt damage and well below the impact energy required to fracture the bolt in the impulsive event.

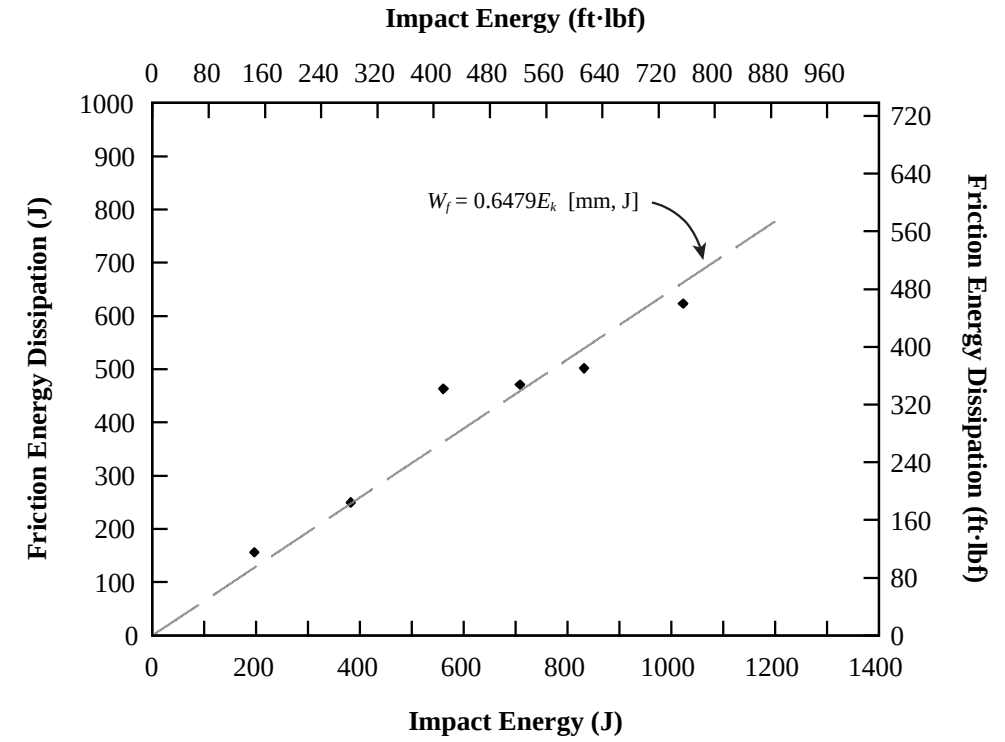

Figure 7.14: Energy dissipation through friction.

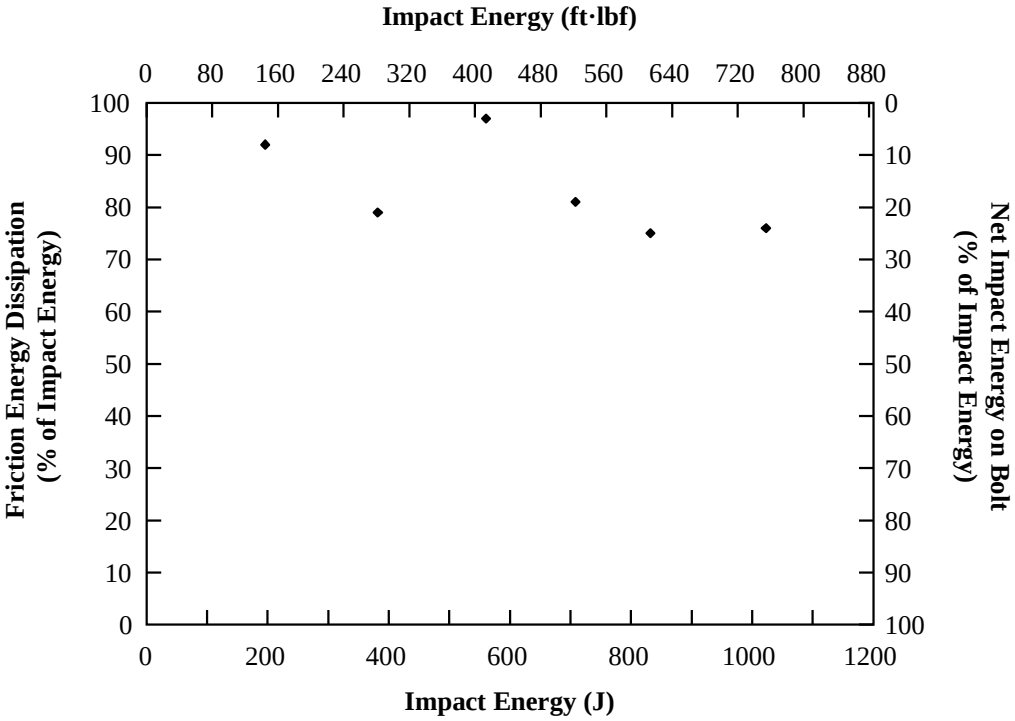

Figure 7.15: Net impact energy on the bolt in a slip-critical connection.

The importance of clamping force and friction resistance in bolted steel connections subjected to an impulsive load cannot be understated. Slip-critical connections substantially protect the structural bolts from damage by dissipating energy through friction. Further, very few structural steel connections in the field are fabricated with a single bolt. As was shown in Equation 7.1, additional bolts have a multiplicative effect on the force required to resist slip and therefore would also increase the energy dissipation through friction in an impulsive event. Current design guidelines do not require the bolts in bearing-type connections to be tightened beyond snug tight. Based on the results presented in this section, requiring that all bolts be pretensioned would significantly increase the survivability of structural bolts to an impulsive load. The effects of friction resistance in a connection should not be neglected for connections subjected to impulsive loads. Furthermore, additional research is required to better measure and quantify the effects of friction resistance under impulsive loads for different types of surface treatments and materials.

7.4.3 Static and Dynamic Friction Coefficients

Based on the static baseline tests and the impulsive event tests, coefficients of static and dynamic friction can be determined as well as the parameters that govern the transition between the two. Table 7.3 shows the calculated coefficient of static friction based on the baseline static tests while Table 7.4 shows the calculated coefficient of dynamic friction based on the impulsive tests. These coefficients of friction are valid for clean mill scale ASTM A572, Grade 50 plates. In the tables, both methods of estimating the bolt tension,

either by assuming a minimum bolt tension of 39,000 lbf (173 kN) (Method 1) or by estimating the bolt tension based on the tightening torque (Method 2) are shown.

Table 7.3: Coefficient of static friction results.

		Method 1		Method 2	
	P_{slip} lbf (kN)	F_p lbf (kN)	μ_s	F_p lbf (kN)	μ_s
B2-325-01	17,946 (79.8)	39,000 (173)	0.46017	39,758	0.45140
B2-325-02	16,628 (74.0)		0.42636	43,070	0.38607
B2-325-03	16,416 (73.0)		0.42093	41,163	0.39880
B2-325-04	19,178 (85.3)		0.49174	42,905	0.44698
B2-325-05	19,802 (88.0)		0.50778	36,953	0.53588
B2-325-06	22,068 (98.2)		0.56384	36,651	0.60210
Average	18,673 (83.1)		0.48	40,083	0.47

Table 7.4: Coefficient of dynamic friction results.

		Method 1		Method 2	
	$P_{peak,impulse}$ lbf (kN)	F_p lbf (kN)	μ_s	F_p lbf (kN)	μ_s
SC-325-01	12,517	39,000 (173)	0.32096	39,072	0.32037
SC-325-02	13,109		0.33613	41,362	0.31694
SC-325-03	11,407		0.29249	42,247	0.27001
SC-325-04	13,863		0.35546	41,026	0.33790
SC-325-05	14,162		0.36313	42,727	0.33146
SC-325-06	13,274		0.34035	41,973	0.31625
Average	13,055		0.33	41,401	0.32

Both methods of determining the coefficients of friction yielded similar results. The average coefficient of static friction based on Method 1 was 0.48 as opposed to 0.47

for Method 2. Similarly, the average coefficient of dynamic friction was 0.33 for Method 1 and 0.32 for Method 2. The coefficient of static friction are slightly higher than expected based on previously reported results [3] where an average for various clean mill scale steels was 0.33. However, ASTM A572, Grade 50 steel was not included in those results and the experimental results from the conducted results were not outside the range of previously reported results. No comparative information for the dynamic friction coefficient for clean mill scale ASTM A572, Grade 50 steel was found, however, a coefficient of dynamic friction that is approximately 2/3 of the coefficient of static friction is a commonly accepted rule of thumb for many materials and the dynamic coefficient of friction results are consistent with that.

For modeling friction behavior and response, the transition between the coefficient of static friction and the coefficient of dynamic friction is important for determining the friction coefficient, μ_c, as a function of the relative velocity. A common method to describe the friction coefficient as a function of the relative velocity, v_{rel}, is [1]:

$$\mu_c(v_{rel}) = \mu_d + (\mu_s - \mu_d)e^{-\lambda|v_{rel}|} \tag{7.12}$$

where λ is the decay coefficient. Using the average values of the coefficients of static and dynamic friction shown in Tables 7.3 and 7.4 and the relative velocity data from the impulsive tests, the collected experimental data were fit to Equation 7.11 to determine an appropriate decay coefficient. The data were fit using the non-linear Levenberg-Marquardt method to minimize error. Figure 7.16 shows the results of the analysis, where again both methods of estimating the preload tension in the bolt are used.

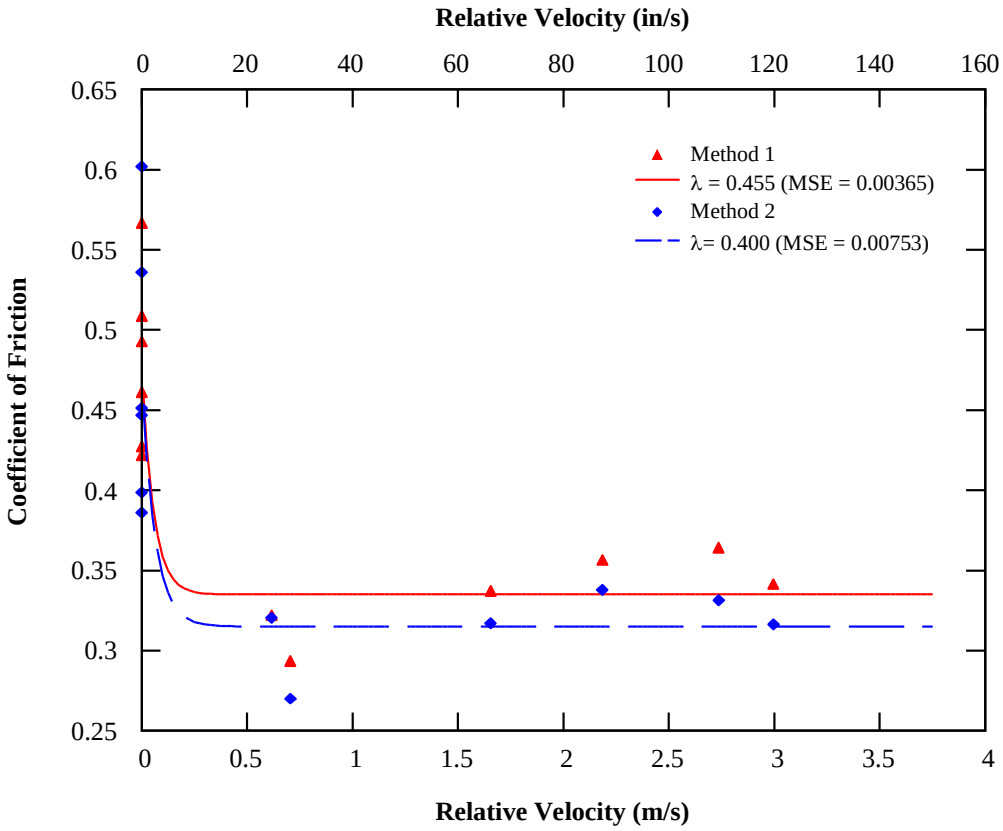

Figure 7.16: Coefficient of friction as a function of relative velocity.

The mean squared error (MSE) is a method to estimate the quality of fit for non-linear functions where values closer to zero indicate a better fit. From the results, both methods yield relatively low MSE values indicating the data fits the curve fairly well. However, the MSE from Method 1 is approximately half the MSE from Method 2. Therefore, it is recommended that a decay coefficient, λ, of 0.455 with the average coefficients of static and dynamic friction from Method 1 be used to determine the coefficient of friction of static friction as a function of the relative velocity of the connected plates.

7.4.4 Residual Capacity of Slip-Critical Connections

Because of the importance of friction in dissipating energy and transferring force between two or more connected members, it is important to understand the residual capacity of slip-critical connections in terms of the residual force required to cause slip, the residual slip displacement until bolt bearing, and the residual preload remaining in the bolt after an impulsive event. Figure 7.17 shows the ratio of the residual force required to cause slip to the average static slip load as a function of the impact energy. The dashed lines represent the range of expected values based on the variability of the baseline static tests. The figure shows that up to an impact energy threshold of approximately 600 J (443 ft·lbf) the bolts maintain 100% of the initial slip load. However, beyond that threshold the residual force required to cause slip decreases rapidly. The threshold of 600 J also corresponds to the threshold where bolt was not fully engaged during the impulsive. Therefore, it appears that the mechanism for loss of preload in the bolt occurs when the bolt is actually engaged by the impact shear plate.

As expected, the magnitude of residual slip before the bolt became fully engaged decreased with increased impact energy from the impulsive event. Figure 7.18 shows the residual slip displacement as a function of the impact energy of the impulsive event. These results follow from the results presented in Figure 7.12 that showed increased maximum slip with increased impact energy. As the impact energy increased, the impact T-section rebounded, oscillated, and eventually came to rest. Interestingly, the residual slip displacement showed a good linear correlation with applied impact energy ($R^2 = 0.97$).

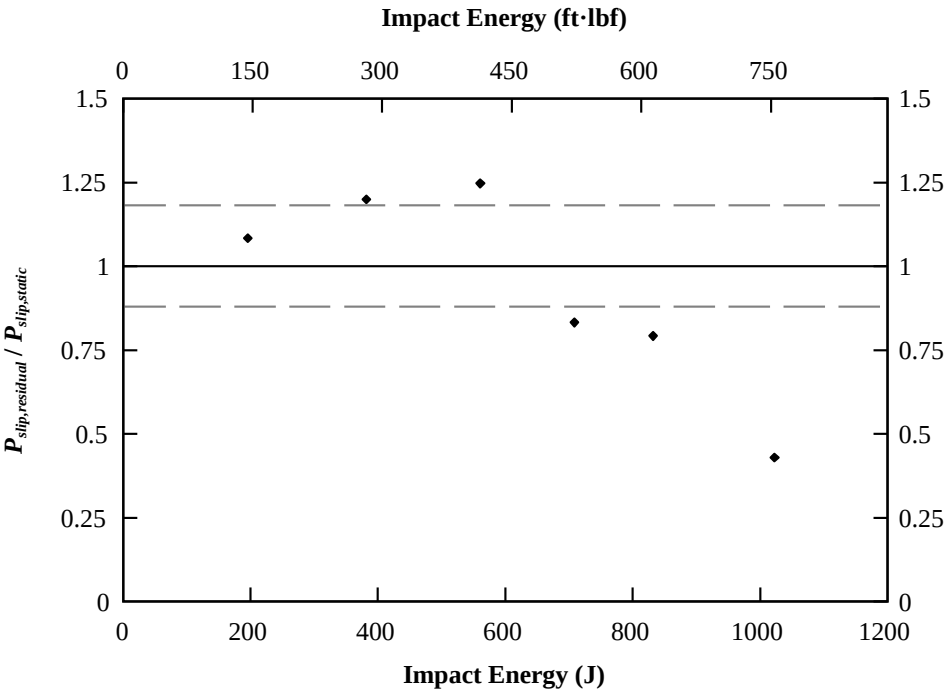

Figure 7.17: Residual slip load.

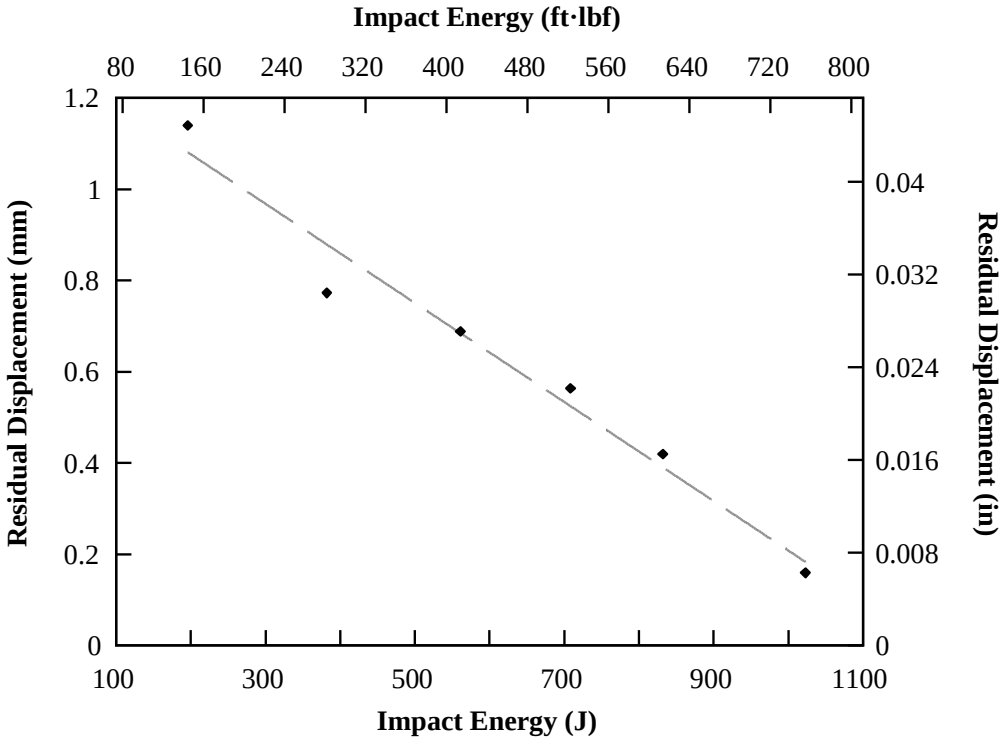

Figure 7.18: Residual slip displacement.

Finally, following the residual capacity test, the bolts were broken and the residual torque in the bolt was measured. Figure 7.19 shows the ratio of break torque to the recorded tightening torque for each test. The solid line represents the average of the results from the baseline static tests while the dashed line represents the range of values observed in the baseline tests. From the figure, it is evident that once again, at impact energies below the bolt becoming fully engaged, the tension in the bolt is consistent with static results. Beyond that threshold, however, the tension in the bolt begins to decrease, indicating that at higher impact energies, additional bolt preload is lost as a result of the impulsive event. These results are consistent with the results presented in Figure 7.17.

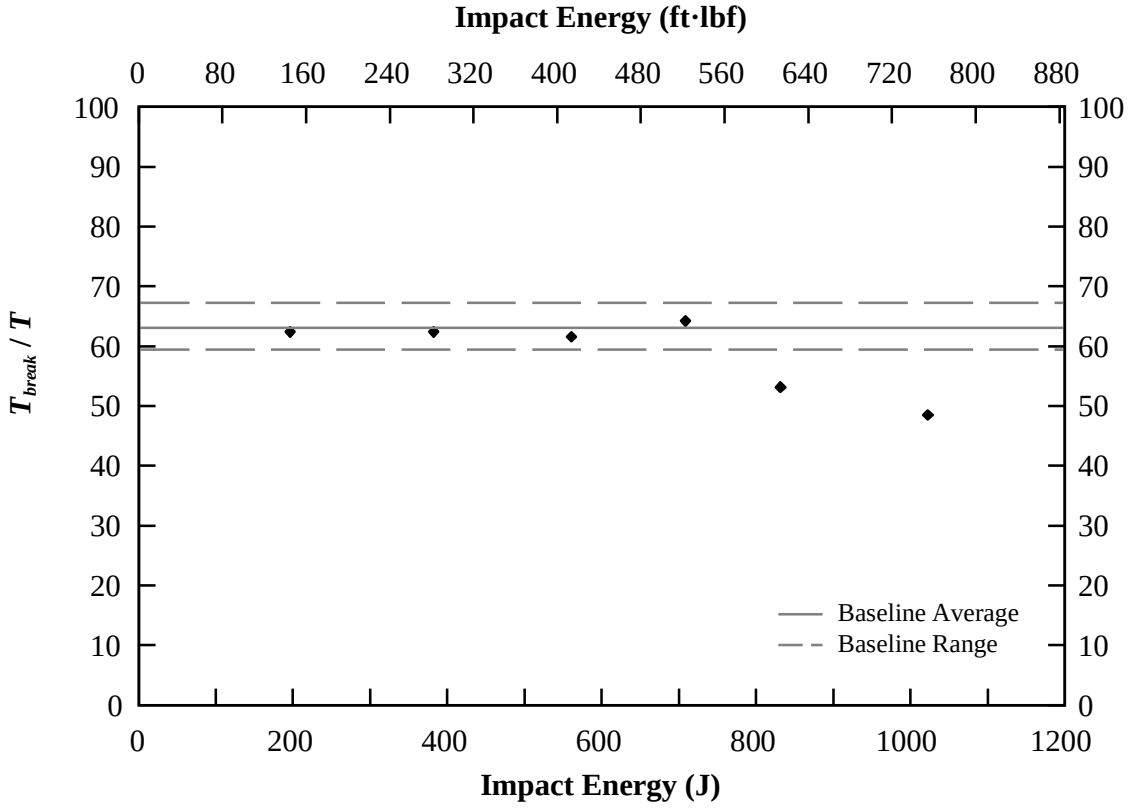

Figure 7.19: Residual break torque.

7.5 Conclusions

An experimental test series was conducted to determine the viability of using the residual capacity experimental test system to investigate the response of slip-critical connections during and after an impulsive loading event. Slip-critical connections were fabricated by using 7/8 inch (22.2 mm) ASTM A325 bolts to connect two ASTM A572, Grade 50 shear plates with a clean mill scale surface condition. The structural bolts were installed using the turn-of-the-nut method to ensure the minimum required clamping force in the connection. The connections were then impacted with a flyer mass at impact energies ranging from approximately 200 J (148 ft·lbf) to 1000 J (738 ft·lbf). Additionally, baseline static tests were conducted for comparative purposes.

Based on the results of this test series and the data that were collected, the residual capacity experimental test system is a viable experimental procedure to investigate the response of slip-critical connections during and after an impulsive event. The experimental test system provided insight into the load required to cause slip during an impulsive event, an estimate of the energy dissipated through friction, as well as the residual capacity of a slip-critical connection after impulse. In addition, the following conclusions regarding the behavior and residual capacity of slip-critical connections can be made:

1. For the impact energy range tested, the peak slip force under a dynamic load is constant regardless of the impact energy. The peak friction force was found to be 75% of the baseline slip load on average. While the peak friction force was expected to be equivalent to the static slip force observed in baseline tests, the results were consistent with

systemic losses observed in impulsive bolt test series. Further investigation is required to ascertain the effects of friction at increased relative velocities.

2. Slip-critical connections maintain a constant impulsive friction resistance below a critical impact energy. Beyond that critical impact energy, impulsive friction resistance decreases rapidly as the increased relative velocity of the shear plates reduces the duration that the friction force can provide resistance.

3. Work due to friction in the slip-critical connection increases linearly with increased impact energy. As a result, within the impact energy range tested, only 20 to 30% of the initial impact energy was transferred to the structural bolt. The effect of clamping force and friction between the connected plates therefore provides the bolt significant protection from damage. Based on these findings, it is recommend that all structural bolts, including those in bearing-type connections, be installed with the minimum bolt tension required in slip-critical connections. Requiring a minimum pretension in the bolt will provide a low cost, effective safety measure for protection against extreme loads.

4. When modeling clean mill scale A572 shear plates, a static coefficient of friction of 0.48 and a dynamic coefficient of friction of 0.33 are recommended. Additionally, to scale the static coefficient of friction based on relative velocity, a decay coefficient of 0.455 is recommended.

5. The experimental test series was limited both in the number of tests conducted and in the parameters that effect slip-critical connections. Therefore, further experimental research is required to investigate varying levels of bolt preload, different connected members, and different surface treatments of connected plates.

7.6 References

[1] Livermore Software Technology Corporation, *LS-DYNA Keyword User's Manual*, 2007.

[2] Bickford, J. H., *An Introduction to the Design and Bahavior of Bolted Joints*, 4 ed. Boca Raton, FL: CRC Press, 2007.

[3] Kulak, G. L., J. W. Fisher, and J. H. Struik, *Guide to Design Criteria for Bolted and Riveted Joints, 2nd ed.* Chicago: American Institute of Steel Construction, 2001.

[4] Persson, B. N. J., *Sliding Friction: Physical Principles and Applications*, 2nd ed. Berlin, Germany: Springer-Verlag, 2000.

[5] Salmon, C. G., J. E. Johnson, and F. A. Malhas, *Steel Structures: Design and Behavior*, 5th ed. Upper Saddle River, NJ: Pearson Prentice Hall, 2009.

CHAPTER 8

EVALUATION OF CURRENT MODELING METHODS

8.1 Introduction

The ability to accurately and efficiently model the behavior of structural bolts subjected to impulsive loads is extremely important in being able to predict the capacity and ductility of structural connections after such an event. Much of the literature [7, 12, 17] has stated that current high fidelity, physics based modeling methods do not accurately predict the behavior of bolts and structural connections subjected to extreme loadings. Because much of the conclusions from that research was conducted on much more complex connections than have been considered in this research, it is important to reduce the problem to understand where issues and inaccuracies arise in these modeling methods by first examining a simple bolted connection. These simulation results can then be compared to collected experimental data. This chapter presents the development of a finite element model of the experimental research conducted in Chapters 5, 6, and 7 and compares the results of the simulation to collected data to ascertain how accurately the models predict behavior. This research investigated the performance of models in the impulsive event, residual capacity, and slip-critical connections.

Simulations were conducted using the finite element software LS-DYNA developed by the Livermore Software Technology Corporation using two Intel Xeon E5-2630 v3 processors (16 cores) at 2.40 GHz on a 64 bit operating system with 32.0 GB of

installed random access memory (RAM). LS-DYNA is a general purpose finite element solver that is used for analyzing the static and dynamic response of structures with large deformations. The software contains both an explicit solver, where the solution time step is determined by the solver using the Courant time step, and an implicit solver where the time step is determined by the user. The time step in an implicit analysis is generally orders of magnitude larger than the time step in an explicit analysis. Therefore, LS-DYNA's explicit solver is generally preferred for dynamic analysis and the implicit solver is generally preferred for static analysis [1]. The explicit solver can be used for static analysis although a significant computational cost is incurred. Both the explicit and the implicit solver were used in the following analysis.

8.2 Finite Element Model

To model the experiments conducted using the bolt residual capacity experimental test system, several important factors must be considered for the model to be accurate. These factors include: 1) the structural model of the setup; 2) the material models used in the simulation; 3) the sensitivity of the finite element mesh; and 4) the calibration of the material models combined with the mesh geometry. This section discusses each of these factors in the development of a model to simulate the bolt residual capacity experimental test system.

8.2.1 Model of Experimental Setup

8.2.1.1 Structural Model

Two separate approaches to the structural model were investigated and compared to determine the most efficient method of conducting simulations of the experimental system. First, a mesh of all of the major components of the structural system was developed based on the model described in detail in Chapter 4. Minor modifications were made to the model to better represent the actual behavior observed. For example, boundary conditions restraining motion in all degrees of freedom except translation in the direction of the load were added to the reaction flange to account for the fact that the reaction T-section was in actuality tensioned to the mounting plate. Additionally, the support rails with artificially fixed boundary conditions were added to prevent rotation of the impact T-section below the plane of the shear plane. Figure 8.1(a) shows an isometric view of the detailed model.

Because of the number of elements in the detailed mesh, the computational expense associated with running the simulations was significant, taking several days to run a full residual capacity simulation with a very coarse bolt mesh. In the development of the experimental system, a mesh that incorporated all of the components was essential in estimating how the experimental setup might perform. In evaluating current modeling methods, the performance of these ancillary components is less significant. Therefore, to reduce the computational expense a simplified mesh was developed to focus only on the pertinent aspects of the simulation. The mesh was therefore reduced to the two shear plates and the specimen bolt, significantly reducing the number of elements, contacts, and other parameters that significantly increase the computational expense.

The ancillary components do, however, play a significant role in the overall behavior during the impulsive event due to inertia effects from the mass of the impact T-section. To account for the additional mass from the impact T-section, the end of the impact shear plate opposite the specimen bolt was given a density that corresponded to the equivalent weight of the impact T-section.

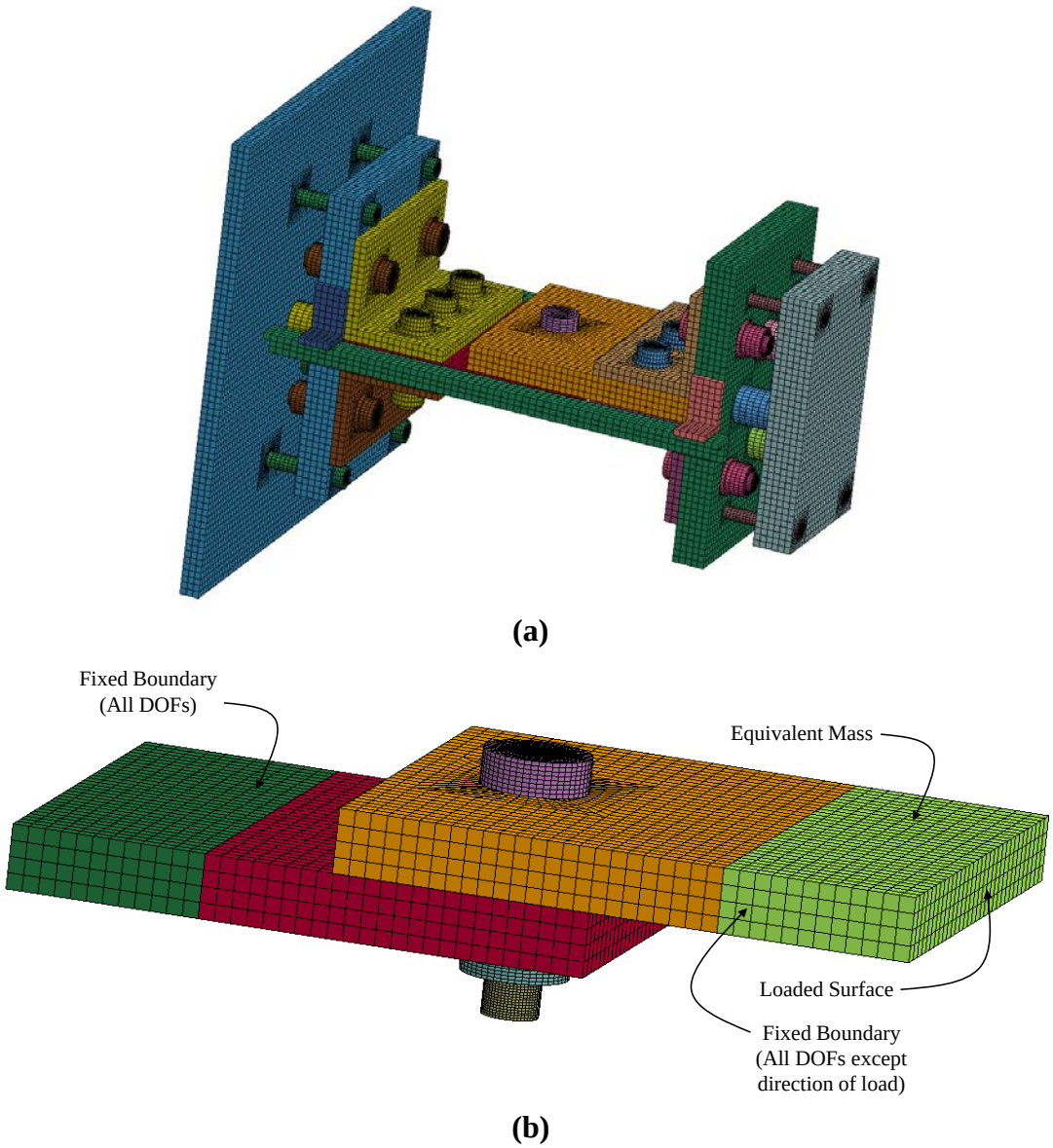

Figure 8.1: Structural model (a) detailed mesh; and (b) reduced mesh.

To account for the rail system in the actual setup, boundary conditions along the edges of the impact T-section that allowed translation only in the direction of the loading were applied. Additionally, to maintain equilibrium of the entire system fixed boundary conditions were applied to the end of the reaction shear plate opposite the specimen bolt. Samples of both models were run for an impulsive event and the results of the models were compared based on the resulting load on the specimen bolt. The solutions were found to be within 2% while the reduced mesh took orders of magnitude less in terms of computational time. Based on these results, the reduced mesh was used for all future simulations.

8.2.1.2 Modeling Methodology

LS-DYNA provides two techniques for running a residual capacity simulation. In the first method, the explicit solver can be used to run the entire simulation. To run the entire simulation using the explicit solver, an impulsive load is applied to the mesh followed by a period of zero load to allow the impact shear plate to stop oscillating due to the response of the impact. A quasi-static load is then applied to load the bolt to failure. This technique has significant draw backs. First, if there is no or very little friction between the two plates, the time required to reduce the oscillations can be large, incurring significant computational cost with very little benefit. Second, to prevent the computational time from being on the order of multiple years, the quasi-static load must be applied at a relatively high rate. While this reduces the computational time, it opens the possibility for both strain rate and inertia effects to skew the results.

A second method to conduct a residual capacity simulation is to conduct the simulation in two distinct iterations – an impulsive phase with the explicit solver and a

separate quasistatic phase with the implicit solver. In this technique, the impulsive event is simulated for the duration of the impulsive load with LS-DYNA's explicit solver. In the explicit analysis, the command *INTERFACE_SPRINGBACK_LSDYNA is used to create an output file, *dynain*, which is used as an input file for the static analysis. The user selects the specific parts of the model to be included in *dynain* and LS-DYNA writes all of the node and element deformations and corresponding stress states at the last time step of the explicit analysis as initial states in the file. Therefore, the *dynain* file contains the deformed mesh and element stresses as a result of the explicit analysis. The *dynain* file is then used as an input file to a second, implicit simulation of the quasi-static loading. This method has several advantages over the explicit-only method. First, the significant dwell period is not required to reduce the oscillations because the *dynain* file does not contain any initial nodal velocities. Second, the implicit solver is much better suited for a static analysis as a much larger time step can be used. This allows for much lower loading rates thereby reducing strain rate and inertia effects. While this method requires a user restart of the analysis, the reduction in overall computational time is significant.

Because of its advantages, the explicit-implicit method was used for all simulations that involved both an impulsive and a quasi-static loading. For simulations that only involved the impulsive event, such as simulations of bolt fracture, only the explicit solver was used. Likewise, for simulations that only involved the quasi-static event only the implicit solver was used. Quasi-static simulations were run for a minimum of 5.0 seconds with a maximum time step of 0.01 seconds. Combining the use of LS-DYNA's implicit and explicit solvers provided the most efficient means of conducting simulations that most closely resembled actual test conditions.

To further gain efficiencies in the simulations, underintegrated solid elements (ELFORM = 1) were used throughout the model. During the initial and detailed model simulations discussed in Chapter 4, significant hourglass modes were observed in the bolt using this type of element formulation. Hourglass modes occur when there are zero-energy modes of deformation that produce no strain and no stress. Visually, they are recognizable by a sudden hourglass shape to an element or group of elements in the simulation. LS-DYNA offers several formulations to control hourglass modes in the model, all of which add pseudo stiffness to the element to prevent the hourglass mode from occurring. However, only the Belytschko-Bindeman formulation (Type 6) is available for both explicit and implicit simulations. The Belytschko-Bindeman formulation assumes a strain co-rotational stiffness and is available only for solid elements. During each simulation, the amount of hourglass energy was verified to ensure the hourglass energy did not exceed the recommended 5 to 10% of the internal energy. In all of the simulations conducted, the hourglass energy did not exceed 2% of the internal energy for each individual part and for the model in its entirety.

8.2.1.3 Applied Loads

To simulate experimental results, it was essential for the applied loads to be as similar to the actual loads from the experiment. For the impulsive loading, a representative test (D-325-05) from the impulsive test series that caused heavy damage to the bolt was selected as the load in the simulation. Figure 8.2 shows the measured force from the impact load cells and the loading used in the simulation. The loading shown is shifted in time for clarity as the actual simulated load began at time zero. The simulated load was simplified to be a ramp load up to the peak load corresponding to the time of the peak load followed

by a linear decay. The total duration of the load was determined by equating the measured impulse, *S*, to the area of the simplified load:

$$t_d = \frac{2S}{P_{peak}} \tag{8.1}$$

As a result, while the applied load may not be entirely equivalent, the impulse of the actual load and the impulse of the simulated load are equal. Impulsive loads were applied to the model as a pressure load over the surface of the impact shear plate end.

For quasi-static simulations, displacement control methods were used to load the bolt rather than pressure loads. Through trial and error, it was found that displacement controlled loads provided more consistent results than pressure loads as they eliminated oscillations in the loading due to the movement of the impact shear plate. Actual static tests were conducted at an average strain rate of 10^{-4} s^{-1}. To reduce simulation time with significantly effecting the results, a strain rate of 10^{-1} s-1 was selected for the simulations. At this strain rate, inertia effects and strain rate effects on the material were negligible. The load was applied using *BOUNDARY_PRESCRIBED_MOTION_SET to advance the impact shear plate at 0.1 in/s (2.54 mm/s). Cross-sections within the model at the impact shear plate, reaction shear plate, and the shear plane in the bolt measured the resulting forces from the displacement control method.

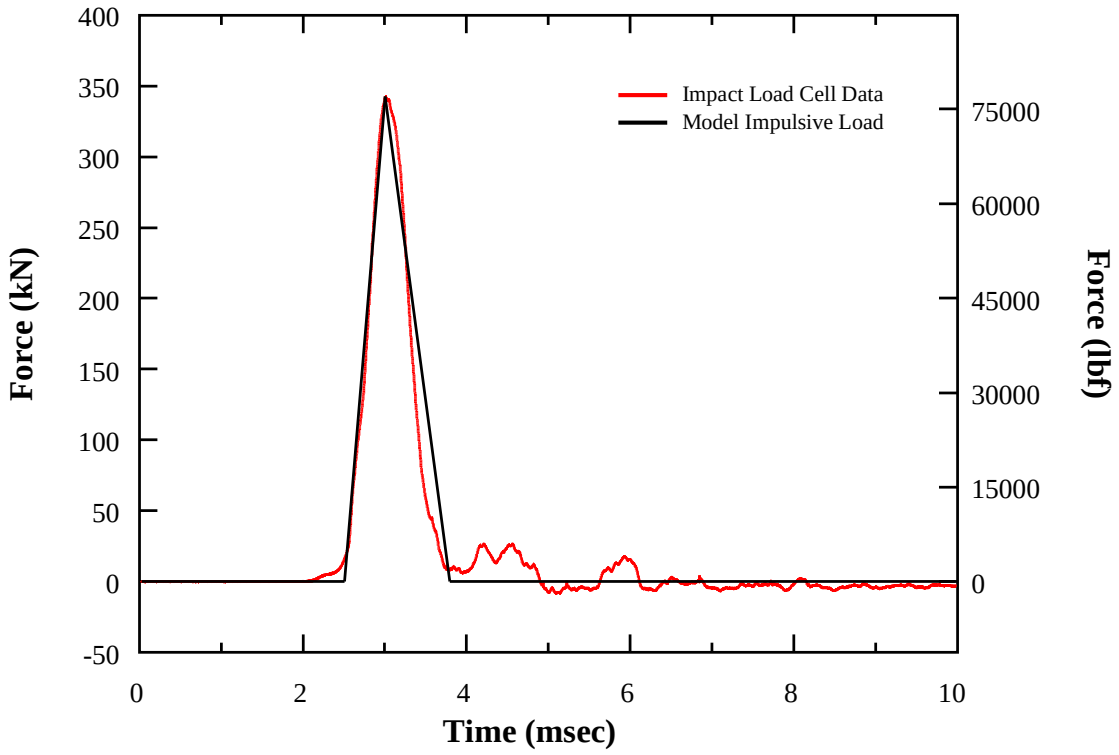

Figure 8.2: Applied impulsive load.

8.2.2 Material Models

8.2.2.1 A325 Stress-Strain Curves

Because direct tension tests of A325 bolts were beyond the scope of this research, a review of relevant literature regarding stress-strain data for A325 bolts and A325 bolt material was conducted to develop potential material models. Three different stress-strain curves for A325 bolts were found in the literature. Calibration tests of A325 bolts were originally conducted by Rumpf et al. in 1963 [15]. A subsequent validation of Rumpf et al.'s calibration in 1992 by Salih et al. [16] found that in the thirty years following the original calibration tests the strength and ductility of A325 structural bolts was significantly higher than previously reported, likely due to a combination of improvements in manufacturing processes and in testing and instrumentation. In the second edition of the

Guide to Design Criteria for Bolted and Riveted Joints, results from coupon tests of A325 bolt material are provided [9]. Figure 8.3 shows the engineering stress strain curves from two direct tension tests and the engineering stress strain curve from the A325 coupon tests. Additionally, a simplified elastic-perfectly plastic model is shown. This model was developed based on ASTM F1325 minimum requirements for A325 bolts (σ_y = 92,000 psi (635 MPa) and σ_u = 120,000 psi (830 MPa)) with a static increase factor of 1.2 included [3]. Because of the widely varying ultimate strengths and ductility of the reported results, no single curve was selected for use in the simulation. Instead, a material model was developed based on each stress-strain curve and the performance of each material was evaluated in the simulation of the residual capacity test.

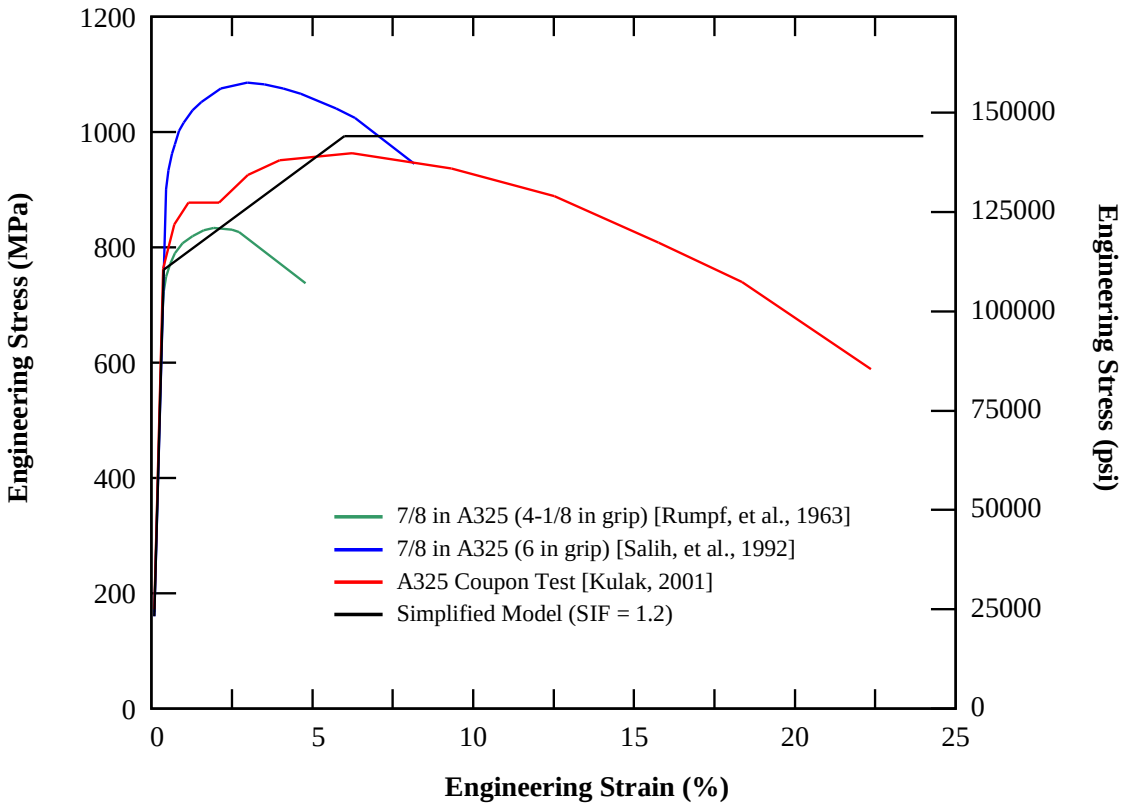

Figure 8.3: A325 bolt direct tension stress-strain curves.

8.2.2.2 A325 Bolt Material Models

The four engineering stress-strain curves shown in Figure 8.3 were used to develop material models for the A325 bolts in the simulations. LS-DYNA provides the user with the option of numerous material models. For the simulations conducted, all A325 bolt materials were modeled with *MAT_PIECEWISE_LINEAR_PLASTICITY (MAT_024). MAT_024 is a versatile material model that provides multiple options for including strain rate effects and multiple methods to define the plastic behavior of the material beyond the elastic limit. This material model requires the user to define the plasticity curve in terms of true stress and true strain. Based on the engineering stress-strain curves shown in Figure 8.3, the true stress, σ_T, and true strain, ε_T, up to the ultimate stress were calculated using the following equations:

$$\sigma_T = \sigma(1 + \varepsilon) \tag{8.2}$$

$$\varepsilon_T = \ln(1 + \varepsilon) \tag{8.3}$$

These equations are only valid through the strain hardening region of the stress-strain curve. At the onset of necking, the model becomes unstable. However, the slope of the true stress-strain curve can be estimated using the relationship in Equation 8.4, which is based on the engineering strain and the true stress at ultimate:

$$\frac{d\sigma_T}{d\varepsilon_T} = \frac{\sigma_{T,u}}{1 + \varepsilon_u} \tag{8.4}$$

The resulting stress-strain curve entered into MAT_024 is therefore significantly different than the engineering stress-strain curve. Figure 8.4 shows the engineering stress-strain curve and the resulting true stress-strain curve for the A325 coupon test.

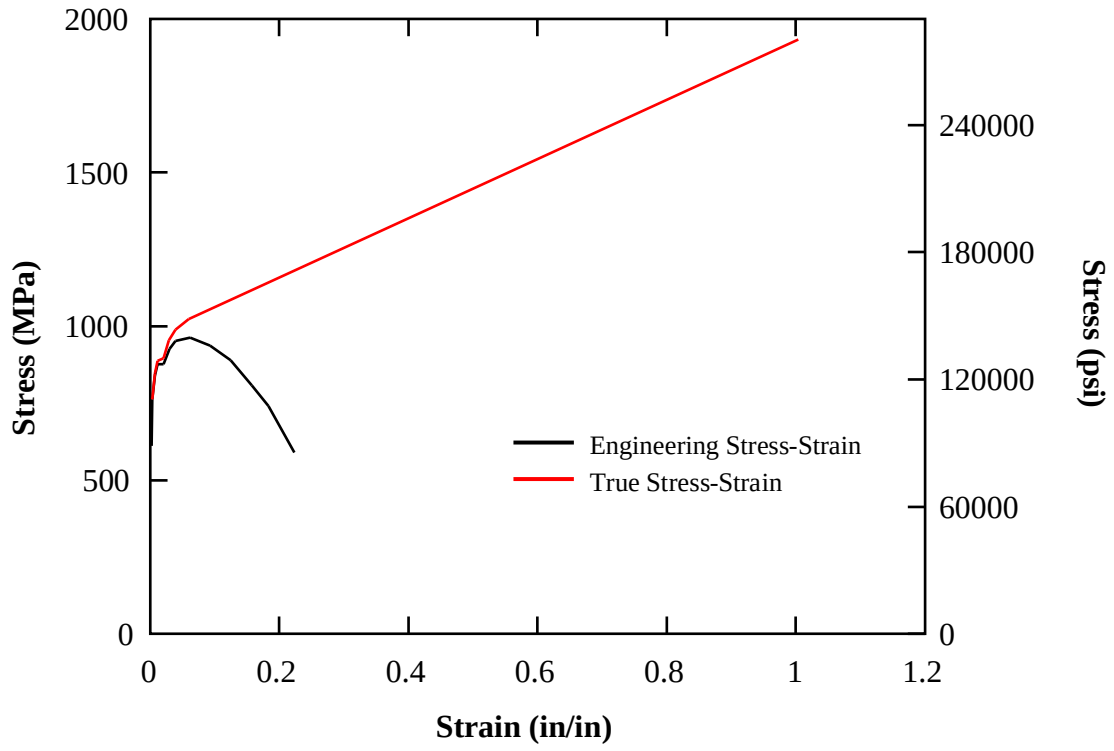

Figure 8.4: Engineering stress-strain versus true stress-strain, A325 coupon test.

MAT_024 defines the elastic portion of the stress-strain curve with the modulus of elasticity. For all four material models developed, a modulus of elasticity of 29,000,000 psi (200,000 MPa) was used. The remainder of the stress-strain curve is defined using the effective plastic strain (EPS), where:

$$EPS = \varepsilon_{T,total} - \frac{\sigma_T}{E} \tag{8.5}$$

$$EPS = \varepsilon_{T,total} - \varepsilon_y \tag{8.6}$$

Equation 8.5 represents the actual effective plastic strain while Equation 8.6 is a simplified approach where only the engineering yield strain is used. This approach has been found to be valid for ductile materials such as steel and was used in the development of these models [1].

During the finite element analysis, once a designated effective plastic strain is reached in an element, MXEPS or FAIL, the element fails and is then eroded from the model. Significant difficulty arises in determining the true fracture strain of the material for use in the material models. Often, values of 0.8 to 0.85 are used for an effective plastic strain at failure for steels [10]. However, from the engineering stress-strain curves in Figure 8.3, it is evident that there is significant variation in ductility for each reported result. Therefore, a maximum effective plastic strain of 0.80 was selected for the A325 coupon model which exhibited the highest ductility in the engineering stress-strain curves and all other material models were scaled based on their relative engineering fracture strain:

$$MXEPS_i = \frac{\varepsilon_{f,i}}{\varepsilon_{f,A325\ Coupon}}(0.80) \tag{8.7}$$

The plasticity models resulting from this analysis can be seen in Figure 8.5. In all models, failure was designated using MXEPS in *MAT_ADD_EROSION as opposed to the limit FAIL internal to MAT_024.

8.2.2.3 Strain Rate Effects

Strain rate effects on material properties were an important consideration for incorporating into the material models because the simulations involve both quasi-static rates and intermediate strain rates. MAT_024 provides a mechanism to account for strain effects using the Cowper-Symonds model, which is a constitutive model that scales the yield stress based on the strain rate [2]:

$$\sigma_y^d = \sigma_y \left(1 + \frac{\dot{\varepsilon}}{D}\right)^{\frac{1}{q}} \tag{8.8}$$

Other methods are available to account for strain rate in MAT_024, however, these generally require experimental data for the specific material.

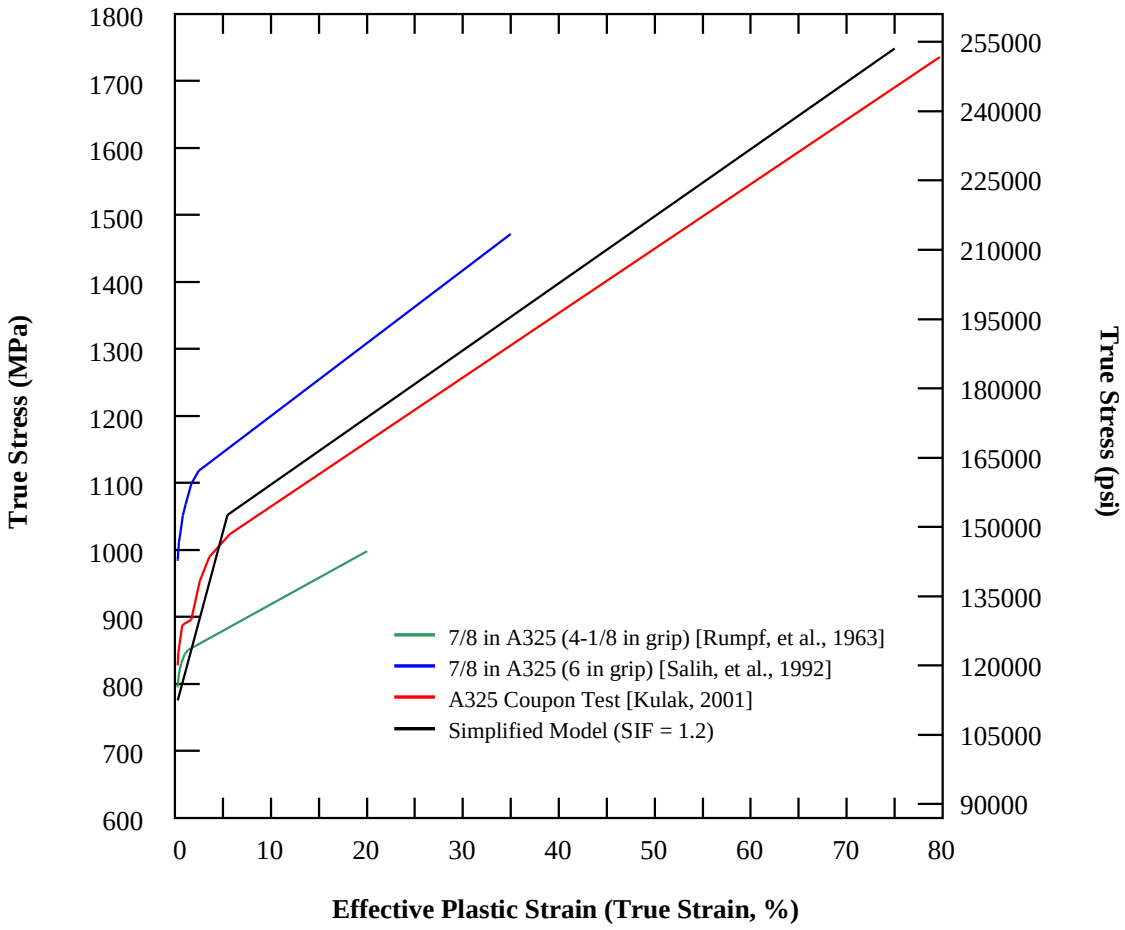

Figure 8.5: MAT_024 A325 bolt material models.

Several researchers [5, 6, 8, 11, 14] have posited values for the Cowper-Symonds model parameters for steels. Figure 8.6 shows the resulting Cowper-Symonds model curves. Each of these tests were conducted on varying types of steel, specimen geometry, and modes (tension or compression). Evident in the figure is that widely varying parameters have been reported.

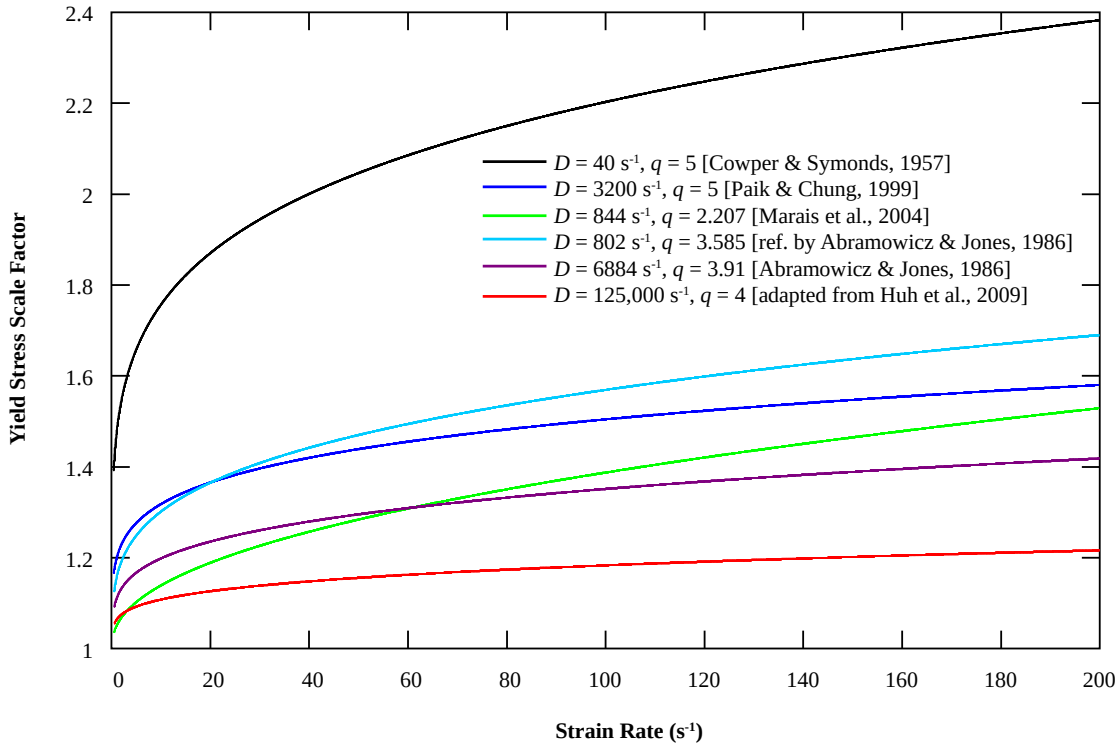

Figure 8.6: Cowper-Symonds model parameters.

Huh et al. [8] tested steel sheets of varying strengths from 40,000 psi (275 MPa) to 100,000 psi (640 MPa) and found that strain rate effects were reduced for higher strength steels. Specifically, they observed a 200% increase for lower strength steel but only a 20% increase in the highest strength steel tested at 200 s^{-1}. Furthermore, they observed the parameter, q, decreased with higher strength steels. Because A325 bolt steel is a high strength steel and no experimental data exist for the Cowper-Symonds model parameters, parameters were chosen to achieve only a 20% increase in yield stress at 200 s^{-1}. As well as a q-value that yielded a similar slope to previous researchers' results. Therefore, parameters selected for all of the material models were D = 125,000 and q = 4. While the D-value is significantly higher than other reported research, it is consistent with Huh et al.'s findings for high strength steels.

8.2.2.4 Shear Plate Material Model

In addition to the A325 bolt material model, an appropriate model for the ASTM A514A shear plates was also required. LS-DYNA material model MAT_024 was used for the shear plates. The effective plastic strain and corresponding stress values were adapted from the ASTM A572, Grade 50 steel material model developed by Kargozian & Case [10] based on experimental data. A572 steel has a minimum yield stress of 50,000 psi (345 MPa) as opposed to A514 steel with a yield stress of 100,000 psi (690 MPa). To account for the higher yield stress, the true stress values in the Kargozian & Case material model were scaled by the yield stress or multiplied by a factor of two. The effective plastic strain at failure in the A572 model was 0.80 and because failure of the shear plates was not a concern in this simulation, the same effective plastic strain at failure was used for the A514 model. The Kargozian & Case model uses experimental data to determine the yield stress at varying strain rates. Because the A514 steel shear plates are a high strength steel, these curves were not incorporated into the model. Instead, strain rate effects in the shear plates were incorporated into the material model using the Cowper-Symonds method where the parameters used were the same as those discussed in the previous section. Figure 8.7 shows the effective plastic strain - true stress curve used for the A514 material model.

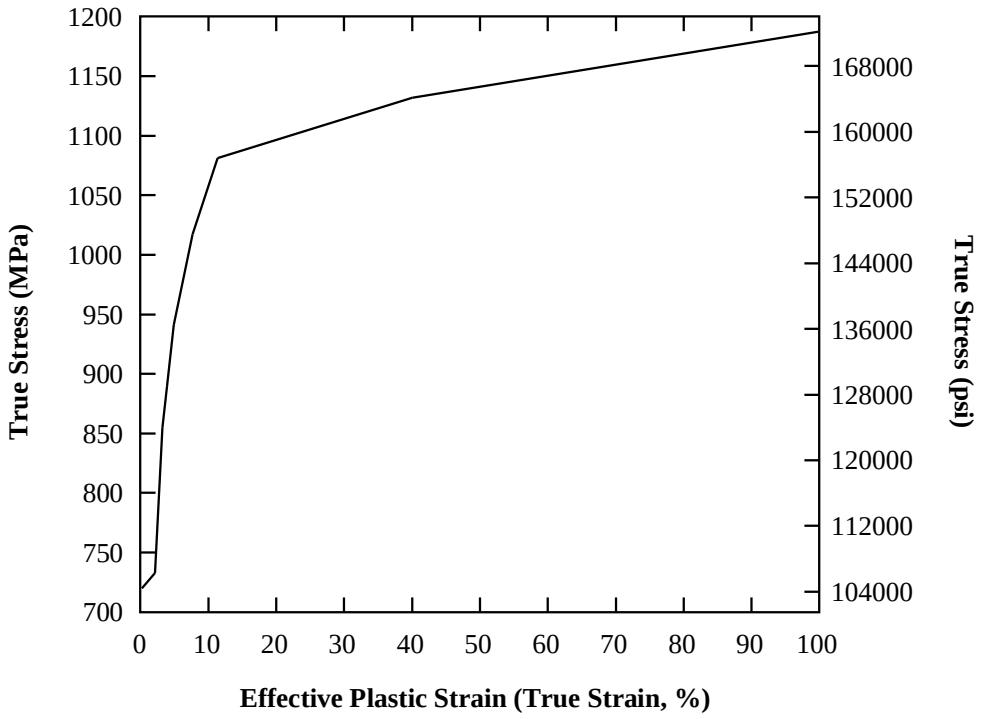

Figure 8.7: ASTM A514A shear plate material model.

8.2.3 Mesh Sensitivity

Performance of the simulations is significantly affected by the size of the mesh used. Of particular concern in these simulations is the mesh size of the specimen bolt. Therefore, a mesh sensitivity study was conducted to determine the effect of mesh size on results. For ease in determining the gauge length and to ensure a standard specimen for the simulation, varying meshes based on a standard tensile test specimen [4] were developed to determine an appropriate mesh size for the specimen bolt. Figure 8.8 shows the ASTM E8 specimen and varying mesh sizes investigated. The coarsest mesh, with element sizes of approximately 0.1113 in (2.83 mm), was based on the same mesh size used in the development of a model to design the experimental test system. The density, D_m, refers to the number of elements within a 90-degree arc of the specimen shaft. The

gauge length, shown as a blue part in the figure, was 2.0 inches (50.8 mm) with a standard 0.5 inch (12.7 mm) diameter.

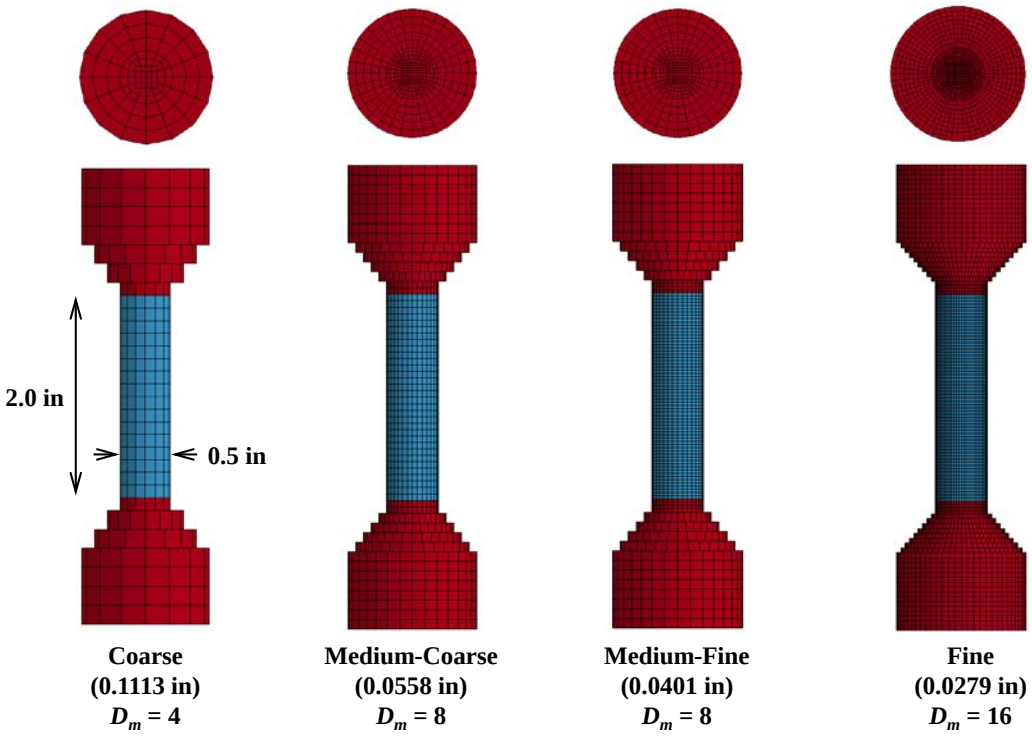

Figure 8.8: Mesh sensitivity specimens.

For all of the mesh sensitivity models, only the simplified A325 material model was used with the assumption that the material model would not affect the results. Nodes at the base were fixed in all degrees of freedom and the specimen was loaded using *BOUNDARY_PRESCRIBED_MOTION_SET. A cross-section at the center of the gauge length measured the force in the bolt. Engineering strain was calculated using the gauge length as the initial length and relative displacements of the nodes at the top and bottom of the gauge length section for the change in length. Figure 8.9 and Table 8.1 summarize the results of the simulations.

Table 8.1: Mesh sensitivity results.

	Coarse	Medium-Coarse	Medium-Fine	Fine
Mesh Density	4	8	8	16
Relative Cost	1.0	8.4	13.9	103.5
Yield (% Difference)	-2.9	-1.1	-0.8	-0.4
Ultimate (% Difference)	-2.9	-0.9	-0.8	-0.4
Ductility (% Difference)	19.1	-5.1	-7.3	-8.6

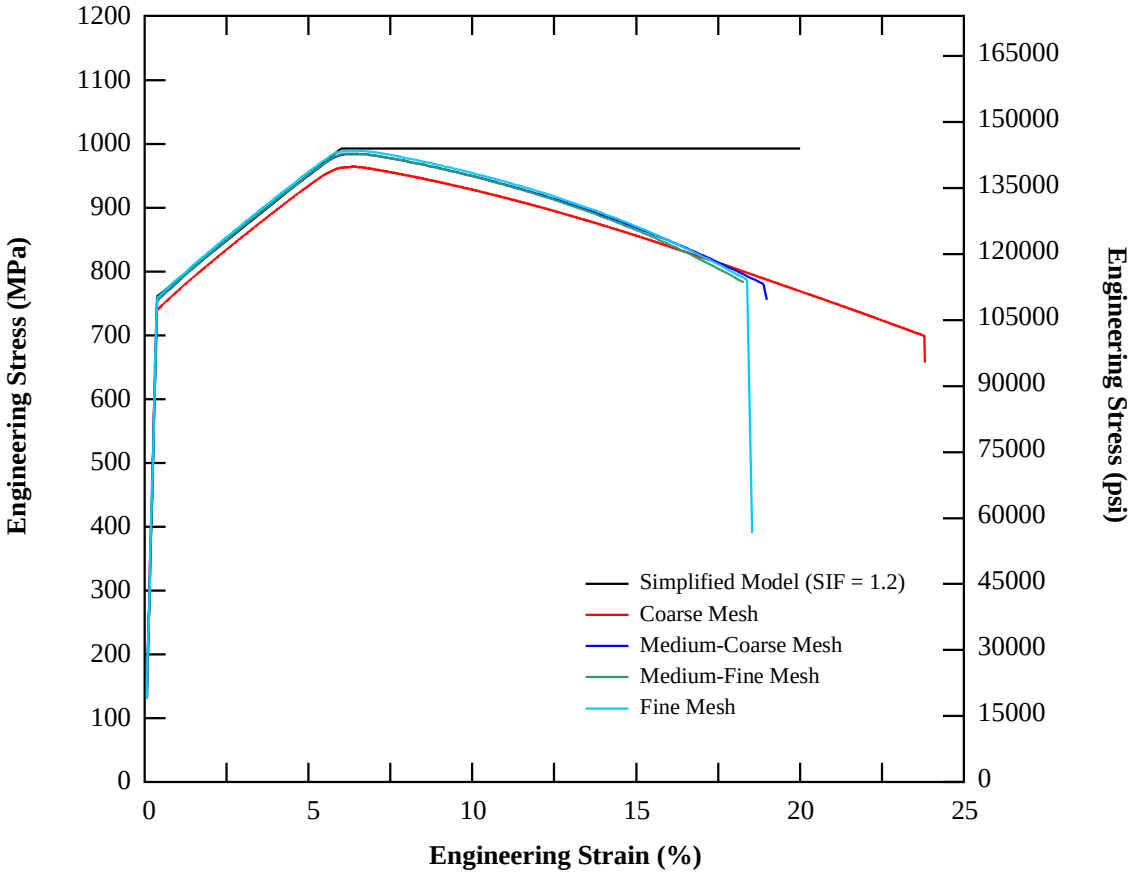

Figure 8.9: Mesh sensitivity results.

Figure 8.9 and Table 8.1 show that strength results improve as the mesh fineness increases. However, the improvements are relatively minor compared to the costs associated with a denser, finer mesh. For example, the fine mesh was 12 times more costly than the medium coarse mesh but only yielded an improvement of 0.7% and 0.5% for the yield strength and ultimate strength, respectively. Ductility is more difficult to accurately capture because the erosion criteria is somewhat arbitrary and erosion of the elements is heavily dependent on the mesh. The coarsest mesh resulted in the largest ductility overestimating the model by 19% while the remaining meshes all underestimated the model between 5 and 9%.

8.2.4 Bolt Tension Simulation

Based on the results of the mesh sensitivity study, a mesh size in the medium-coarse to medium fine range was selected for the specimen bolt. Such a mesh size would accurately capture the material behavior of the bolt without significant, unnecessary computational cost. Figure 8.10 shows the bolt mesh used for all of the simulations. Due to the larger diameter of the bolt compared to the tensile test specimen, a density, D_m, of 12 was used for the bolt. The resulting inner element size of the bolt shank was approximately 0.030 in (0.762 mm) while the outer element size was slightly larger at 0.044 in (1.118 mm). Because the bolt head and nut were represented as circular rather than hexagonal in the model for element size consistency, a determination had to be made for the diameter of the bolt head and nut. Because the experimental tests always oriented the width of the points along the direction of the load, the width of the points was selected for the diameter.

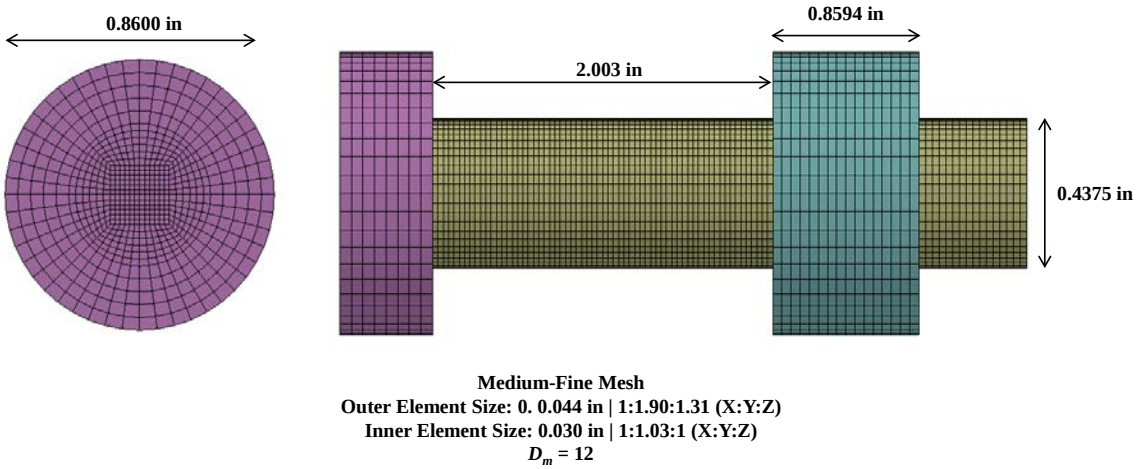

Figure 8.10: Specimen bolt mesh.

To ascertain the influence of the bolt mesh geometry, mesh size, and A325 bolt material models developed, each material model was tested with the bolt mesh in a direct tension test. As in the mesh sensitivity investigation, the bolts were tested quasi-statically using LS-DYNA's implicit solver. The nodes of the nut were fixed in all degrees of freedom while the bolt head was advanced at a constant velocity using the prescribed motion set command. Figure 8.11 shows the simulation engineering stress-strain results for each material model compared to the actual reported direct tension results.

All of the material models are consistent with their corresponding stress-strain curves up to the point of necking. After necking, the material models vastly overestimate the ductility of the bolt and are significantly stiffer in the necking region than the actual direct tension tests showed. Attempts were made to calibrate the models by reducing the stiffness of the material model after the onset of necking and reducing the effective plastic strain at fracture to more closely resemble the results of the actual direct tension tests. However, these attempts proved fruitless because altering these values resulted in element

instabilities in the form of negative volumes. To more closely match the results after necking, a more refined mesh would be required but, as was concluded in the previous section, the incrementally greater accuracy in the necking region was not worth the computational cost associated with a more refined mesh. Therefore, the "default" values determined in Section 8.2.1.2 were used for all simulations.

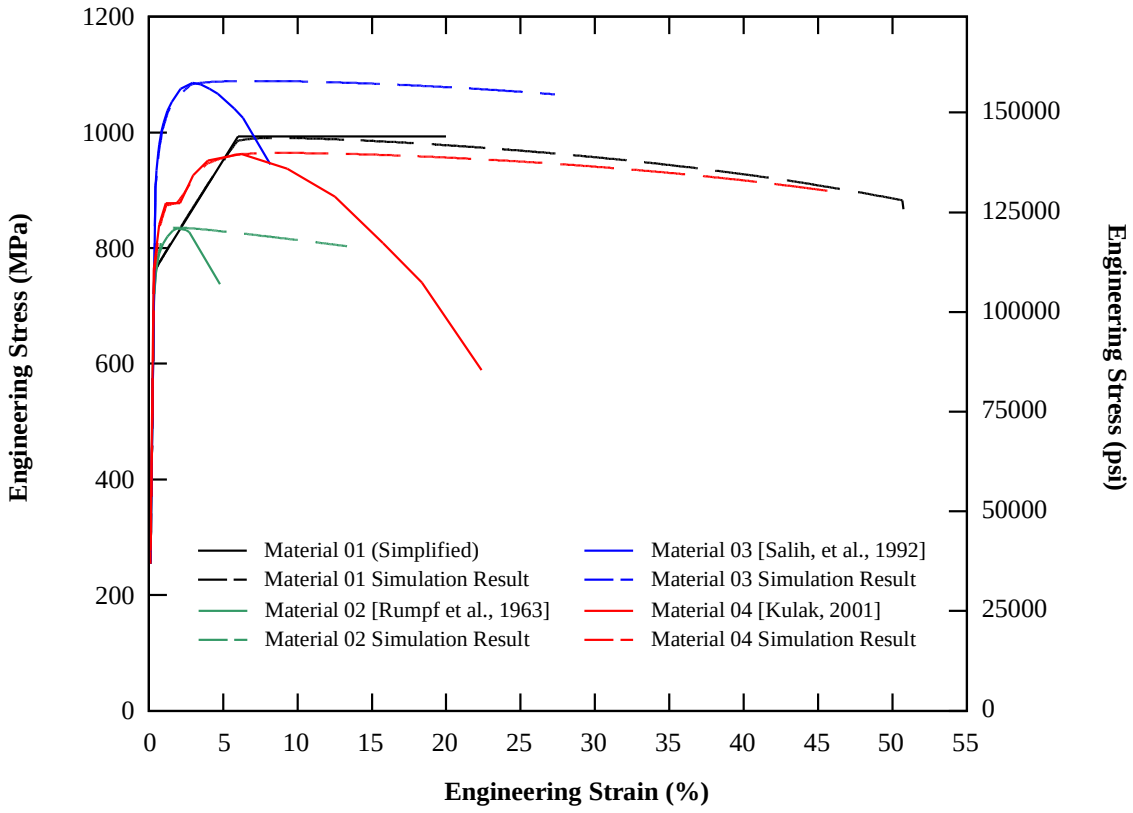

Figure 8.11: A325 bolt direct tension test simulations.

8.3 Simulation Results

Using the A325 material models and structural models described in the previous sections, a series of simulations were run to determine how accurately the simulations

captured observed behavior from the experimental tests. Simulations were run of the impulsive event, residual capacity, fracture during the impulsive event, and of the slip-critical connection tests. Analysis of ultimate strength and ductility were performed on the simulation using the same methodology as the experimental tests to ensure consisting when comparing results. Variations from the previously described modeling methods, techniques, loadings, and materials used are also presented in each subsection.

8.3.1 Impulsive Event and Residual Capacity Simulation

Each of the four material models were simulated in the impulsive event and residual capacity event. Table 8.2 shows the impulsive event and residual capacity simulation results. Table 8.2 shows the shear capacity, V_u, and shear deformation, δ, for the following phases of the experimental tests: 1) a quasi-static only simulation comparable to the baseline static tests; 2) an impulsive event simulation; and 3) a residual capacity simulation. In addition, the total deformation, combining the impulsive event deformation and the residual capacity deformation, are compared to the total deformation determined through experimental tests.

The materials under predict the static shear strength of the bolt. All of the material models were reasonably close to the theoretical minimum shear capacity for A325 structural bolts but were on average 17% less than theoretical shear capacity based on the material models' ultimate capacity. The closest material model to the observed experimental data was Material 03 as it was only 7% less than the experimental data. This follows from the fact that Material 03 also had the highest ultimate tensile stress. The discrepancy in static shear capacity is likely a result of the mesh sensitivity in tension

versus shear. A more refined mesh may have resulted in more accurate ultimate static shear capacities, indicating that the mesh for a shear analysis is more sensitive than a tensile analysis.

Materials 01 and 04 were reasonably accurate in predicting the static ductility of the bolt with differences of 13% and 22%, respectively. Materials 02 and 03 were much too brittle and predicted very little ductility in the bolt. These results are most significantly impacted by the value input for the effective plastic strain at failure, MXEPS. These results indicate that the initial selected values were not significantly off and through an iterative process, could be refined to predict the ductility quite accurately.

Material 02, which had the lowest strength and ductility, fractured during the impulsive event. However, the three remaining material models accurately captured the impulsive resistance of the structural bolt with all of the models predicting the peak resistance within 10%. It should be noted, however, that were the static capacities of the bolts closer to the experimental results, these results would have been approximately 25% higher than the experimental reaction values.

Given that the reaction load cell measurement was approximately 25% less than the theoretical impulse due to other losses in the real system, the results would be reasonably accurate. All of the materials over predicted the plastic deformation in the bolt due to the impulsive event and most were as much as twice the experimental results. This is most likely due to the fact that the material models do not account for the increased stiffness of the bolt during the impulsive event that was observed during the experimental tests.

Table 8.2: Impulsive event and residual capacity simulation results.

	Experimental Data	Material 01	Material 02	Material 03	Material 04
$V_{u,static}$, lbf (kN)	54,122 (241)	44,404 (198)	39,923 (178)	50,293 (224)	44,776 (199)
$V_{u,static} / V_{u,exp}$		0.82	0.74	0.93	0.83
δ_{static} , in (mm)	0.2321 (5.90)	0.2628 (6.68)	0.0770 (1.96)	0.1358 (3.45)	0.2828 (7.18)
$\delta_{static} / \delta_{exp}$		1.13	0.33	0.59	1.22
$V_{u,impulse}$, lbf (kN)	55,629 (247)	53,752 (239)	48,933 (218)	60,900 (271)	54,225 (241)
$V_{u,impulse} / V_{u,exp}$		0.97	0.88	1.09	0.97
$\delta_{impulse}$, in (mm)	0.0482 (1.22)	0.1138 (2.89)	0.0970 (2.46)	0.0883 (2.24)	0.1117 (2.84)
$\delta_{impulse} / \delta_{exp}$		2.36	2.01	1.83	2.32
$V_{u,residual}$, lbf (kN)	54,320 (242)	44,779 (199)	–	50,628 (225)	48,451 (216)
$V_{u,residual} / V_{u,exp}$		0.82	–	0.93	0.89
$V_{u,residual} / V_{u,static}$		1.01	–	1.01	1.08
$\delta_{residual}$, in (mm)	0.1793 (4.55)	0.1876 (4.77)	0.0000	0.0575 (1.46)	0.1591 (4.04)
$\delta_{residual} / \delta_{exp}$		1.05	0.00	0.32	0.89
δ_{total} , in (mm)	0.2391 (6.07)	0.3014 (7.66)	0.0970 (2.46)	0.1457 (3.70)	0.2708 (6.88)
$\delta_{total} / \delta_{exp}$		1.26	0.41	0.61	1.13
$\delta_{total} / \delta_{static}$		1.15	1.26	1.07	0.96

In general, all of the material models with the exception of Material 02 accurately captured the residual capacity behavior observed during the physical tests. The materials that did not fracture during the impulsive event had generally the same residual capacity after impulse as that of a virgin bolt simulation. While the simulation values were less than the experimental results, they were consistent with the baseline simulation results. Similarly, the total deformation – accounting for both the impulsive event and the residual capacity event – yields results consistent with what was observed during the experiment tests.

Based on the simulation results, it is clear that the modeling method used accurately captures the overall behavior of the impulsive and residual capacity events. The peak impulsive resistance of the bolt, residual capacity, and total ductility are within reasonable limits given the modeling methods used. Material 04, based on the A325 coupon stress strain curve from *Guide to Design Criteria for Bolted and Riveted Joints* [9] provided the most accurate response with the exception of ductility. The effective plastic strain at failure could be refined through an iterative process to match more closely the static and total ductility of the bolt in the simulation. The permanent shear deformation from the impulsive event could in part be addressed by increasing the stiffness of the material for the impulsive phase of the event to reduce the ductility and more closely match experimental results. However, more experimental data is necessary to determine the relationship between strain rate and the increase in rigidity of the bolt.

8.3.2 Fracture During Impulsive Event Simulation

During experimental testing, the A325 bolt fractured during the impulsive event in test RC-325-10. From this event, it was observed that the fracture strain of the bolt at the higher loading rate resulted in lower ductility of the bolt. This phenomena has been observed previously [13, 18] and LS-DYNA provides a mechanism to input the effective plastic failure strain as a function of the strain rate using the *MAT_ADD_EROSION command. An effective plastic failure strain at fracture was estimated based on the engineering fracture strain of the bolt at failure, the engineering fracture strain from the static event, and the effective plastic failure strain developed in the residual capacity simulations:

$$MXEPS_{impulsive} = \frac{\varepsilon_{f,impulsive}}{\varepsilon_{f,static}}(MXEPS) \tag{8.9}$$

Because little is known about the transition from the static fracture strain to the impulsive or dynamic fracture strain, a simplified curve was developed that would capture the behavior in both the static and intermediate strain rate range. Figure 8.11 shows the effective plastic strain at failure as a function of strain rate used in the simulation. For the impulsive fracture tests, only Material 04 was used due to its best overall performance in the residual capacity simulations.

The load applied to the bolt fracture simulations was developed from the impact load cell data from Test RC-325-10 following the same method previously described. Figure 8.12 shows the applied load, again shifted in time for clarity.

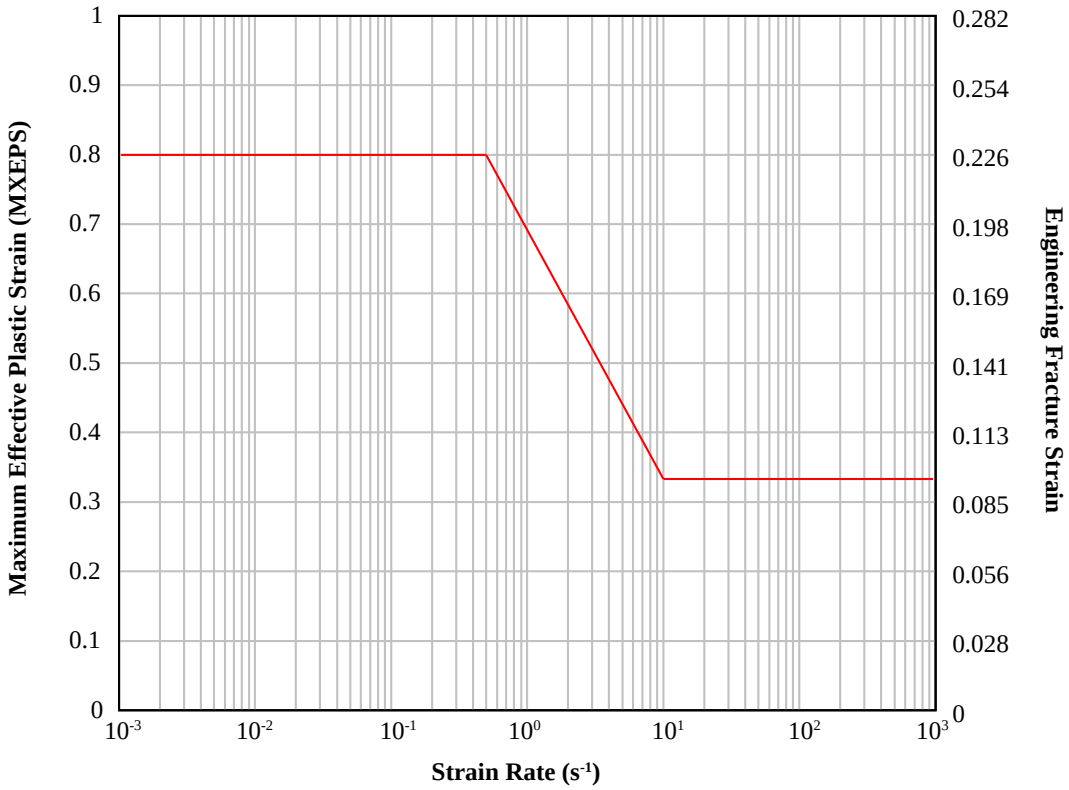

Figure 8.12: Model effective plastic strain at fracture as a function of strain rate.

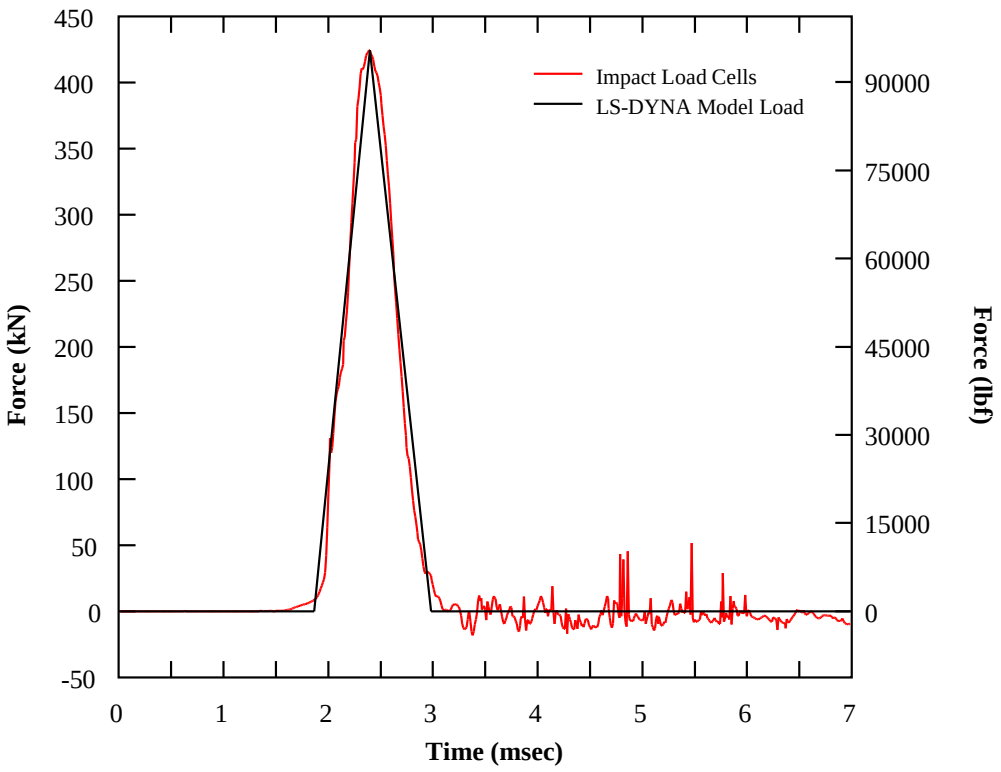

Figure 8.13: Bolt fracture simulation loading.

Three separate simulations of the bolt fracture were conducted: 1) a base simulation in which the scaled maximum effective plastic strain rate was not used; 2) a simulation with the scaled maximum effective plastic strain rate; and 3) a simulation with the scaled effective plastic strain rate and the material stiffness doubled. Figure 8.14 and Table 8.3 show the results of the bolt fracture simulations along with the quasi-static simulation and the actual reaction load cell data from the experimental test for comparison. The bolt fracture results demonstrate that the modeling method, with the maximum effective plastic strain set appropriately, has the ability to accurately predict fracture at different strain rates. All simulations accurately predicted the load on the structural bolt.

In the first simulation where the fracture strain was not input as a function of the strain rate, the bolt did not fracture and behaved the same as the impulsive tests from the simulations described in Section 8.3.1.

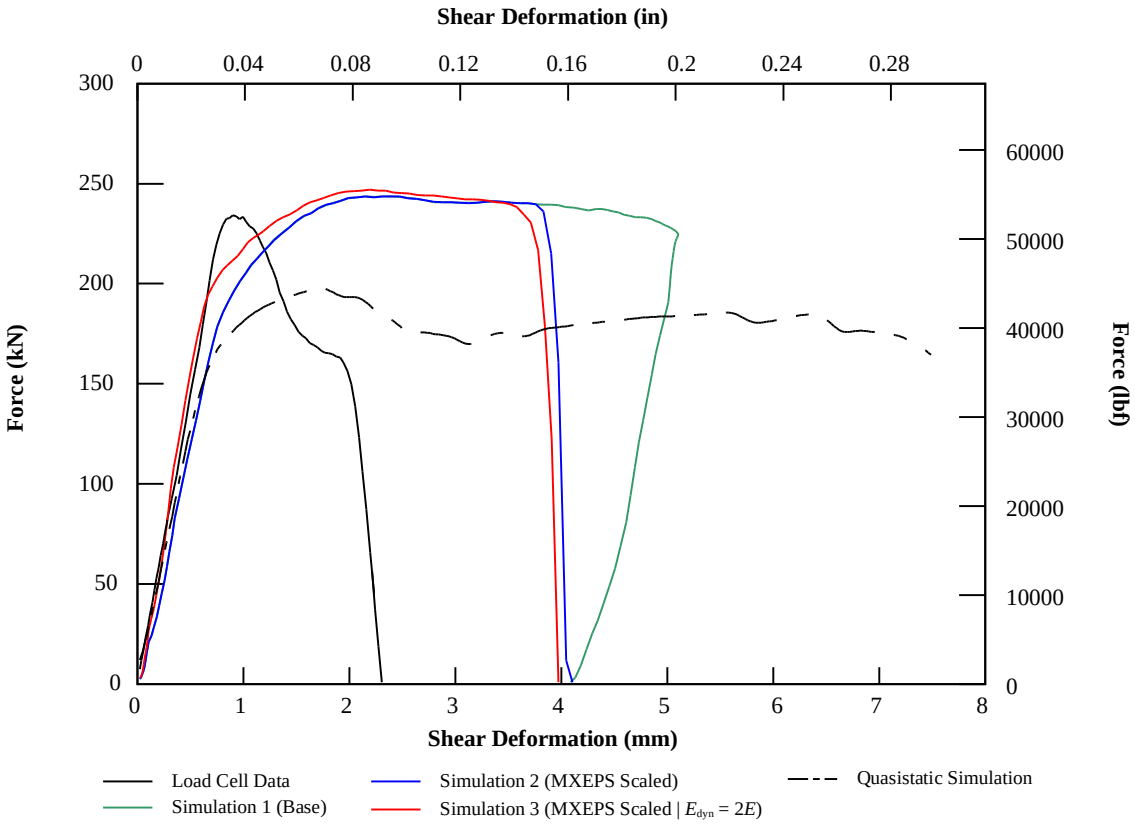

Figure 8.14: Bolt fracture simulation results.

Table 8.3: Bolt fracture simulation results.

	Experimental Data	**Simulation 1**	**Simulation 2**	**Simulation 3**
$V_{u,static}$, lbf (kN)	52,632 (234)	54,770 (244)	54,791 (243)	55,554 (247)
$V_{u,static} / V_{u,exp}$		1.04	1.04	1.06
δ_{static} , in (mm)	0.0909 (2.31)	–	0.1596 (4.05)	0.1565 (3.98)
$\delta_{static} / \delta_{exp}$		–	1.76	1.72

Once the maximum effective plastic failure strain was scaled based on strain rate, the bolts fractured during the impulsive event. In the third simulation, the increased rigidity in the bolt observed in the experimental test was predicted by increasing the stiffness which had the added effect of decreasing the fracture strain during the impulsive event. Compared to the experimental data, the simulations exhibited much more ductility after yield, which is potentially a result of the Cowper-Symonds model parameters used in the simulation. These results show that the use of scaling the maximum effective plastic strain as a function of the strain rate is an effective tool for handling the phenomena that the bolts have significantly less fracture ductility at higher strain rates. Further experimental research would enhance the development of a model to determine the relationship between fracture strain and strain rate.

8.3.3 Slip-critical Connection Simulation

Simulations were also conducted to investigate how well the models predict the effects of friction in slip-critical bolted connections. In LS-DYNA it is possible to establish friction parameters when defining the contact surfaces between two parts. Contact sliding friction is based on a Coulomb formulation where the friction is essentially modeled as an equivalent elastic-plastic spring [1]. In the *CONTACT card, the friction parameters include the static coefficient of friction, μ_s, the dynamic coefficient of friction, μ_d, and the exponential decay coefficient, λ, which determine the contact friction, μ_c. The contact friction is a function of the static friction, dynamic friction, and relative velocity of contact surfaces. Contact friction is given by [2]:

$$\mu_c = \mu_d + (\mu_s - \mu_d)e^{-\lambda|v_{rel}|} \tag{8.10}$$

Because the coefficients of static friction, dynamic friction, and the decay coefficient must be determined experimentally, the parameters developed in Chapter 7 were used for the slip-critical simulations. Additionally, the coefficient of viscous friction, *VC*, used to limit the shear friction between two sliding plates, was defined based on the yield strength of the shear plates [2]:

$$VC = \frac{\sigma_y}{\sqrt{3}} \tag{8.11}$$

In addition to defining the friction parameters between the two shear plates, between the nut and the reaction shear plate, and between the bolt head and the impact shear plate, it is necessary to preload the specimen bolt to provide the clamping force exerted on the shear plates. Preload on the specimen bolt was done through the command *CONTROL_DYNAMIC_RELAXATION where the shear plane of the bolt was loaded with an initial stress using the command *INITIAL_STRESS_SECTION. Because of the variability in bolt preload discussed in Chapter 7, the bolts were preloaded with 84,000 psi (580 MPa), which is equivalent to the proof load or 70% the minimum tensile strength of the bolt. Other options are available to preload the bolt such as through thermal effects or interference contacts, however, these methods require iterative solutions to achieve the proper pretension in the bolt.

A total of six slip-critical simulations were conducted corresponding to the six experimental tests conducted. The loads for each simulation were developed using the same methodology previously described based on impact load cell data from the experimental test. Table 8.4 shows the peak impulsive load, P_{peak}, the time of peak load, t_{peak}, and the total duration, t_D, for each simulation conducted. Simulations were selected to examine the full range of impulses tested experimentally.

Table 8.4: Slip-critical load parameters.

	Experimental Test	P_{peak} lbf (kN)	t_{peak} (msec)	t_D (msec)
Simulation 1	SC-325-01	12,517 (55.7)	1.830	3.808
Simulation 2	SC-325-03	28,963 (128.8)	1.210	1.962
Simulation 3	SC-325-06	48,678 (216.5)	0.903	1.519

The results of the slip-critical simulations were evaluated and compared to experimental data based on the peak friction force developed during the impulsive event, $P_{impulse}$, the maximum shear plate displacement developed during the impulsive event, $d_{impulse}$, and the peak residual friction force required to cause slip, $P_{slip,residual}$. Also compared were baseline static slip-critical simulations and experimental results. In the experimental baseline static tests, the average force to cause major slip in the connection was 18,673 lbf (83.1 kN). The baseline static simulation result was reasonably close to the average at 18,222 lbf (81.1 kN) or approximately 2.4% less than the experimental results. Table 8.5 shows the results of the three slip-critical simulations.

The predicted peak impulses from the impulsive event were higher than what was actually observed. While the simulation involving the lowest impact was most accurate, the accuracy of the model in terms of the peak friction force appears to decrease as the impulse increases. The model results are logical based on the formulation of static friction in the model since in order for the impact shear plate to move, it must first overcome static friction. However, experimental data suggests that in such an impulsive event, likely due to the rate at which the loading occurs, the peak static friction is not reached and a

maximum resistance of approximately 75% of the static friction is the only frictional resistance.

Table 8.5: Slip-critical simulation results.

		Simulation 1	**Simulation 2**	**Simulation 3**
Experimental $P_{peak,impulse}$	lbf (kN)	12,535 (55.8)	14,782 (65.8)	13,261 (59.0)
Simulation $P_{peak,impulse}$		12,538 (55.8)	17,900 (79.6)	17,988 (80.0)
P_{sim} / P_{exp}		1.00	1.21	1.36
Experimental $d_{impulse}$	in (mm)	0.0660 (1.68)	0.0866 (2.20)	0.1689 (4.29)
Simulation $d_{impulse}$		0.0007 (0.02)	0.0293 (0.74)	0.1503 (3.82)
P_{sim} / P_{exp}		0.01	0.33	0.89
Experimental $P_{slip,residual}$	lbf (kN)	20,236 (90.0)	23,289 (103.6)	8,027 (35.7)
Simulation $P_{slip,residual}$		18,188 (80.9)	16,641 (74.0)	13,910 (61.9)
P_{sim} / P_{exp}		0.90	0.71	1.73
P_{resid} / P_{static}		1.00	0.91	0.76

Conversely, the accuracy of the models increase in terms of the shear plate displacement as the applied impulse increases. In Simulation 1, hardly any movement in the impact shear plate was detected in the simulation while in Simulation 3, 89% of the measured displacement was predicted. Likewise, the accuracy of the residual force required to cause slip in the connection decreased as the applied impulse increased. The simulation results showed a steady trend of decreased slip force whereas the experimental data – both in terms of the force required to cause slip in the connection and the torque required to break the connection – showed little degradation in the force required to cause slip until a certain input energy threshold. This is likely due to the manner in which LS-DYNA handles relaxation in the bolt of the initial preload.

8.4 Conclusions

The results of the impulsive event, residual capacity, and bolt fracture during impulse demonstrate that LS-DYNA finite element modeling software can accurately predict the behavior of a simple connection subjected to an impulsive shear load and predict its residual capacity. At lower impact energies, the models accurately predict the force required to cause slip in a preloaded connection. The models had the most difficulty in predicting bolt ductility during and after the impulsive event. Additionally, the slip-critical models had difficulty in predicting the friction resistance at high impact energies and the shear displacement at lower impact energies. However, many of the issues do not appear symptomatic of the modeling methods, but with model calibration.

Sufficient data for the maximum effective plastic strain rate during an impulsive event and for quasi-static simulations do not currently exist to calibrate the material models, and so the user must guess at input parameters which may or may not lead to accurate results. The combination of mesh size, maximum effective plastic strain values, and strain rate all influence the response and more experimental data is necessary to be able to accurately provide modeling software with the proper parameters to predict behavior. However, the fact that the models were able to capture the overall behavior of a residual capacity event is promising in that with properly calibrated and validated models, these simulations might provide the expanded data set to calibrate and validate simplified tools such as an artificial neural network, response surface, or simple multi-degree of freedom model. These predictive tools would be implemented more widely and be much less computationally expensive than using high fidelity physics based models.

8.5 References

[1] Livermore Software Technology Corporation, *LS-DYNA Theory Manual*, 2006.

[2] Livermore Software Technology Corporation, *LS-DYNA Keyword User's Manual*, 2007.

[3] American Society for Testing and Materials, *Standard Specification for High Strength Structural Bolts, Steel and Alloy Steel, Heat Treated, 120 ksi (830 MPa) and 150 ksi (1040 MPa) Minimum Tensile Strength, Inch and Metric Dimensions*, ASTM F3125-15A, 2015.

[4] American Society for Testing and Materials, *Standard Test Methods for Tension Testing of Metallic Materials*, ASTM E8/E8M-16A, 2016.

[5] Abramowicz, W. and N. Jones, "Dynamic progressive buckling of circular and square tubes," *International Journal of Impact Engineering*, vol. 4, no. 4, pp. 243-270, 1986.

[6] Cowper, G. R. and P. S. Symonds, "Strain-hardening and strain-rate effects in the impact loading of cantilever beams," Brown Univ Providence Ri1957.

[7] Hadjioannou, M., D. Stevens, and M. Barsotti, "Development and Validation of Bolted Connection Modeling in LS-DYNA® for Large Vehicle Models," in *14th International LS-DYNA Users Conference*, Dearborn, MI, 2016.

[8] Huh, H., J. Lim, and S. Park, "High speed tensile test of steel sheets for the stress-strain curve at the intermediate strain rate," *International Journal of Automotive Technology*, vol. 10, no. 2, pp. 195-204, 2009.

[9] Kulak, G. L., J. W. Fisher, and J. H. Struik, *Guide to Design Criteria for Bolted and Riveted Joints, 2nd ed.* Chicago: American Institute of Steel Construction, 2001.

[10] Malvar, L. J., "Review of static and dynamic properties of steel reinforcing bars," *American Concrete Institute Materials Journal*, vol. 95, no. 5, pp. 609-616, 1997.

[11] Marais, S., R. Tait, T. Cloete, and G. Nurick, "Material testing at high strain rate using the split Hopkinson pressure bar," *Latin American Journal of Solids and Structures*, vol. 1, no. 3, pp. 219-339, 2004.

[12] Morrill, K. B., J. E. Crawford, J. M. Magallanes, and H. J. Choi, "Development of simplified tools to predict blast response of steel beam-column connections," in *Structural Engineering Research Frontiers*, 2007, pp. 1-10.

[13] Munoz-Garcia, E., J. Davison, and A. Tyas, "Analysis of the response of structural bolts subjected to rapid rates of loading," in *4th European Conference on Steel and Composite Structures (EUROSTEEL)*, 2005, vol. 100, p. 4.10.

[14] Paik, J. G. and J. Y. Chung, "A basic study on static and dynamic crushing behavior of a stiffened tube," *Transactions of the Korean Society of Automotive Engineers*, vol. 7, no. 1, pp. 219-219, 1999.

[15] Rumpf, J. and J. Fisher, "Calibration of A325 bolts," *Proc. ASCE*, vol. Vol. 89 (ST6), no. December 1963, Reprint No. 232 (63-18), 1963.

[16] Salih, N., J. Smith, H. M. Aktan, and M. Usmen, "An experimental appraisal of the load-deformation properties of A325 high-strength bolts," *Journal of Testing and Evaluation*, vol. 20, no. 6, pp. 440-448, 1992.

[17] Stoddart, E., M. Byfield, and A. Tyas, "Blast modeling of steel frames with simple connections," *Journal of Structural Engineering*, vol. 140, no. 1, p. 04013027, 2012.

[18] Whittington, W. R. *et al.*, "Capturing the effect of temperature, strain rate, and stress state on the plasticity and fracture of rolled homogeneous armor (RHA) steel," *Materials Science and Engineering: A*, vol. 594, pp. 82-88, 2014.

CHAPTER 9

CONCLUSIONS AND FUTURE WORK

9.1 Conclusions

Terror attacks employing explosives continue to increase in frequency domestically and around the globe. Even relatively small explosive events can cause structural damage to surrounding infrastructure due to the extreme nature of the load. The loss or decreased capacity of a load bearing structural element has the potential to cause a progressive collapse response process to ensue. Ideally, the existing dead and service loads are transferred to surviving structural elements such that the structure is stable long enough to enable occupants to escape. Connections are the critical link in the transfer of these loads, yet their behavior and response is the least understood.

In modern steel frame structures, bolted connections play a significant role in the response of the structure during the extreme event and after the extreme event has dissipated. A more thorough understanding of the behavior of bolted steel connections during and after extreme loading events is necessary to predict and prevent progressive collapse of structures. Connections ensure ductility and transfer loads to non-damaged and less damaged structural elements. To this point, relatively little experimental research has been done on the behavior of structural bolts subjected to impulsive shear loadings and no research has evaluated the residual shear capacity of bolts or connections after an extreme loading event. The research presented in this thesis begins to fill that gap with an

experimental test program of structural bolts and simple bolted steel connections. By simplifying the problem from the more complex connections found in the field, insights can be gleaned on the fundamental behaviors and response of the bolted connection.

An experimental residual capacity test system was developed to subject bolts and bolted connections to an impulsive shear event and then test the residual static capacity of the bolt in-situ after the event. In the test system, impulsive loads were generated through the use of a high speed hydraulic actuator to accelerate a flyer mass to a desired impact velocity. The residual capacity experimental test system used dynamic load cells to measure the force-time histories of both the impact and the reaction of the system. High speed video was used to measure the displacement-time history of the flyer mass and capture data regarding the response at the specimen bolt. A modular system was design to be installed within the impulsive setup to apply a quasi-static load after the impulsive event. The quasi-static apparatus measured the shear force-displacement of the specimen bolt. While a single structural bolt served as the primary specimen for this research, the system can be adapted to accommodate any number of bolted connection configurations. The system can also be easily adapted to investigate different types of bolts, pins, rods, dowels or connected plate materials and surface treatments.

The residual capacity experimental test system was used to investigate three fundamental aspects of bolted steel connections under impulsive loads: 1) the response and behavior of structural bolts during an impulsive event; 2) the residual capacity of structural bolts after an impulsive event; and 3) the response and behavior of clamping force and friction during and after an impulsive event in slip-critical connections. The experimental

tests were intended to be a starting point for understanding structural bolts and bolted steel connections and not an exhaustive investigation.

The response and behavior of structural bolts during an impulsive event was investigated by subjecting ASTM A307 and ASTM A325 structural bolts to varying impulsive loads. Impulsive loads were generated in the intermediate strain rate range, typical of the structural response strain rate from a blast load. Key findings of this investigation included an observed increase in the rigidity of structural bolts within the tested strain rate range, recommended static and dynamic increase factors for structural bolts for design and simplified analysis, a linear relationship between impact energy and residual permanent shear strain in the bolt, and decreased ductility as compared to static ductility at higher rates.

Investigation of the residual capacity of structural bolts after an impulsive load was conducted by quasi-statically testing impulsively damaged ASTM A307 and ASTM A325 structural bolts. Key findings of this investigation included the observation that below a certain impact energy threshold, the residual capacity of a structural bolt is equivalent to the virgin capacity of the bolt. The threshold was observed to be comparatively high compared to the impact energy that would cause fracture within the bolt during the impulsive event. The residual ductility of the damaged bolt was found to decrease with increased impact energy. However, the total ductility, considering both the permanent deformation from the impulsive event and the residual deformation, was generally equivalent to the ductility of a virgin bolt. This indicates that within the limited strain rate range tested, typical load-unload-reload behavior is present regardless the strain rate range in which the damage was developed. Finally, a response model to predict the impulsive

plastic strain and resulting residual capacity for a bolt subjected to an impulsive shear load was developed. Shown in Figure 9.1 (A307 bolts) and Figure 9.2 (A325 bolts), the model accounts for the four apparent behavior zones based on the impact energy applied to the bolt. Because of the limited number of tests conducted, further experimental research is needed to improve the model.

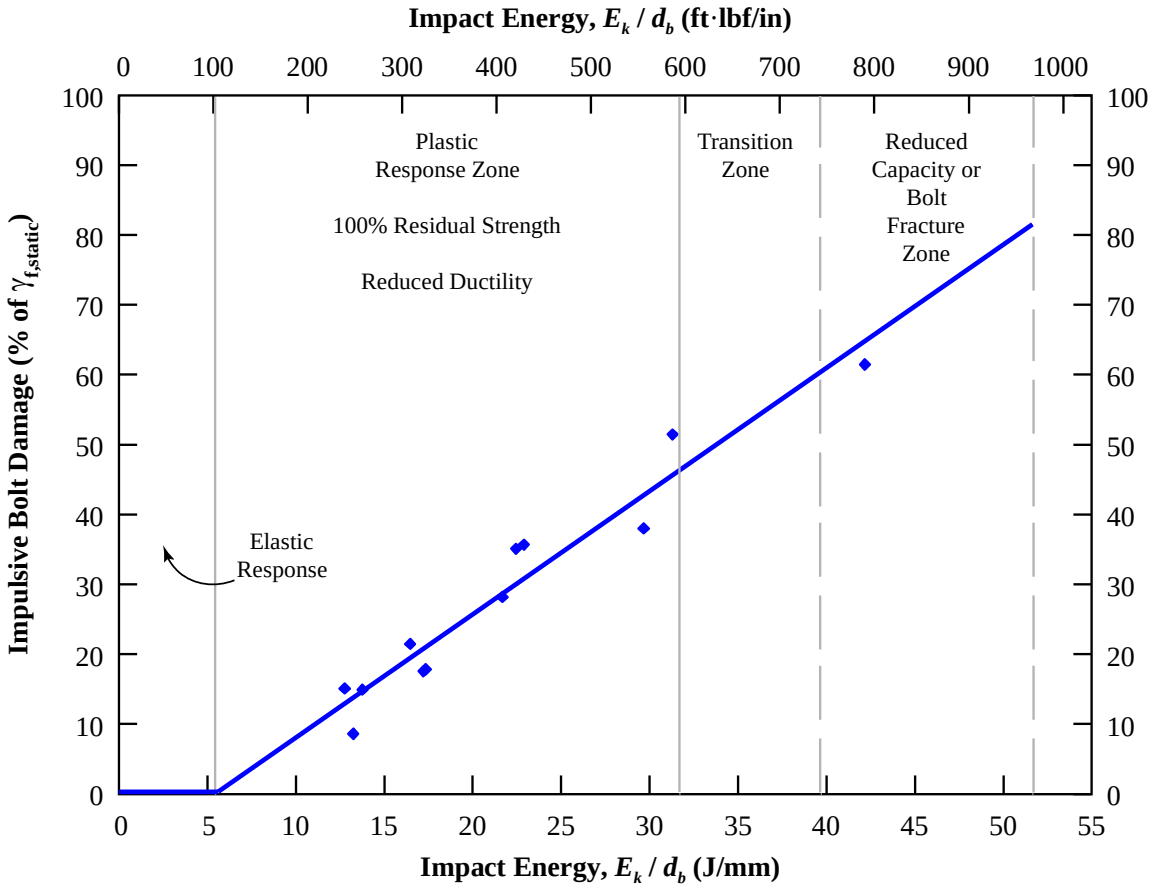

Figure 9.1: A307 bolt damage and residual capacity response model.

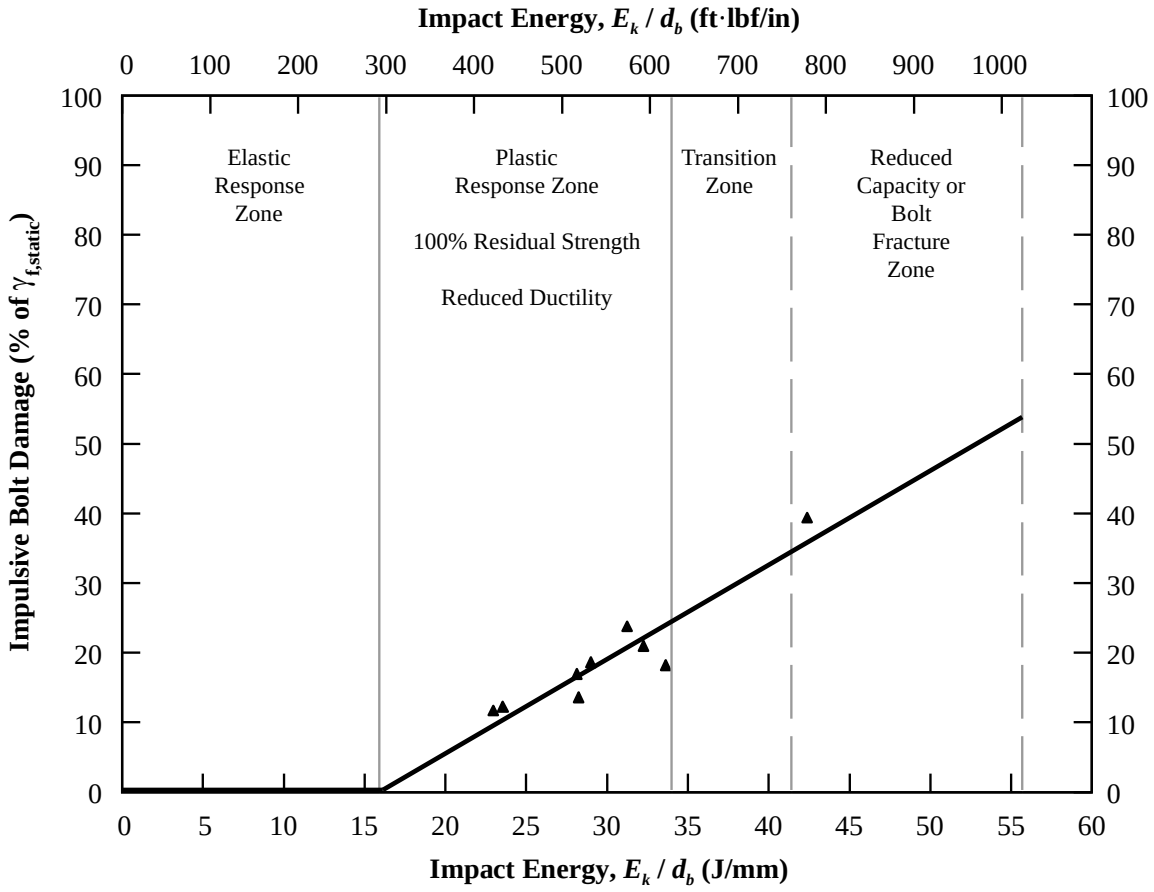

Figure 9.2: A325 bolt damage and residual capacity response model.

The response, behavior, and residual capacity of slip-critical connections subjected to an impulsive load was conducted by using the residual capacity experimental test system to test single bolt, slip-critical connections fabricated using current design standards. Key findings of this investigation included a lower peak friction resistance under impulsive loads than static loads, work due to fiction increases linearly with increased impact energy. As a result only 20 to 30% of the initial impact energy is transferred to the structural bolt in bearing. Because the friction resistance increases with the number of structural bolts in the connection, friction resistance has the potential to significantly protect structural bolts from damage in a structural bolt and should not be neglected. Below a critical impact

energy threshold, the residual slip capacity of slip-critical connections is generally equivalent to the static slip capacity. Beyond that threshold, the residual slip capacity decreases significantly and preload in the bolt exhibits relaxation. Finally, for the plate material and surface conditions used, coefficients of static and dynamic friction as well as a decay coefficient describing the transition from static friction to dynamic friction are recommended. This data is particularly important for modeling slip-critical connections.

A numerical study was conducted to investigate how well current, state of the art high fidelity physics based models capture the behavior observed in the impulsive, residual capacity, and slip-critical experimental tests. The investigation employed common modeling methodologies inherent to the finite element solver, LS-DYNA. A simplified model of the experimental test setup was developed to gain efficiencies and reduce computational expense. Tensile stress-strain data from the literature was used to develop four different material models for ASTM A325 bolts. A mesh sensitivity study was conducted to investigate the influence of mesh size on results. Representative simulations of the experimental test series were conducted and results compared to the experimental data. In general, the models predict the overall impulsive and residual capacity behavior observed in experimental tests. However, due to lack of calibration data, the models significantly over predict the ductility in the connections. Similarly, in slip-critical simulations the current models fail to accurately predict relaxation of preload in the bolt and subsequently over predict the friction resistance observed in slip-critical connections. The experimental research conducted in this work provides the starting point for calibration data, but more experimental research is needed to confirm and predict behavior.

In summary, the following key conclusions regarding this research can be made, particularly with respect to the four research questions posed in Chapter 3:

1. An experimental method was developed to investigate the response and residual capacity of structural bolts, pins, rods, and dowels subjected to impulsive loads. Using a high-speed, hydraulic actuator, the experimental method can be adapted to investigate the dynamic and residual shear response of a wide variety of materials and connection configurations.

2. Residual plastic shear deformation in structural bolts subjected to an impulsive load increases linearly with increasing impact energy. Static and dynamic increase factors of 1.15 and 1.10, respectively, are recommended for structural bolts with respect to the minimum proof strength. The modulus of rigidity in structural bolts increased by a factor of two under impulsive loading conditions.

3. The residual strength of slightly, moderately, and heavily damaged bolts is commensurate with that of virgin bolts that were not damaged. Severely damaged bolts demonstrated reduced strength. Residual ductility is decreased in damaged bolts but the total ductility, determined by combining the permanent plastic deformation and the residual ductility, is approximately the same as that of a virgin bolt. Further experimental research is required to investigate the reduction in capacity for severely damaged bolts.

4. The clamping force and resulting friction between connected members in slip-critical joints significantly protects the bolt from damage during an impulsive event. Due to the energy dissipated by friction, only 20-30% of the impact energy was transferred to the bolt in the impact energy range tested. Therefore, it is recommended that all structural bolts, including those in bearing type connections, be installed with the minimum

pretension required for slip-critical connections to provide a low cost, effective safety measure for extreme loads.

5. Current high fidelity, physics-based modeling methods predict the overall behavior of structural bolts subjected to an impulsive load and then reloaded statically to fracture but are not accurate in their predictions. Models predicted the capacity of the bolt during the impact and the residual capacity under quasistatic loads. However, the models fail to accurately capture the ductility in the bolt or accurately predict the fracture strain. Experimentally validated material parameters are needed to improve model accuracy.

9.2 Contributions and Significance

The research presented in this thesis is significant in that it begins to fill the current gap in knowledge of structural bolts and bolted connections subjected to extreme loads. Further, the research provides a path forward to generate the data necessary, both experimental and numerical, to continue to further understanding in this area. The research presented in this thesis makes several contributions to the current body of knowledge regarding the response of steel bolted connections during impulsive events and the residual capacity of those connections after such an event. These contributions include:

1. Developed a novel experimental method to investigate impulsive shear in bolts, pins, rods, and dowels.

2. Quantified the residual permanent shear deformation of a structural bolt subjected to an impulsive load. The data set can be used to help calibrate models of steel bolts and predict damage based on impact energy.

3. Quantified an increase in modulus of rigidity for structural bolts subjected to impulsive shear loads.

4. Developed a novel experimental method to investigate the in-situ residual capacity bolts and bolted steel connections.

5. Created a response model to predict the residual capacity of structural bolts and bolted connections subjected to impulsive shear loadings that accounts for multiple energy regimes.

6. Proposed a potential new method for identifying bolt fracture strain under impulsive loads based on the static stress-strain curve.

7. Conducted the first, deliberate experimental investigation of slip-critical connections subjected to impulsive loads along with an investigation of the residual capacity of the connection. Validated that the residual capacity experimental test system can be used for further impulsive investigations of slip-critical connections.

8. Conducted a rigorous evaluation of current modeling methods, identified shortcomings in those methods, and recommended ways to improve those models in the future.

9.3 Recommendations for Future Work

As the research presented in this thesis was essentially a proof of concept study to investigate the behavior of structural bolts and steel bolted connections, many areas exist for future research. Recommendations for future work are aimed at either filling gaps

identified in this research, expanding the existing data set, or improving current modeling methods.

There is a need to improve the data set for structural bolts subjected to impulsive loads, particularly ASTM A325 and ASTM A490 bolts. A true analysis of variance (ANOVA) study should be conducted to generate statistically significant data regarding the behavior of both types of structural bolts under impulsive loads. Additional variables not included in this research such as bolt diameter and grip length should also be considered. Further, more advanced methods of directly measuring strain in the bolt, such as digital image correlation, should be incorporated for more accurate and consistent results.

Further experimental research is needed to identify the response of structural bolts in the transition zone identified in the bolt residual capacity model developed in Chapter 6. This transition zone is particularly important for predicting the response of a steel bolted connection and currently insufficient data is available to truly understand the behavior in this zone. This research would also serve to improve the understanding of the fracture strain parameters necessary to accurately calibrate models to predict the ductility of a structural bolt subjected to an impulsive load.

This research focused on minimizing localized failure of the shear plates to generate damage in the structural bolt itself. However, the bolt shear plate interaction is particularly important in understanding the true response and residual capacity of a connection more likely to be fabricated in the field. Therefore, further experimental testing of different shear plate – bolt material combinations would provide further insight into the behavior and response of the connection holistically.

Further investigation of the fracture strain and ductility under impulsive loads is also needed. The observation that shear fracture strain under high rates may be predicted from the static stress-strain curve within a limited strain rate range, while interesting, needs much more conclusive data to draw any hard conclusions. A test series aimed at observing structural bolts that fracture under impact is needed to investigate whether or not this is an actual phenomena or merely a coincidence in the collected data. Such a test series would be critical for improving modeling efforts as well. An identified shortcoming of modeling methods presented in Chapter 8 is a model of the true fracture strain as a function of strain rate.

This research also focused only on the response of a single structural bolt in shear. Further research is necessary to investigate the response of connections with multiple bolts for both bearing-type connections and slip-critical connections to further understand the multiplicative effects of multi fastener connections. Additionally, in any typical steel structure there are connections with differing modes of carrying loads, including tension and combined tension and shear. Using the same methodology presented in this thesis, the response and residual capacity of structural bolts in tension should also be investigated. Combined with an improved shear data set, more complex connections and stress states that are typically found in steel structures can then be investigated.

Finally, once high fidelity physics based models are properly calibrated and accurately predict the response and residual capacity of steel bolted connections, a fast running model should be developed, such as an artificial neural network, a response surface, or a mechanism to incorporate connection behavior into simple single and multi-

degree of freedom models. These models would be highly implementable and much less computationally expensive than high fidelity physics based models.

APPENDIX A

RESIDUAL CAPACITY TEST SYSTEM FABRICATION DRAWINGS

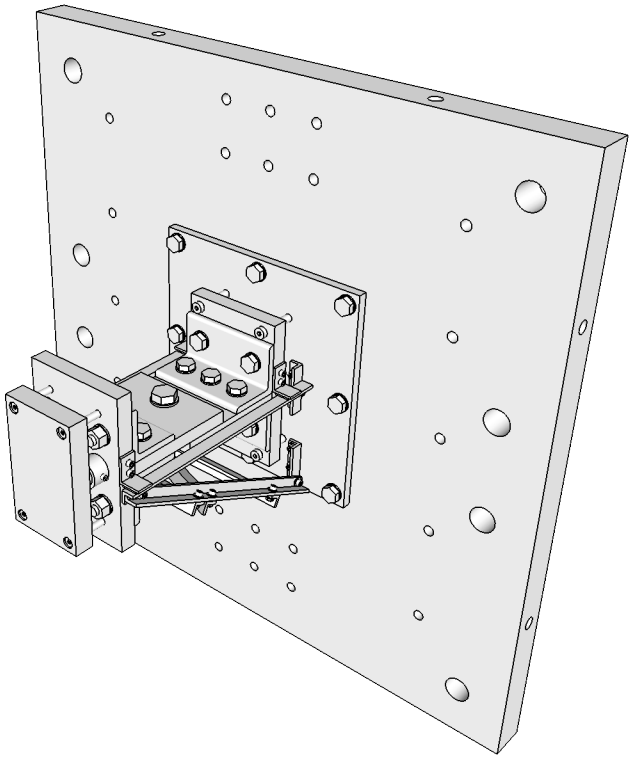

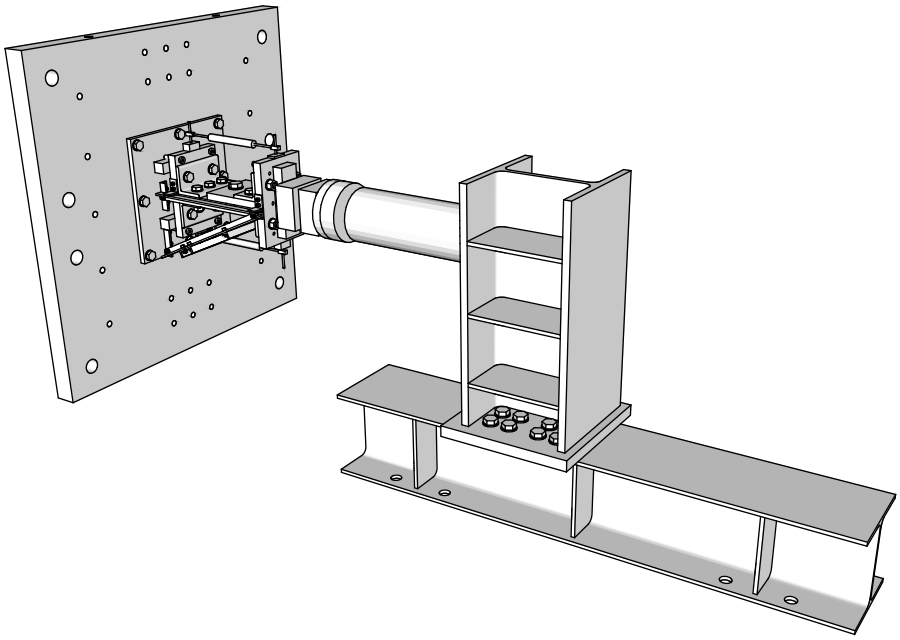

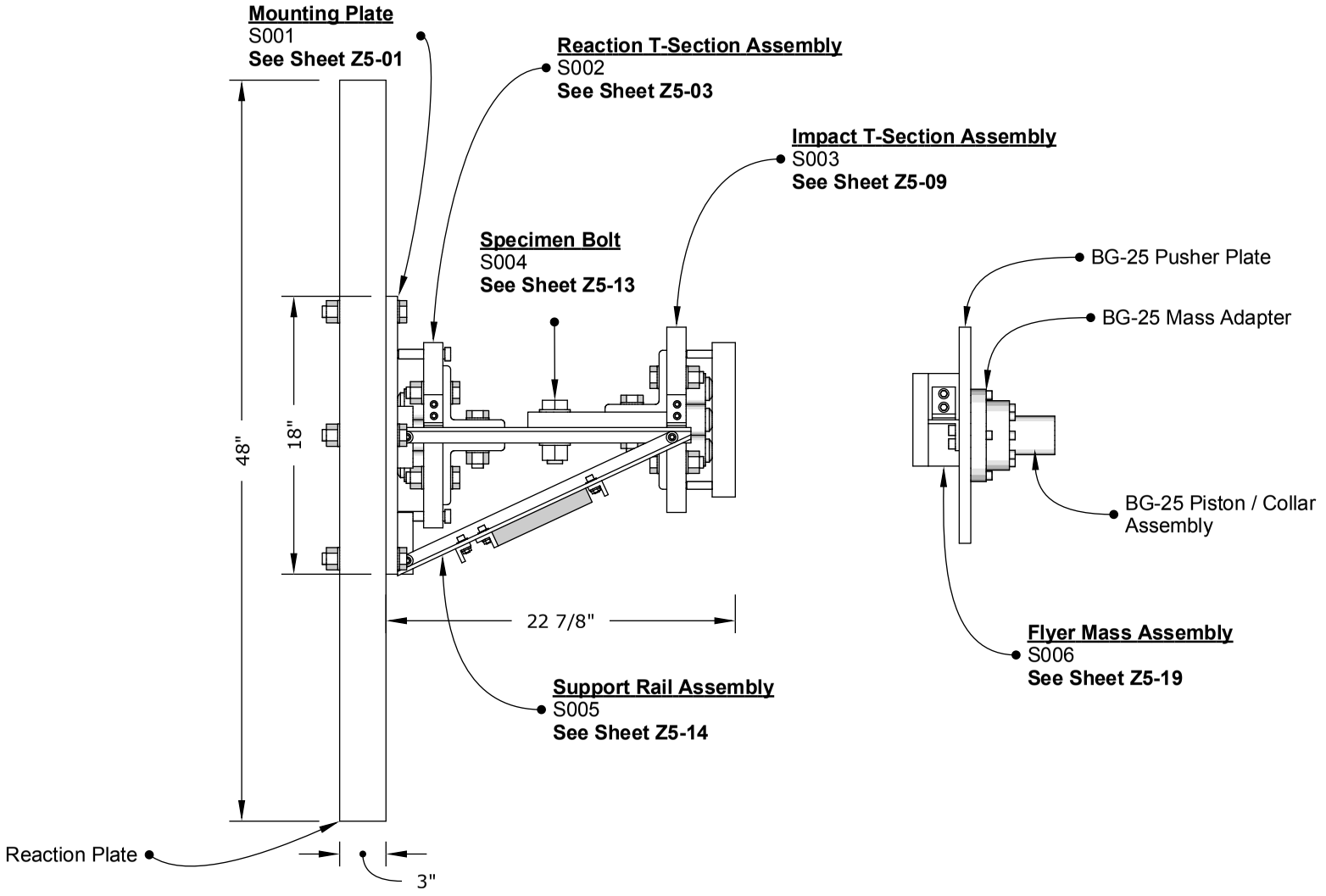

Project:	Component:	Sheet Description:		
Residual Capacity Test System	Dynamic Test System	Component Overview	**Z1**	01

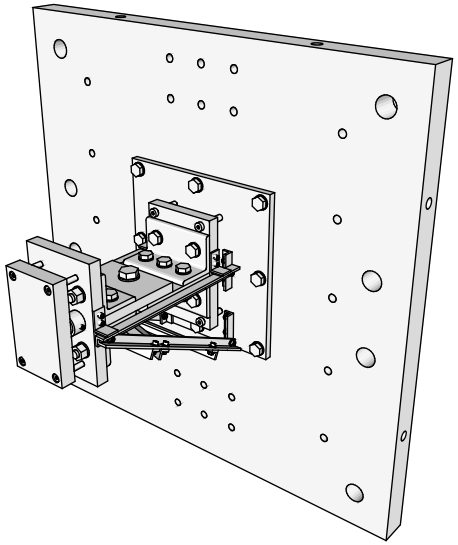

ISOMETRIC VIEW

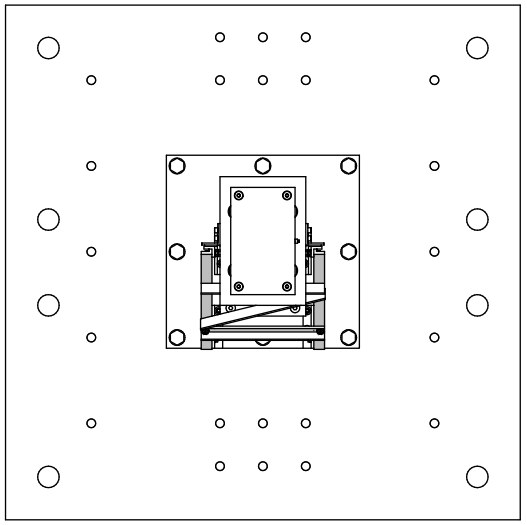

FRONT VIEW (DIRECTION OF IMPACT)

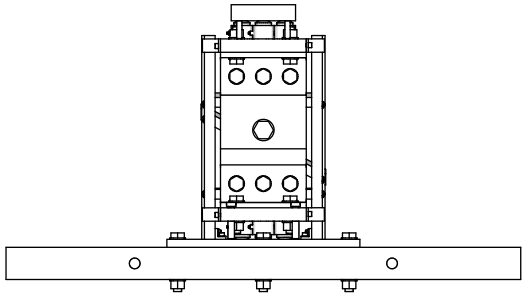

TOP VIEW

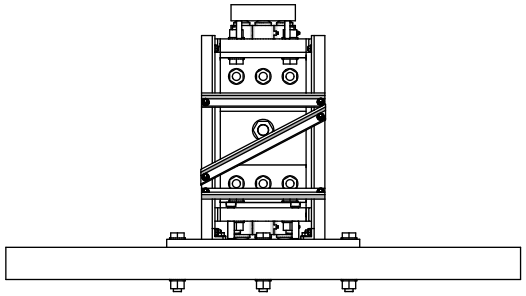

BOTTOM VIEW

Project:	Component:	Sheet Description:		
Residual Capacity Test System	Dynamic Test System	Component Overview, Alternate Views	**Z1**	02

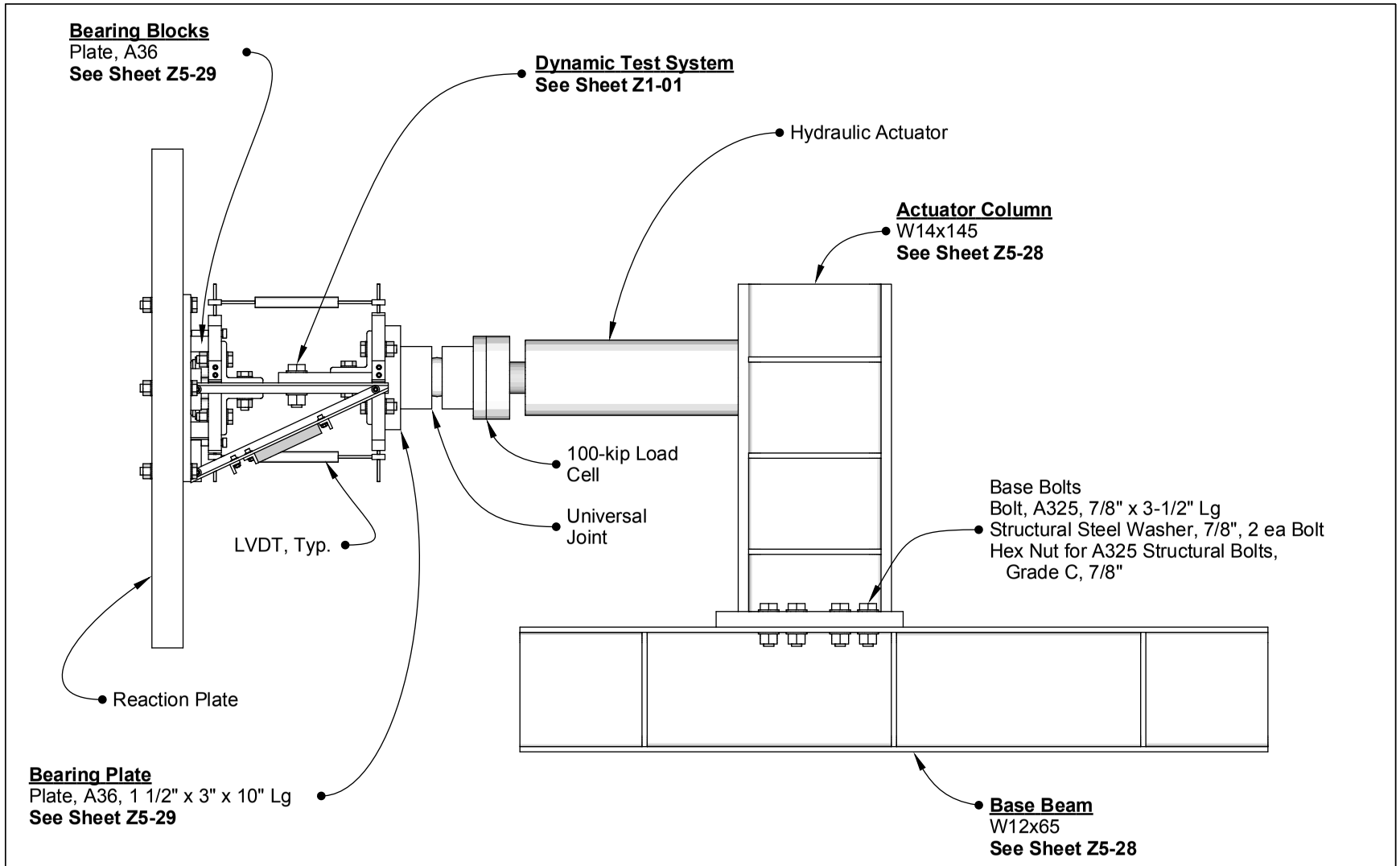

Project:	Component:	Sheet Description:		
Residual Capacity Test System	Static Test System	Component Overview	**Z1**	03

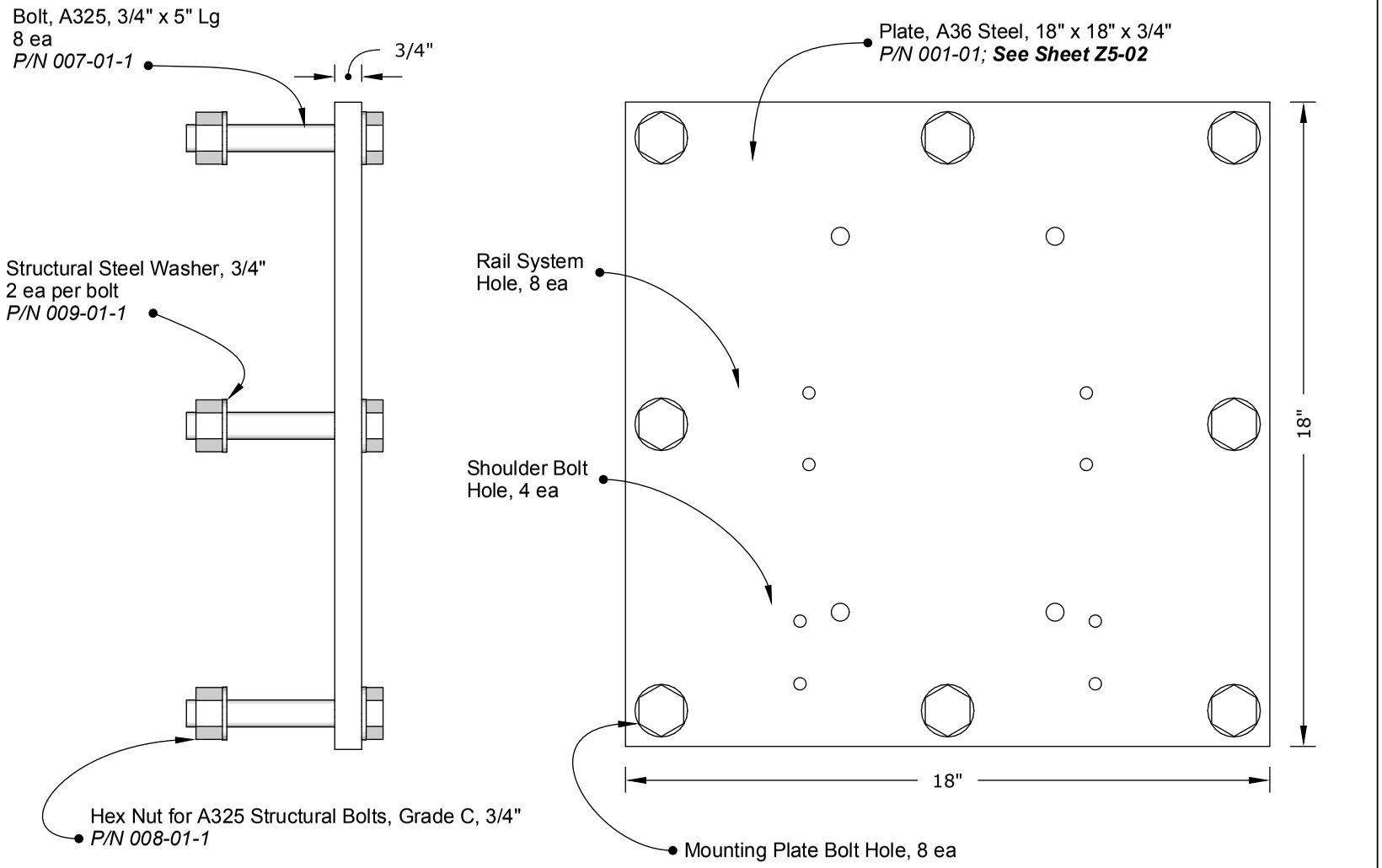

Project:	Component:	Sheet Description:		
Residual Capacity Test System	Dynamic Test System	Mounting Plate Detail, S001	**Z5**	01

Hole ID	# Hole	Ø Hole	Fit Class	Thread	Depth
Z502-A	8 ea	0.813 (13/16")	Normal	None	Thru
Z502-B	4 ea	0.5 (1/2")	3A	1/2-13 UNC	Thru
Z502-C	8 ea	0.313 (5/16")	3A	5/16-18 UNC	Thru

NOTES: 1. MATERIAL: ASTM A36 STEEL
2. COMPONENT MASS: 69 LB
3. TOLERANCES ± 1/32"

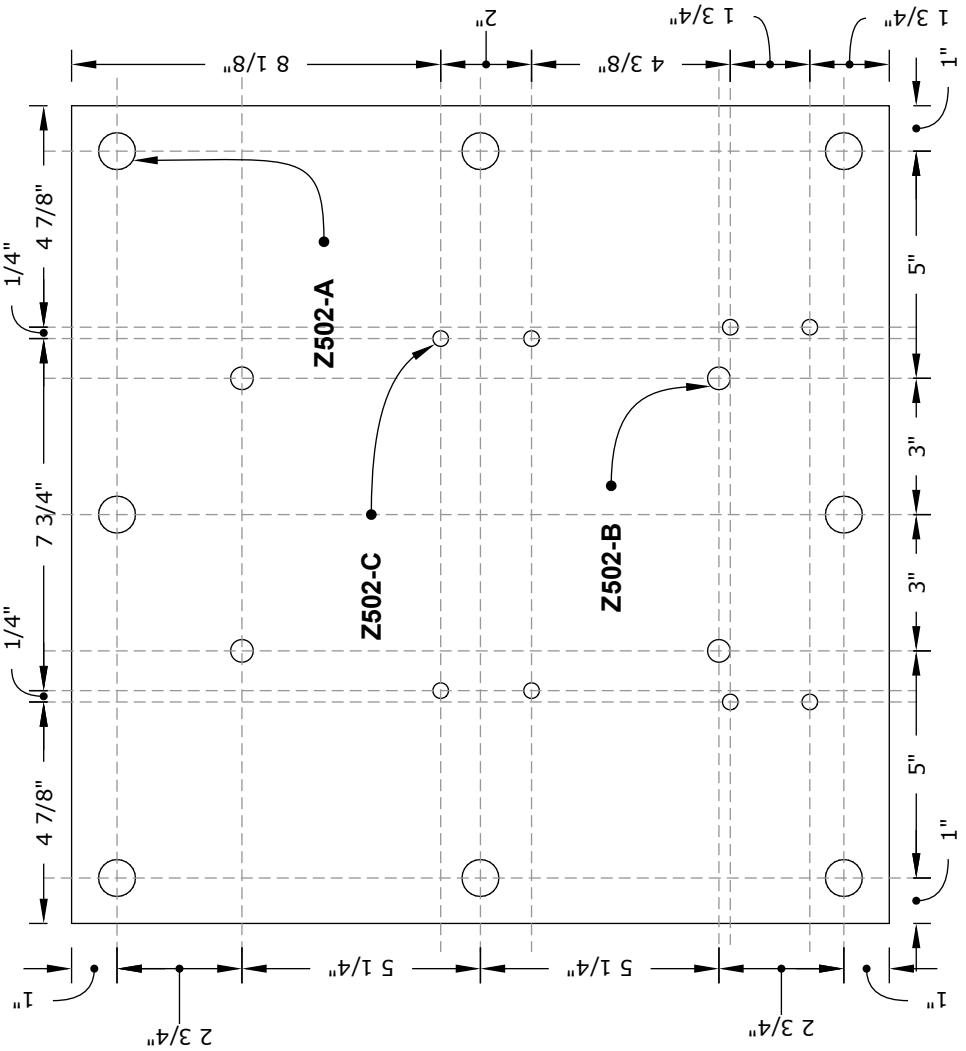

Project: Residual Capacity Test System
Component: Dynamic Test System
Sheet Description: Mounting Plate Detail, P/N 001-01
Z5 02

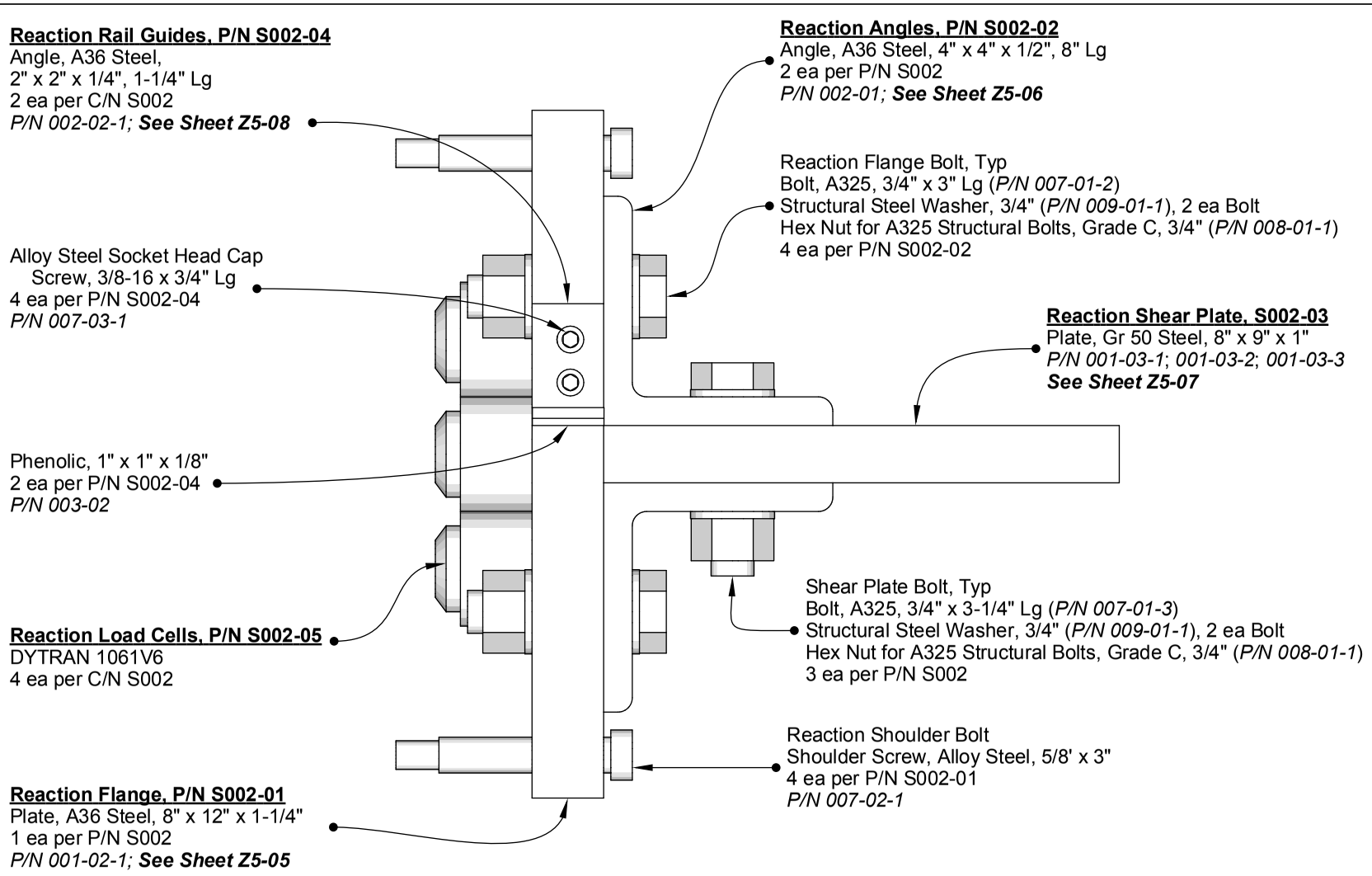

Project:	Component:	Sheet Description:		
Residual Capacity Test System	Dynamic Test System	Reaction T-Section Assembly Detail, S002	**Z5**	03

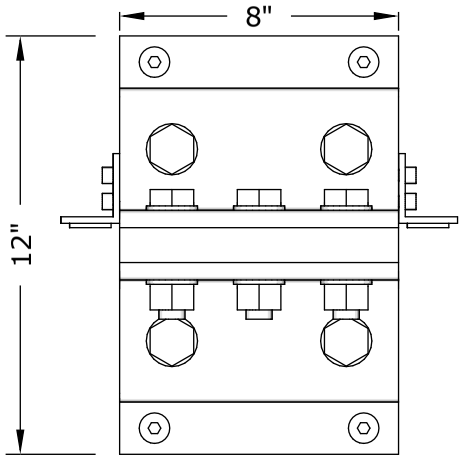

FRONT VIEW

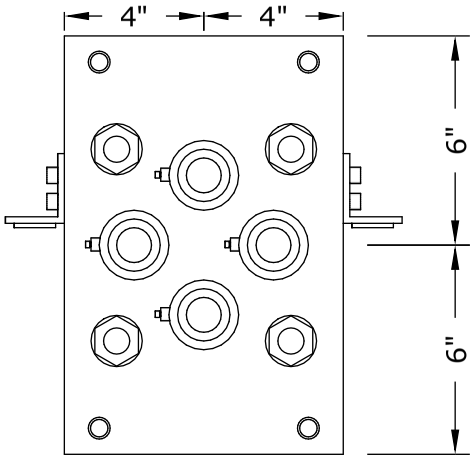

BACK VIEW

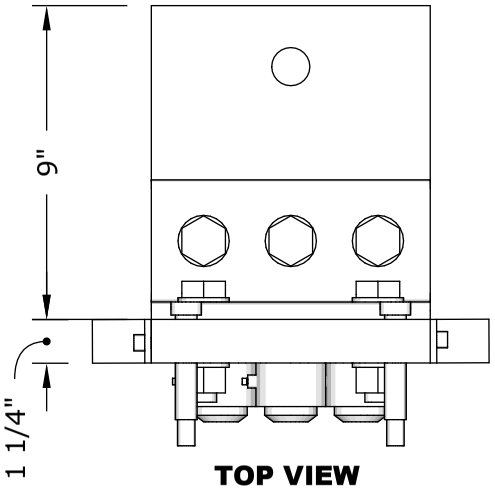

TOP VIEW

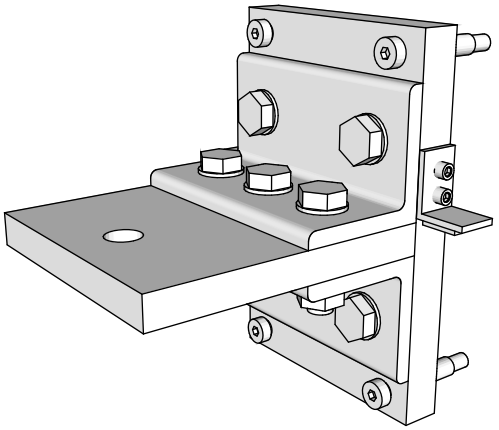

ISOMETRIC VIEW

Project:	Component:	Sheet Description:		
Residual Capacity Test System	Dynamic Test System	Reaction T-Section Assembly, S002, Alternate Views	Z5	04

Hole ID	# Hole	Ø Hole	Fit Class	Thread	Depth
Z505-A	4 ea	0.688 (11/16")	Normal	None	Thru
Z505-B	4 ea	0.813 (13/16")	Normal	None	Thru
Z505-C	4 ea	0.375 (3/8")	2B	3/8-16 UNC	Thru
Z505-D	4 ea	0.375 (3/8")	3A	3/8-16 UNC	7/8"

NOTES: 1. MATERIAL: ASTM A36 STEEL
2. COMPONENT MASS: 34 LB
3. TOLERANCES ± 1/32"

Project: Residual Capacity Test System

Component: Dynamic Test System

Sheet Description: Reaction Flange Detail, P/N 001-02-1

Z5 05

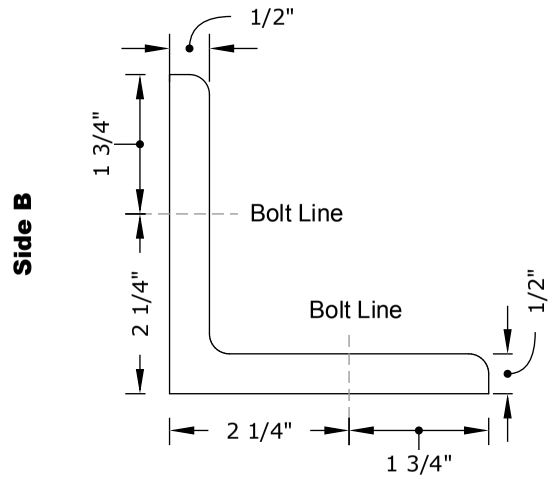

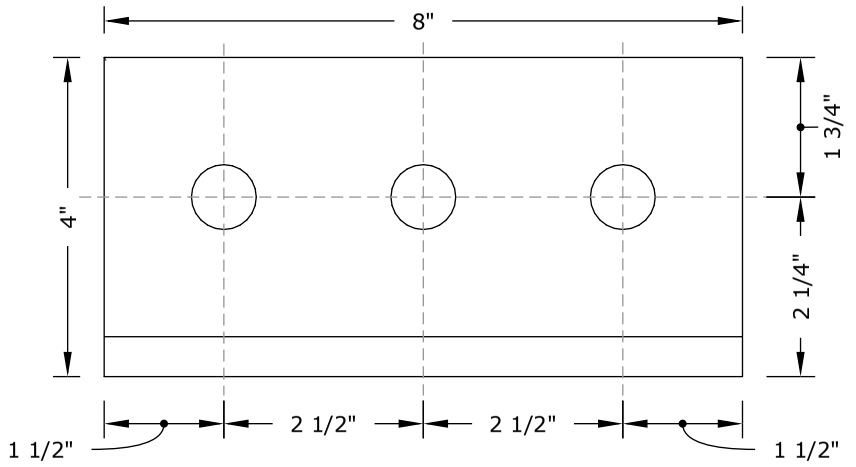

Hole ID	# Hole	Ø Hole	Fit Class	Thread	Depth
Z506-A	5 ea	0.813 (13/16")	Normal	None	Thru

NOTES: 1. MATERIAL: ASTM A36 STEEL
2. COMPONENT MASS: 8.5 LB
3. TOLERANCES ± 1/32"

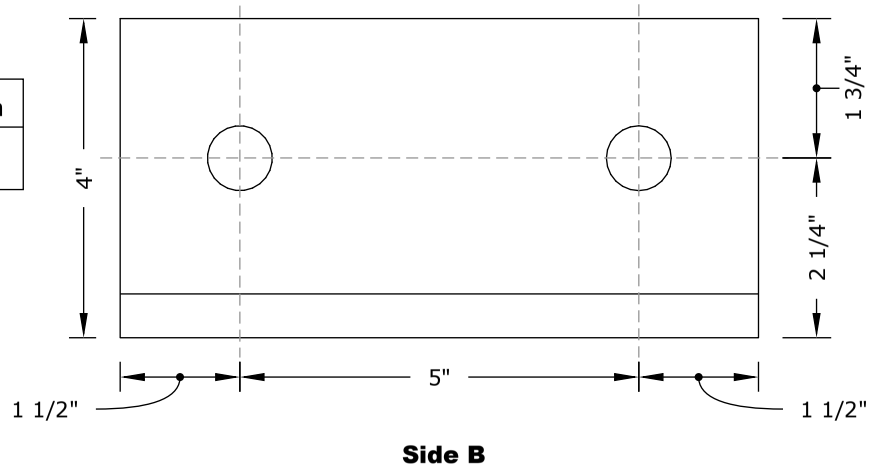

Project:	Component:	Sheet Description:		
Residual Capacity Test System	Dynamic Test System	Angle Detail, P/N 002-01	Z5	06

P/N 001-03-1

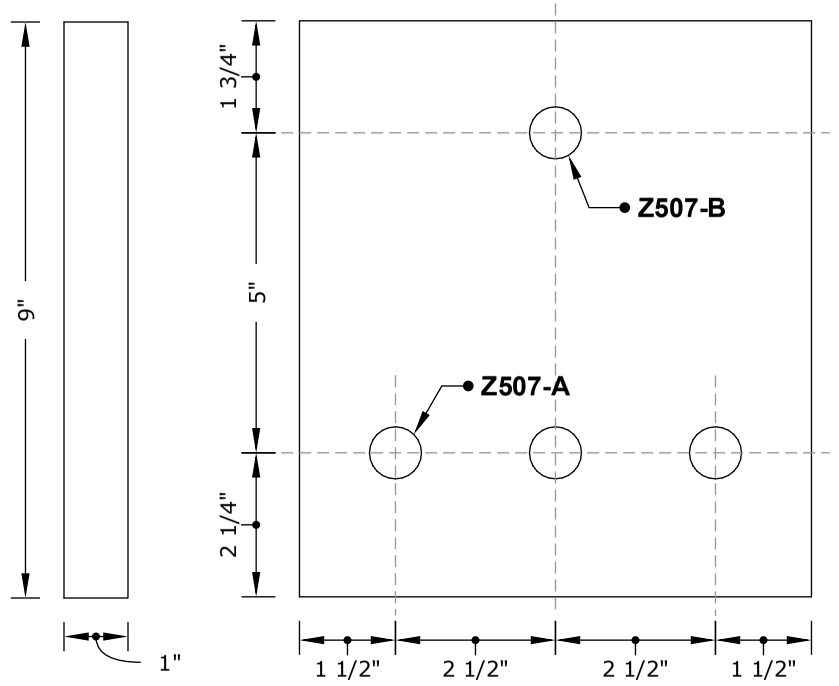

P/N 001-03-2, -3

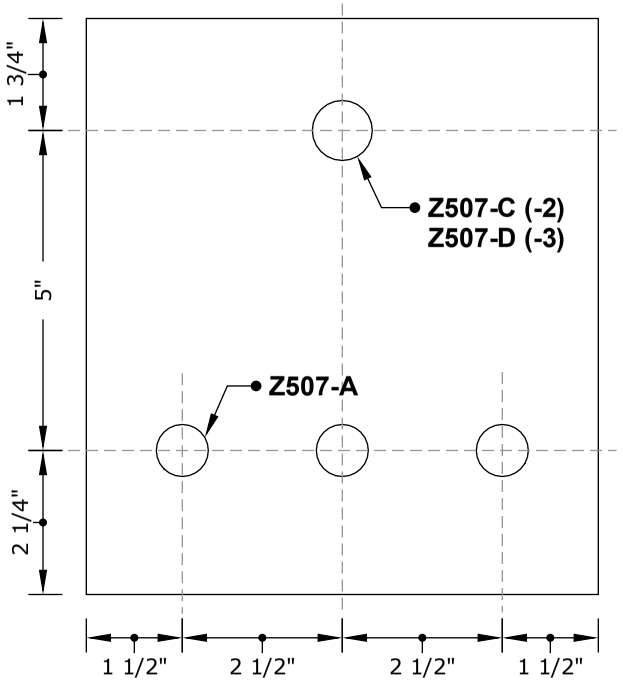

Hole ID	# Hole	Ø Hole	Fit Class	Thread	Depth
Z507-A	3 ea	0.813 (13/16")	Normal	None	Thru
Z507-B	1 ea	0.813 (13/16")	Normal	None	Thru
Z507-C	1 ea	0.938 (15/16")	Normal	None	Thru
Z507-D	1 ea	1.094 (1-3/32")	Normal	None	Thru

NOTES:
1. MATERIAL: ASTM A572 GR 50 STEEL OR ASTM A514 STEEL
2. COMPONENT MASS: 20.5 LB
3. TOLERANCES ± 1/32"

Project:	Component:	Sheet Description:		
Residual Capacity Test System	Dynamic Test System	Shear Plate Detail, P/N 001-03-1, -2, -3	Z5	07

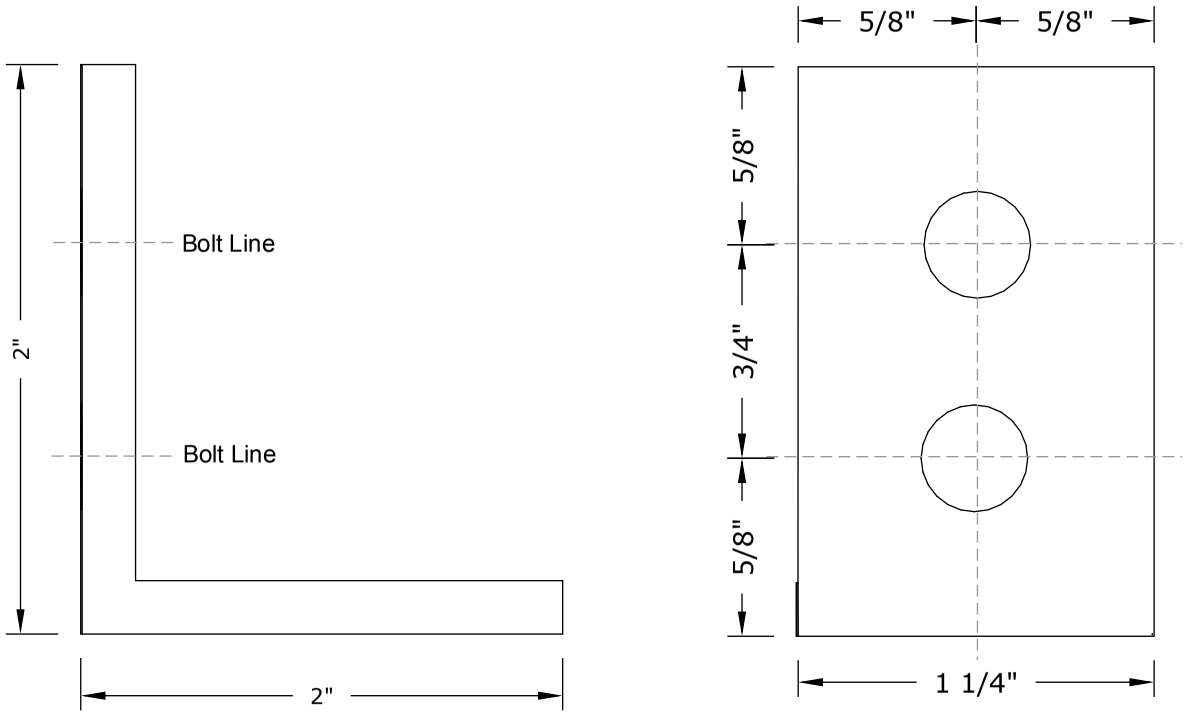

Hole ID	# Hole	Ø Hole	Fit Class	Thread	Depth
Z508-A	2 ea	0.406 (13/32")	Normal	None	Thru

NOTES: 1. MATERIAL: ASTM A36 STEEL
2. COMPONENT MASS: 8.5 LB
3. TOLERANCES ± 1/32"; ± 0.005

Project:	Component:	Sheet Description:		
Residual Capacity Test System	Dynamic Test System	Rail Guide Detail, P/N 002-02-1, -2	Z5	08

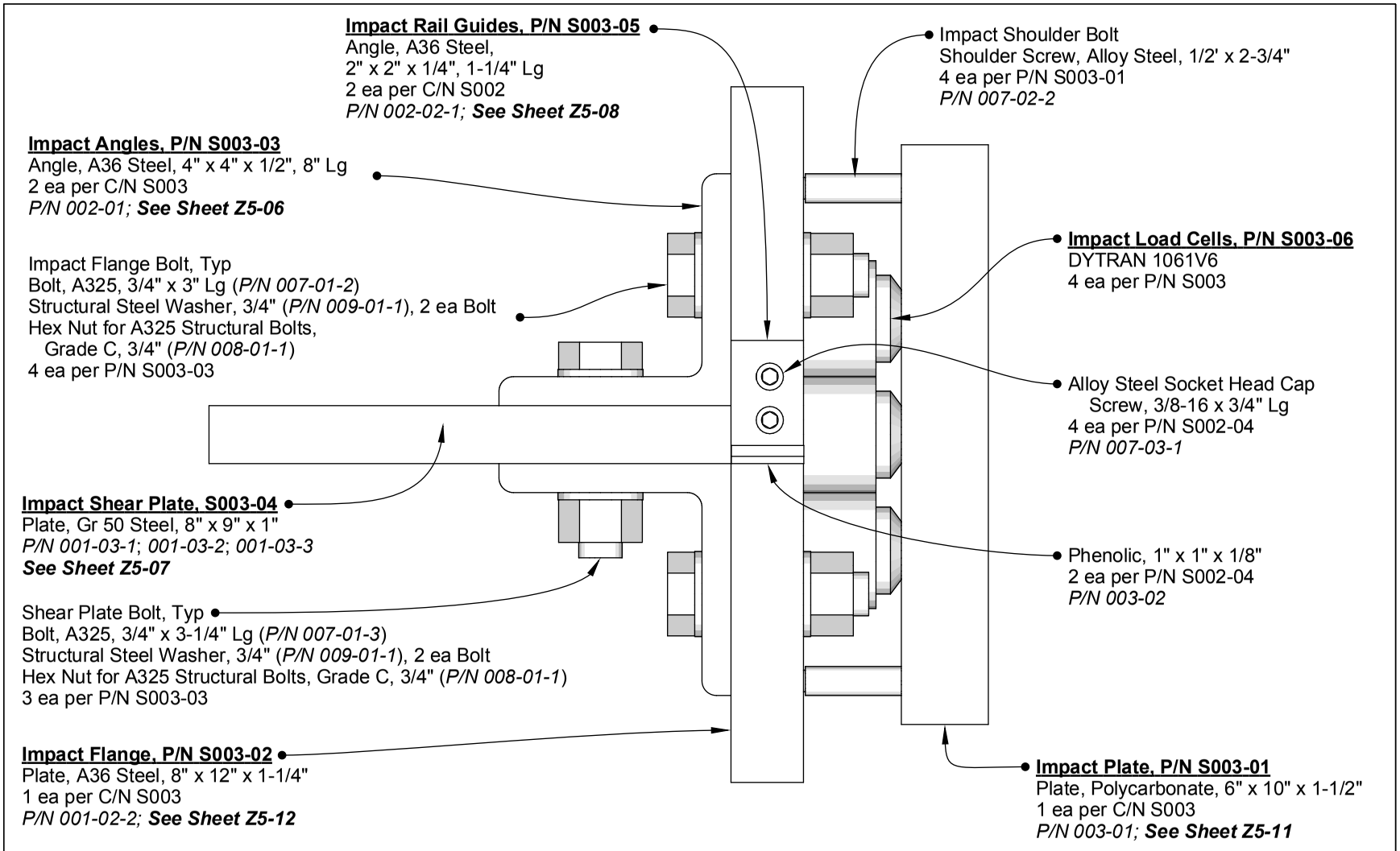

Project:	Component:	Sheet Description:		
Residual Capacity Test System	Dynamic Test System	Impact T-Section Assembly Detail, S003	**Z5**	09

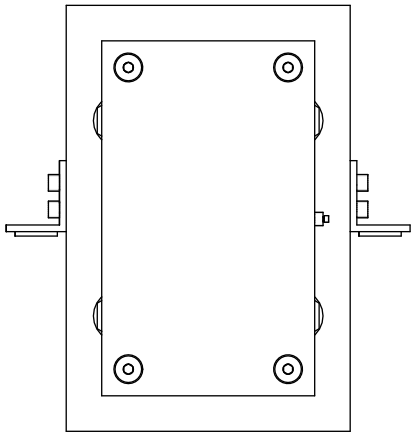

FRONT VIEW

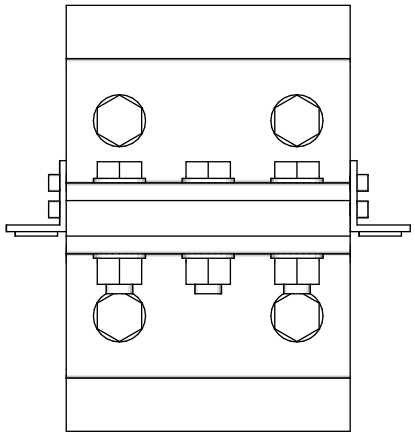

BACK VIEW

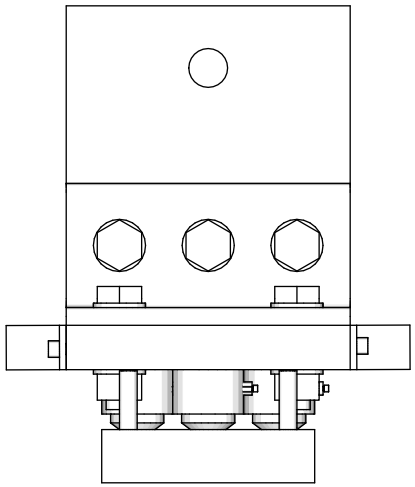

TOP VIEW

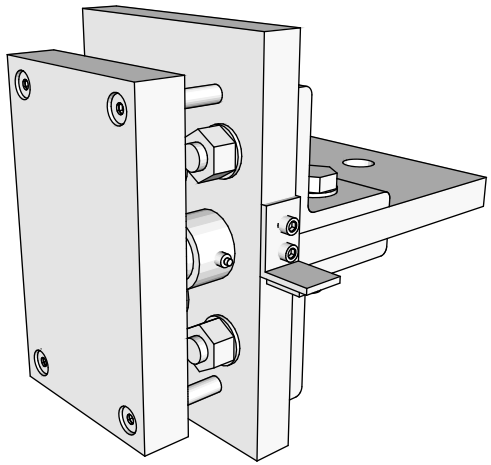

ISOMETRIC VIEW

Project:	Component:	Sheet Description:		
Residual Capacity Test System	Dynamic Test System	Impact T-Section Assembly, S003, Alternate Views	Z5	10

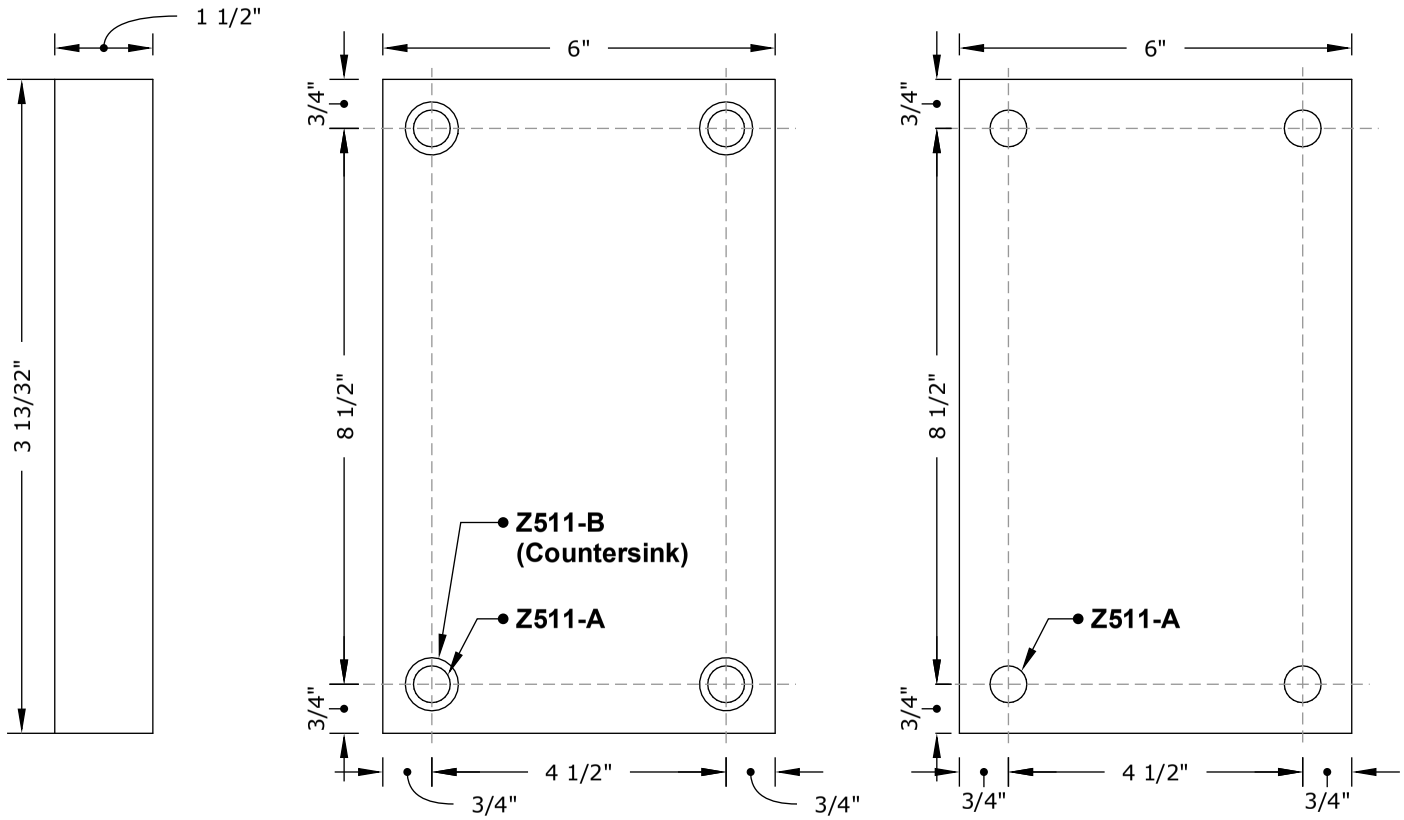

Hole ID	# Hole	Ø Hole	Fit Class	Thread	Depth
Z511-A	4 ea	0.562 (9/16")	Normal	None	Thru
Z511-B	4 ea	0.812 (13/16")	Normal	None	1/4"

NOTES:
1. MATERIAL: POLYCARBONATE, MACHINE GRADE
2. COMPONENT MASS: 3.9 LB
3. TOLERANCES ± 1/32"; ± 0.005"

Project:	Component:	Sheet Description:		
Residual Capacity Test System	Dynamic Test System	Impact Plate Detail, P/N 003-01	Z5	11

Hole ID	# Hole	Ø Hole	Fit Class	Thread	Depth
Z512-A	4 ea	0.375 (3/8")	3A	3/8-16 UNC	Thru
Z512-B	4 ea	0.813 (13/16")	Normal	None	Thru
Z512-C	4 ea	0.375 (3/8")	2B	3/8-16 UNC	Thru
Z512-D	4 ea	0.375 (3/8")	3A	3/8-16 UNC	7/8"

NOTES: 1. MATERIAL: ASTM A36 STEEL
2. COMPONENT MASS: 34.0 LB
3. TOLERANCES ± 1/32"; ± 0.005"

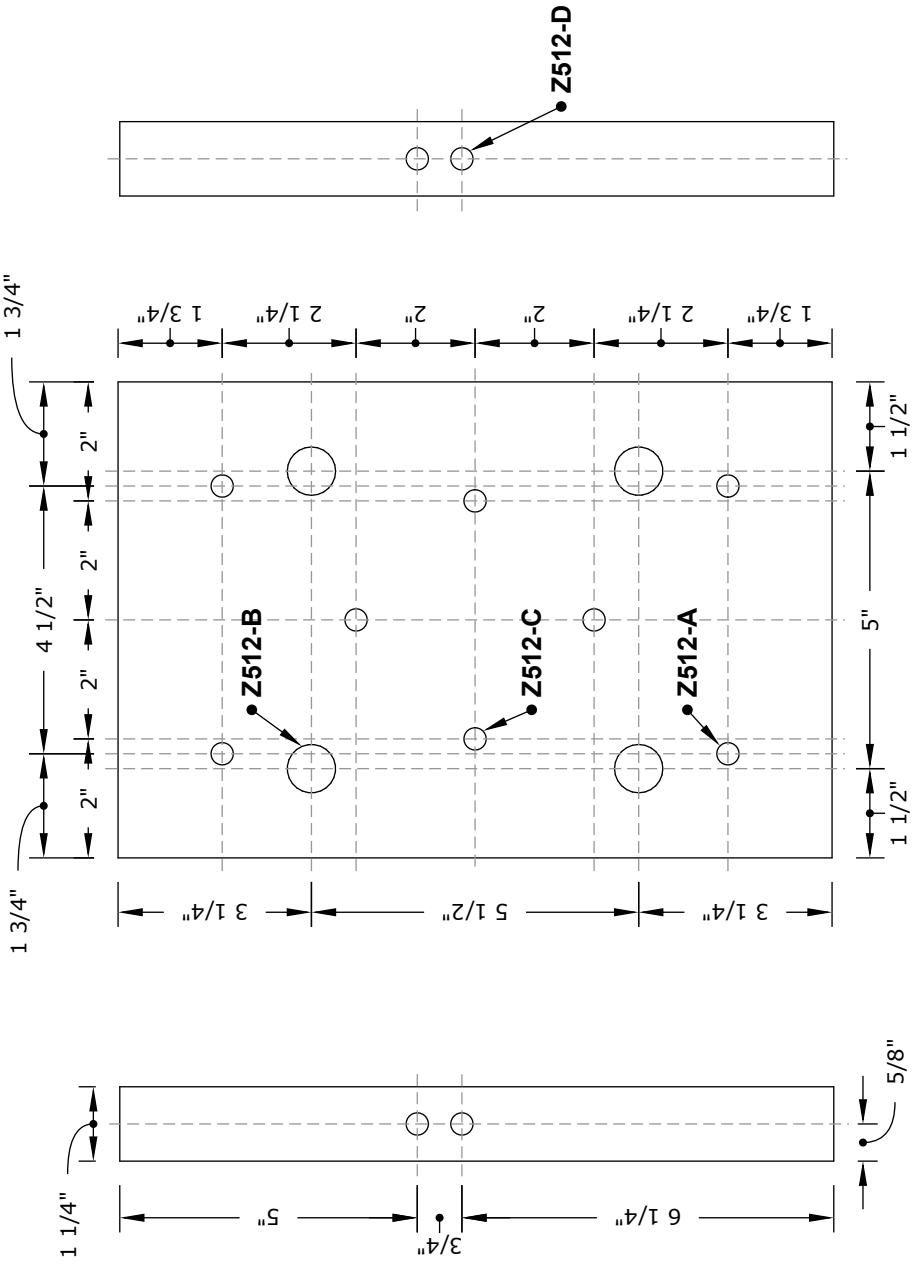

Project: Residual Capacity Test System
Component: Dynamic Test System
Sheet Description: Impact Plate Detail, P/N 003-01
Z5 12

P/N 007-01-4

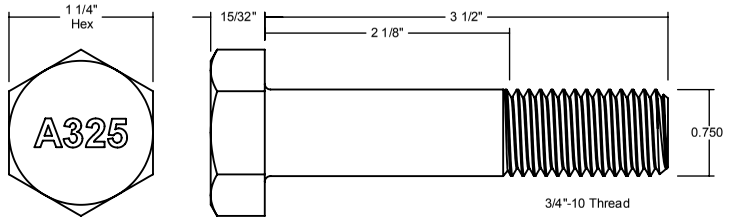

3/4 in A325 Bolt

P/N 007-01-5

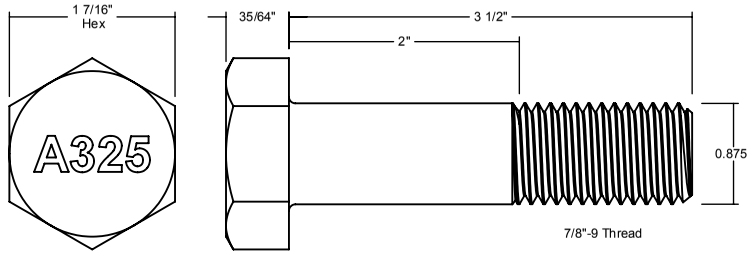

7/8 in A325 Bolt

P/N 007-01-6

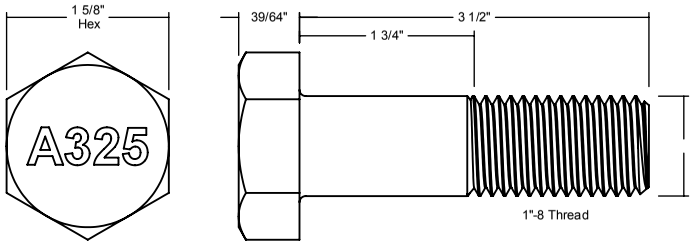

Project:	Component:	Sheet Description:		
Residual Capacity Test System	Dynamic Test System	Specimen Bolt Detail, S004	Z5	13

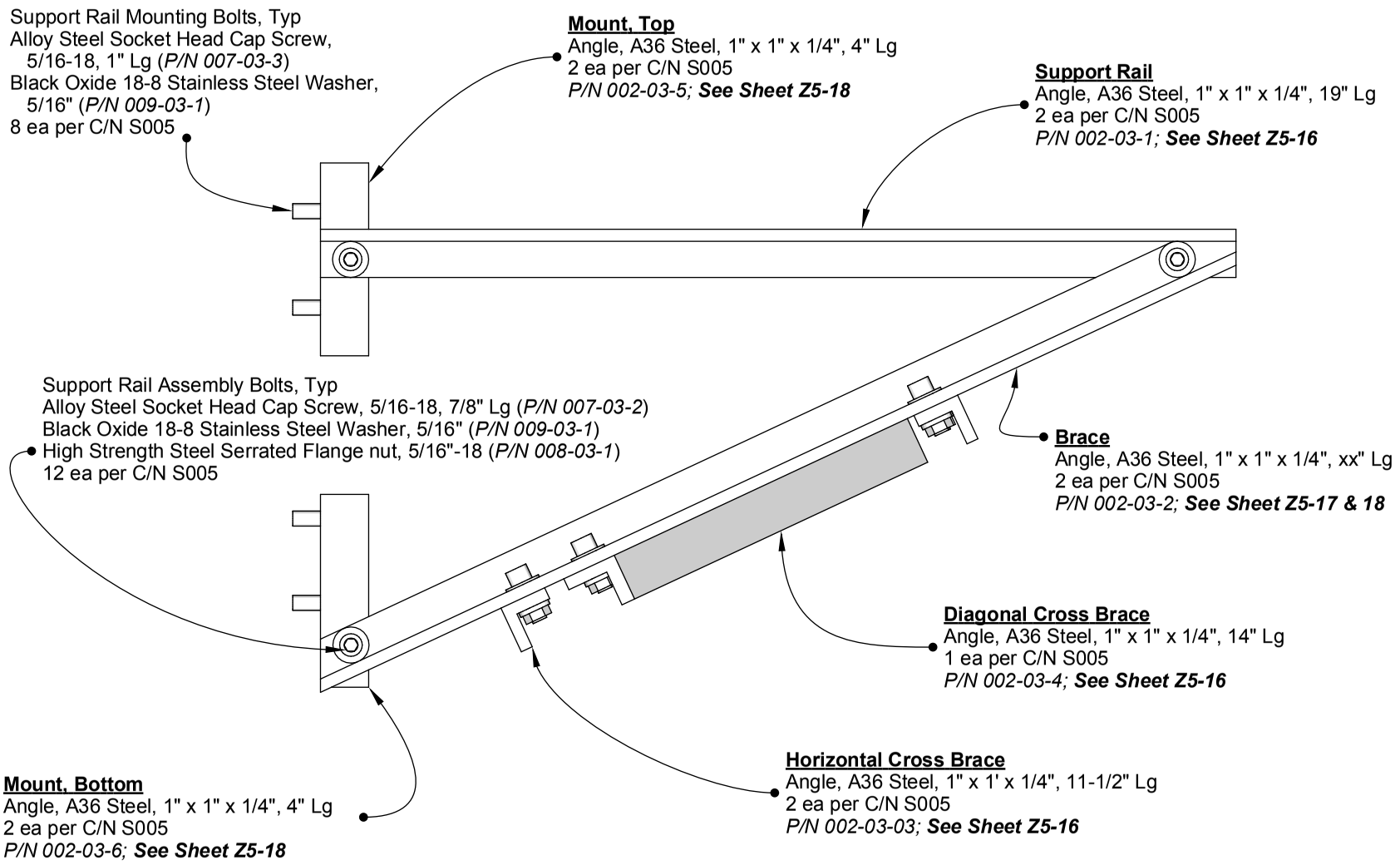

Project:	Component:	Sheet Description:		
Residual Capacity Test System	Dynamic Test System	Rail System Detail, S005	Z5	14

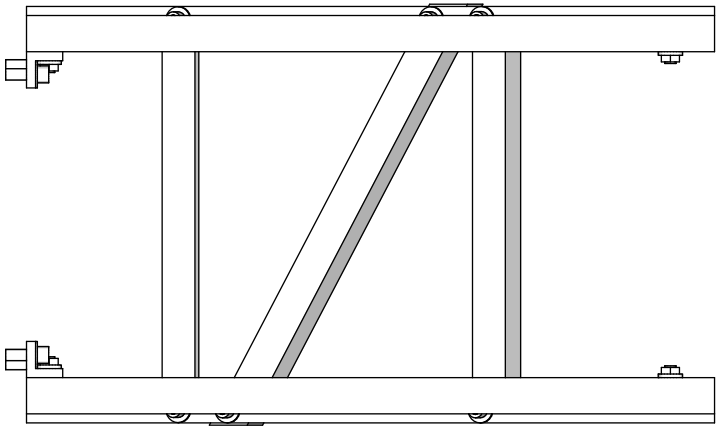

TOP VIEW

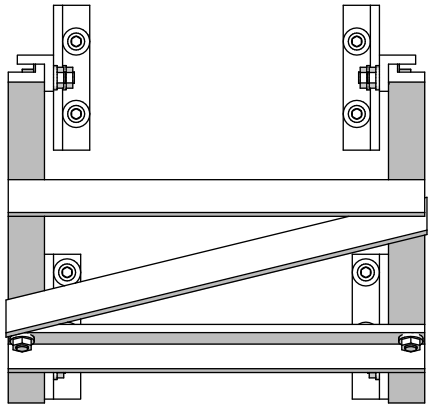

BACK VIEW

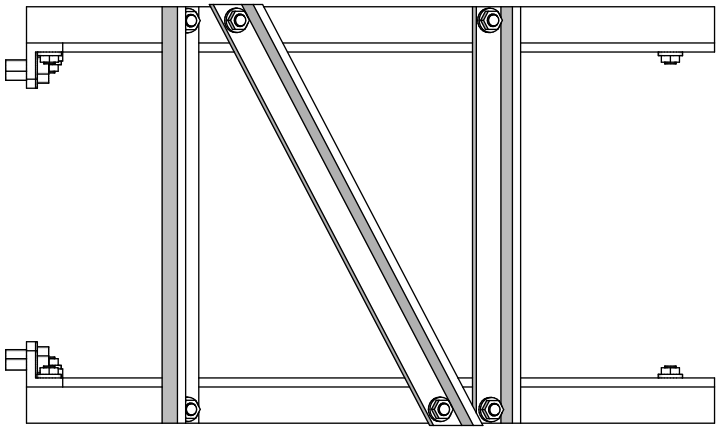

BOTTOM VIEW

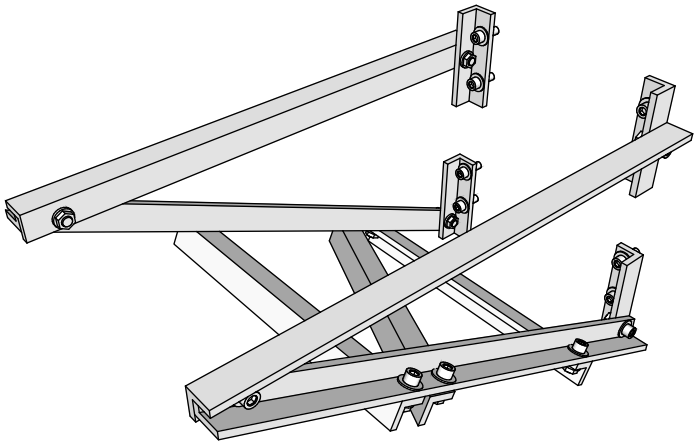

ISOMETRIC VIEW

Project:	Component:	Sheet Description:		
Residual Capacity Test System	Dynamic Test System	Rail System Detail, S005, Alternate Views	Z5	15

P/N 002-03-1

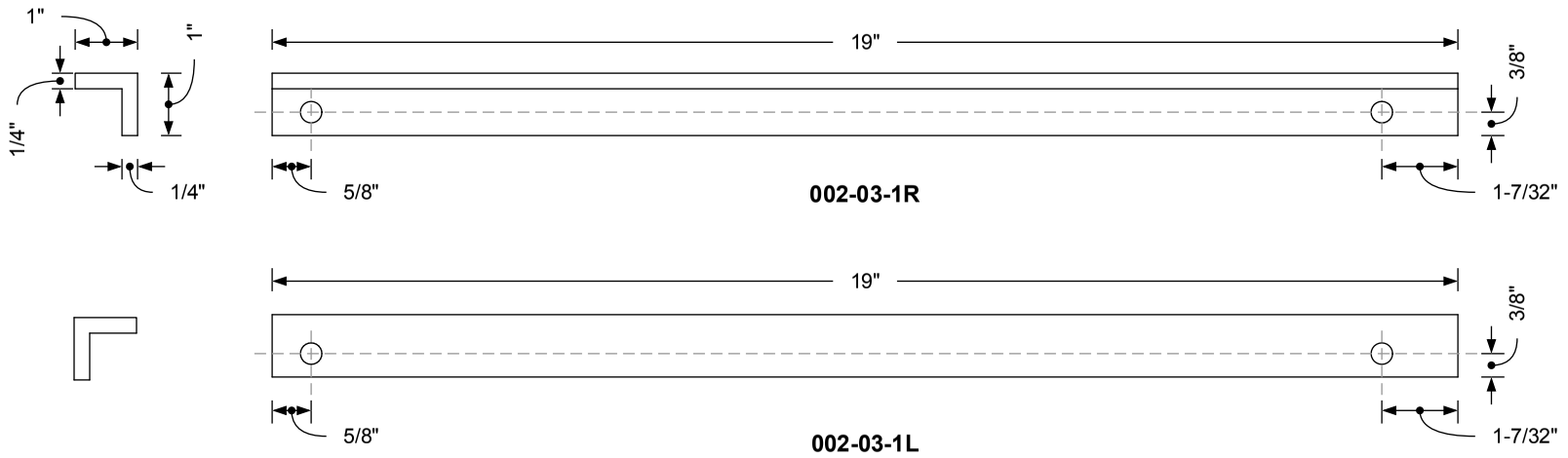

P/N 002-03-3

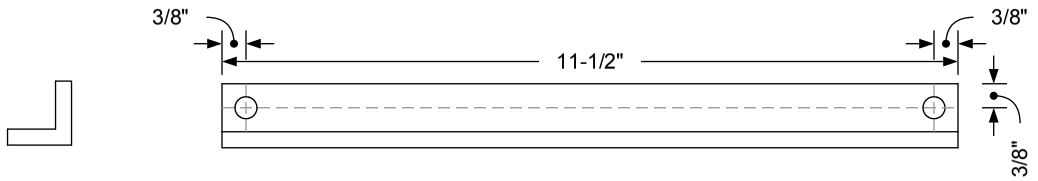

NOTE: BOLT HOLES IN ALL PARTS ARE ID Z516-A

P/N 002-03-4

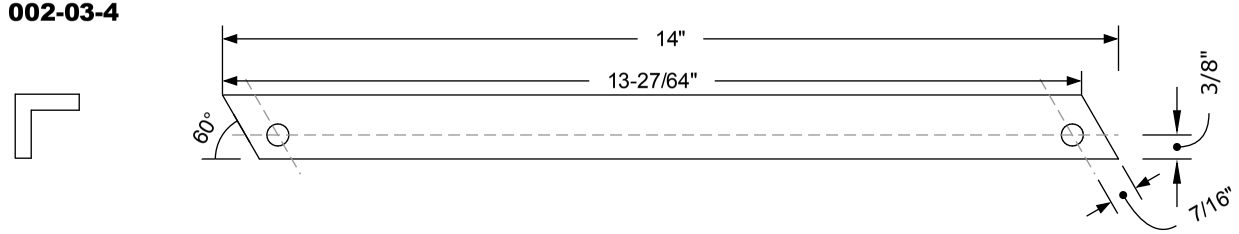

Project:	Component:	Sheet Description:		
Residual Capacity Test System	Dynamic Test System	Rail System Detail, P/N 002-03-X	Z5	16

NOTE: BOLT HOLES IN ALL PARTS ARE ID Z516-A

P/N 002-03-2

002-03-2R

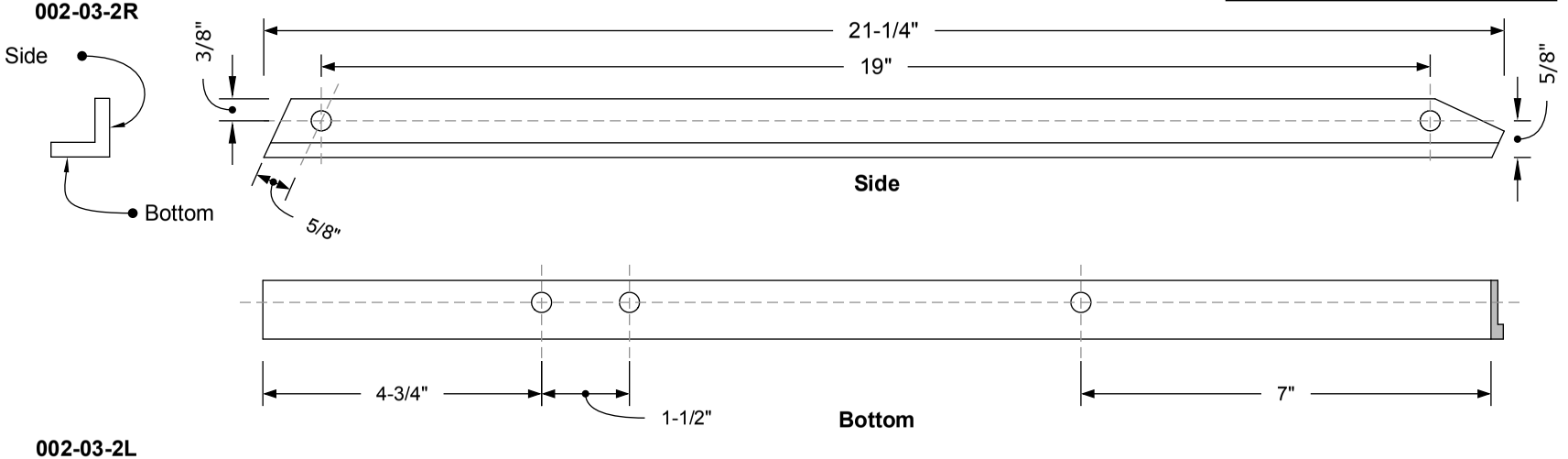

002-03-2L

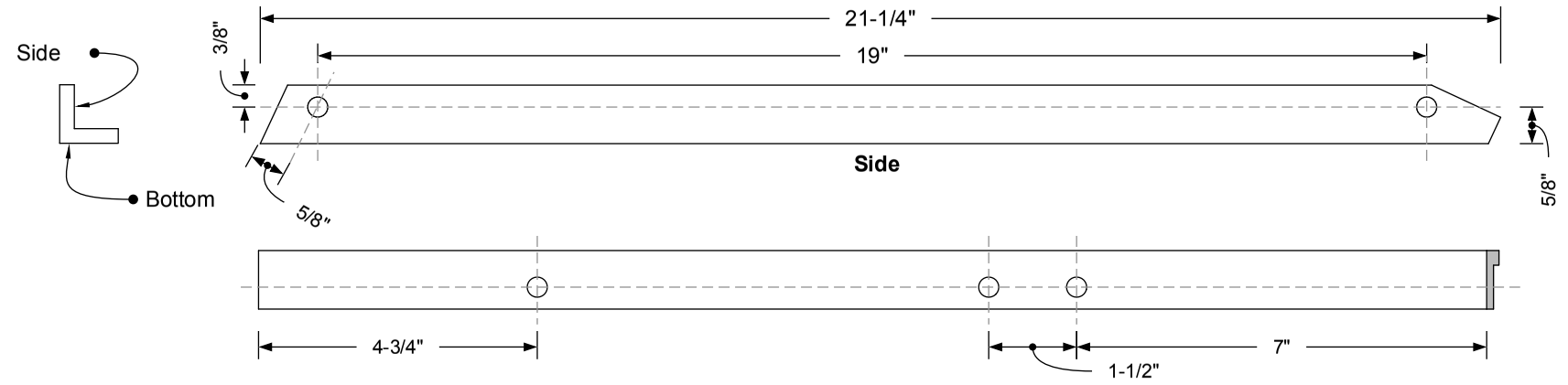

See Sheet Z5-18 for angle details

Project:	Component:	Sheet Description:		
Residual Capacity Test System	Dynamic Test System	Rail System Detail, P/N 002-03-X	Z5	17

P/N 002-03-5

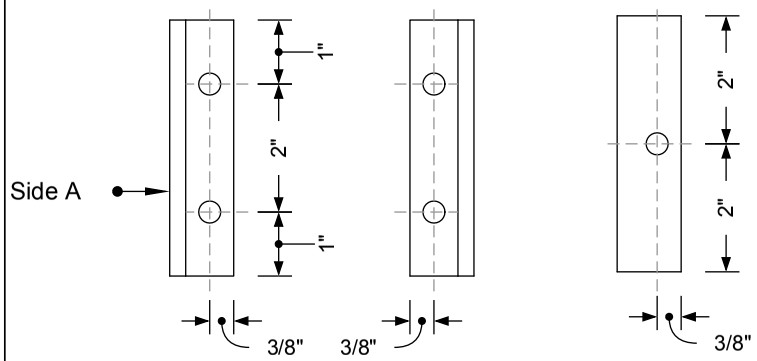

002-03-5R | 002-03-5L | Side A, Typ

P/N 002-03-6

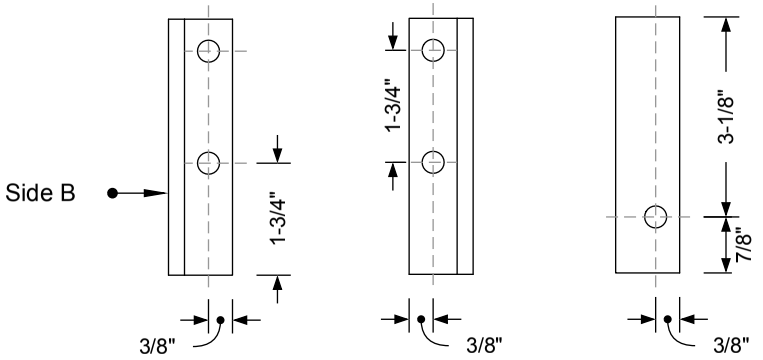

002-03-6R | 002-03-6L | Side B, Typ

NOTE: BOLT HOLES IN ALL PARTS ARE ID Z516-A

P/N 002-03-2

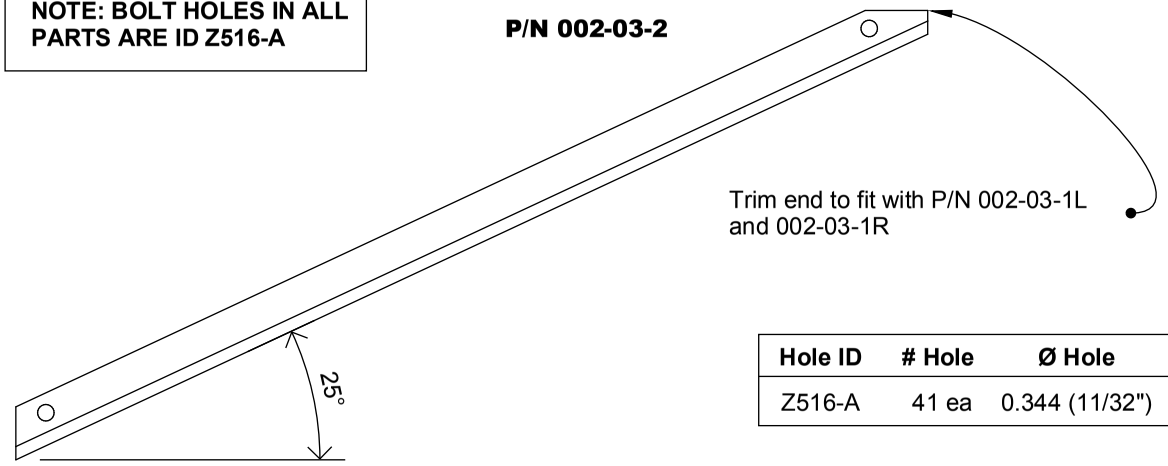

Hole ID	# Hole	Ø Hole	Fit Class	Thread	Depth
Z516-A	41 ea	0.344 (11/32")	Normal	None	Thru

Project:	Component:	Sheet Description:		
Residual Capacity Test System	Dynamic Test System	Rail System Detail, P/N 002-03-X	Z5	18

Programmer
Neoprene, High Strength, 6" x 8" x 1"
1 ea per C/N S006
P/N 003-02-1; ***See Sheet Z5-19***

Flyer Bracket
Angle, A36 Steel, 2" x 2" x 1/4", 1.5" Lg
2 EA per C/N S006
P/N 002-02-2; ***See Sheet Z5-21***

BG Pusher Plate
MOD-2; ***See Sheet Z5-22***

Pusher Plate Bracket
Angle, A36 Steel, 2" x 2" x 1/4", 1.5" Lg
2 ea per C/N S006
P/N 002-02-2; ***See Sheet Z5-21***

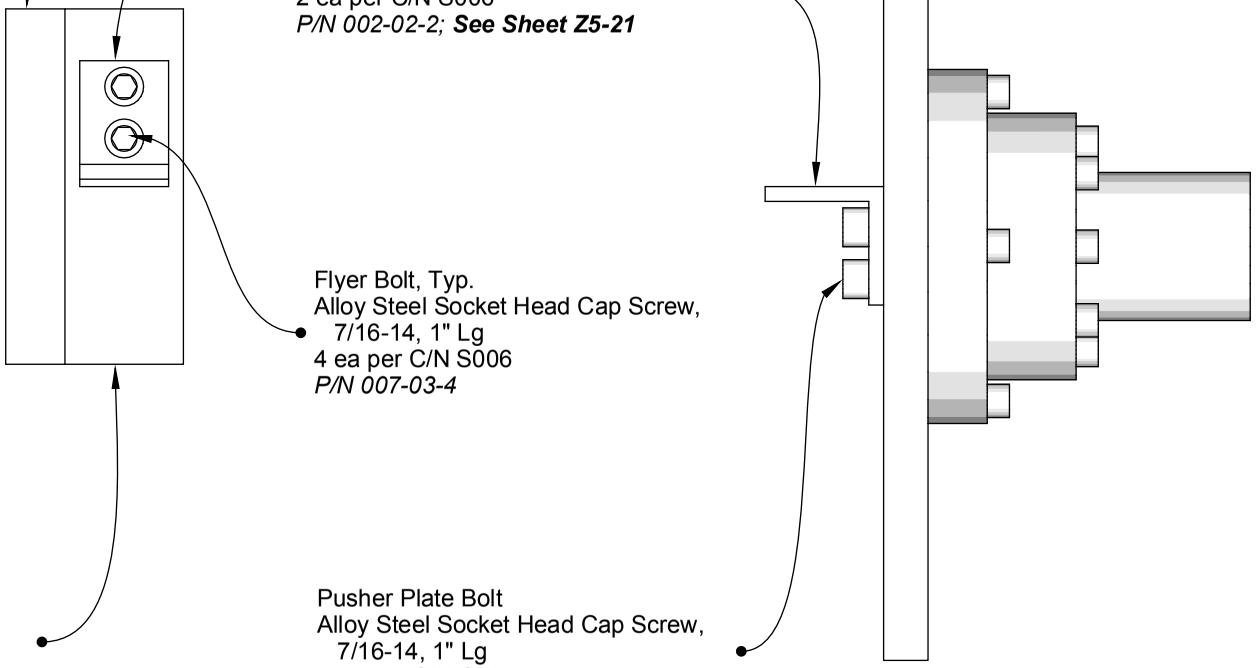

Flyer Bolt, Typ.
Alloy Steel Socket Head Cap Screw,
7/16-14, 1" Lg
4 ea per C/N S006
P/N 007-03-4

Flyer Mass
Plate, A36 Steel, 6" x 8" x 2"
1 ea per C/N S006
P/N 001-04; ***See Sheet Z5-20***

Pusher Plate Bolt
Alloy Steel Socket Head Cap Screw,
7/16-14, 1" Lg
4 ea per C/N S006
P/N 007-03-4

Project:	Component:	Sheet Description:		
Residual Capacity Test System	Dynamic Test System	Flyer Mass Detail, S006	Z5	19

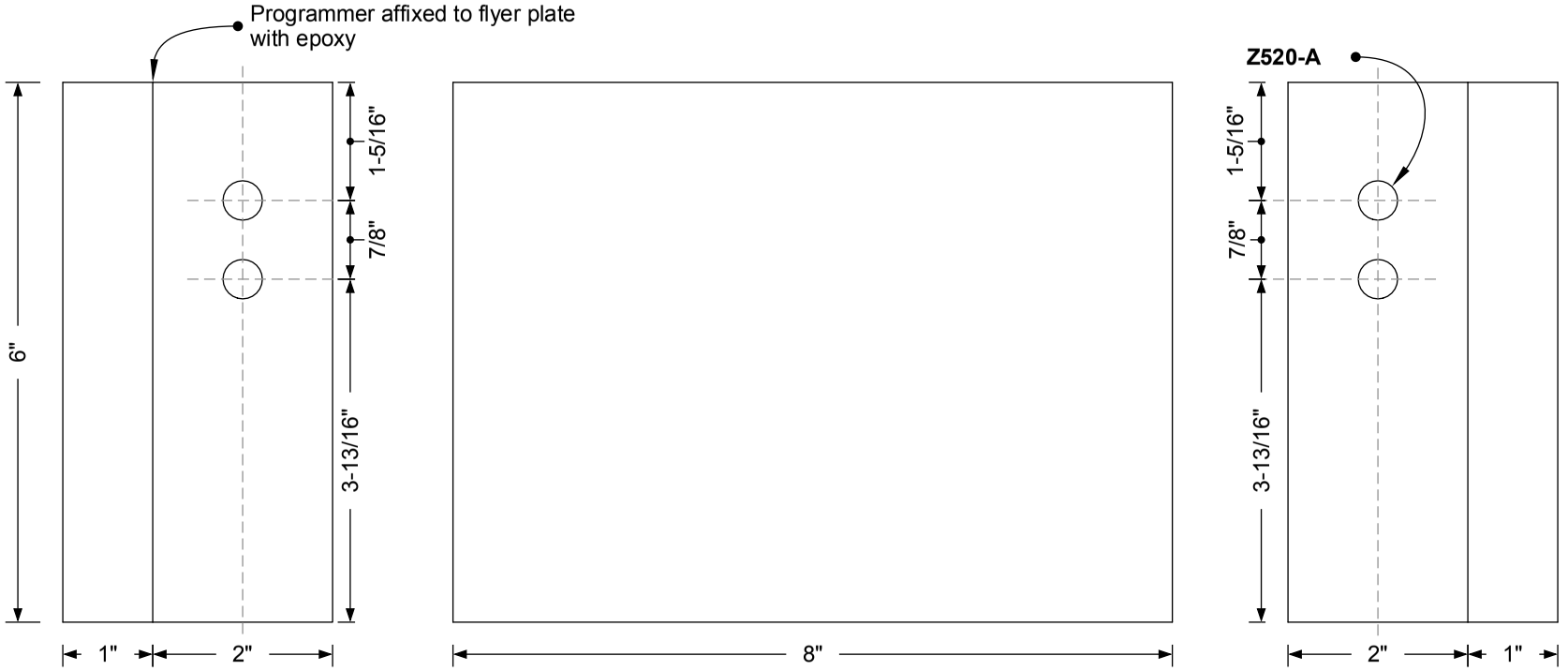

Hole ID	# Hole	Ø Hole	Fit Class	Thread	Depth
Z520-A	4 ea	0.438 (7/16")	3A	7/16-14	1"

NOTES:
1. MATERIAL: ASTM A36 STEEL
2. COMPONENT MASS: 25.0 LB
3. TOLERANCES ± 1/32"; ± 0.005"

Project:	Component:	Sheet Description:		
Residual Capacity Test System	Dynamic Test System	Flyer Mass Detail, P/N 001-04	Z5	20

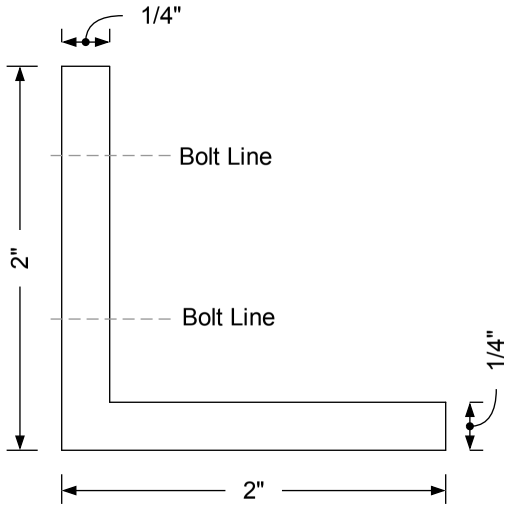

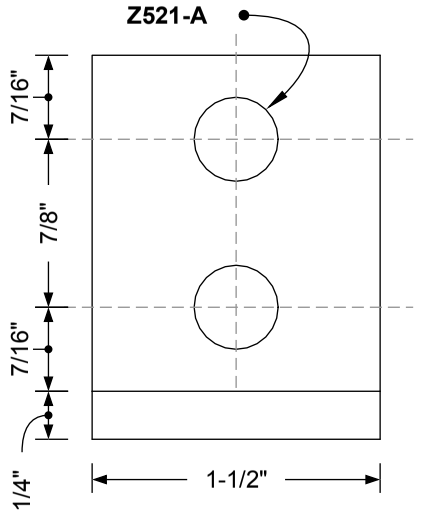

Hole ID	# Hole	Ø Hole	Fit Class	Thread	Depth
Z521-A	4 ea	0.469 (15/32")	Normal	None	Thru

NOTES: 1. MATERIAL: ASTM A36 STEEL
2. COMPONENT MASS: 2.3 LB
3. TOLERANCES ± 1/32"; ± 0.005"

Project:	Component:	Sheet Description:		
Residual Capacity Test System	Dynamic Test System	Flyer Mass Detail, P/N 002-02-2	Z5	21

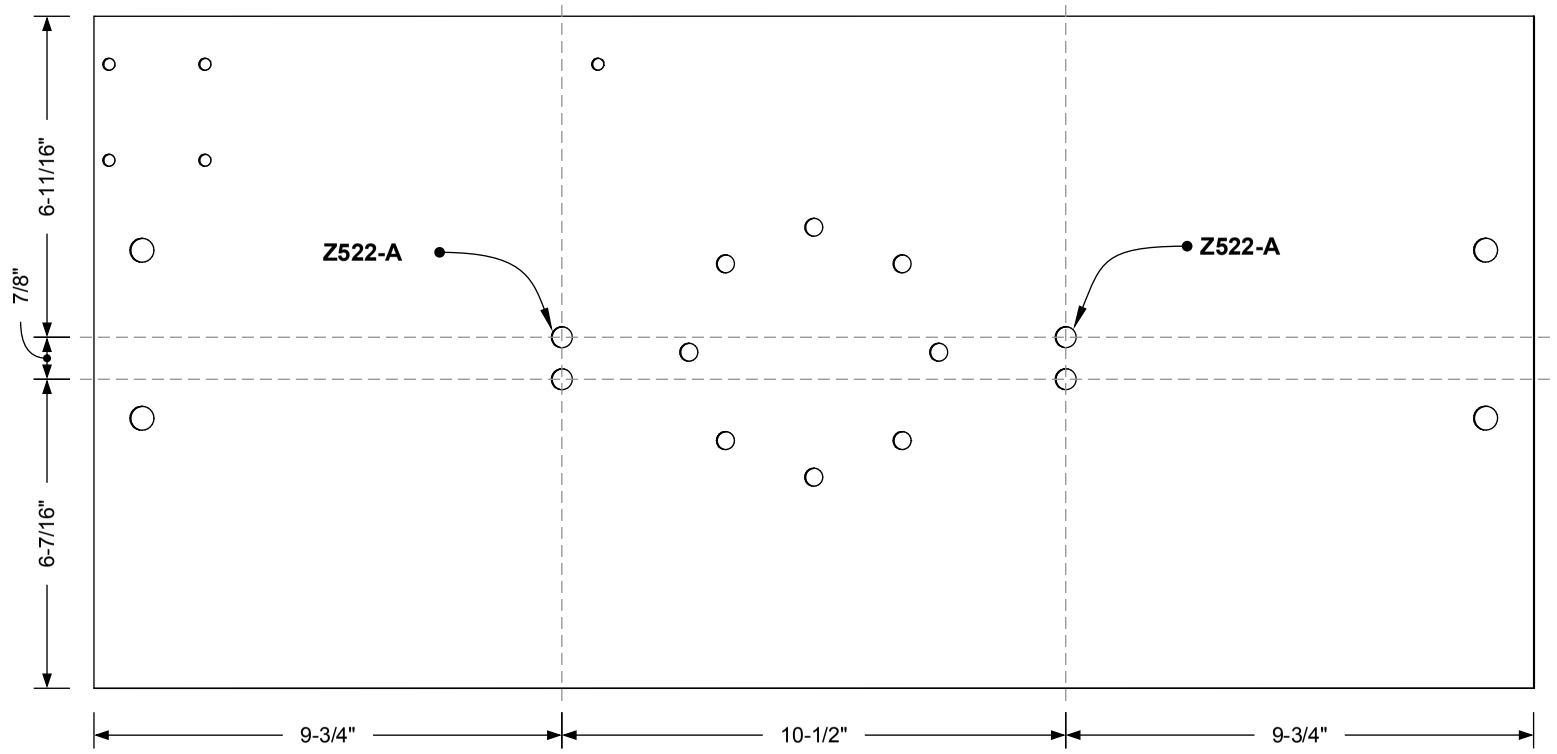

Hole ID	# Hole	Ø Hole	Fit Class	Thread	Depth
Z522-A	4 ea	0.438 (7/16")	3A	7/16-14	Thru

NOTES:
1. MATERIAL: 1024-T6 ALUMINUM
2. COMPONENT MASS: 34.0 LB
3. TOLERANCES ± 1/32"; ± 0.005"
4. ALL HOLES EXCEPT 2522-A ARE PRE-MACHINED

Project:	Component:	Sheet Description:		
Residual Capacity Test System	Dynamic Test System	Pusher Plate Detail, MOD-2	Z5	22

		QTY	CNTGCY	Total QTY	Vendor	Vendor P/N	Pkg Qty
S001	***Mounting Plate***	***1***					
001-01	Plate, A36 Steel, 18" x 18" x 3/4"	1	0	1	Metals Depot	P134	1
007-01-1	Bolt, A325, 3/4" x 5" Lg	8	0	8	McMaster-Carr	91571A310	1
009-01-1	Steel Washer for Structural Applications (3/4")	16	0	16	McMaster-Carr	98038A274	50
008-01-1	Hex Nut for A325 Structural Bolts, Grade C (3/4")	8	0	8	McMaster-Carr	90580A325	10
S002	***Reaction T Assembly***	***1***					
S002-01	*Reaction Flange*						
001-02-1	Plate, A36 Steel, 8" x 12" x 1-1/4"	1	0	1	Metals Depot	P1114	1
007-02-1	Alloy Steel Shoulder Screw, 5/8" x 3" Shoulder (1/2-13)	4	4	8	McMaster-Carr	91259A806	1
S002-02	*Reaction Angles*						
002-01	Angle, A36 Steel, 4" x 4" x 1/2", 8" Lg	2	0	2	Metals Depot	A231238	1
007-01-2	Bolt, A325, 3/4" x 3" Lg	4	8	12	McMaster-Carr	91571A298	5
007-01-3	Bolt, A325, 3/4" x 3-1/4" Lg	3	6	9	McMaster-Carr	91571A302	5
009-01-1	Steel Washer for Structural Applications (3/4")	14	0	14	McMaster-Carr	98038A274	50
008-01-1	Hex Nut for A325 Structural Bolts, Grade C (3/4")	7	0	7	McMaster-Carr	90580A325	10
S002-03	*Reaction Shear Plate*						
001-03-1	Plate, Gr 50 Steel, 8" x 9" x 1", 3/4" Bolt Hole	2	1	3	Speedy Metals	50P1-8X9	1
001-03-2	Plate, Gr 50 Steel, 8" x 9" x 1", 7/8" Bolt Hole	2	1	3	Speedy Metals	50P1-8X9	1
001-03-3	Plate, Gr 50 Steel, 8" x 9" x 1", 1" Bolt Hole	2	1	3	Speedy Metals	50P1-8X9	1
S002-04	*Reaction Rail Guides*						
002-02-1	Angle, A36 Steel, 2" x 2" x 1/4", 1-1/4" Lg	2	2	4	Metals Depot	A12214	1
007-03-1	Alloy Steel Socket Head Cap Screw, 3/8-16 x 3/4" Lg	4	4	8	McMaster-Carr	91251A622	25
003-02	Phenolic, 1" x 1" x 1/8"	2	2	4	Amazon	B0013HO3MK	12
S003	***Impact T Assembly***	***1***					
S003-01	*Impact Plate*						
003-01	Plate, Polycarbonate, Machine Grade, 6" x 10" x 1-1/2"	1	1	2	Professional Plastics	SPCMG1.500	1
007-02-2	Alloy Steel Shoulder Screw, 1/2" x 2-3/4" Shoulder (3/8-16)	4	4	8	McMaster-Carr	91259A723	1
S003-02	*Impact Flange*						
001-02-2	Plate, A36 Steel, 8" x 12" x 1-1/4"	1	0	1	Metals Depot	P1114	1
S003-03	*Impact Angles*						
002-01	Angle, A36 Steel, 4" x 4" x 1/2", 8" Lg	2	0	2	Metals Depot	A231238	1
007-01-2	Bolt, A325, 3/4" x 3" Lg	4	8	12	McMaster-Carr	91571A298	5
007-01-3	Bolt, A325, 3/4" x 3-1/4" Lg	3	6	9	McMaster-Carr	91571A302	5
009-01-1	Steel Washer for Structural Applications (3/4")	14	0	14	McMaster-Carr	98038A274	50
008-01-1	Hex Nut for A325 Structural Bolts, Grade C (3/4")	7	0	7	McMaster-Carr	90580A325	10
S003-04	*Impact Shear Plate*						
001-03-1	Plate, Gr 50 Steel, 8" x 9" x 1", 3/4" Bolt Hole	2	1	3	Speedy Metals	50P1-8X9	1
001-03-2	Plate, Gr 50 Steel, 8" x 9" x 1", 7/8" Bolt Hole	2	1	3	Speedy Metals	50P1-8X9	1
001-03-3	Plate, Gr 50 Steel, 8" x 9" x 1", 1" Bolt Hole	2	1	3	Speedy Metals	50P1-8X9	1
S003-05	*Impact Rail Guides*						
002-02-1	Angle, A36 Steel, 2" x 2" x 1/4", 1-1/4" Lg	2	0	2	Metals Depot	A12214	1
007-03-1	Allow Steel Socket Head Cap Screw, 3/8-16 x 3/4" Lg	4	0	4	McMaster-Carr	91251A622	25
003-02	Phenolic, 1" x 1" x 1/8"	2	0	2	Amazon	B0013HO3MK	12
S004	***Specimen Bolts***	***1***					
007-01-4	Bolt, A325, 3/4" x 3-1/2" Lg	15	15	30	McMaster-Carr	91571A304	5
009-01-1	Steel Washer for Structural Applications (3/4")	30	30	60	McMaster-Carr	98038A274	50
008-01-1	Hex Nut for A325 Structural Bolts, Grade C (3/4")	15	15	30	McMaster-Carr	90580A325	10
007-01-5	Bolt, A325, 7/8" x 3-1/2" Lg	15	15	30	McMaster-Carr	91571A324	1
009-01-2	Steel Washer for Structural Applications (7/8")	30	30	60	McMaster-Carr	98119A037	25
008-01-2	Hex Nut for A325 Structural Bolts, Grade C (7/8")	15	15	30	McMaster-Carr	90580A330	10
007-01-6	Bolt, A325, 1" x 3-1/2" Lg	15	15	30	McMaster-Carr	91571A336	1
009-01-3	Steel Washer for Structural Applications (1")	30	30	60	McMaster-Carr	98119A038	10
008-01-3	Hex Nut for A325 Structural Bolts, Grade C (1")	15	15	30	McMaster-Carr	90580A335	5
S005	***Support Rail Assembly***	***1***					
002-03-1	Angle, A36 Steel, 1" x 1" x 1/4", 19" Lg (Rail)	2	2	4	Metals Depot	A11114	1
002-03-2	Angle, A36 Steel, 1" x 1" x 1/4", 24" Lg (Brace)	2	2	4	Metals Depot	A11114	1
002-03-3	Angle, A36 Steel, 1" x 1" x 1/4", 11-1/2" Lg (Horizontal)	2	2	4	Metals Depot	A11114	1
002-03-4	Angle, A36 Steel, 1" x 1" x 1/4", 15" Lg (Diagonal)	1	1	2	Metals Depot	A11114	1
002-03-5	Angle, A36 Steel, 1" x 1" x 1/4", 4" Lg (Mount, Top)	2	2	4	Metals Depot	A11114	1
002-03-6	Angle, A36 Steel, 1" x 1" x 1/4", 4" Lg (Mount, Bottom)	2	2	4	Metals Depot	A11114	1
007-03-2	Alloy Steel Socket Head Cap Screw, 5/16-18, 7/8" Lg	12	12	24	McMaster-Carr	91251A582	50
007-03-3	Alloy Steel Socket Head Cap Screw, 5/16-18, 1" Lg	8	8	16	McMaster-Carr	91251A583	50
009-03-1	Black Oxide 18-8 Stainless Steel Washer (5/16")	20	20	40	McMaster-Carr	96765A145	100
008-03-1	High Strength Steel Serrated Flange Nut (5/16-18)	12	12	24	McMaster-Carr	95922A120	100
S006	***Flyer Mass***	***1***					
001-04	Plate, A36 Steel, 6" x 8" x 2"	1	0	1	Metals Depot	P12	1
003-02-1	Neoprene, High Strength (50A Medium), 6" x 8" x 1"	1	2	3	McMaster-Carr	1290N42	1
002-02-2	Angle, A36 Steel, 2" x 2" x 1/4", 1.5" Lg	4	0	4	Metals Depot	A12214	1
007-03-4	Alloy Steel Socket Head Cap Screw, 7/16-14, 1" Lg	8	0	8	McMaster-Carr	91251A669	25
003-02	Phenolic, 1.5" x 1.75" x 1/8"	4	4	8	Amazon	B0013HO3MK	12

P/N	Part Description	Single SU	Total Qty	Sheet	Hole ID	# Hole Per Piece	Ø Hole Dec (in)	Ø Hole Nom (in)	Fit Class	Thread	Depth (in)
001-01	Plate, A36 Steel, 18" x 18" x 3/4"	1	1	Z502	Z502-A	8	0.813	13/16	Normal	None	Thru
					Z502-B	4	0.5	1/2	3A	1/2-13 UNC	Thru
					Z502-C	8	0.313	5/16	3A	5/16-18 UNC	Thru
001-02-1	Plate, A36 Steel, 8" x 12" x 1-1/4"	1	1	Z505	Z505-A	4	0.688	11/16	Normal	None	Thru
					Z505-B	4	0.813	13/16	Normal	None	Thru
					Z505-C	4	0.375	3/8	2B	3/8-16 UNC	Thru
					Z505-D	4	0.375	3/8	3A	3/8-16 UNC	7/8
001-02-2	Plate, A36 Steel, 8" x 12" x 1-1/4"	1	1	Z512	Z512-A	4	0.375	3/8	3A	3/8-16 UNC	Thru
					Z512-B	4	0.813	13/16	Normal	None	Thru
					Z512-C	4	0.375	3/8	2B	3/8-16 UNC	Thru
					Z512-D	4	0.375	3/8	3A	3/8-16 UNC	7/8
001-03-1	Plate, Gr 50 Steel, 8" x 9" x 1"; 3/4" Specimen Bolt	2	6	Z507	Z507-A	3	0.813	13/16	Normal	None	Thru
					Z507-B	1	0.813	13/16	Normal	None	Thru
001-03-2	Plate, Gr 50 Steel, 8" x 9" x 1"; 7/8" Specimen Bolt	2	6	Z507	Z507-A	3	0.813	13/16	Normal	None	Thru
					Z507-C	1	0.938	15/16	Normal	None	Thru
001-03-3	Plate, Gr 50 Steel, 8" x 9" x 1"; 1" Specimen Bolt	2	6	Z507	Z507-A	3	0.813	13/16	Normal	None	Thru
					Z507-D	1	1.094	1-3/32	Normal	None	Thru
001-04	Plate, A36 Steel, 6" x 8" x 2"	1	1	Z520	Z520-A	4	0.438	7/16	3A	7/16-14 UNC	1
002-01	Angle, A36 Steel, 4" x 4" x 1/2" x 8" Lg	4	4	Z506	Z506-A	5	0.813	13/16	Normal	None	Thru
002-02-1	Angle, A36 Steel, 2" x 2" x 1/4" x 1-1/4" Lg	4	4	Z508	Z508-A	2	0.406	13/32	Normal	None	Thru
002-02-2	Angle, A36 Steel, 2" x 2" x 1/4", 1-1/2" Lg	4	4	Z521	Z521-A	4	0.469	15/32	Normal	None	Thru
002-03-1R	Angle, A36 Steel, 1" x 1" x 1/4", 19" Lg (Rail)	1	2	Z516	Z516-A	2	0.344	11/32	Normal	None	Thru
002-03-1L	Angle, A36 Steel, 1" x 1" x 1/4", 19" Lg (Rail)	1	2	Z516	Z516-A	2	0.344	11/32	Normal	None	Thru
002-03-2R	Angle, A36 Steel, 1" x 1" x 1/4", 24" Lg (Brace)	1	2	Z517	Z516-A	5	0.344	11/32	Normal	None	Thru
002-03-2L	Angle, A36 Steel, 1" x 1" x 1/4", 24" Lg (Brace)	1	2	Z517	Z516-A	5	0.344	11/32	Normal	None	Thru
002-03-3	Angle, A36 Steel, 1" x 1" x 1/4", 11-1/2" Lg (Horizontal)	2	4	Z516	Z516-A	2	0.344	11/32	Normal	None	Thru
002-03-4	Angle, A36 Steel, 1" x 1" x 1/4", 14" Lg (Diagonal)	1	2	Z516	Z516-A	2	0.344	11/32	Normal	None	Thru
002-03-5R	Angle, A36 Steel, 1" x 1" x 1/4", 4" Lg (Mount, Top)	2	2	Z516	Z516-A	3	0.344	11/32	Normal	None	Thru
002-03-5L	Angle, A36 Steel, 1" x 1" x 1/4", 4" Lg (Mount, Top)	2	2	Z516	Z516-A	3	0.344	11/32	Normal	None	Thru
002-03-6R	Angle, A36 Steel, 1" x 1" x 1/4", 4" Lg (Mount, Bottom)	2	2	Z516	Z516-A	3	0.344	11/32	Normal	None	Thru
002-03-6L	Angle, A36 Steel, 1" x 1" x 1/4", 4" Lg (Mount, Bottom)	2	2	Z516	Z516-A	3	0.344	11/32	Normal	None	Thru
003-01	Plate, Polycarbonate, Machine Grade, 6" x 10" x 1-1/2"	1	2	Z511	Z511-A	4	0.562	9/16	Normal	None	Thru
					Z511-B	4	0.812	13/16	Normal	None	1/4
MOD-2	BG Pusher Plate, MOD-2	1	1	Z522	Z522-A	4	0.438	7/16	3A	7/16-14 UNC	Thru

FRONT VIEW

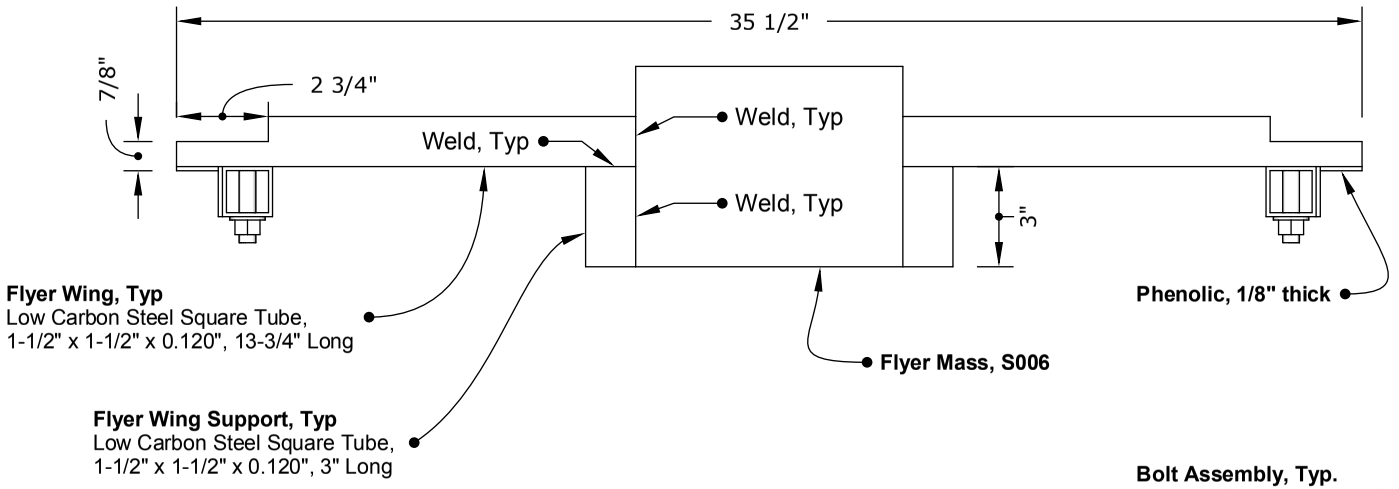

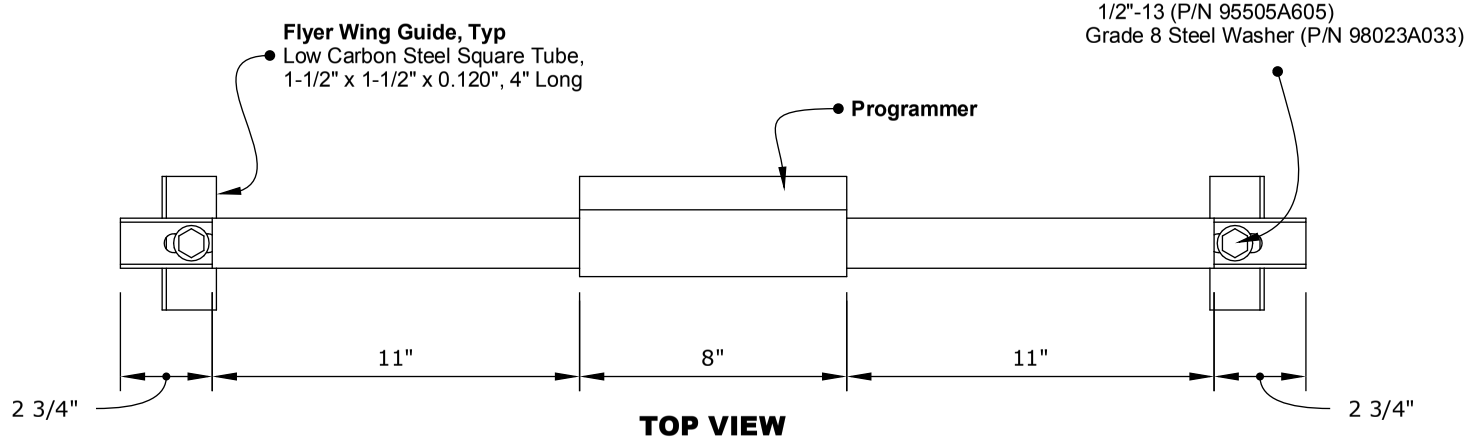

TOP VIEW

Project:	Component:	Sheet Description:		
Residual Capacity Test System	Dynamic Test System	Flyer Mass Assembly, MOD-1	Z5	25

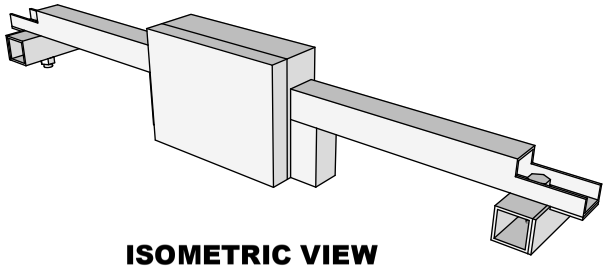

ISOMETRIC VIEW

FLYER WING

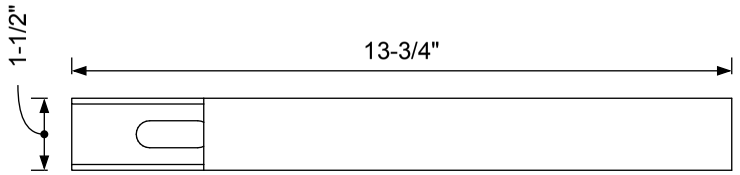

Top

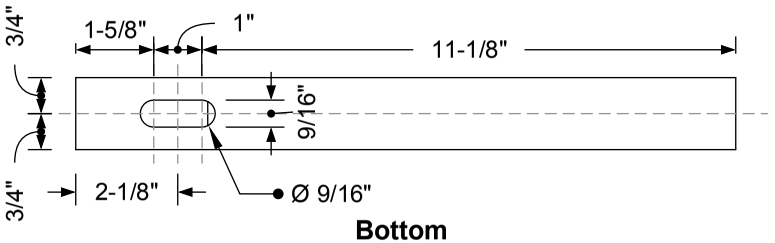

Bottom

FLYER WING GUIDE

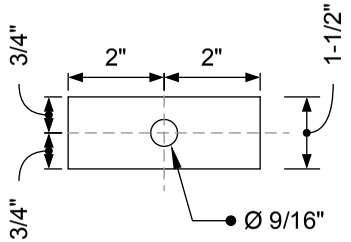

Top & Bottom

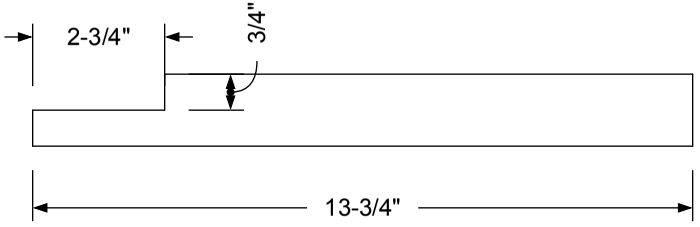

Side

Project:	Component:	Sheet Description:		
Residual Capacity Test System	Dynamic Test System	Flyer Mass Assembly, MOD-1	Z5	26

TOP VIEW

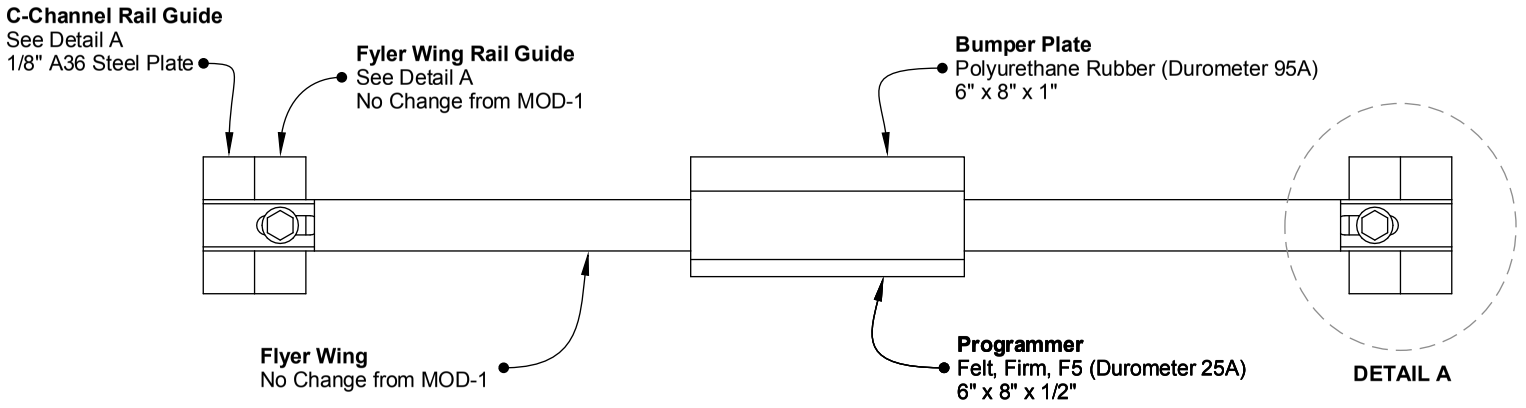

DETAIL A

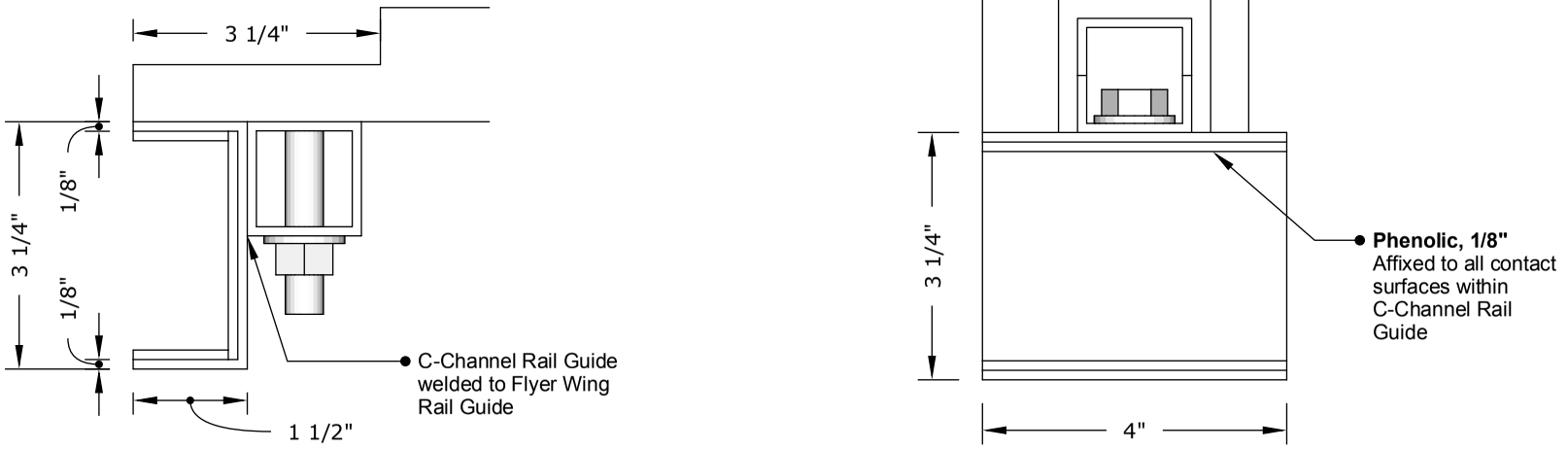

Project:	Component:	Sheet Description:		
Residual Capacity Test System	Dynamic Test System	Flyer Mass Assembly, MOD-2	Z5	27

ACTUATOR COLUMN

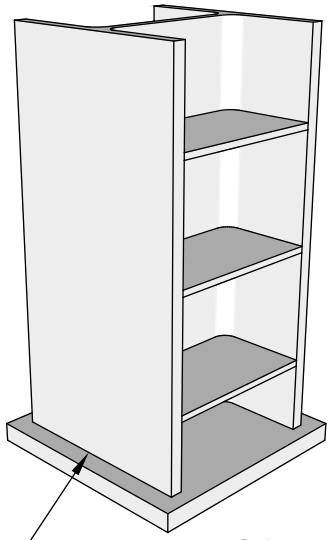

Column welded to
18" x 18" x 1 1/2" base

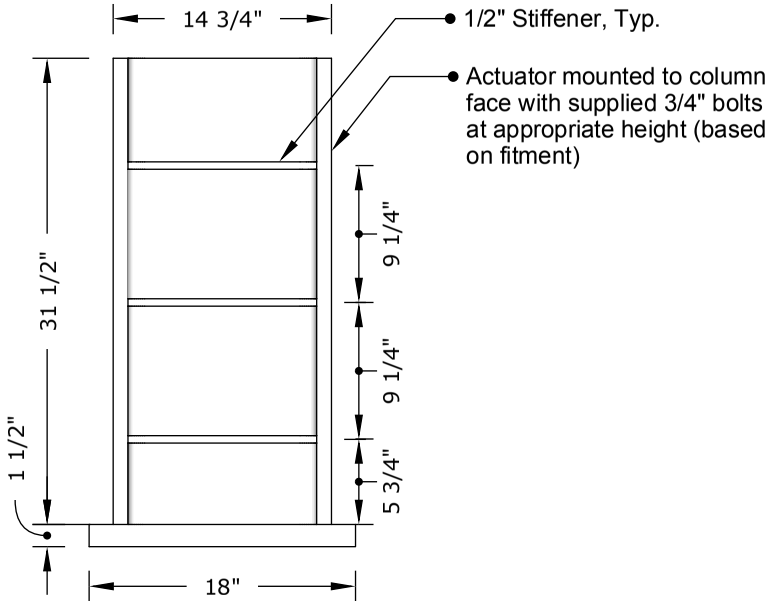

BASE BEAM

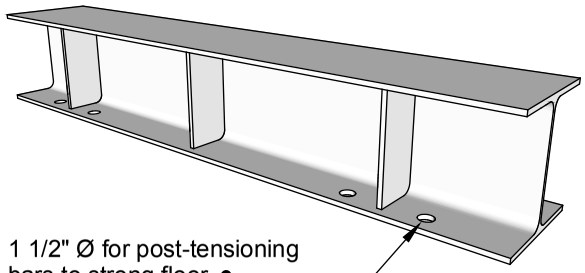

1 1/2" Ø for post-tensioning
bars to strong floor

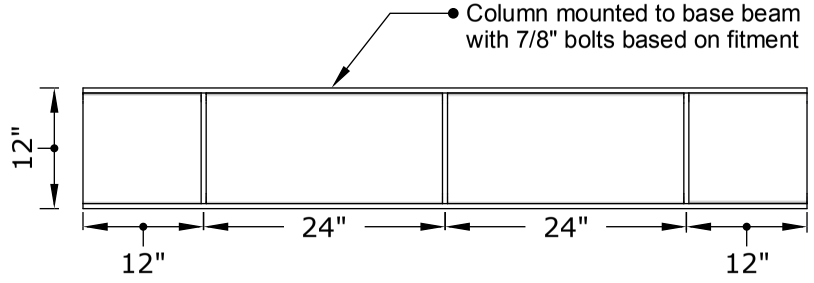

Project:	Component:	Sheet Description:		
Residual Capacity Test System	Static Test System	Main Structural Components	Z5	28

BEARING BLOCKS

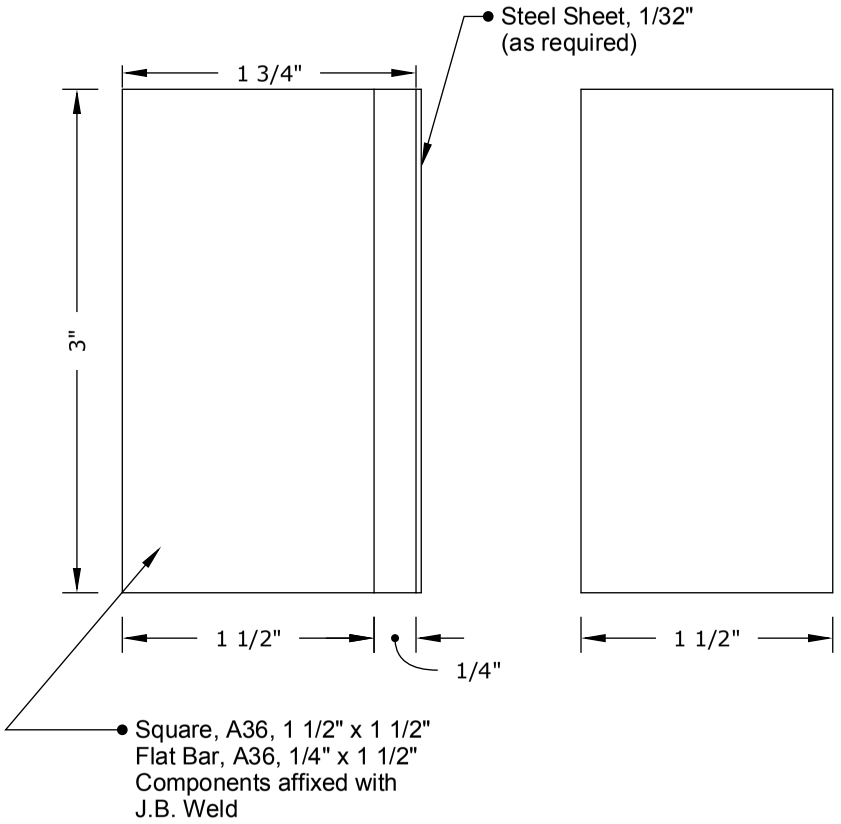

BEARING PLATE

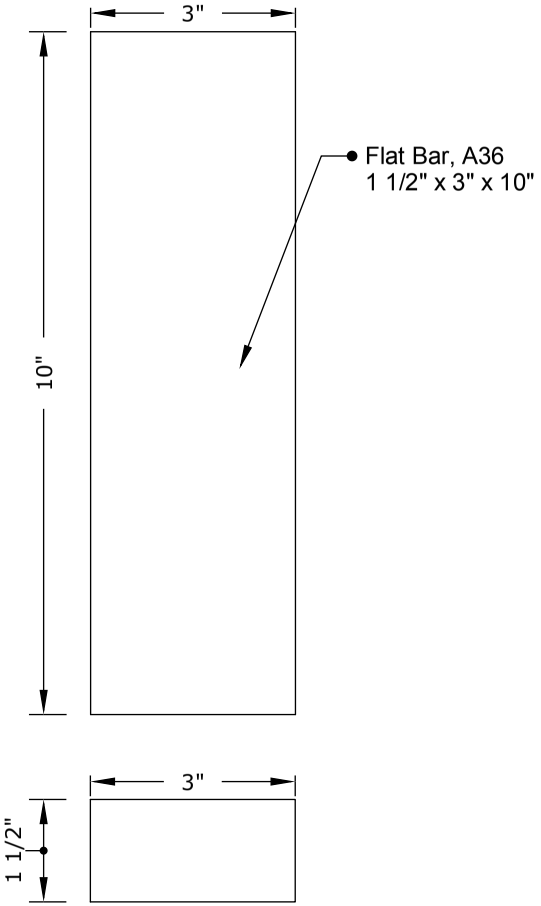

Project:	Component:	Sheet Description:		
Residual Capacity Test System	Static Test System	Bearing Components	Z5	29

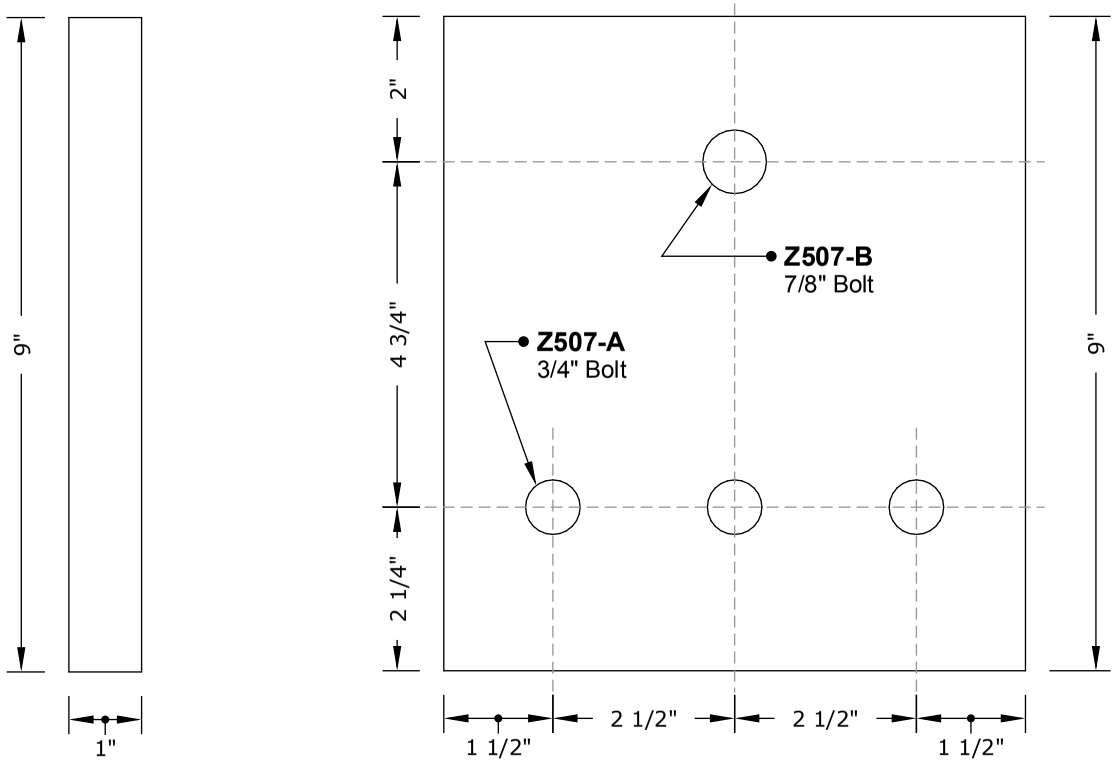

Hole ID	# Hole	Ø Hole	Fit Class	Thread	Depth
Z507-A	3 ea	0.813 (± 0.005")	Normal	None	Thru
Z507-B	1 ea	0.906 (+0.005")	Close	None	Thru

NOTES:
1. MATERIAL: ASTM A514A STEEL (fy = 100 ksi)
2. COMPONENT MASS: 20.5 LB
3. TOLERANCES: ± 1/32"

Project:	Component:	Sheet Description:		
Residual Capacity Test System	Dynamic Test System	Shear Plate Detail, P/N 001-03-1, MOD-1	Z5	30

APPENDIX B

EXPERIMENTAL TEST DATA

TEST RC-307-01

7/8 inch A307 | 272.5 in/s

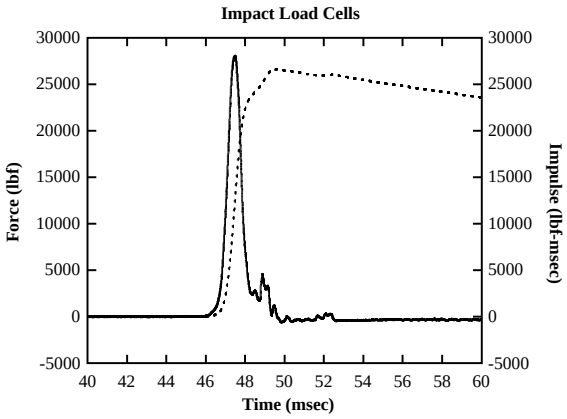

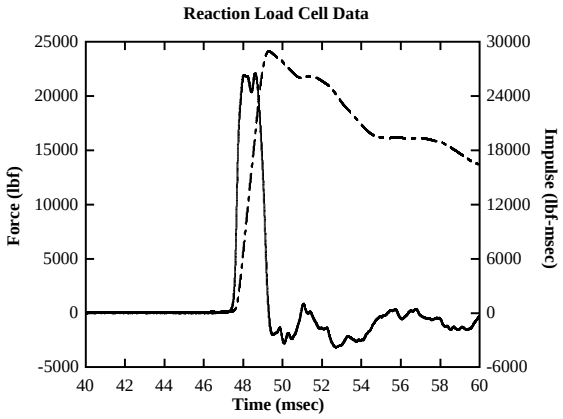

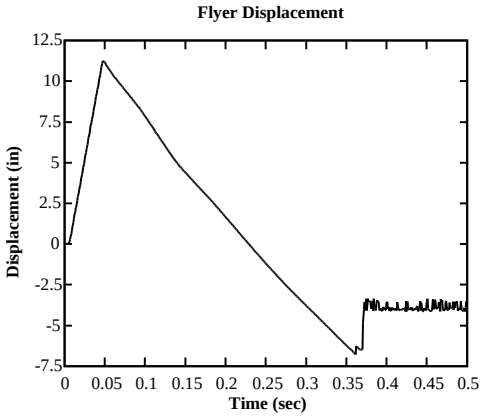

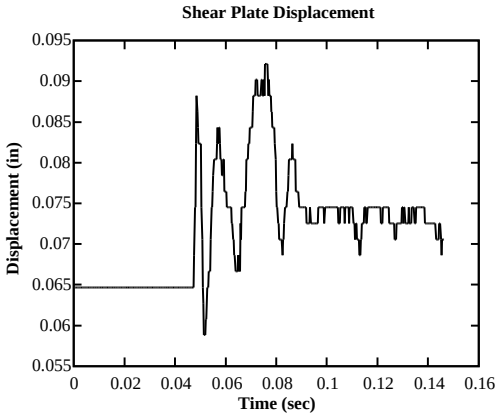

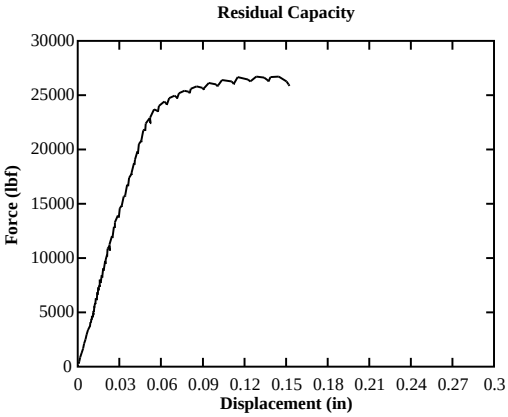

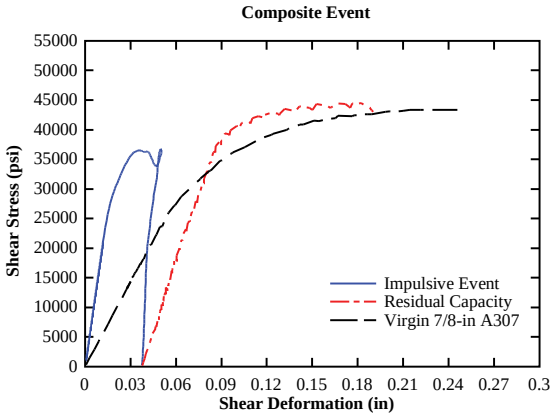

TEST RC-307-02

7/8 inch A307 | 277.7 in/s

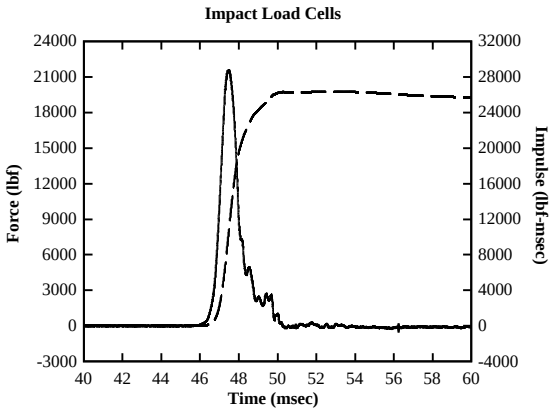

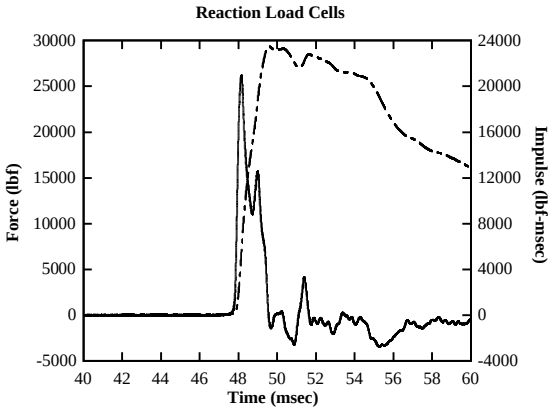

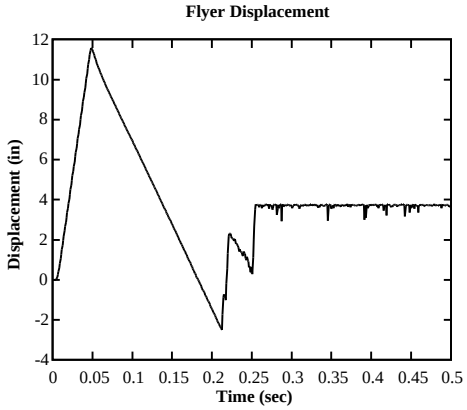

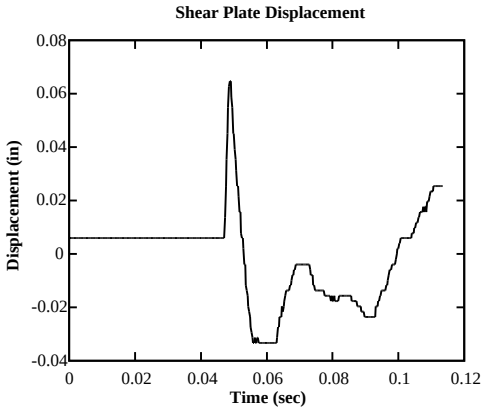

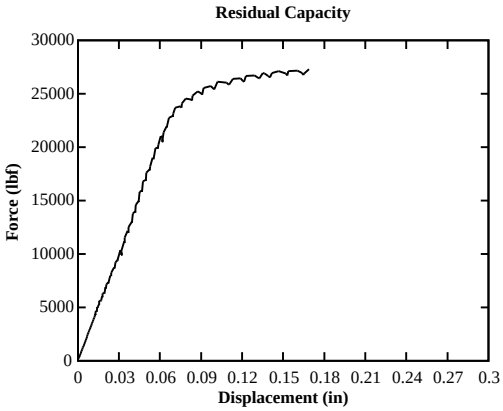

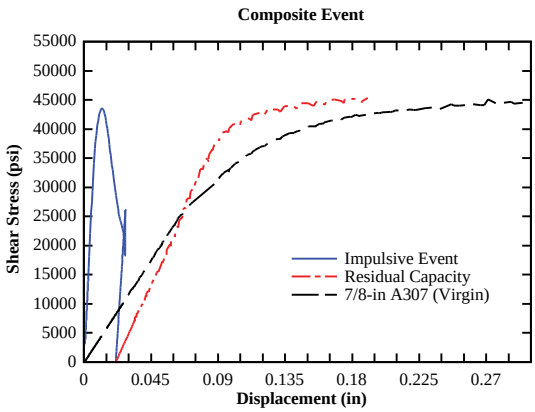

TEST RC-307-03

7/8 inch A307 | 283.0 in/s

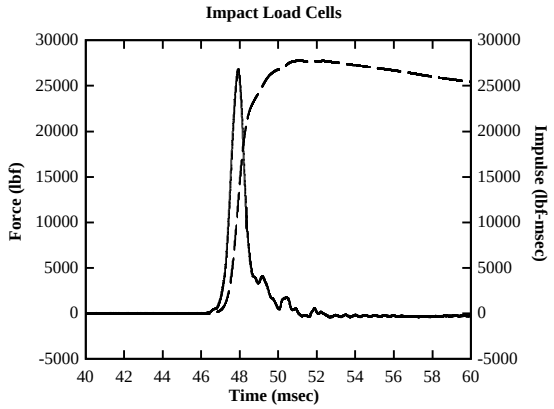

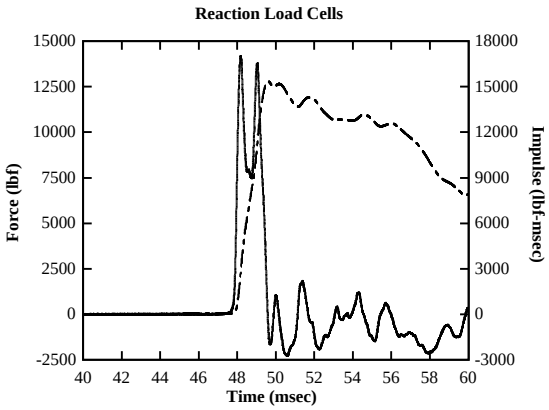

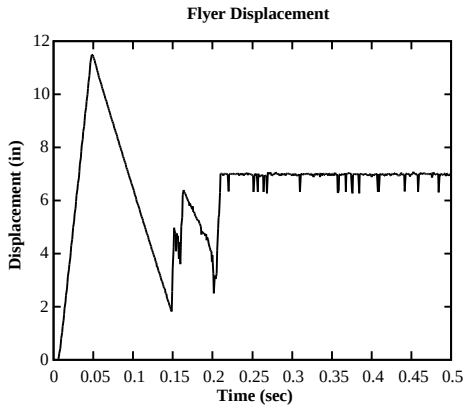

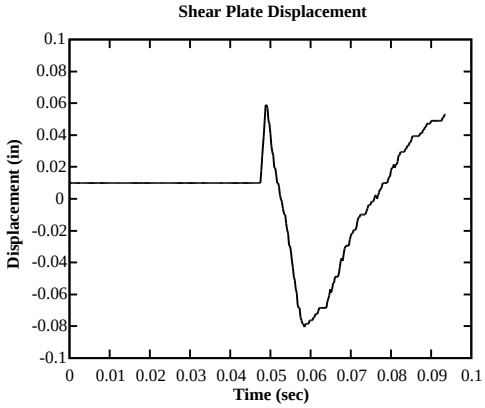

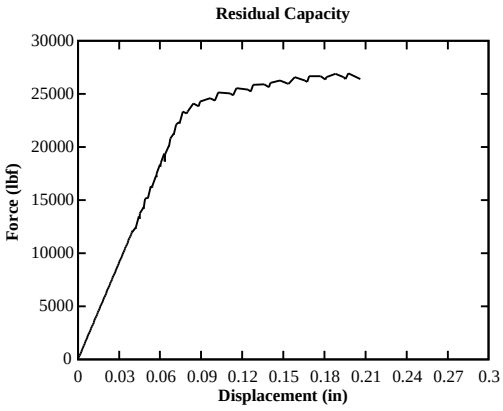

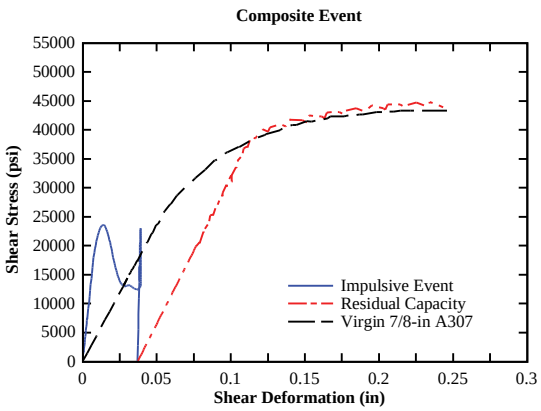

TEST RC-307-04

7/8 inch A307 | 316.5 in/s

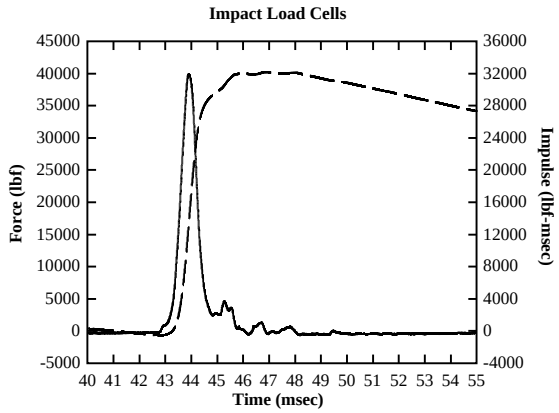

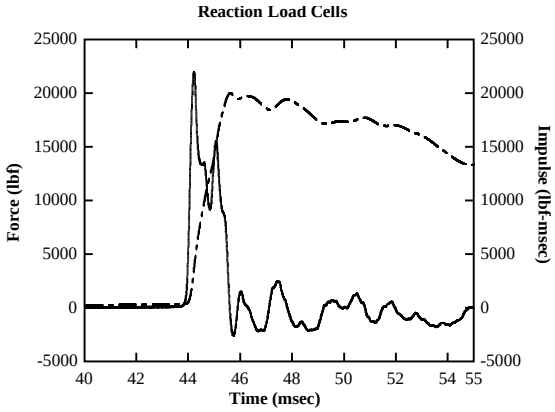

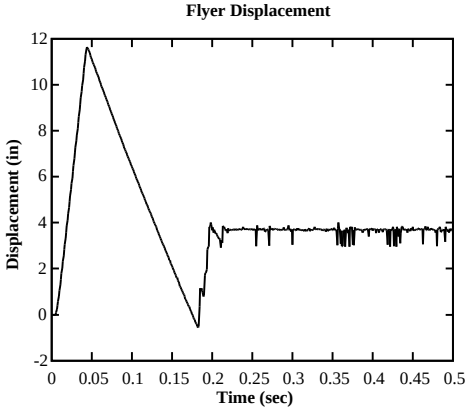

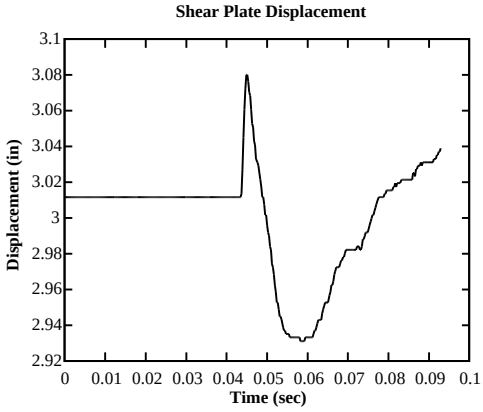

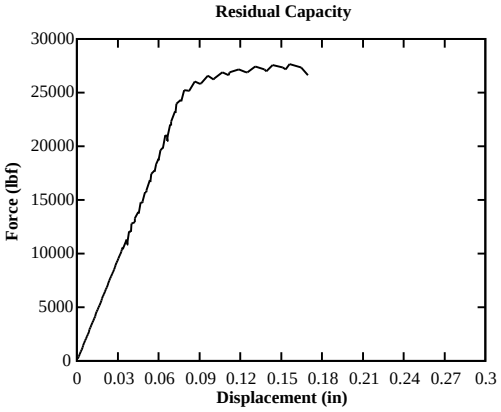

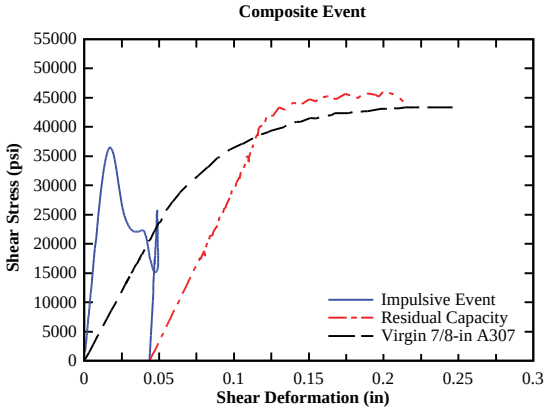

TEST RC-307-05

7/8 inch A307 | 309.5 in/s

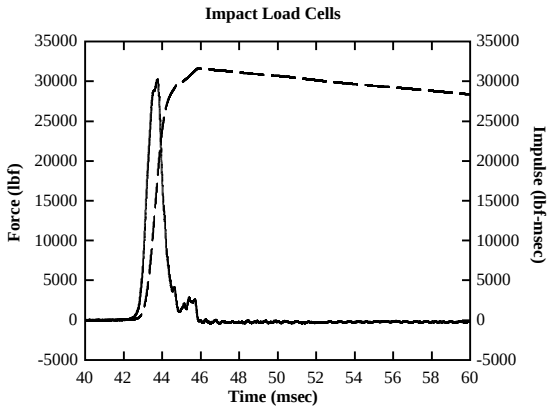

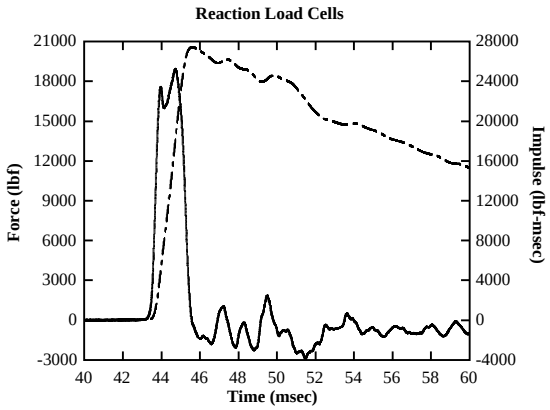

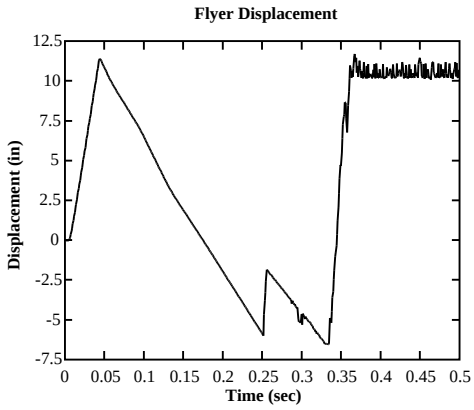

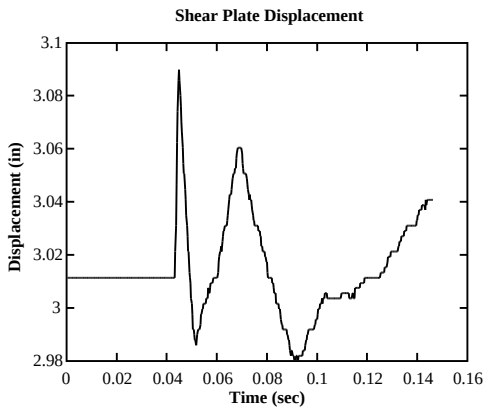

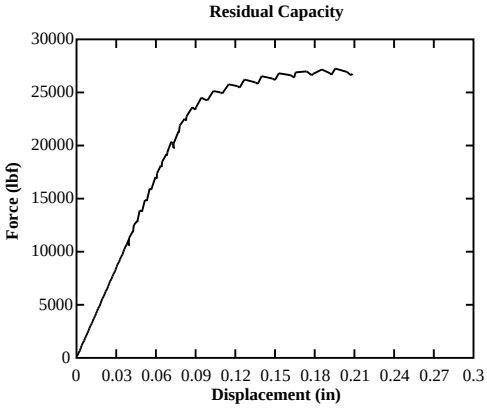

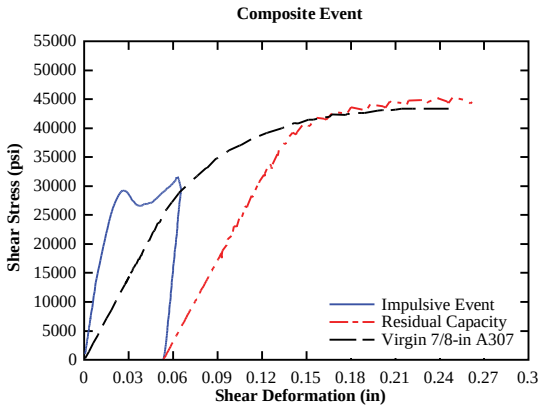

TEST RC-307-06

7/8 inch A307 | 317.7 in/s

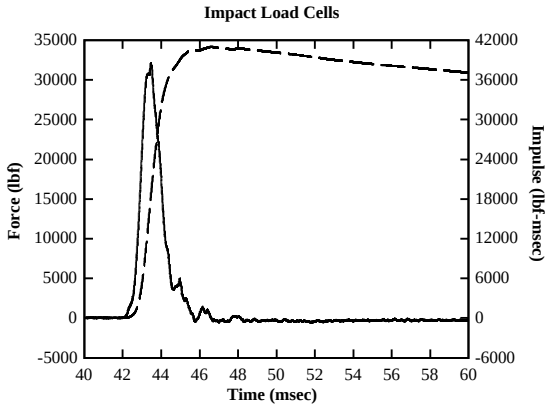

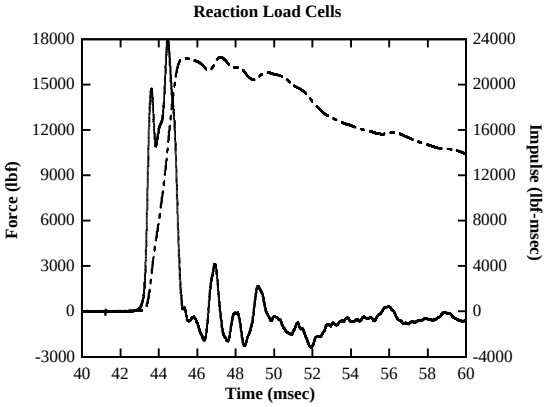

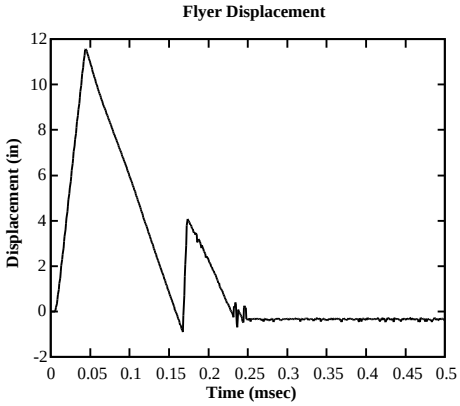

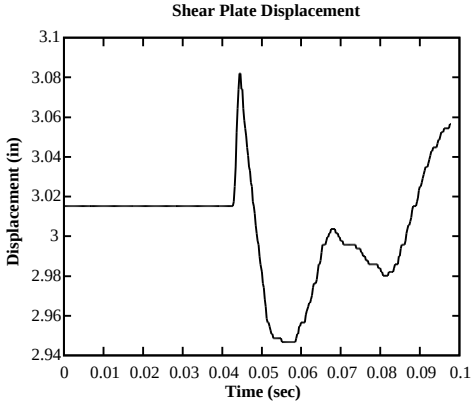

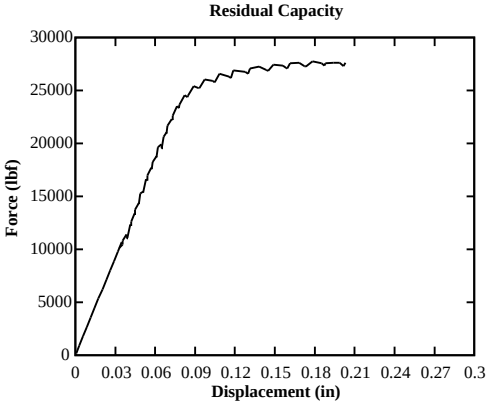

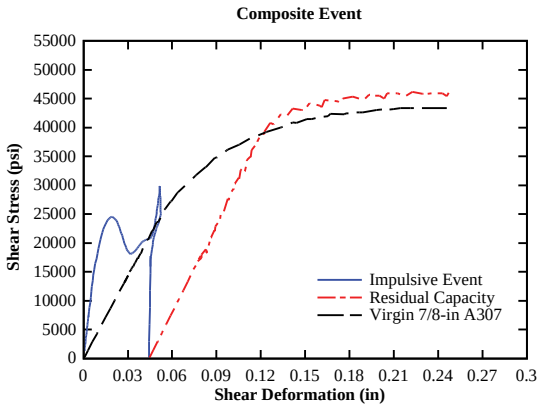

TEST RC-307-07

7/8 inch A307 | 361.4 in/s

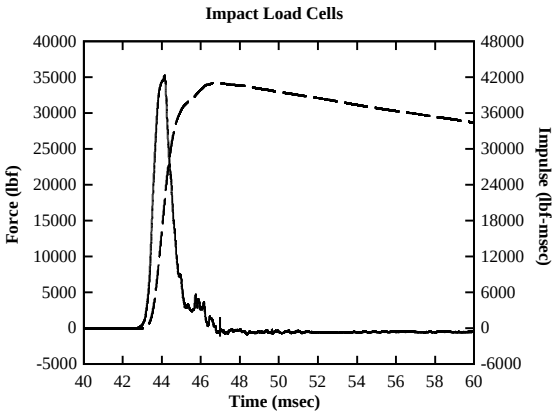

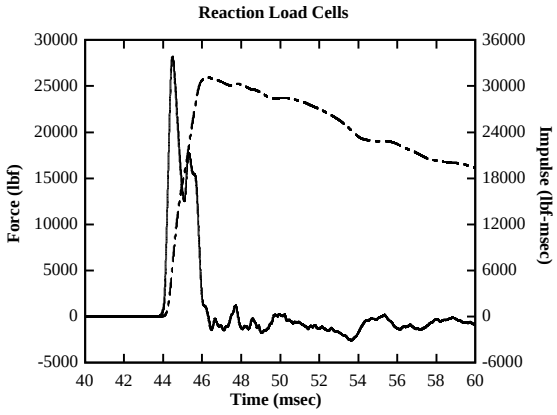

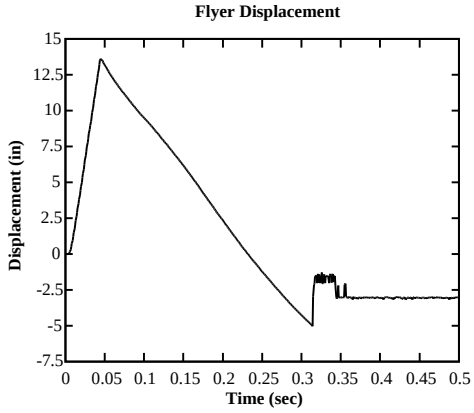

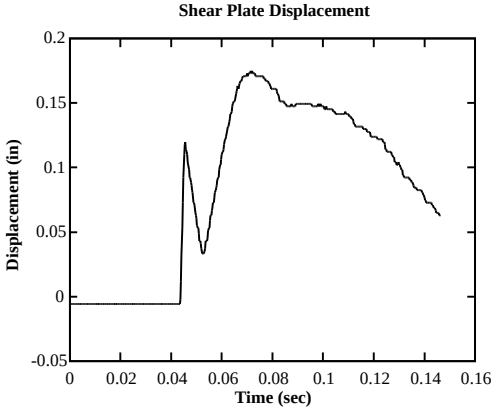

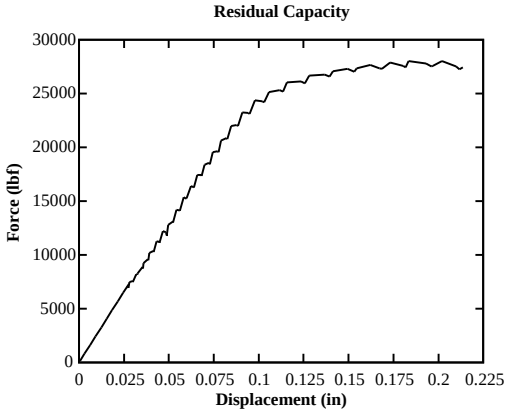

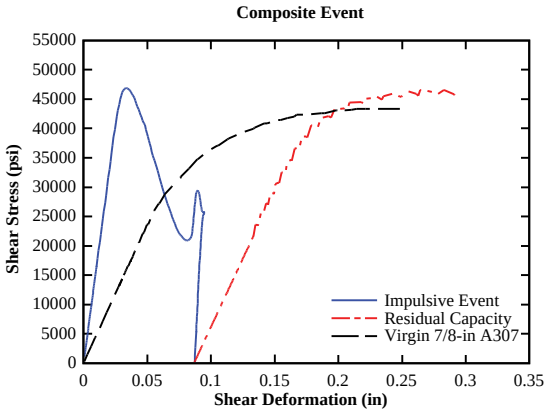

TEST RC-307-08

7/8 inch A307 | 365.0 in/s

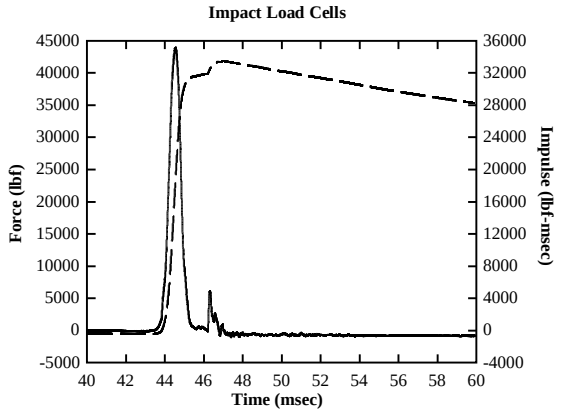

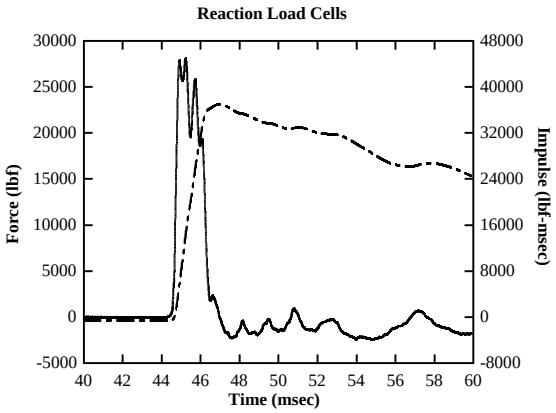

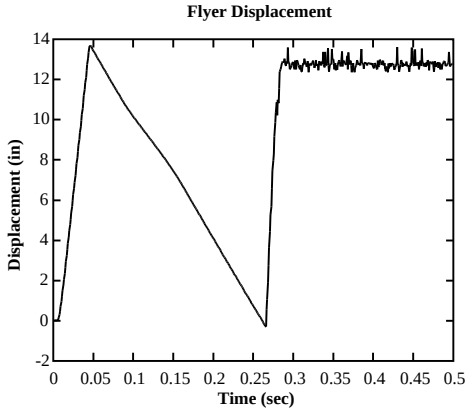

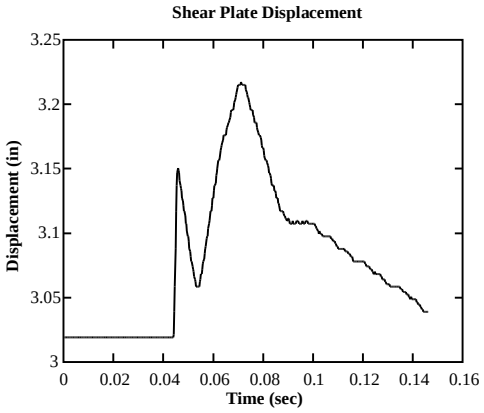

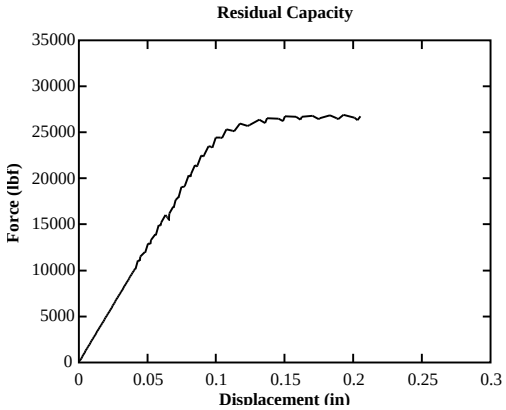

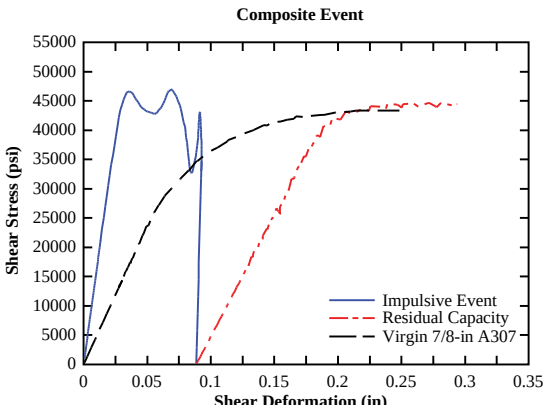

TEST RC-307-09

7/8 inch A307 | 355.2 in/s

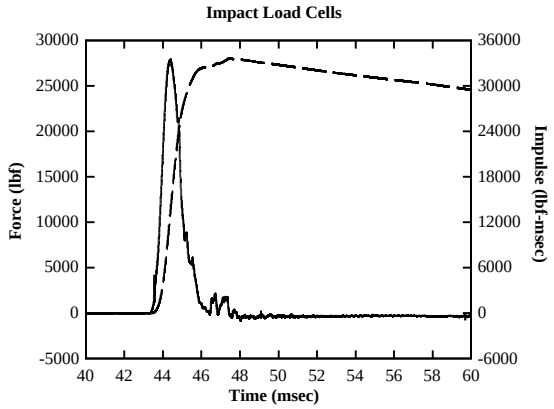

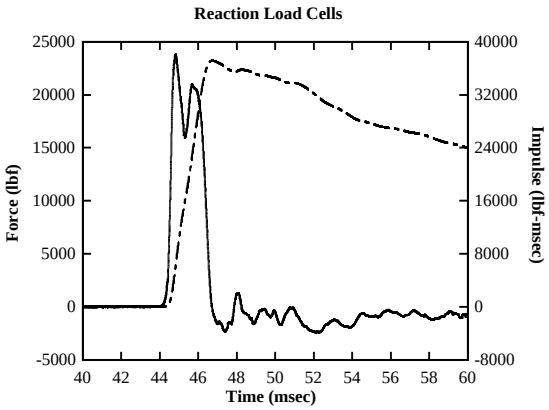

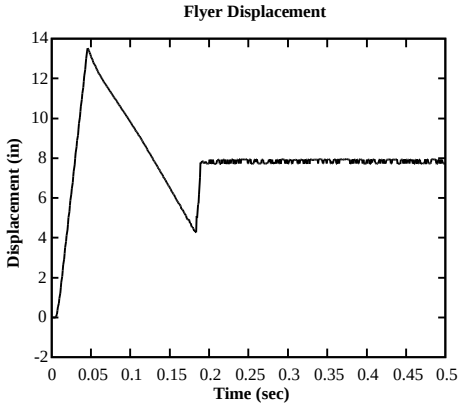

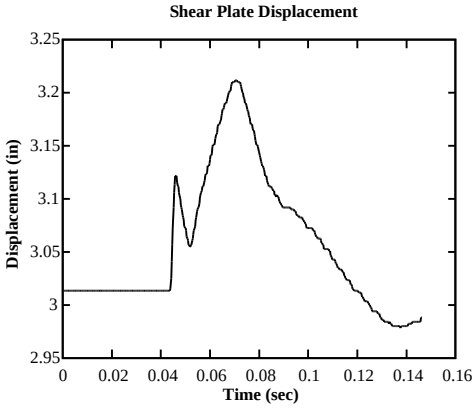

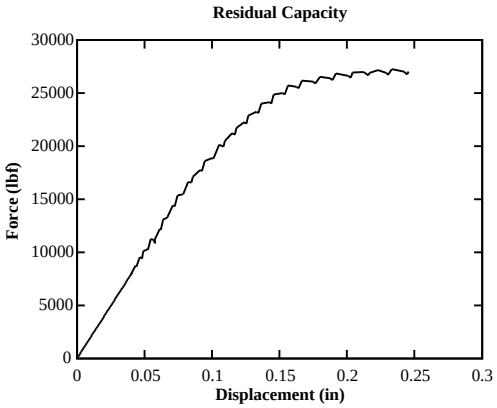

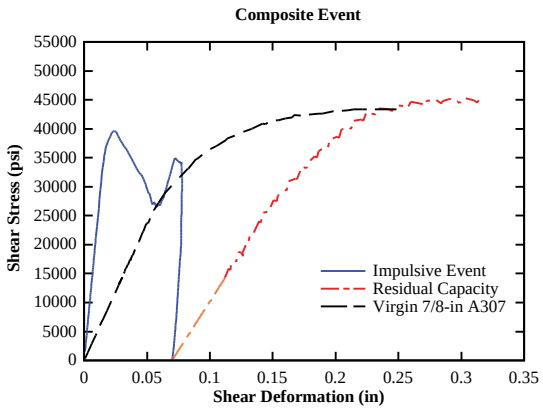

TEST RC-307-10

7/8 inch A307 | 393.1 in/s

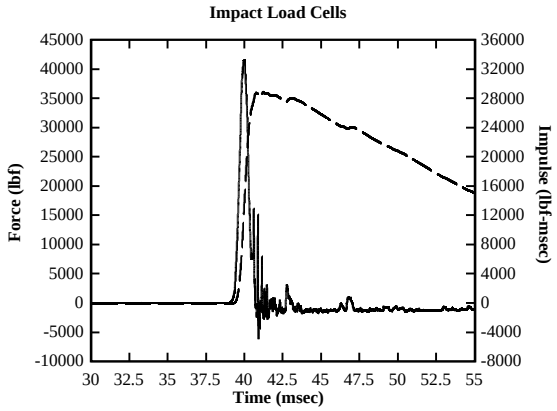

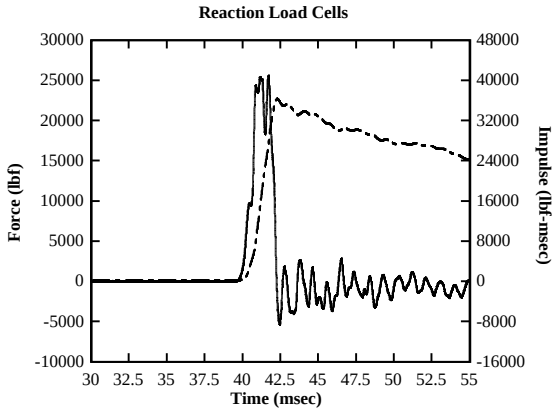

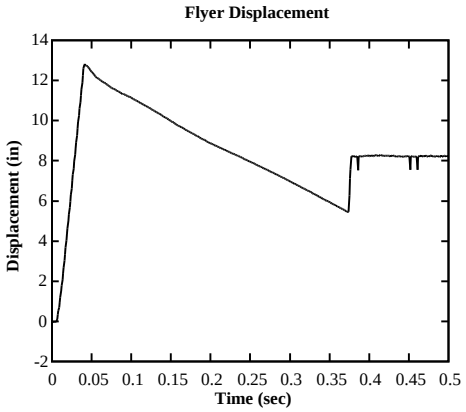

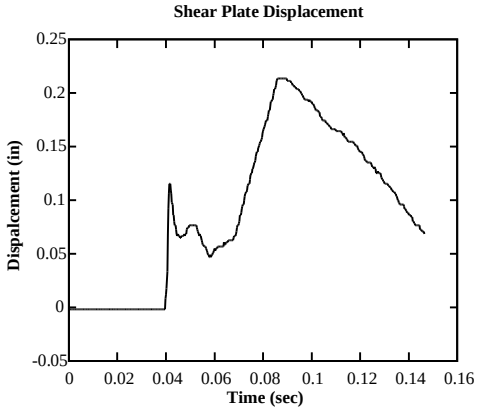

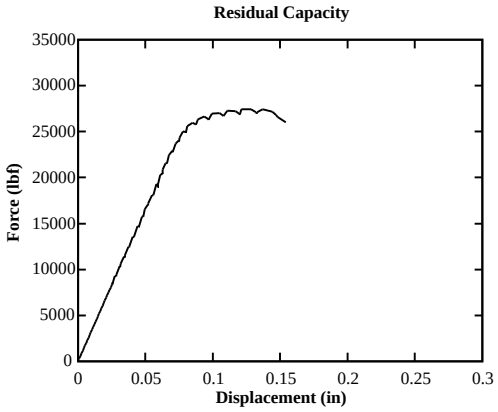

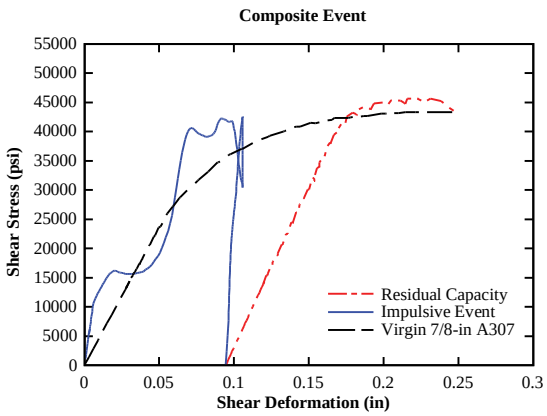

TEST RC-307-11

7/8 inch A307 | 403.8 in/s

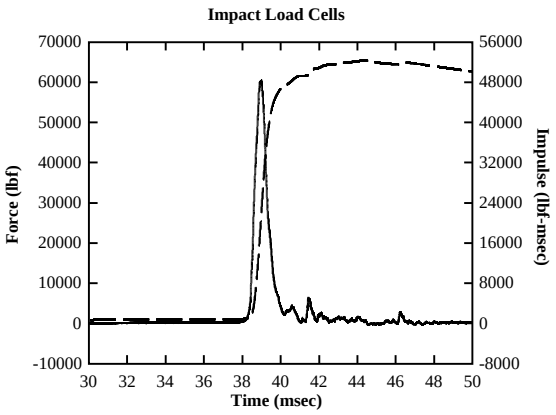

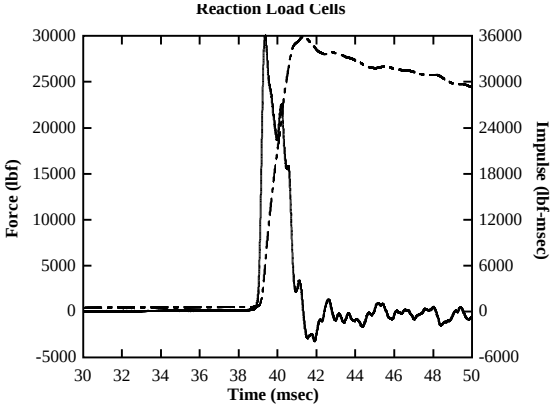

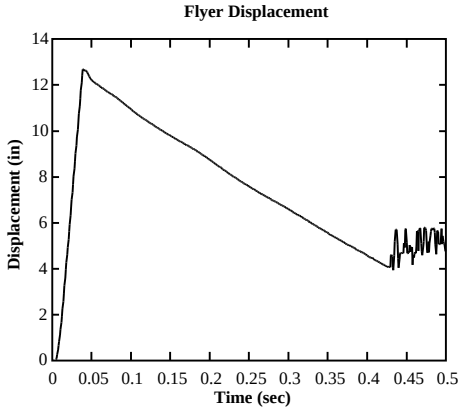

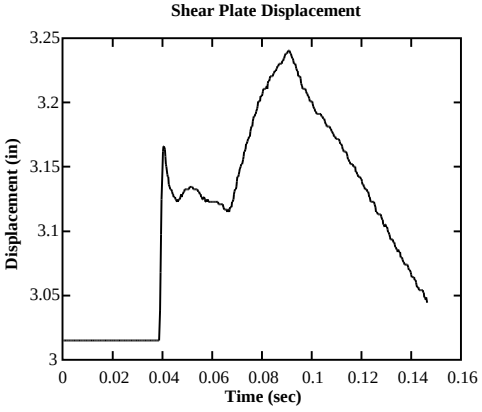

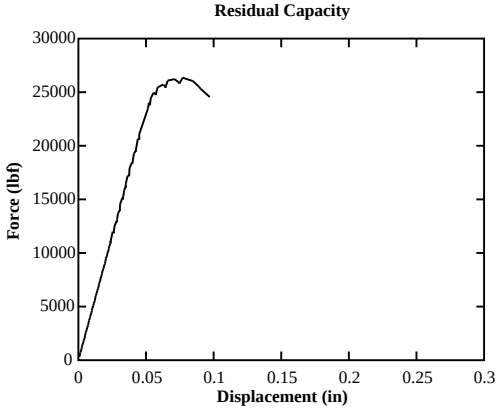

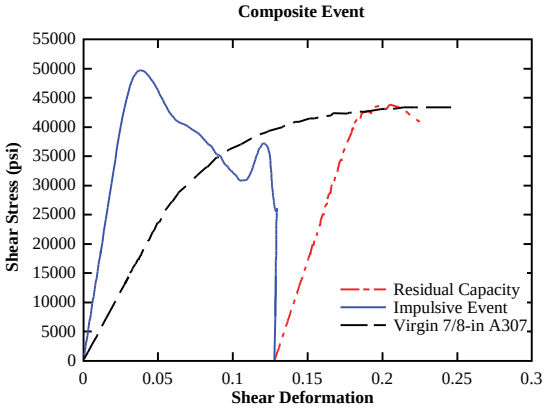

TEST RC-307-12

7/8 inch A307 | 468.7 in/s

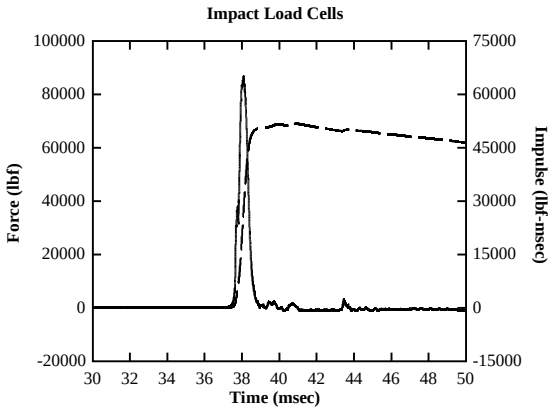

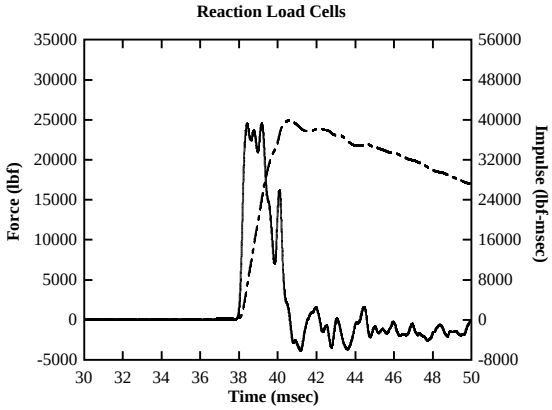

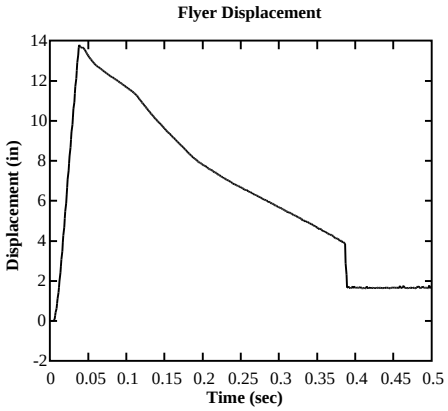

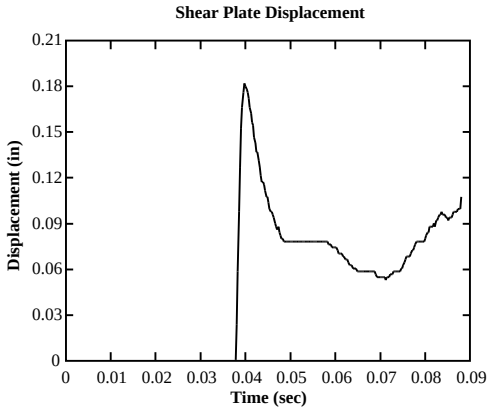

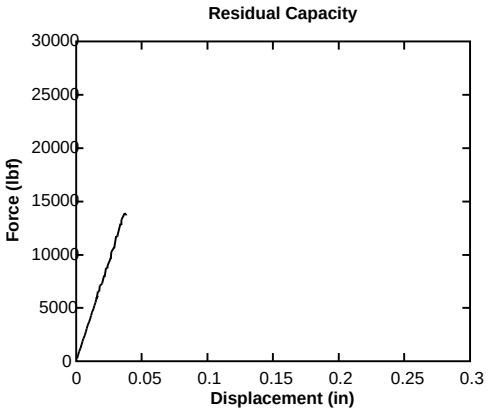

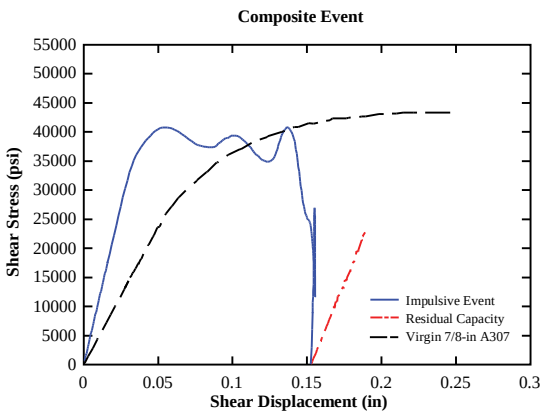

TEST RC-325-01

7/8 inch A325 | 370.2 in/s

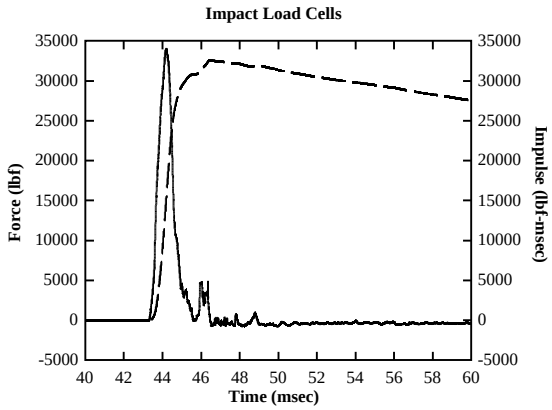

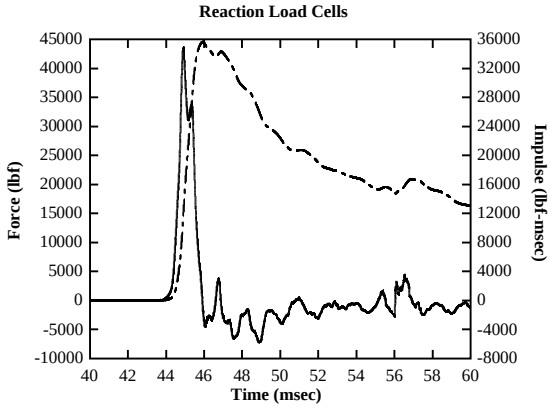

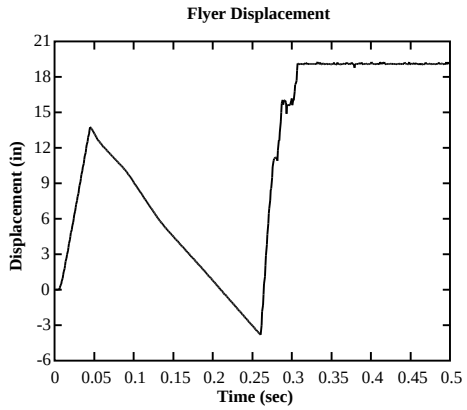

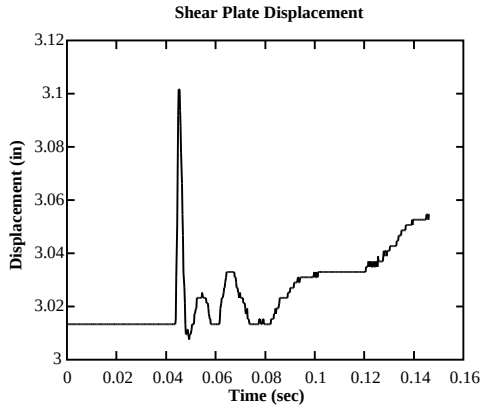

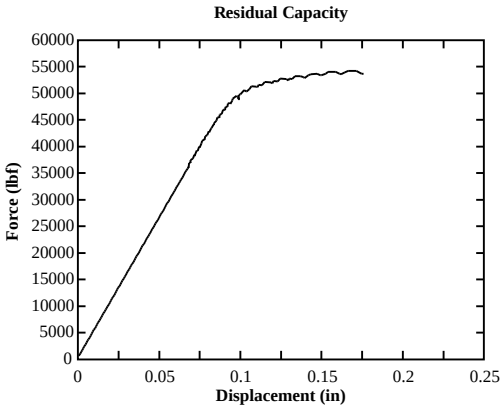

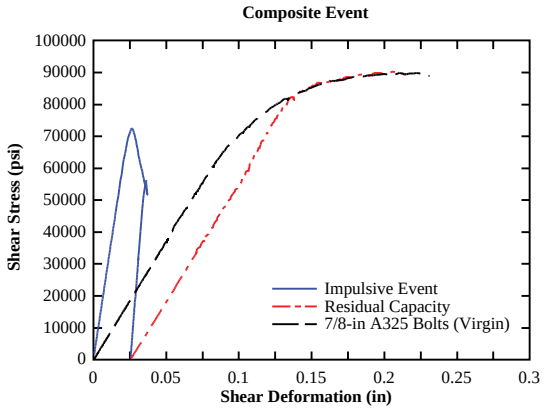

TEST RC-325-02

7/8 inch A325 | 365.5 in/s

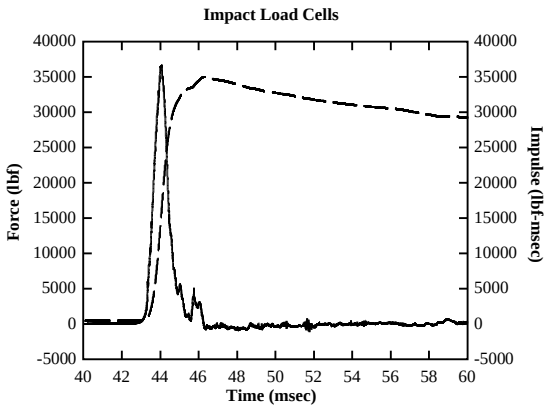

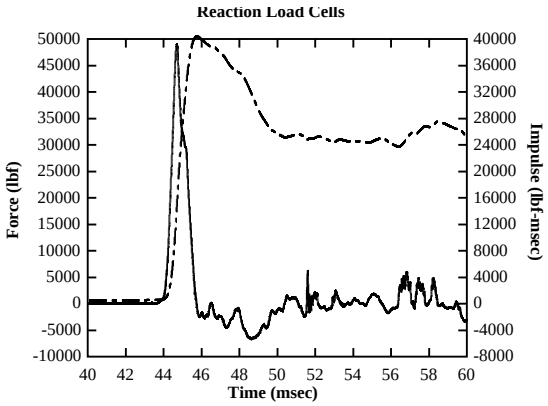

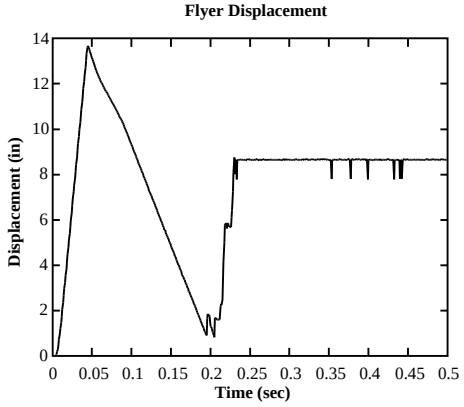

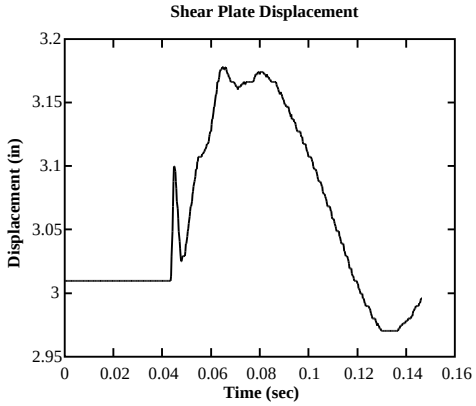

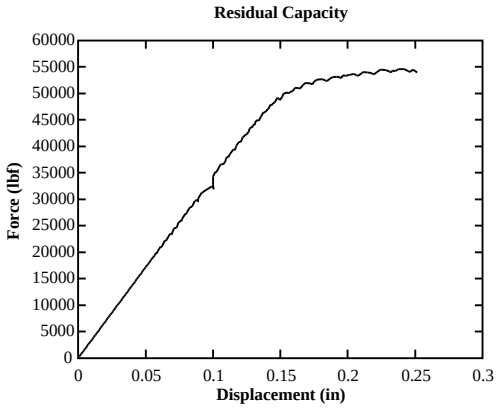

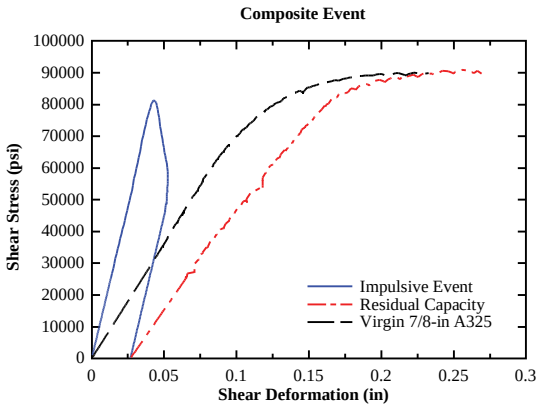

TEST RC-325-03

7/8 inch A325 | 374.9 in/s

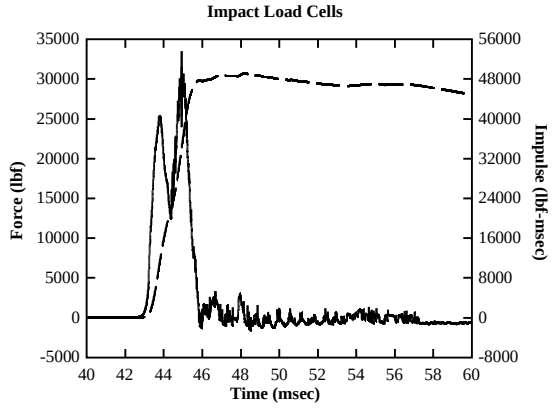

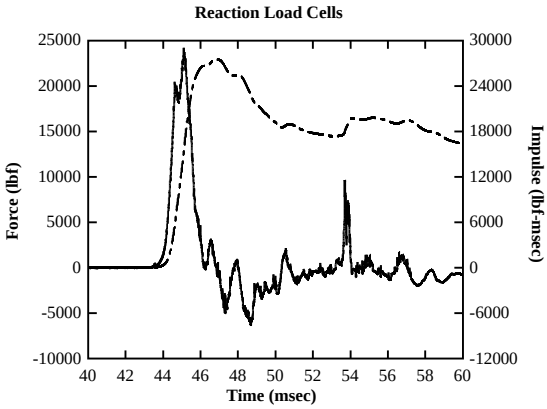

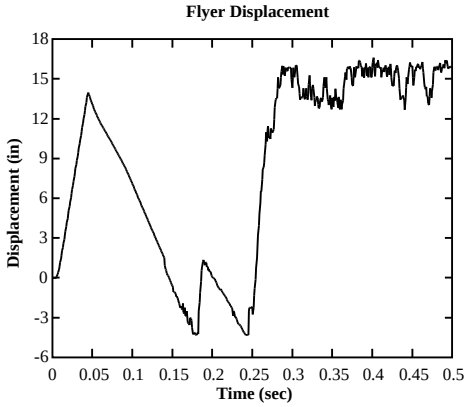

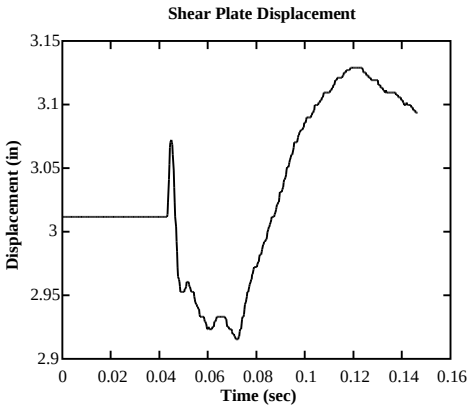

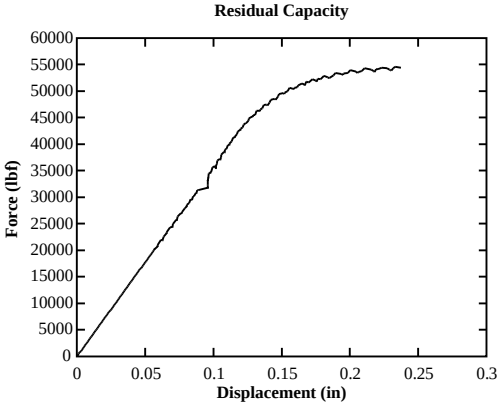

Composite curve data not available due to unusable data from reaction load cells and shear plate displacement.

Flyer did not impact setup directly.

TEST RC-325-04

7/8 inch A325 | 404.6 in/s

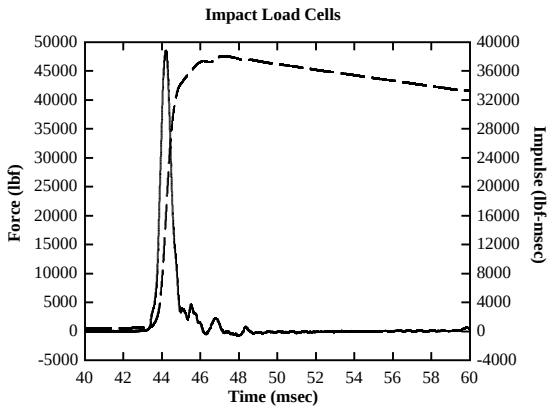

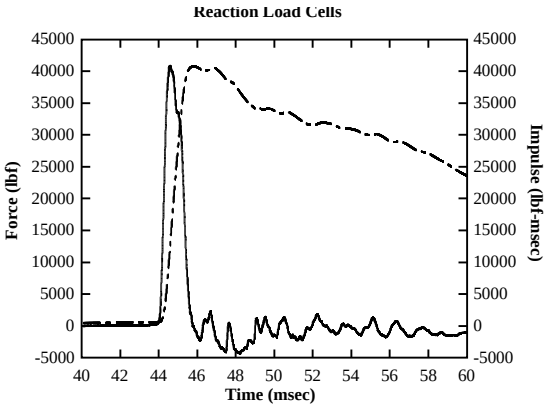

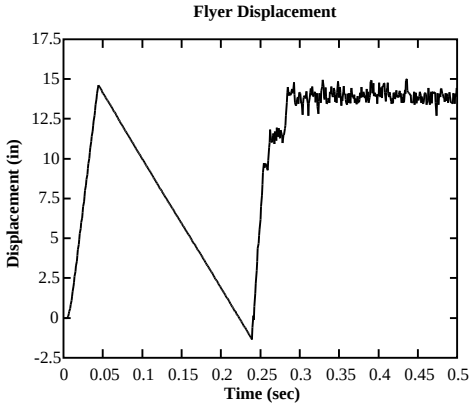

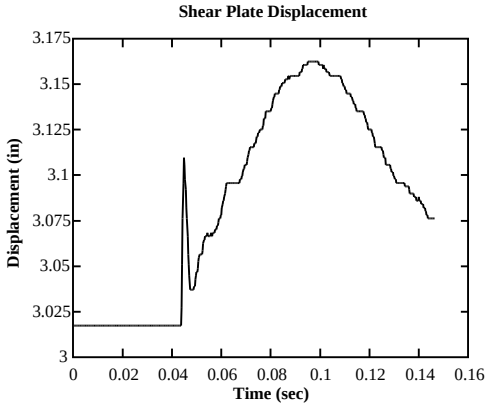

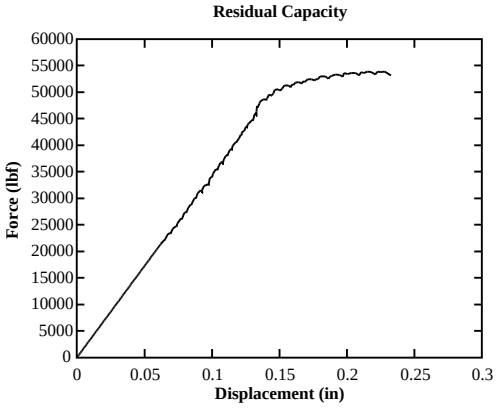

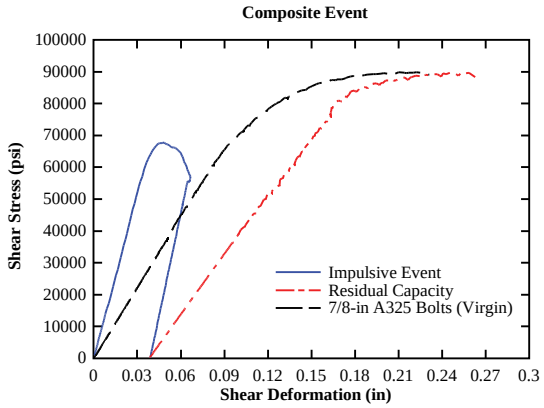

TEST RC-325-05

7/8 inch A325 | 405.4 in/s

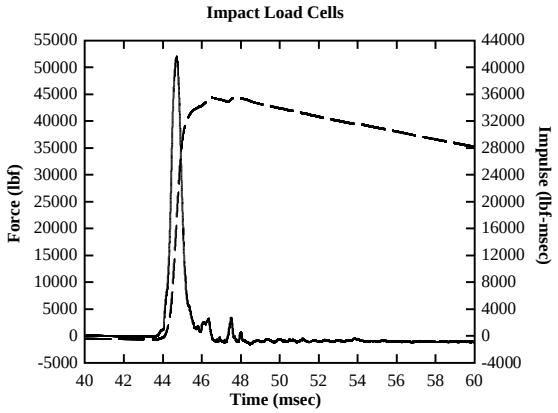

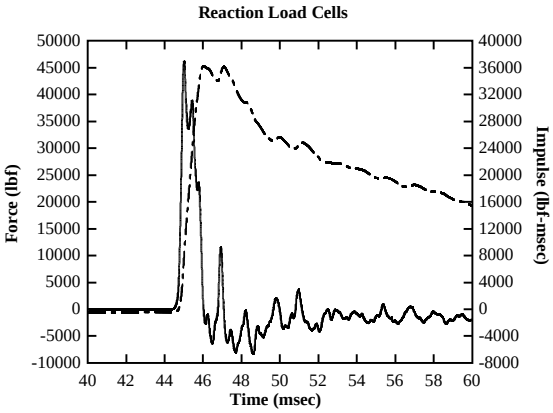

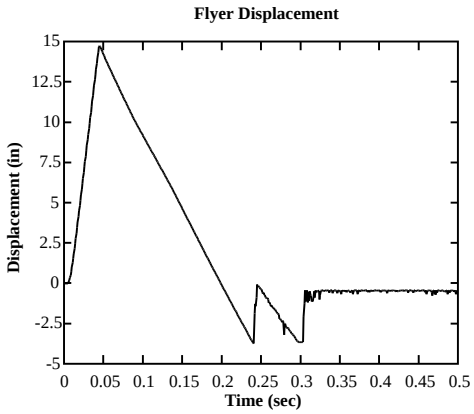

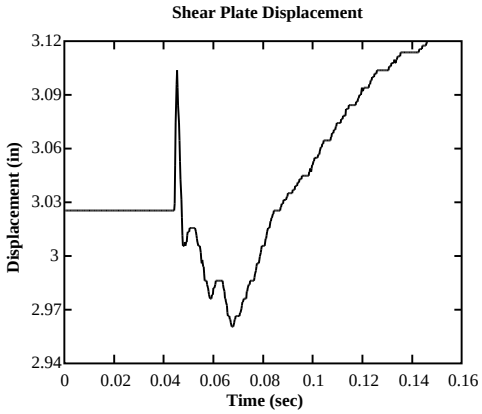

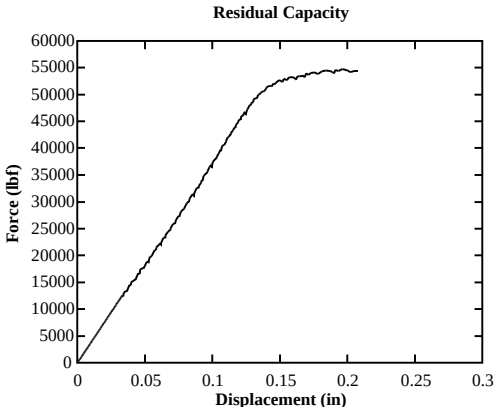

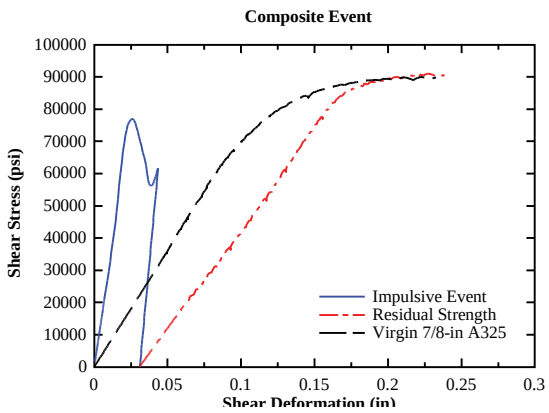

TEST RC-325-06

7/8 inch A325 | 410.8 in/s

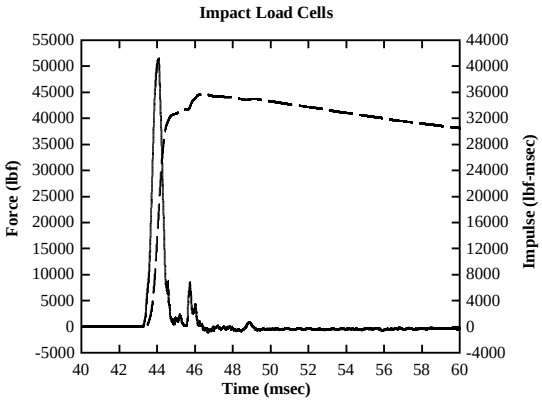

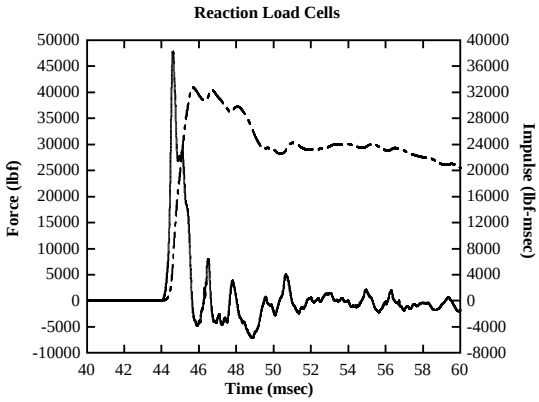

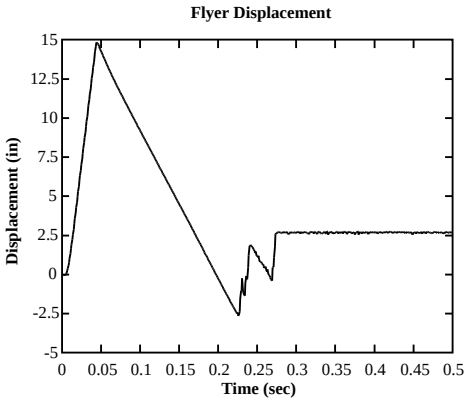

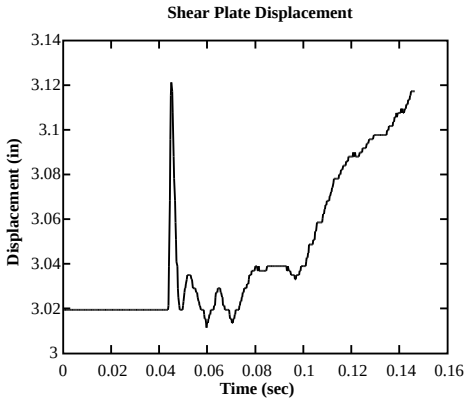

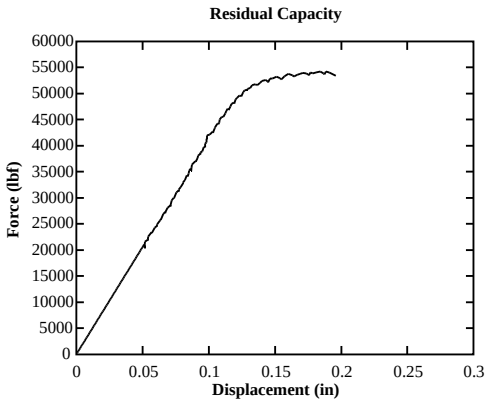

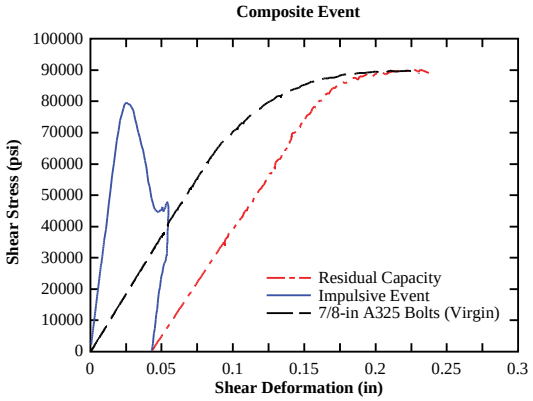

TEST RC-325-07

7/8 inch A325 | 426.4 in/s

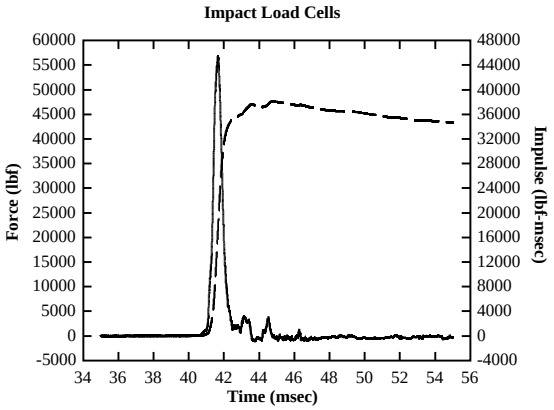

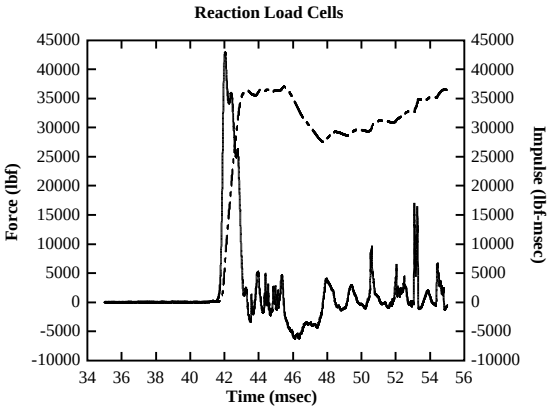

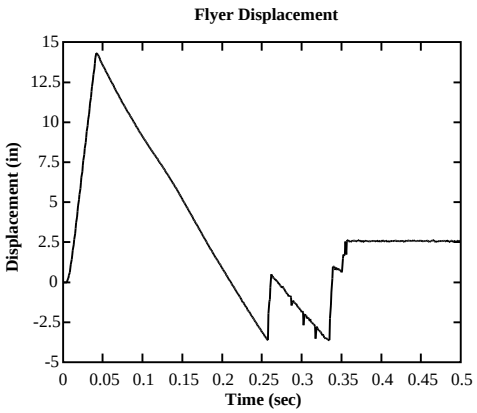

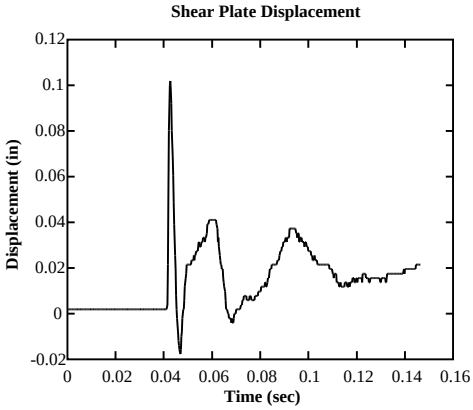

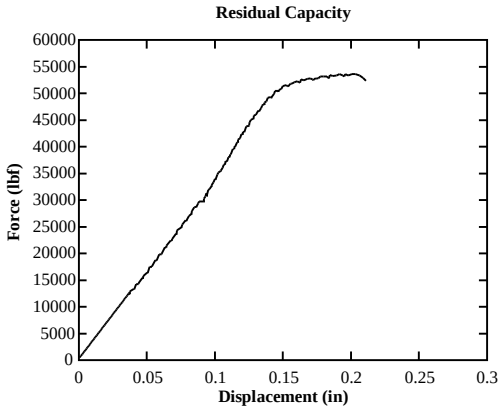

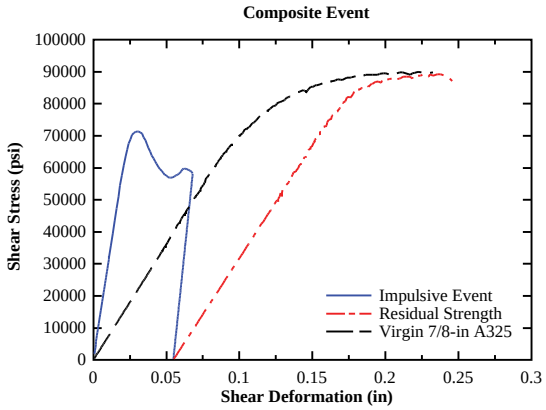

TEST RC-325-08

7/8 inch A325 | 433.2 in/s

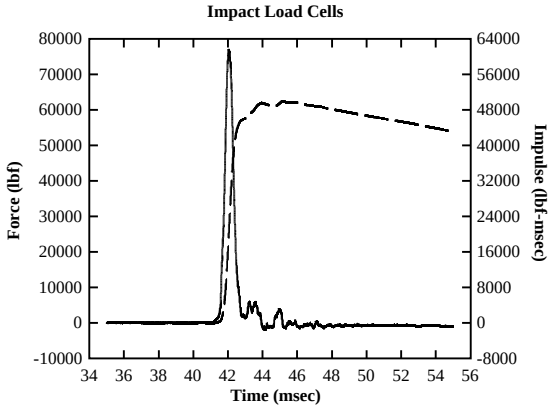

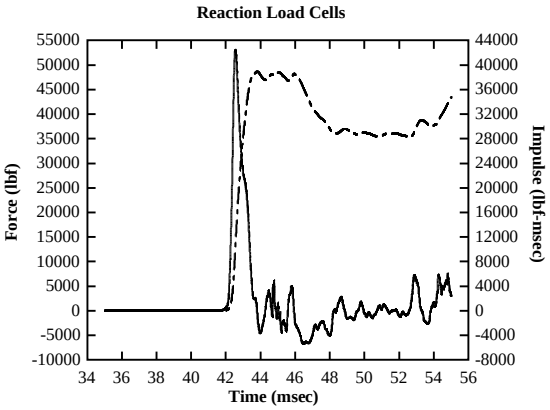

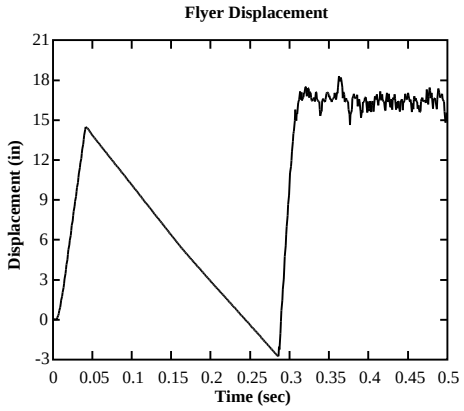

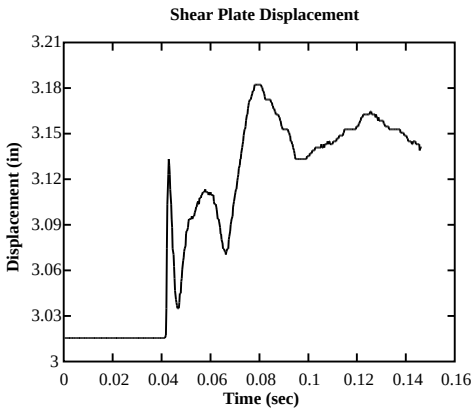

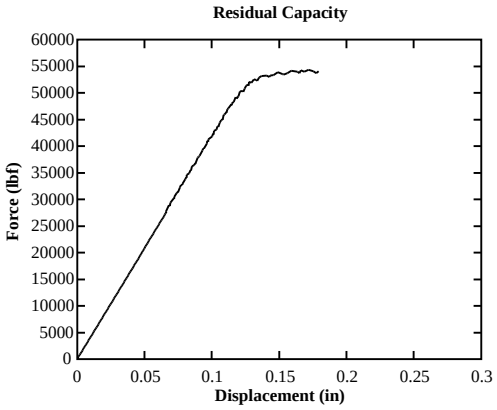

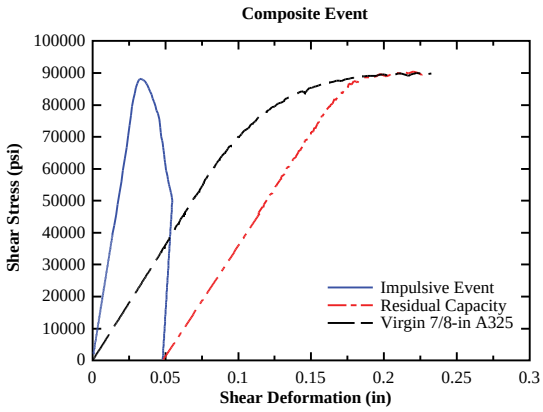

TEST RC-325-09

7/8 inch A325 | 442.4 in/s

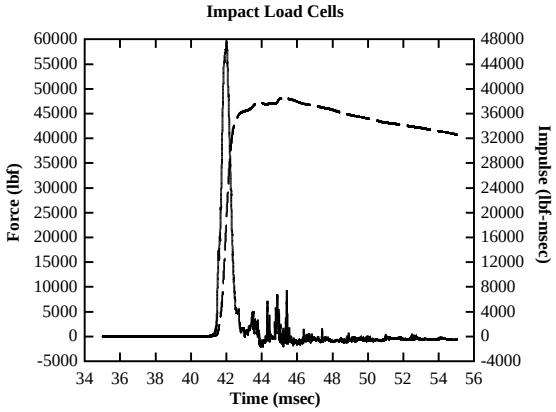

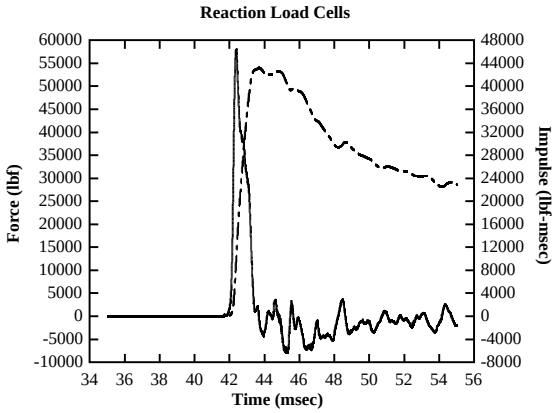

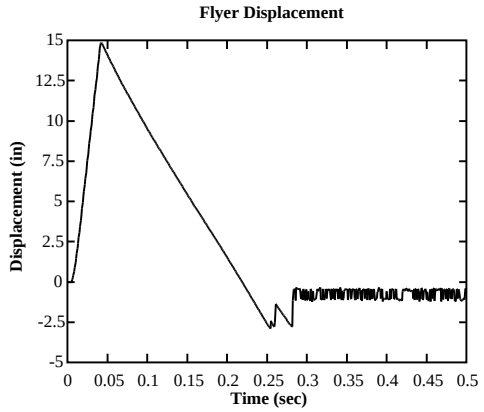

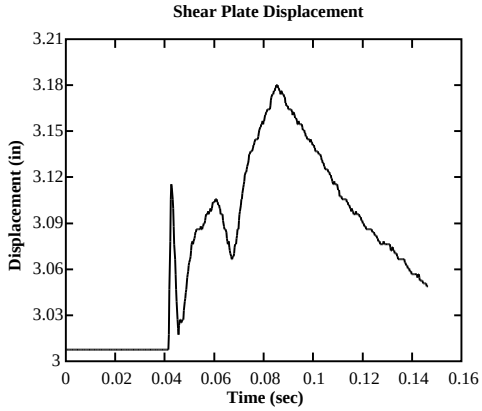

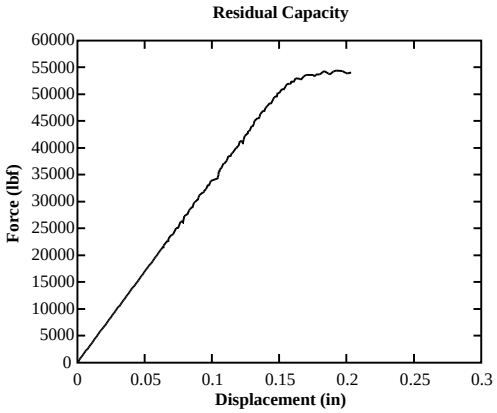

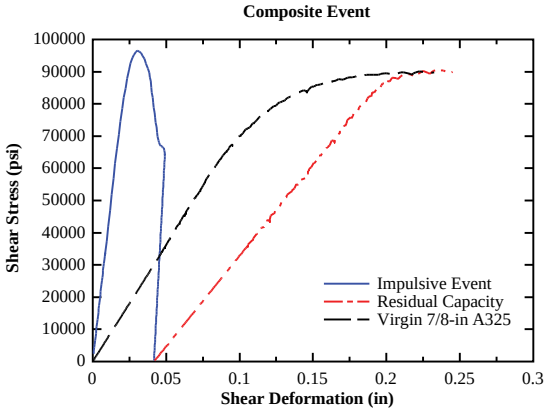

TEST RC-325-10

7/8 inch A325 | 496.6 in/s

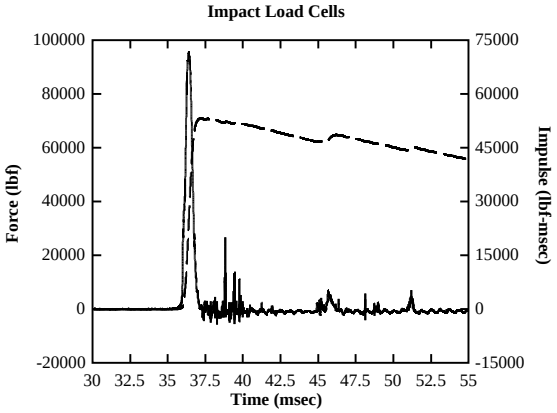

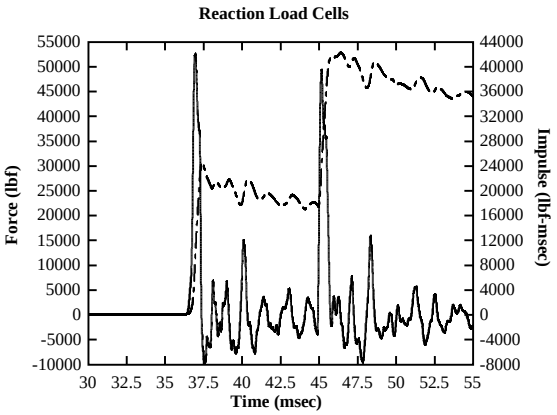

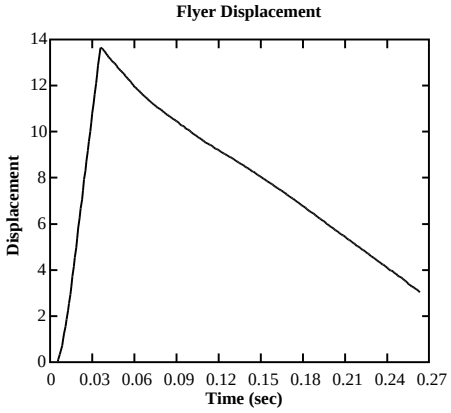

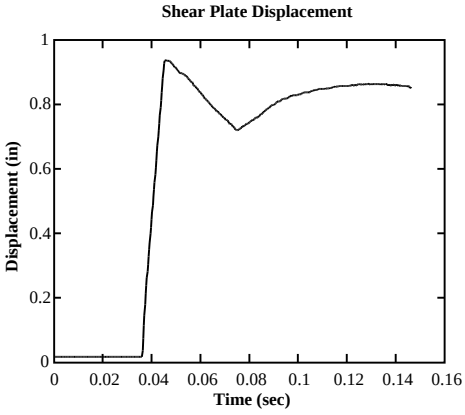

Bolt fractured during impulsive event, therefore there is no residual capacity.

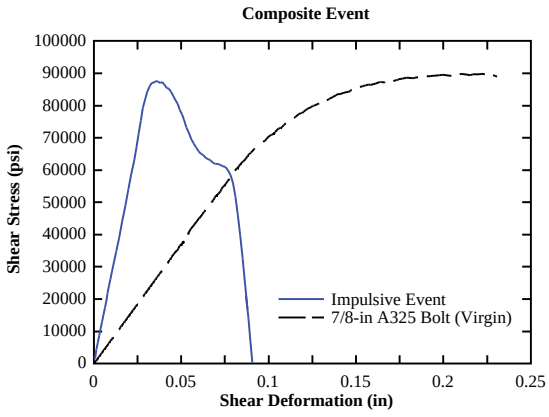

TEST SC-325-01

7/8 inch A325 | 177.64 in/s
Initial Torque: 569.8 ft·lbf | Break Torque: 355.5 ft·lbf

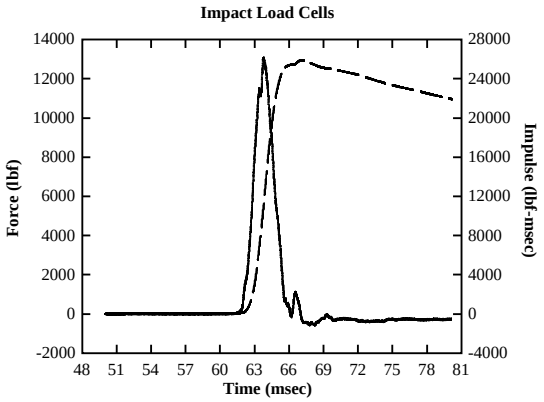

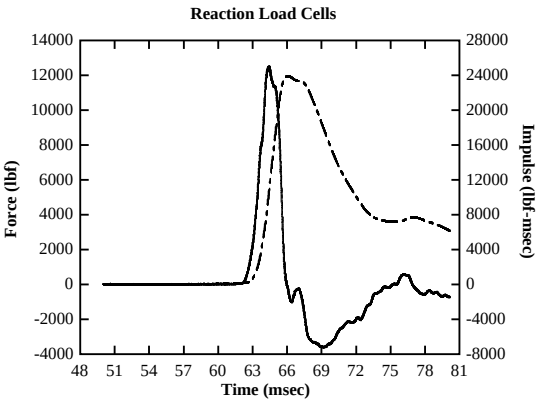

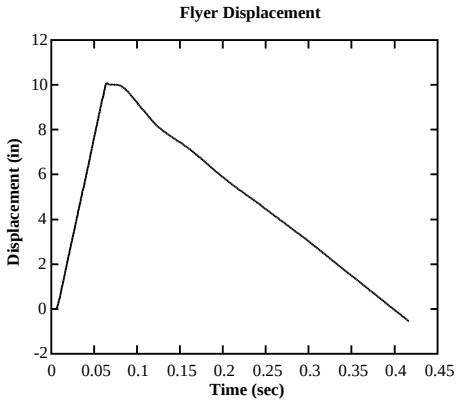

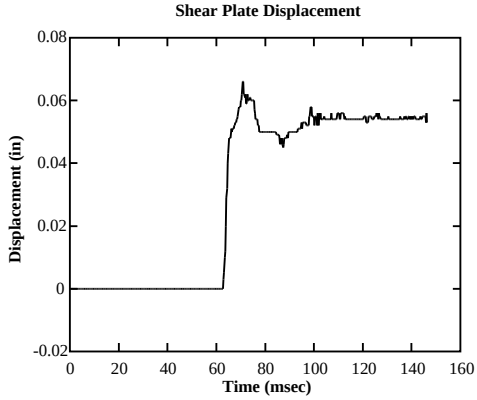

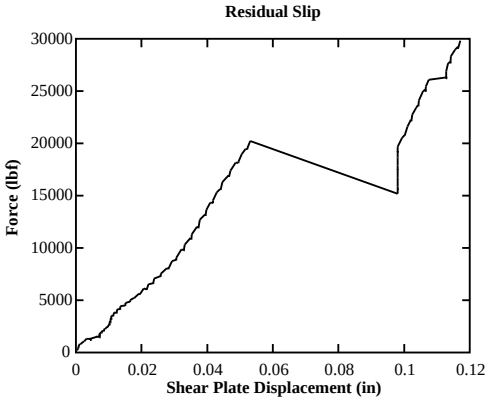

TEST SC-325-02

7/8 inch A325 | 248.0 in/s
Initial Torque: 603.2 ft·lbf | Break Torque: 376.3 ft·lbf

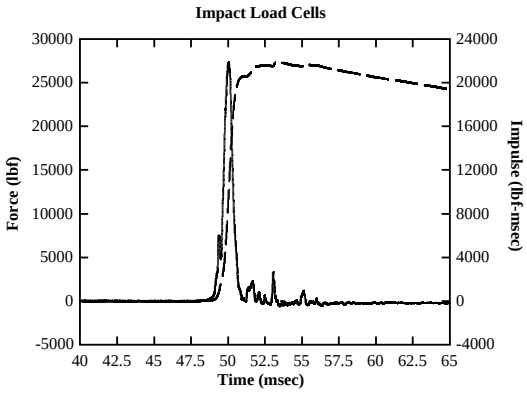

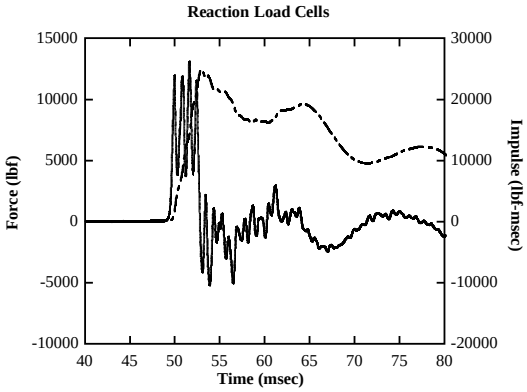

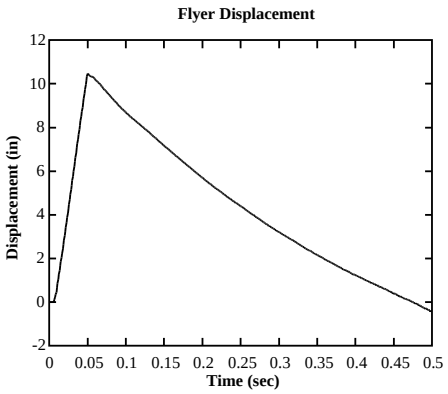

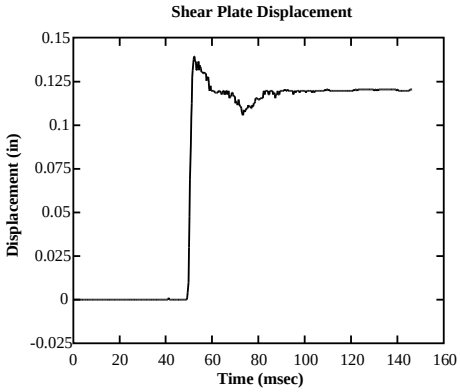

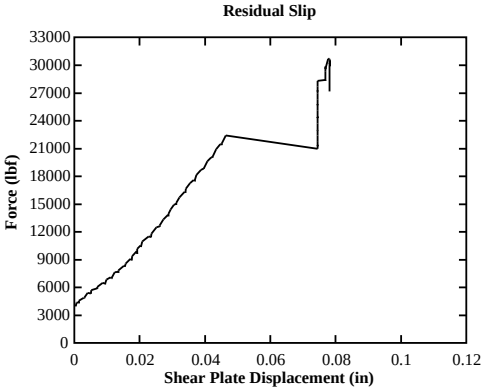

TEST SC-325-03

7/8 inch A325 | 300.5 in/s
Initial Torque: 616.1 ft·lbf | Break Torque: 379.5 ft·lbf

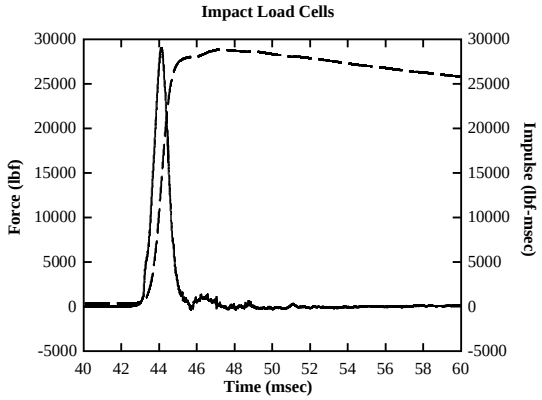

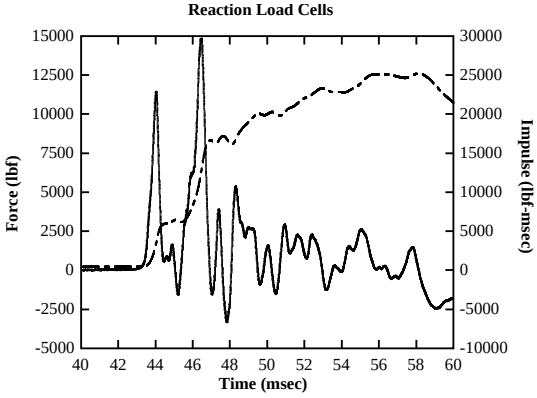

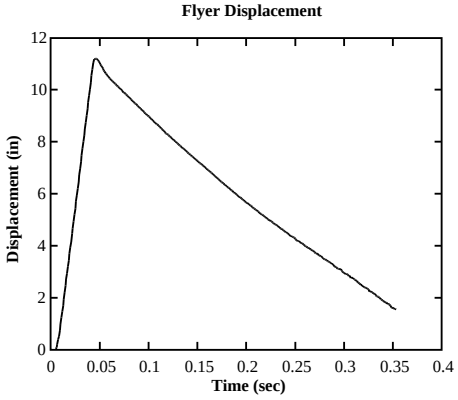

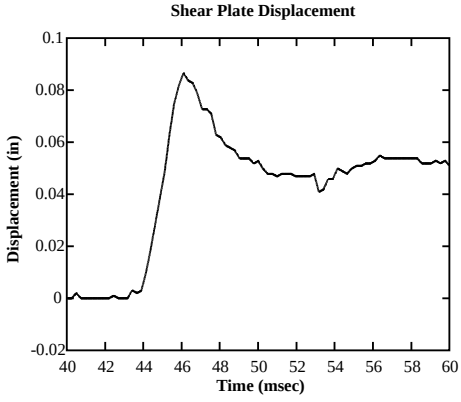

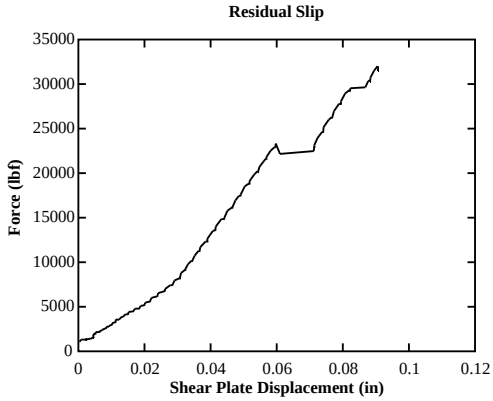

TEST SC-325-04

7/8 inch A325 | 337.7 in/s
Initial Torque: 598.3 ft·lbf | Break Torque: 384.1 ft·lbf

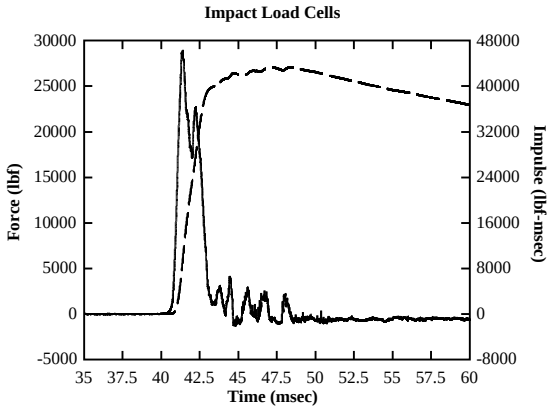

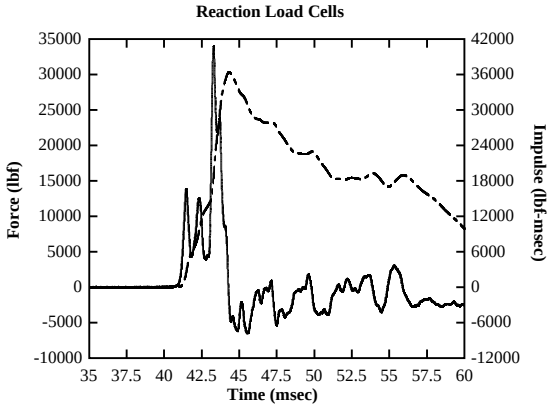

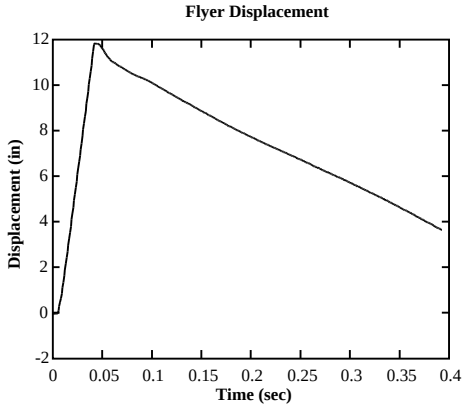

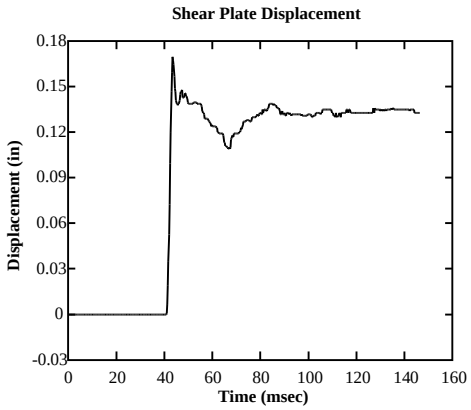

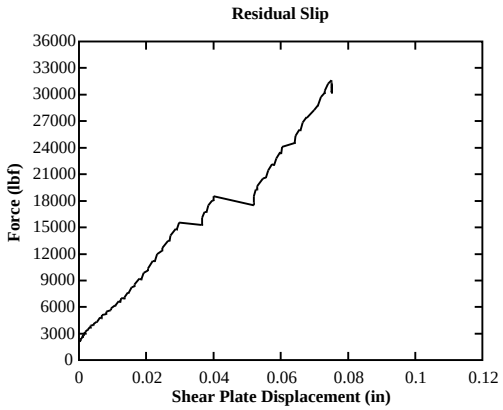

TEST SC-325-05

7/8 inch A325 | 365.9 in/s
Initial Torque: 623.1 ft·lbf | Break Torque: 331.2 ft·lbf

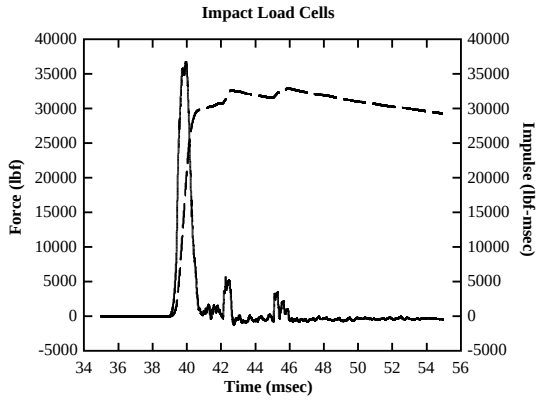

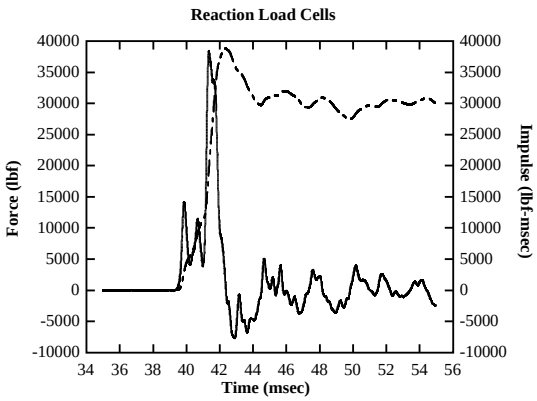

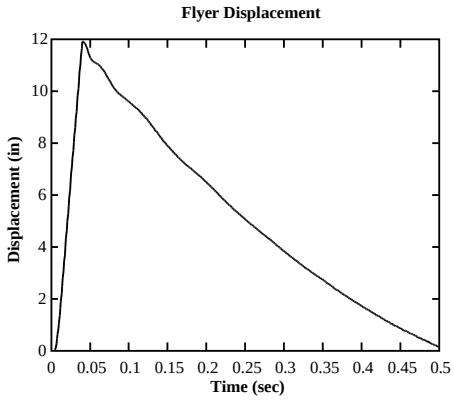

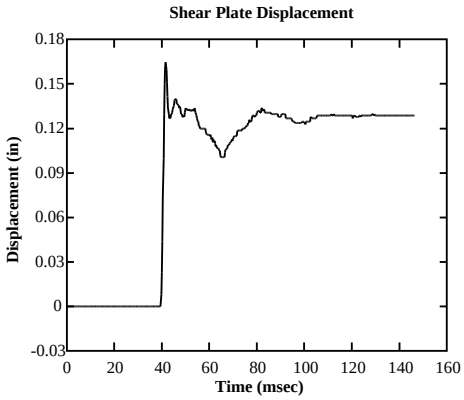

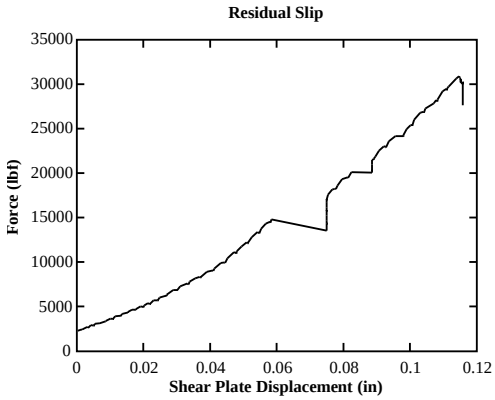

TEST SC-325-06

7/8 inch A325 | 405.8 in/s
Initial Torque: 612.1 ft·lbf | Break Torque: 296.9 ft·lbf

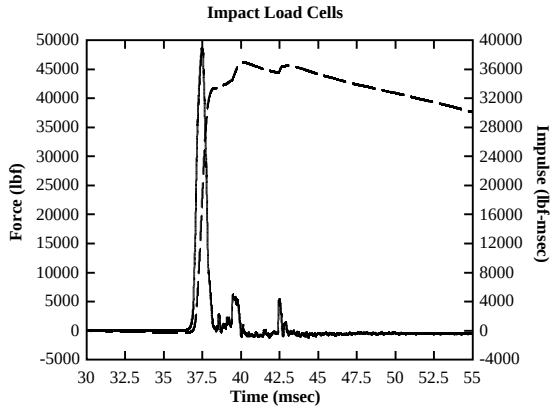

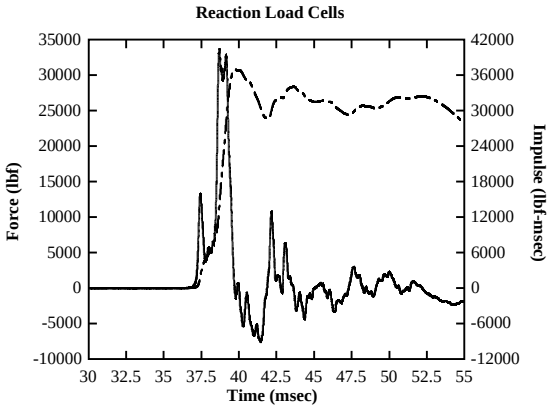

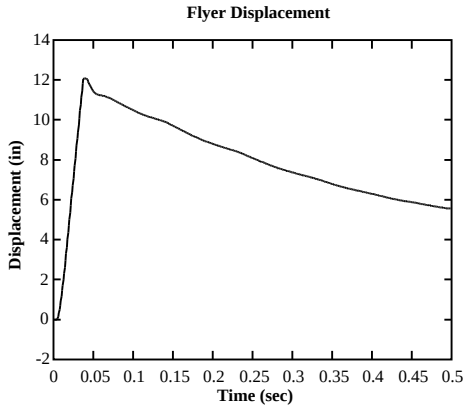

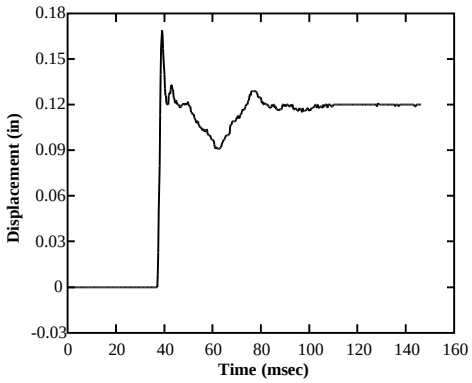

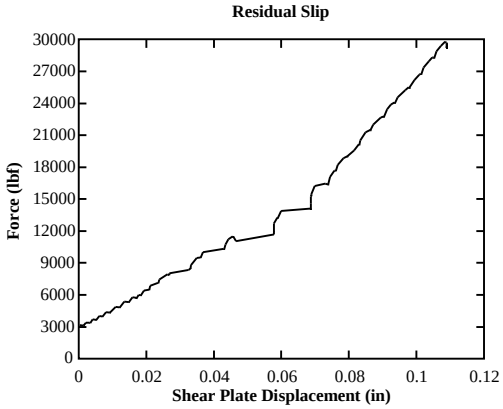

A307 BASELINE STATIC TESTS

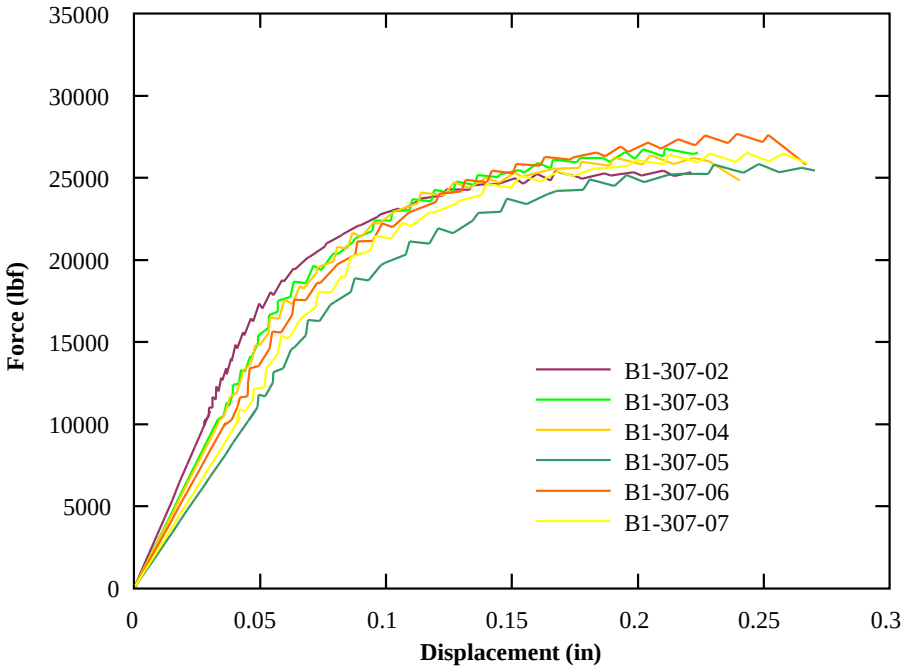

A325 BASELINE STATIC TESTS

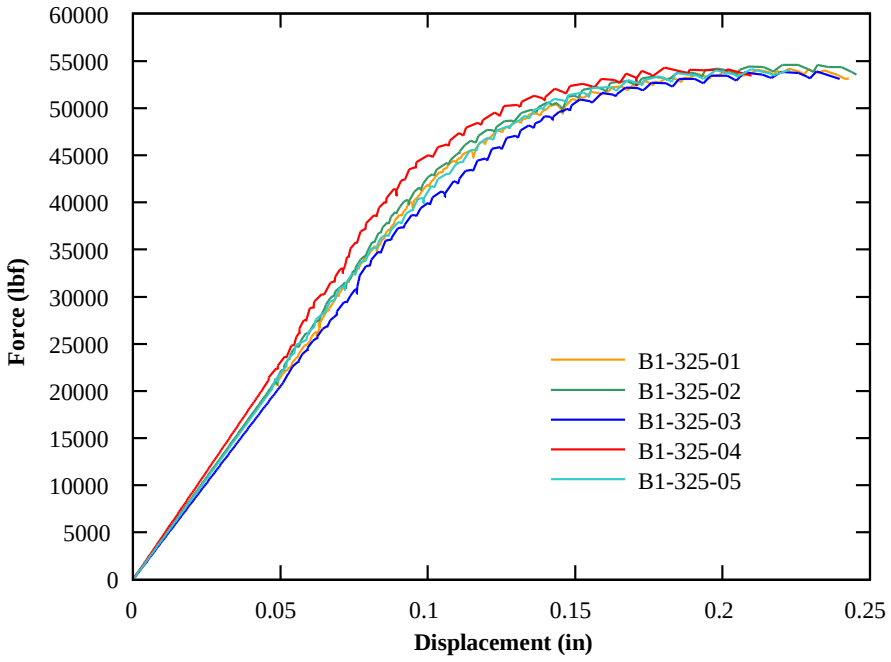

SLIP-CRITICAL BASELINE STATIC TESTS